ISSN 0021-9673

VOL. 605 NO. 2 JULY 17, 1992

THIS ISSUE COMPLETES VOL. 605

JOURNAL OF CHROMATOGRAPHY

INCLUDING ELECTROPHORESIS AND OTHER SEPARATION METHODS

ELSEVIER

JOURNAL OF CHROMATOGRAPHY

INCLUDING ELECTROPHORESIS AND OTHER SEPARATION METHODS

Scope. The *Journal of Chromatography* publishes papers on all aspects of chromatography, electrophoresis and related methods. Contributions consist mainly of research papers dealing with chromatographic theory, instrumental development and their applications. The section *Biomedical Applications*, which is under separate editorship, deals with the following aspects: developments in and applications of chromatographic and electrophoretic techniques related to clinical diagnosis or alterations during medical treatment; screening and profiling of body fluids or tissues with special reference to metabolic disorders; results from basic medical research with direct consequences in clinical practice; drug level monitoring and pharmacokinetic studies; clinical toxicology; analytical studies in occupational medicine.

Submission of Papers. Manuscripts (in English; *four* copies are required) should be submitted to: Editorial Office of *Journal of Chromatography*, P.O. Box 681, 1000 AR Amsterdam, Netherlands, Telefax (+31-20) 5862 304, or to: The Editor of *Journal of Chromatography, Biomedical Applications*, P.O. Box 681, 1000 AR Amsterdam, Netherlands. Review articles are invited or proposed by letter to the Editors. An outline of the proposed review should first be forwarded to the Editors for preliminary discussion prior to preparation. Submission of an article is understood to imply that the article is original and unpublished and is not being considered for publication elsewhere. For copyright regulations, see below.

Publication. The *Journal of Chromatography* (incl. *Biomedical Applications*) has 39 volumes in 1992. The subscription prices for 1992 are:

J. Chromatogr. (incl. *Cum. Indexes, Vols. 551–600*) + *Biomed. Appl.* (Vols. 573–611):
Dfl. 7722.00 plus Dfl. 1209.00 (p.p.h.) (total *ca.* US$ 4880.25)

J. Chromatogr. (incl. *Cum. Indexes, Vols. 551–600*) only (Vols. 585–611):
Dfl. 6210.00 plus Dfl. 837.00 (p.p.h.) (total *ca.* US$ 3850.75)

Biomed. Appl. only (Vols. 573–584):
Dfl. 2760.00 plus Dfl. 372.00 (p.p.h.) (total *ca.* US$ 1711.50).

Subscription Orders. The Dutch guilder price is definitive. The US$ price is subject to exchange-rate fluctuations and is given as a guide. Subscriptions are accepted on a prepaid basis only, unless different terms have been previously agreed upon. Subscriptions orders can be entered only by calender year (Jan.–Dec.) and should be sent to Elsevier Science Publishers, Journal Department, P.O. Box 211, 1000 AE Amsterdam, Netherlands, Tel. (+31-20) 5803 642, Telefax (+31-20) 5803 598, or to your usual subscription agent. Postage and handling charges include surface delivery except to the following countries where air delivery via SAL (Surface Air Lift) mail is ensured: Argentina, Australia, Brazil, Canada, China, Hong Kong, India, Israel, Japan*, Malaysia, Mexico, New Zealand, Pakistan, Singapore, South Africa, South Korea, Taiwan, Thailand, USA. *For Japan air delivery (SAL) requires 25% additional charge of the normal postage and handling charge. For all other countries airmail rates are available upon request. Claims for missing issues must be made within three months of our publication (mailing) date, otherwise such claims cannot be honoured free of charge. Back volumes of the *Journal of Chromatography* (Vols. 1–572) are available at Dfl. 217.00 (plus postage). Customers in the USA and Canada wishing information on this and other Elsevier journals, please contact Journal Information Center, Elsevier Science Publishing Co. Inc., 655 Avenue of the Americas, New York, NY 10010, USA, Tel. (+1-212) 633 3750, Telefax (+1-212) 633 3990.

Abstracts/Contents Lists published in Analytical Abstracts, Biochemical Abstracts, Biological Abstracts, Chemical Abstracts, Chemical Titles, Chromatography Abstracts, Clinical Chemistry Lookout, Current Contents/Life Sciences, Current Contents/Physical, Chemical & Earth Sciences, Deep-Sea Research/Part B: Oceanographic Literature Review, Excerpta Medica, Index Medicus, Mass Spectrometry Bulletin, PASCAL-CNRS, Pharmaceutical Abstracts, Referativnyi Zhurnal, Research Alert, Science Citation Index and Trends in Biotechnology.

US Mailing Notice. *Journal of Chromatography* (main section ISSN 0021-9673, *Biomedical Applications* section ISSN 0378-4347) is published (78 issues/year) by Elsevier Science Publishers (Sara Burgerhartstraat 25, P.O. Box 211, 1000 AE Amsterdam, Netherlands). Annual subscription price in the USA US$ 4880.25 (subject to change), including air speed delivery. Application to mail at second class postage rate is pending at Jamaica, NY 11431. **USA POSTMASTERS:** Send address changes to *Journal of Chromatography*, Publications Expediting, Inc., 200 Meacham Avenue, Elmont, NY 11003. Airfreight and mailing in the USA by Publication Expediting.

See inside back cover for Publication Schedule, Information for Authors and information on Advertisements.

0021-9673/92/$05.00

This issue is printed on acid-free paper.

Printed in the Netherlands

CONTENTS

(Abstracts/Contents Lists published in Analytical Abstracts, Biochemical Abstracts, Biological Abstracts, Chemical Abstracts, Chemical Titles, Chromatography Abstracts, Current Contents/Life Sciences, Current Contents/Physical, Chemical & Earth Sciences, Deep-Sea Research/Part B: Oceanographic Literature Review, Excerpta Medica, Index Medicus, Mass Spectrometry Bulletin, PASCAL-CNRS, Referativnyi Zhurnal, Research Alert and Science Citation Index)

REGULAR PAPERS

Column Liquid Chromatography

Gas Chromatography

Continued overleaf

In articles with more than one author, the name of the author to whom correspondence should be addressed is indicated in the article heading by a 6-pointed asterisk (*).

Journal of Chromatography, 605 (1992) 151–159
Elsevier Science Publishers B.V., Amsterdam

CHROM. 24 248

Analytic solution for volume-overloaded gradient elution chromatography

Giorgio Carta and W. Butler Stringfield

Center for Bioprocess Development, Department of Chemical Engineering, University of Virginia, Charlottesville, VA 22903-2442 (USA)

(First received January 23rd, 1992; revised manuscript received April 7th, 1992)

ABSTRACT

An analytic solution to a partial differential equation model for gradient elution chromatography is obtained. The model is restricted to linear isotherms and treats mass transfer effects with the linear driving force approximation. The solution is obtained for periodic, rectangular feed pulses, with an arbitrary gradient shape and type, and is given in the form of a convergent series that allows a direct calculation of the effluent profile and of the average product concentration. Calculations for small feed pulses, show that the solution gives the retention time and peak spreading predicted by the linear solvent strength theory for reversed phase chromatography, in the limit of Gaussian peaks. For larger feed pulses the solution predicts asymmetric peaks with concentrations exceeding that of the feed sample. The theory developed is succesfully used to predict volume overload effects in gradient elution from isocratic elution data for an experimental system.

INTRODUCTION

Gradient elution chromatography is frequently used for both analytical and preparative applications, especially for the separation of mixtures whose components have a broad spectrum of retentivity [1,2] and for biopolymer separations [3]. While in analytical applications small feed pulses are used, in preparative applications the feed pulses are larger and may be have the shape of a rectangular slug. Often preparative gradient elution is carried out in industry with only slight concentration overloading during feed injection, but with considerable volume overloading, since such conditions tend to be the most reproducible to operate. There is a need, therefore, for simple solutions to the equations that describe linear gradient elution that can be used by the industrial practitioner for the purpose of interpretation of results and parameter optimization.

Correspondence to: Dr. G. Carta, Center for Bioprocess Development, Department of Chemical Engineering, University of Virginia, Charlottesville, VA 22903-2442, USA.

Gradient elution chromatography has been studied theoretically by many authors with the assumption of linear adsorption equilibrium [3–12]. These analyses are restricted to solutions that are sufficiently dilute that adsorption is governed by Henry's law, or when a high initial solvent strength is used to maximize resolution [13]. Non-linear adsorption, on the other hand, must be considered for concentration overloading conditions, but this generally requires numerical simulation methods, such as Craig simulations [14,15], or orthogonal collocation [1,2, 16]. However, in gradient elution chromatography, the equilibrium distribution coefficient of each solute decreases rapidly as the solvent strength is increased. As a consequence, in many cases non-linear adsorption affects only the initial feed loading step and the initial phase of gradient elution. The linear approximation can then still provide an adequate representation of non-equilibrium spreading effects, if the equilibrium remains linear for most of the separation time [12,13].

The most comprehensive treatment of gradient elution chromatography appears to be the linear

0021-9673/92/$05.00

solvent strength (LSS) theory of Snyder and coworkers (see refs. 3 and 7). The theory is developed for infinitesimal feed pulses with a linear gradient of the modifier concentration, φ

$$\varphi = \varphi^0 + \beta t \tag{1}$$

and for solutes for which the dependence of the linear adsorption coefficient K on φ has the form

$$\ln K = \ln \kappa - S\varphi \tag{2}$$

Here κ and S are characteristic constants for each solute. Assuming that the modifier propagates through the bed as an ideal, undistorted wave, the retention time of a component is given by

$$t_R = \frac{\varepsilon z}{u} + \frac{1}{S\beta} \ln \left[1 + \frac{S\beta z}{u} K_0(1 - \varepsilon) \right] \tag{3}$$

K_0 is the distribution coefficient for the component at the start of the gradient, when $\varphi = \varphi^0$. The standard deviation of the component peak in time units is

$$\sigma = C \frac{z/u}{\sqrt{N}} \left[\varepsilon + \frac{K_0(1 - \varepsilon)}{K_0(1 - \varepsilon)S\beta z/u + 1} \right] \tag{4}$$

where N is the plate number measured under isocratic conditions for a peak that elutes with retention time t_R and C is a band compression factor given by

$$C = \frac{(1 + p + p^2/3)^{1/2}}{1 + p} \tag{5}$$

with

$$p = \frac{\varepsilon K_0(1 - \varepsilon)S\beta z/u}{\varepsilon + K_0(1 - \varepsilon)} \tag{6}$$

Frey [12] has recently generalized the treatment, providing asymptotic relations for preparative gradient elution chromatography, which converge to the results of the LSS theory for infinitesimally small feed pulses.

The objective of this paper is to provide an analytic solution in the form of explicit expressions, which are valid for both small and large (rectangular) feed pulses and which are applicable to any arbitrary gradient shape and type. The solution is restricted to linear isotherms and neglects the accumulation of solute in the mobile phase in the column. Thus, the solution is applicable only to systems in which the solutes are retained significantly by the stationary phase, but with a linear relationship between the concentration in the stationary phase and that in the mobile phase. However, the solution is general with respect to sample size, to the way in which the modifier concentration is varied, and to the functional relationship between the distribution coefficient and the modifier concentration. Thus, the solution applies to both narrow and wide feed pulses and to different branches of chromatography, such as reversed-phase and ion-exchange, since it can take into account the different characteristic dependencies of the distribution coefficient (or retention factor) on the modifier concentration.

MATHEMATICAL MODEL

We consider a fixed-bed which is supplied with a periodic, square wave feed of rectangular pulses, each of duration t_F, as shown in Fig. 1. For each period of duration t_P, after introduction of the feed slug, the solvent composition is changed in a prescribed way, either continuously or in a stepwise fashion. At the end of the period, the solvent composition is returned to the original value and a new feed slug is introduced. The corresponding variation of K for a solute is sketched in Fig. 1. The gradient ends at time $t_F + t_G$, after which K is held constant at a value K_G.

Neglecting axial dispersion and using a film model to describe mass transfer between the mobile phase

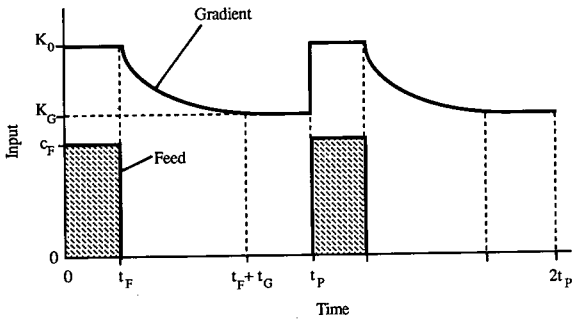

Fig. 1. Input for gradient elution chromatography. The gradient line shows the effect of the modifier concentration on K.

and the stationary phase, the conservation equations for a solute in the bed may be written as

$$\varepsilon \frac{\partial c}{\partial t} + (1 - \varepsilon) \frac{\partial q}{\partial t} + u \frac{\partial c}{\partial z} = 0 \tag{7}$$

$$(1 - \varepsilon) \frac{\partial q}{\partial t} = k_0 a \left(c - \frac{q}{K} \right) \tag{8}$$

with boundary conditions

$$\begin{aligned} c(0,t) &= c_F, \quad (j-1)t_P \leqslant t < (j-1)t_P + t_F \\ c(0,t) &= 0, \quad (j-1)t_P + t_F \leqslant t < jt_P \\ & \qquad j = 1, 2, 3 \ldots \end{aligned} \tag{9}$$

Here we seek only the purely time-periodic solution, which is approached after a sufficiently large number of cycles. In this case, initial conditions are unimportant.

In the remainder of the development we neglect the mobile phase accumulation of solute; *i.e.*, we neglect the first term in eqn. 7. This is permissible when, throughout the gradient run, the retention factor k' satisfies the relationship

$$k' = \frac{K(1 - \varepsilon)}{\varepsilon} > 1 \tag{10}$$

We also assume that the modifier is not retained by the stationary phase. For these conditions, when eqn. 10 is valid, only the temporal variation of K needs to be accounted for. A similar assumption has been made by Gibbs and Lightfoot [10] in their treatment of gradient elution, and yields that everywhere in the bed

$$K = K(\varphi) = K(t) \tag{11}$$

We define the following dimensionless variables

$$X = \frac{K(t)}{K_0} \cdot \frac{c}{c_F} \tag{12}$$

$$Y = \frac{q}{K_0 c_F} \tag{13}$$

$$n = \frac{k_0 a z}{u} \tag{14}$$

$$\frac{d\vartheta}{dt} = \frac{k_0 a}{(1 - \varepsilon)K}, \quad \vartheta = 0 \quad \text{for} \quad t = 0 \tag{15}$$

X and Y are dimensionless mobile and stationary phase concentrations, n is the number of transfer units in the bed, and ϑ a dimensionless time. Since in gradient elution K decreases with time, the dimensionless time ϑ runs slowly at the beginning of the gradient run and faster towards the end. Eqns. 7–9 in dimensionless form are

$$\frac{\partial X}{\partial n} = -X + Y \tag{16}$$

$$\frac{\partial Y}{\partial \vartheta} = X - Y \tag{17}$$

$$\begin{aligned} X(0,\vartheta) &= 1, \quad 2\pi r(j-1) \leqslant \vartheta < 2\pi r(j-1) + \pi r_F \\ X(0,\vartheta) &= 0, \quad 2\pi r(j-1) + \pi r_F \leqslant \vartheta < 2\pi r j \\ & \qquad j = 1, 2, 3 \ldots \end{aligned} \tag{18}$$

The quantities

$$2\pi r = \int_0^{t_P} \frac{k_0 a}{(1 - \varepsilon)K(t)} \, dt \tag{19}$$

$$\pi r_F = \int_0^{t_F} \frac{k_0 a}{(1 - \varepsilon)K(t)} \, dt = \frac{k_0 a t_F}{(1 - \varepsilon)K_0} \tag{20}$$

are the dimensionless durations of the total period and of each feed slug.

A time-periodic solution of eqns. 16–18 with period $2\pi r$ is easily found by applying the residue theorem to the general inversion integral of the Laplace transform solution of these equations [17]. We obtain eqn. 21. The solution consists of a series of terms with a sinusoidal component that determines the location of the peak, and an exponential decay that determines the spreading of the peak caused by mass transfer resistance. The convergence of this series has been discussed [17,18]. Four of five terms may be sufficient when mass transfer resistance is significant, but many more, perhaps 100 or more, if mass transfer is very effective. Note that this equation is totally general with respect to gradient shape and time and applies to both continuous and stepwise gradients. What varies is the definition of the dimensionless time, ϑ, that depends upon the integral of $1/K(t)$ per eqn. 15.

The time-average effluent concentration $\bar{c}$ between two times t_1 and t_2 is of interest in preparative applications to determine the purity of a product cut. This can be found directly from eqn. 21 as eqn. 22. Because of the $1/k^2$ term, this series is much more rapidly convergent than eqn. 21.

$$X = \frac{r_F}{2r} + \frac{2}{\pi}\sum_{k=1}^{\infty}\frac{1}{k}\exp\left(-\frac{k^2 n}{k^2 + r^2}\right)\sin\left(\frac{k\pi r_F}{2r}\right)\cos\left(\frac{k\vartheta}{r} - \frac{k\pi r_F}{2r} - \frac{krn}{k^2 + r^2}\right) \quad (21)$$

$$\bar{c} = \frac{1}{t_2 - t_1}\int_{t_1}^{t_2} c(z,t)\mathrm{d}t = \frac{c_F K_0(1-\varepsilon)}{k_0 a(t_2 - t_1)}\int_{\vartheta_1}^{\vartheta_2} X(n,\vartheta)\mathrm{d}\vartheta = \frac{c_F K_0(1-\varepsilon)}{k_0 a(t_2 - t_1)}\left\{\frac{r_F(\vartheta_2 - \vartheta_1)}{2r} + \right.$$

$$\left. + \frac{4r}{\pi}\sum_{k=1}^{\infty}\frac{1}{k^2}\exp\left(-\frac{k^2 n}{k^2 + r^2}\right)\sin\left(\frac{k\pi r_F}{2r}\right)\cdot\sin\left[\frac{k(\vartheta_2 - \vartheta_1)}{2r}\right]\cos\left[\frac{k(\vartheta_2 + \vartheta_1)}{2r} - \frac{k\pi r_F}{2r} - \frac{krn}{k^2 + r^2}\right]\right\} \quad (22)$$

These equations can be generalized to account for axial dispersion, external film mass transfer resistance, and intraparticle pore diffusion, by using the linear driving force approximation [19,20]. In this case eqns. 21 and 22 can be used as a good approximation if the mass transfer parameter $k_0 a$ is calculated from

$$\frac{1}{k_0 a} = \frac{\varepsilon D_L}{u^2} + \frac{1}{1-\varepsilon}\left(\frac{d_p}{6k_f} + \frac{d_p^2}{60\varepsilon_p D_p}\right) \quad (23)$$

where D_L is the axial dispersion coefficient, d_p the particle diameter, k_f the external film mass transfer coefficient, and D_p the pore diffusivity of the solute. The relationship between the number of transfer units, n, and the plate number, N, or the height equivalent to a theoretical plate, H, is also well known [21,22]

$$N = \frac{z}{H} \approx \frac{n}{2} \quad (24)$$

Thus, $k_0 a$ can be calculated directly from H obtained in isocratic experiments.

Use of eqns. 21 and 22 requires a knowledge of the temporal variation of K in the bed. For linear gradients we have

$$\varphi = \varphi^0 + \beta(t - t_F) \quad \text{for} \quad t_F < t \leqslant t_F + t_G$$
$$\varphi = \varphi^G \quad \text{for} \quad t_F + t_G < t \leqslant t_P \quad (25)$$

We consider here three examples of application of linear gradients: reversed-phase liquid chromatography (RPLC), ion-exchange chromatography (IEC), and stepwise elution (SE). In the first case the relationship between K and φ is given by eqn. 2. In the second case we assume

$$K = A\varphi^{-b} \quad (26)$$

which has been shown to be valid for biopolymers [23] as well as small ions [16]. Finally, for stepwise elution we assume an abrupt change of K from an initial value K_0 to a final value K_G, independent of the particular type of chromatography. The expressions for the transformed time ϑ and the peak profile c corresponding to these three cases are given in Table I. In each case, X is calculated from eqn. 21. Different gradient shapes and other relationships between K and φ can be readily handled via eqn. 15.

Calculation examples and discussion

The parameter values shown in Table II were used for calculations using eqns. 21 and 22, and with the appropriate definitions of ϑ given in Table I. The parameters were chosen arbitrarily to test the theory over a range of conditions. The parameter values, however, are similar to those obtained for an experimental system discussed below, and are representative of typical high-performance liquid chromatographic preparative separations. To insure accuracy, 100 terms were used in the series and a spreadsheet was used to carry out the computations.

Fig. 2 shows calculated peaks for gradient elution RPLC with small feed pulses and different gradient steepness ($\propto 1/t_G$). For these conditions the total period, t_P, chosen is sufficiently long that there is no interference from peaks generated by each injection on the next. The peaks become sharper as the

TABLE I

TRANSFORMED TIME FOR GRADIENT ELUTION

πr_F and πr_G are the values of ϑ at $t = t_F$ and $t = t_F + t_G$, respectively.

Linear gradients: $\varphi = \varphi^0 + \beta t$			Stepwise elution
Time	RPLC	IEC	
$0 < t \leqslant t_F$	$\vartheta = \dfrac{k_0 a}{(1-\varepsilon)K_0} t$	$\vartheta = \dfrac{k_0 a}{(1-\varepsilon)K_0} t$	$\vartheta = \dfrac{k_0 a}{(1-\varepsilon)K_0} t$
	$c = c_F X$	$c = c_F X$	$c = c_F X$
$t_F < t \leqslant t_F + t_G$	$\vartheta = \pi r_F + \dfrac{k_0 a[e^{S\beta(t-t_F)} - 1]}{(1-\varepsilon)K_0 S\beta}$	$\vartheta = \pi r_F + \dfrac{k_0 a\{[\varphi^0 + \beta(t-t_F)]^{b+1} - (\varphi^0)^{b+1}\}}{(1-\varepsilon)(b+1)A\beta}$	$\vartheta = \dfrac{k_0 a}{(1-\varepsilon)K_0} t$
	$c = c_F X e^{S\beta(t-t_F)}$	$c = c_F X K_0[\varphi^0 + \beta(t-t_F)]^b / A$	$c = c_F X$
$t_F + t_G < t \leqslant t_P$	$\vartheta = \pi r_G + \dfrac{k_0 a(t - t_G - t_F)}{(1-\varepsilon)K_G}$	$\vartheta = \pi r_G + \dfrac{k_0 a(t - t_G - t_F)}{(1-\varepsilon)K_G}$	$\vartheta = \pi r_G + \dfrac{k_0 a(t - t_G - t_F)}{(1-\varepsilon)K_G}$
	$c = c_F X K_0 / K_G$	$c = c_F X K_0 / K_G$	$c = c_F X K_0 / K_G$

TABLE II

SIMULATED OPERATING CONDITIONS

Parameter	Value	Units
z	10	cm
u	0.1	cm s^{-1}
$k_0 a$	5	s^{-1}
K_0	10	–
K_G	2	–
ε	0.33	–
t_P	2000	s

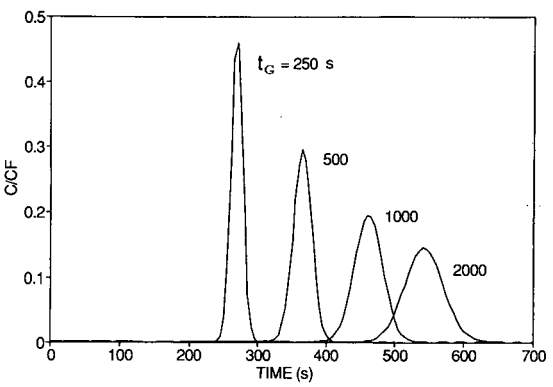

Fig. 2. Gradient elution chromatography peaks for RPLC obtained with eqn. 21 for different values of the gradient time t_G. Parameter values from Table II with t_F = 10 s. CF = feed concentration.

gradient steepness is increased. Note that for t_G = 250 s, a significant portion of the peak exists from the bed after K has reached its final constant value K_G. The first moment and the standard deviation of the computed peaks are given in Fig. 3, in comparison with the results of the LSS theory, eqns. 3 ($\mu \approx t_R$) and 4. The dotted lines show the results of the LSS theory if the same approximation that the mobile phase accumulation is negligible is made in eqns. 3 and 4; *i.e.*, taking $\varepsilon z/u \approx 0$. The error resulting from this approximation is small for the conditions simulated, and it would be much less for

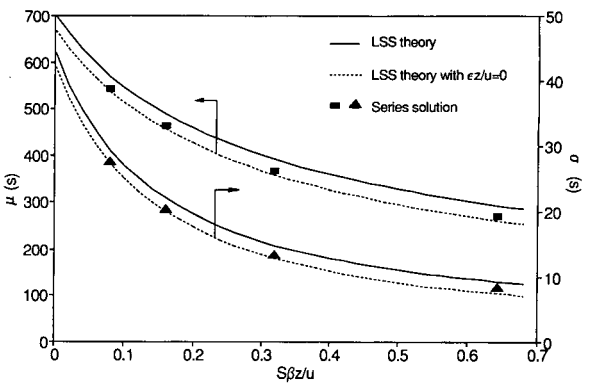

Fig. 3. Comparison of first moment and standard deviation for peaks in Fig. 2 with results of LSS theory.

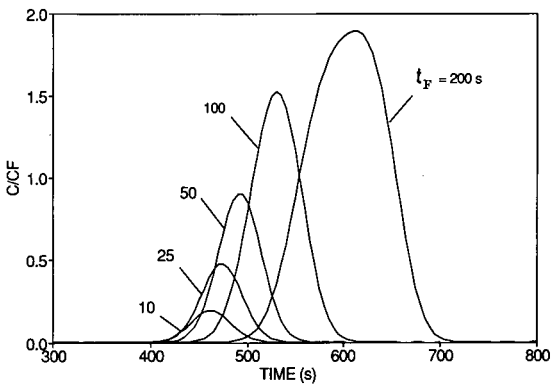

Fig. 4. Effect of feed slug size on gradient elution peaks for RPLC calculated from eqn. 21. Parameter values from Table II with t_G = 1000 s. CF = feed concentration.

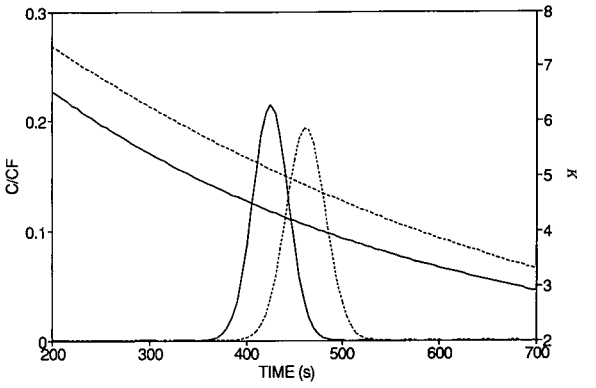

Fig. 5. Gradient shape and chromatographic peaks calculated from eqn. 21 for RPLC (– – –) and IEC (———). Parameter values from Table II with t_F = 10 s, t_G = 1000 s, and A = 10, b = 2, φ^0 = 1 for IEC. CF = feed concentration.

cases where K remains higher during the gradient run. The absolute deviation of the predicted peak position is equal to the quantity $\varepsilon z/u$ and can be easily estimated. The agreement between the series solution and the LSS theory is excellent for these small feed pulses.

The effects of volume overloading are shown in Fig. 4 which gives the calculated peaks obtained by varying the feed injection time t_F. The peaks are Gaussian for small t_F values, but they become increasingly asymmetrical as the loading is increased, reaching concentrations above the feed concentration. This occurs when solute accumulated in the stationary phase is desorbed as a result of the change in K induced by the gradient. Then, if the number of plates is sufficiently large, the component is concentrated into a band which may be narrower than the feed slug. It should be noted that the retention time of the peak also increases with volume loading, as a result of the delay in the gradient introduced by the finite size of the feed slug. The time-average effluent concentration between any two times t_1 and t_2 may be calculated directly from eqn. 22 for any of these peaks. Thus, the concentration and product recovery in any chosen fraction is easily obtained from the theoretical treatment. For example, with reference to the peak obtained with a feed injection time of 200 s (Fig. 4), eqn. 22 yields directly an average concentration $\bar{c}/c_F$ = 1.61 for a fraction between 550 and 650 s, corresponding to a recovery of 80.5% of the injected feed. This may be compared with an average concentration $\bar{c}/c_F$ = 0.741 obtained from eqn. 22 for a fraction between 450 and 720 s, corresponding to essentially 100% recovery.

Fig. 5 shows calculated peaks for gradient elution IEC for a narrow feed pulse with the operating conditions of Table II. Thus, the initial and final K values are the same as in the previous calculations for RPLC. The variation of K with time is, however, different. For these calculations we have chosen A = 10, b = 2 and ϑ^0 = 1, in consistent units. As shown in Fig. 5, for these parameter values, the effect of ϑ on K is more dramatic for IEC than for RPLC. Thus, the IEC peak is eluted faster and is sharper than the RPLC peak. Considerations on peak asymmetry and height similar to those made for RPLC can of course also be made for IEC, and are entirely predicted by the analytic solution.

Calculated peaks for stepwise gradient elution with the conditions of Table II are shown in Fig. 6, for small feed pulses. In the isocratic case, the peak is symmetrical and broad, since elution takes place with the initially large K value. For t_G = 625 s, however, we see that a portion of the peak elutes for isocratic conditions as the initial K value. When the step change in K occurs, the portion of the peak still within the column is sharpened and exits the bed as a narrow, more concentrated band. The abrupt transition in Fig. 6 is the result of having neglected the mobile phase accumulation term in eqn. 7. A smoother transition would, of course, be observed in practice. When t_G is reduced to values lower than

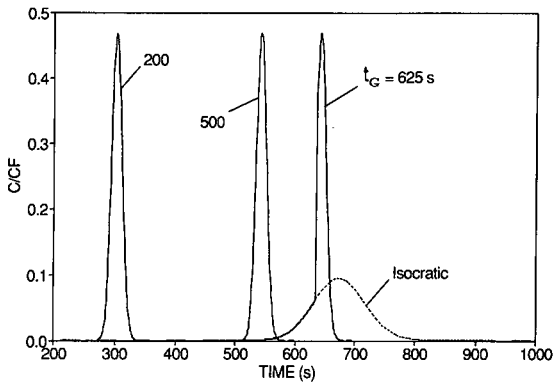

Fig. 6. Peaks calculated from eqn. 21 for stepwise elution chromatography. Parameters from Table II with t_F = 10 s. CF = feed concentration.

500 s, the solute band is well within the bed when the step change occurs. Since K is initially large, the solute band makes little headway through the bed, before the step change. As a result the peak shape and spreading is nearly independent of t_G.

EXPERIMENTAL

Equipment and materials

A Waters (Milford, MA, USA) liquid chromatograph with a Rheodyne Model 7010 injection valve was used. The injection valve was fitted with different loops with volumes of 0.02, 0.8, 2.2 and 4.1 cm^3, which were constructed of 0.039 in. I.D. stainless-steel tubing. The equipment dwell volume and gradient linearity were determined from blank methanol–water gradient runs, using 1% acetone in the methanol as a tracer. Measurements with flow-rates of 1–2.5 cm^3/min gave a value of the dwell volume of 2.1 $\pm$ 0.1 cm^3. Gradients with a maximum deviation from linearity of less than 2% were obtained with and without the column. The column packing was a bonded-phase octadecyl silica 55–105 μm irregular particles (Megabond; Waters), packed in a 25 $\times$ 0.46 cm I.D. stainless-steel column obtained from Biotage. This material is often used in large-scale preparative high-performance liquid chromatography equipment [24]. The void fraction of the packed column was estimated to be ε = 0.33 $\pm$ 0.06 from pressure drop measurements. The experiments were carried out at room temperature (23 $\pm$ 2°C) with UV detection at 254 nm.

Ethyl paraben (Sigma) was used as a test compound. Samples of ethyl paraben containing 0.008 g/l were prepared with various methanol–water mixtures to match the composition of the initial eluent used in gradient elution experiments. The linear adsorption coefficient of ethyl paraben, K, and H were determined from experimental peaks obtained isocratically for various eluent compositions, using the 0.02-cm^3 loop. K and H were calculated numerically from the first and second moments of the digitized experimental peaks. The results are shown in Fig. 7. The linear adsorption coefficient depends on the methanol volume fraction, φ, in the manner predicted by eqn. 2, with only a minor deviation at the highest φ value. The values of ln κ and S obtained from a regression of the data are 5.87 and 8.61, respectively. The linearity of the equilibrium was checked over the range of φ values from 0.3 to 0.7, by varying the amount of ethyl paraben injected with the various sample loops.

H was also found to vary with the methanol volume fraction in the eluent. This can be attributed to changes in viscosity and solute diffusivity that occur when the solvent composition is changed. The variation was, however, very small and limited to about $\pm$ 7% of a mean value of 0.145 cm in the range of φ from 0.3 to 0.6. The corresponding value of the mass transfer parameter k_0a is obtained from eqns. 14 and 24, yielding a value of k_0a = 3.5 s^{-1}.

RESULTS AND COMPARISON WITH THEORY

Gradient elution experiments were carried out with the larger sample loops, in order to test the

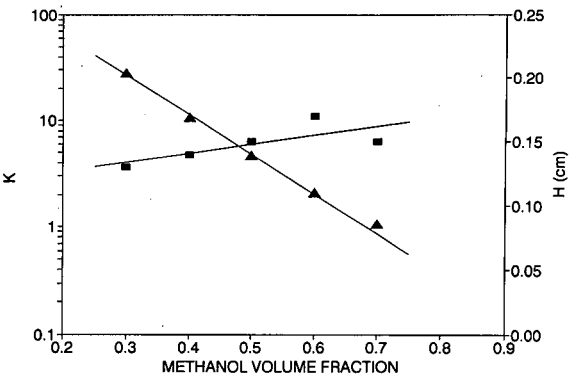

Fig. 7. Linear adsorption coefficient, K (▲) and H (■) for ethyl paraben obtained from isocratic elution experiments at 2.5 cm^3/min with different eluent compositions. K = exp (5.87 – 8.61 φ).

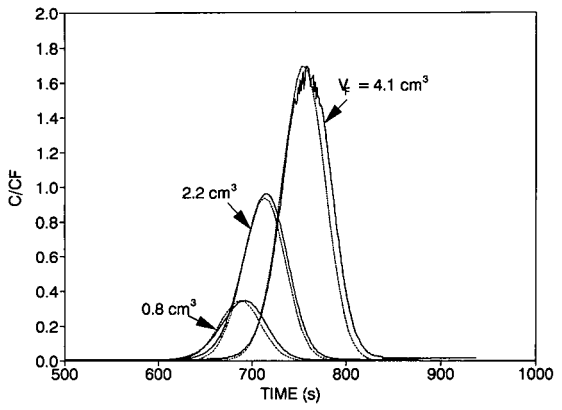

Fig. 8. Comparison of experimental (———) and predicted (· · · ·) gradient elution profiles for ethyl paraben. Gradient from 30 to 60% (v/v) methanol in water, in 15 min at 2.5 cm^3/min. V_F is the volume of the injected sample and CF the feed sample concentration (= 0.008 g/l).

ability of the theory to simulate gradient elution behavior from isocratic elution data, and to correctly predict volume overloading effects. A gradient of 30 to 60% methanol in 15 min was used at a flow-rate of 2.5 cm^3/min. After the start of the gradient, injection of the samples was delayed by an amount of time equal to the equipment dwell time, so that, the gradient started immediately after introduction of the feed slug. The results are shown in Fig. 8 in comparison with the peaks predicted by the theory. Since the fluid phase accumulation term has been neglected in the model, the theory would underestimate the elution time of the peak (see Fig. 3). Thus, in order to provide a clearer comparison of predicted and experimental peak shapes, the calculated peaks were shifted to the right by the quantity $\varepsilon z/u$ = 32.9 s. This correction is less then 5% of the mean retention time. Aside from this correction, the theory requires no adjustable parameter; *i.e.*, the values of K and H obtained from isocratic experiments are used to predict the gradient elution behavior. The volume overloading effects are well predicted by the theory. As the volume injected is increased, the peak becomes increasingly asymmetrical and reaches maximum concentrations that exceed the feed value. Only a small discrepancy between experimental and predicted peaks is observed. This may be due to the inability of the theory to provide an exact description of dispersion in gradient elution with the single lumped mass transfer parameter k_0a.

CONCLUSIONS

The analytic solution presented here is totally general with respect to gradient shape and type; *i.e.*, it applies to linear and non-linear gradients, to multiple step gradients, and to different relationships between K and the modifier concentration. The equations are limited to linear isotherms and to gradient conditions in which the linear adsorption coefficient remains large during the gradient run. The solution is explicit and allows a direct calculation of the effluent concentrations. The first moment and standard deviation of calculated peaks converge to the predictions of the LSS theory in the limit of small feed pulses and Gaussian peaks. Yet, the solution presented here is uniformly valid for small pulses and large, rectangular feed slugs. The series solution is also easy to use, although a programmable calculator or a personal computer may be needed to compute a sufficiently large number of terms to insure adequate precision. A significant advantage is that the solution can be formally integrated, so that the average concentration of any chosen product cut, may be calculated directly. This is convenient to select the product cuts that will provide a desired purity in preparative applications.

The theory was found to be able to correctly predict volume overload effects in gradient elution which were observed experimentally for a model system. The prediction was based solely on data obtained isocratically for k' and H. The close agreement between the theory and the experimental results would indicate that a single mass transfer parameter may be used to represent dispersion in gradient elution with reasonable accuracy.

Finally, it should be noted that the solution provides the time-periodic response obtained with periodic feed pulses. On the other hand, if the response to a single isolated pulse is desired, this is easily accomplished by selecting a sufficiently large total period to avoid interference from repeated injections, as we have done with the sample calculations reported here.

ACKNOWLEDGEMENTS

This research was supported by Biotage, Inc. and the Virginia Center for Innovative Technology.

SYMBOLS

A parameter in IEC, eqn. 26
b parameter in IEC, eqn. 26
c mobile phase concentration
$\bar{c}$ average value of c in a product cut
c_F feed concentration
C peak compression factor in LSS theory, eqn. 5
d_p particle diameter
D_L axial dispersion coefficient
D_p pore diffusivity
H height equivalent to a theoretical plate
k term number in series solution
k' retention factor
k_0a film mass transfer parameter
k_f external film mass transfer coefficient
K linear adsorption coefficient
K_0 initial value of K
K_G final value of K
n number of transfer units, eqn. 14
N plate number
p parameter defined by eqn. 6
q stationary phase concentration
r dimensionless period, eqn. 19
r_F dimensionless duration of feed injection, eqn. 20
r_G dimensionless gradient duration
S constant in eqn. 2
t time
t_F duration of feed injection
t_G duration of gradient
t_R retention time
t_P total period
u mobile phase superficial velocity
V_F feed volume
X dimensionless mobile phase concentration, eqn. 12
Y dimensionless stationary phase concentration, eqn. 13
z column length

Greek symbols

β gradient slope
ε bed void fraction
ε_p particle porosity
ϑ dimensionless time, eqn. 15
κ constant in eqn. 2
μ first moment of peak
σ standard deviation of peak
φ modifier concentration or volume fraction
φ^0 value of φ at the start of gradient run
φ^G value of φ at the end of the gradient run

REFERENCES

1 F. D. Antia and Cs. Horváth, *J. Chromatogr.*, 484 (1989) 65.
2 F. D. Antia and Cs. Horváth, in C. A. Costa and J. S. Cabral (Editors), *Chromatographic and Membrane Processes in Biotechnology*, Kluwer, Dordrecht, 1991, pp. 115–136.
3 L. R. Snyder and M. A. Stadalius, in Cs. Horváth (Editor), *High-Performance Liquid Chromatography —Advances and Perspectives*, Vol. 1, Academic Press, New York, 1986, pp. 195–235.
4 B. Drake, *Arkiv. Kemi.*, 8 (1955) 1.
5 E. C. Freiling, *J. Am. Chem. Soc.*, 77 (1955) 2067.
6 P. J. Schoenmakers, H. A. H. Billiet, R. Tijssen and L. de Galan, *J. Chromatogr.*, 149 (1978) 519.
7 L. R. Snyder, in Cs. Horváth (Editor), *High-Performance Liquid Chromatography —Advances and Perspectives*, Vol. 1, Academic Press, New York, 1980, pp. 208–316.
8 S. Yamamoto, K. Nakanishi, R. Matsuno and T. Kamikubo, *Biotechnol. Bioeng.*, 25 (1983) 1465.
9 P. Jandera and J. Churáček, *Gradient Elution in Column Liquid Chromatography —Theory and Practice*, Elsevier, Amsterdam, New York, 1985.
10 S. J. Gibbs and E. N. Lightfoot, *Ind. Eng. Chem. Fundam.*, 25 (1986) 490.
11 K. Kang and B. J. McCoy, *Biotechnol. Bioeng.*, 33 (1989) 786.
12 D. D. Frey, *Biotechnol. Bioeng.*, 35 (1990) 1055.
13 S. Yamamoto, K. Nakanishi and R. Matsuno, *Ion Exchange Chromatography of Proteins*, Marcel Dekker, New York, 1988.
14 J. E. Eble, R. L. Grob, P. E. Antle and L. R. Snyder, *J. Chromatogr.*, 405 (1987) 51.
15 L. R. Snyder, G. B. Cox and P. E. Antle, *J. Chromatogr.*, 444 (1988) 303.
16 G. Carta, J. P. DeCarli, II, C. H. Byers and W. G. Sisson, *Chem. Eng. Commun.*, 79 (1989) 207.
17 G. Carta and R. L. Pigford, *Chem. Eng. Sci.*, 41 (1986) 511.
18 G. Carta, *Chem. Eng. Sci.*, 43 (1988) 2877.
19 E. Glueckauf, *Trans. Faraday Soc.*, 51 (1955) 1540.
20 D. M. Ruthven, *Principles of Adsorption and Adsorption Processes*, Wiley, New York, 1984, pp. 242–244.
21 P. Schneider and J. M. Smith, *AIChE J.*, 14 (1968) 762.
22 T. K. Sherwood, R. L. Pigford and C. R. Wilke, *Mass Transfer*, McGraw-Hill, New York, 1975, pp. 561–578.
23 A. Valeyudhan and Cs. Horváth, *J. Chromatogr.*, 367 (1986) 160.
24 *Technical Bulletin*, Biotage, Inc., Charlottesville, VA, 1991.

Journal of Chromatography, 605 (1992) 161–166
Elsevier Science Publishers B.V., Amsterdam

CHROM. 24 240

Computer simulation of three scenarios for the separation of non-racemic mixtures by chromatography on achiral stationary phases

M. Jung and V. Schurig

Institut für Organische Chemie, Universität Tübingen, Auf der Morgenstelle 18, D-7400 Tübingen (Germany)

(First received December 30th, 1991; revised manuscript received April 1st, 1992)

ABSTRACT

With the aid of a general chromatography simulation program based on the theoretical plate model, three scenarios rationalizing the phenomenon of the separation of non-racemic mixtures into racemate and excess enantiomers by chromatography on achiral stationary phases were simulated. The separation, repeatedly observed in high-performance liquid chromatography and gas chromatography, can be explained by the formation of homo- and heterochiral self-associates (*i.e.* RR, SS and RS). The kinetic calculations were performed using a Runge–Kutta routine. This program offers for the first time a general means of simulating dynamic chromatographic elution profiles involving any type of reaction occurring during chromatographic separation. Thus computer simulation of experimental elution profiles is no longer limited to first-order reactions such as enantiomerizations or isomerizations.

INTRODUCTION

The chromatographic separation of non-racemic mixtures into racemate and excess enantiomers by high-performance liquid chromatography (HPLC) and gas chromatography has been reported by several workers [1–3]. Systematic studies for additional classes of compounds were performed and fractions of high optical purity were isolated [4]. This non-trivial phenomenon, which has gained much interest in the realm of non-linear effects [5] (the EE effect [3]) is caused by diastereomeric interactions between the enantiomers R and S in enriched mixtures, *e.g.* self-association to dimers RR, SS and RS (the latter being identical with SR). Indeed, the chromatographic separation of the racemic mixture from the enantiomer in excess was found to be concentration-dependent and to require stationary or mobile phases, or both, that favour the formation of dimers [4].

Three models have been described as a theoretical basis for the simulation of dynamic chromatographic processes: (i) the discontinuous plate (Craig) model [6–9]; (ii) the stochastic model, assuming a Gauss function for the elution at the end of the column [10,11]; and (iii) the continuous flow model [7,12–14]. There are several reports on the simulation of chromatograms, using models i [15,16], ii [17–19] and iii [12–14]. We have chosen the discontinuous theoretical plate model [15] for the development of an improved, general simulation program* of elution profiles (considering dynamic effects

Correspondence to: Professor. V. Schurig, Institut für Organische Chemie, Universität Tübingen, Auf der Morgenstelle 18, D(W)-7400 Tübingen, Germany.

* The program (and the variation described here) on the basis of the theoretical plate model, written in FORTRAN 77 and usable on any large computer, is available from the authors on request as a source code and has been accepted by the Quantum Chemistry Program Exchange (QCPE) [24]. It can be adapted to various problems in dynamic chromatography. An unlimited number of solutes may be injected in variable amounts, and a special procedure allows different plate numbers within one chromatographic run.

0021-9673/92/$05.00

during chromatography) because of its mathematical simplicity and the possibility of application to systems with more complicated, higher-order kinetics. The program has been presented and used elsewhere for the determination of rate constants of enantiomerization by computer simulation of experimental elution profiles [16].

Using a variation of this program, three scenarios suitable for the rationalization of the phenomenon of the separation of non-racemic mixtures into racemate and excess enantiomers by chromatography on an achiral stationary phase were simulated. In principle, all combinations of these scenarios are also suitable for the explanation of the phenomenon. It should be noted that these studies are strictly theoretical in character. Rather than simulating experimental chromatograms, the aim of this study was to rationalize non-linear effects between enantiomers in achiral chromatography by a general theoretical approach, often resorting to different or more extreme conditions than those so far observed in practice. For the chromatograms observed experimentally, even different mechanisms might in principle apply [20].

EXPERIMENTAL

Initially it is necessary to assume values for the capacity factors k' of all five species (R, S, RR, SS and RS), the injected amounts of R and S, the theoretical plate number n, the total volumes of mobile and stationary phase, the dead time t_M and the forward and backward rate constants for all equilibria of dimerization occurring. It has to be recalled that a second-order reaction such as this dimerization is concentration-dependent, which means that the injected amounts of R and S and the total volumes of the phases have an influence on the chromatograms, not only their ratios. The capacity factors and rate constants have to be carefully chosen in agreement with the principles described under Theoretical.

It has to be emphasized that the capacity factors k' of the five species are not directly related to the retention times observed in the chromatogram. They only refer to the phase distribution equilibria, the respective phase distribution coefficients K being given by

$$K = \beta k' \quad (1)$$

where β is the phase ratio. If, in addition, reactions occur between the five species during chromatographic separation, the retention times t_R according to the usual relationship

$$k' = (t_R/t_M) - 1 \quad (2)$$

will not be observed in the resulting chromatogram. For example, if monomer R is injected and dimerization takes place in the stationary phase, but not in the mobile phase, and if the dead time t_M is 1 min and the capacity factor k' for R is 0.001 (implying that R is present only in the mobile phase and not in the stationary phase), then the peak in the chromatogram may be found at a retention time much longer than the expected 1.001 min due to dimerization in the stationary phase.

The chromatographic separation is treated as a discontinuous process by assuming that all processes proceed repeatedly in separate uniform sections of the multicompartmentalized column containing n theoretical plates considered as chemical reactors. The processes taking place in the chromatographic column are separated into three steps: (i) establishment of the distribution (partitioning) equilibrium of all species between the mobile and stationary phases; (ii) reactions between the species during a time period Δt (here the reversible dimerization of the enantiomers R and S in both phases with the respective rate constants); and (iii) transportation (shifting) of the mobile phase to the adjacent section of the column while the stationary phase is retained. The species are initially "injected" into the mobile phase of the first plate (initial amounts in mol), and the content of the mobile phase of the last section (theoretical plate) is recorded in a digital form after every mobile phase shift (in units of mol/min).

In addition to the usual procedure, scenarios 2 and 3 described in the following (involving a permanent interconversion of species with significantly different retentions) were simulated by a slightly modified program. In this instance (to better approach the total equilibrium of all five species in both phases of a theoretical plate) the usual procedure for every plate (step 1, distribution; step 2, association and dissociation, separately for every phase during a time interval Δt; step 3, transportation of the mobile phase) was improved as follows: step 1 and step 2 were performed alternately ten times with only $\Delta t/10$ for step 2, only then does step 3 take place. This procedure is certainly more realistic,

but for the investigated examples it yielded almost identical results.

The kinetic calculations were performed by a fourth-order Runge–Kutta routine [21] with variable step sizes. If too extreme values are chosen for the plate number or the rate constants, the computer may need an excessively long time to perform the calculations. A CONVEX C 220 computer was used. The digitalized chromatograms were transferred to a personal computer for plotting with standard graphics software. The curves shown refer to monomers, *i.e.* a dimer, say RR, that is eluted at the column end is treated like two molecules of R in the detector. Thus the total elution curve is defined as [total] = 2([RS]+[RR]+[SS]) + [R]+[S]. The curve for the racemate is [rac]. (Note that one molecule S together with one molecule R yields two molecules of racemate). The curve of the excess enantiomer is [enant] = [total] − [rac]. For example, let ten molecules RR, five molecules SS, two molecules RS, two molecules R and one molecule S be eluted. This yields a total of $2 \cdot (10 + 5 + 2) + 2 + 1 = 37$ monomer molecules, consisting of 24 molecules R and thirteen molecules S, *i.e.* 26 molecules of racemate and $37 - 26 = 11$ molecules of excess enantiomer R.

THEORETICAL

The simulation is based on the following conditions. All dimerization equilibria are fast and reversible. For the enantiomers R and S and for RR and SS the same rate and equilibrium constants and distribution coefficients are always valid. The kinetics of dimerization (association) is second order and that of dissociation is first order. Thus the following equilibria occur:

mobile phase (m):	stationary phase (s):
$R_{(m)} + S_{(m)} \underset{k^m_{-1}}{\overset{k^m_1}{\rightleftharpoons}} RS_{(m)}$	$R_{(s)} + S_{(s)} \underset{k^s_{-1}}{\overset{k^s_1}{\rightleftharpoons}} RS_{(s)}$
$2R_{(m)} \underset{k^m_{-2}}{\overset{k^m_2}{\rightleftharpoons}} RR_{(m)}$	$2R_{(s)} \underset{k^s_{-2}}{\overset{k^s_2}{\rightleftharpoons}} RR_{(s)}$
$2S_{(m)} \underset{k^m_{-2}}{\overset{k^m_2}{\rightleftharpoons}} SS_{(m)}$	$2S_{(s)} \underset{k^s_{-2}}{\overset{k^s_2}{\rightleftharpoons}} SS_{(s)}$

In addition, the distribution equilibria for all five species occur, so that the system consists of a total of eleven equilibria. The distribution coefficients $K_R = K_S$, $K_{RR} = K_{SS}$ and K_{RS} are determined by the respective capacity factors used as a basis for the simulation (see under Experimental). The rates of dissociation k^m_{-1} and k^m_{-2} are assumed to be equal, as are k^s_{-1} and k^s_{-2}. If RS, RR and SS are assumed to have the same thermodynamic stability in the mobile phase (see under Results and discussion), then it is necessary for statistical reasons[a] that $k^m_1 = 2k^m_2$.

If all the rate constants and thereby all the equilibrium constants for the mobile phase as well as all the distribution coefficients are given, then the equilibrium constants for the stationary phase K^s_1 and K^s_2 can no longer be freely chosen, but are determined by the following expressions according to the principle of microscopic reversibility [15,16]:

$$K^s_1 = K^m_1 \cdot K_{RS}/(K_R K_S) \quad (3)$$

and

$$K^s_2 = K^m_2 \cdot K_{RR}/K^2_R = K^m_2 \cdot K_{SS}/K^2_S \quad (4)$$

This means that the thermodynamic stability of the dimers (K^m_1, K^m_2, K^s_1, K^s_2) is directly connected with the retention behaviour of the species, *i.e.* the distribution coefficients.

RESULTS AND DISCUSSION

If the dimers have significantly longer retention times than the monomers, dimerization takes place mainly in the stationary phase and a peak heading will be observed (see scenario 3 later). In the opposite instance a peak tailing will arise.

In scenario 1 a practically complete dimerization of the enantiomers R and S in both the mobile and stationary phases is assumed. The assumption of significantly different retention times of the heterochiral (RS) and homochiral (RR, SS) species renders a baseline separation (theoretically) feasible if dimer formation and dissociation are sufficiently fast (Fig. 2). Scenario 2 is based on a partial dimerization

[a] This is verified by an experiment: if pairs of two beads are randomly taken out of a container with 100 red and 100 white beads, then on average 50 times the combination red–white and only 25 times each of the combinations white–white and red–red will be obtained.

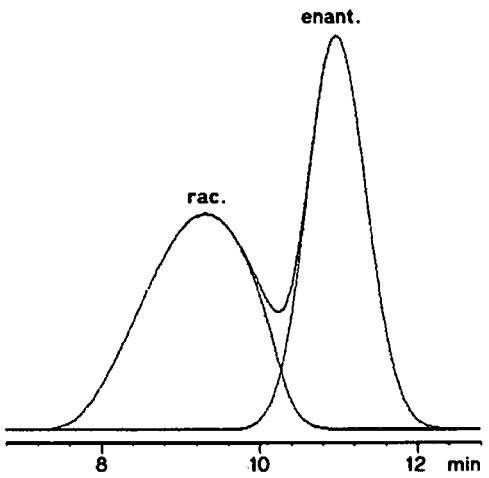

Fig. 1. Simulated chromatogram for scenario 1 (almost complete dimerization in both phases) with higher retention for RR and SS compared with RS. The total elution curve and the curves for the racemate and the excess enantiomer R are shown. The simulation is based on the following data: total volume of the mobile phase, 5 ml; total volume of the stationary phase, 5 ml; injected amounts, $3 \cdot 10^{-9}$ mol R, $1 \cdot 10^{-9}$ mol S, dead time t_M, 1 min; plate number n, 800; capacity factors k' of RS, RR, SS, R and S, 8, 11, 11, 4 and 4; rate constants of dimerization, k_1^m, k_2^m, k_1^s and k_2^s(in 10^{15} l mol^{-1} min^{-1}), 1.0, 2.0, 1.0 and 1.4; rate constants of dissociation of the dimers k_1^m, k_2^m, k_1^s and k_2^s (in min^{-1}), 1, 1, 0.9 and 0.9. At the column end almost exclusively dimers are eluted.

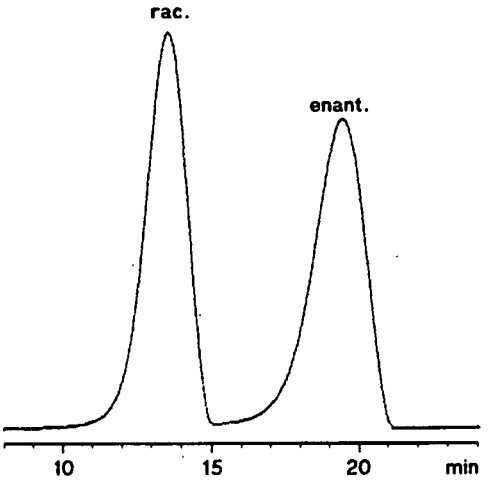

Fig. 2. Simulated chromatogram for scenario 1 (almost complete dimerization in both phases) with higher retention for RR and SS compared with RS. Only the total elution curve is shown. The assumption of significantly different retention times of the heterochiral (RS) and homochiral (RR, SS) species renders a baseline separation (theoretically) feasible if dimer formation and dissociation are sufficiently fast. The simulation is based on the following data: total volume of the mobile phase, 5 ml; total volume of the stationary phase 5 ml; injected amounts, $3 \cdot 10^{-9}$ mol R, $1 \cdot 10^{-9}$ mol S; dead time t_M, 1 min; plate number n, 500; capacity factors k' of RS, RR, SS, R and S, 8, 20, 20, 4 and 4; rate constants of dimerization k_1^m, k_2^m, k_1^s and k_2^s (in 10^{14} l mol^{-1} min^{-1}), 1.0, 2.0, 1.0 and 0.737; rate constants of dissociation of the dimers k_1^m, k_2^m, k_1^s and k_2^s (in min^{-1}), 100, 100, 47.4 and 47.4. At the column end almost exclusively dimers are eluted.

which takes place to a larger extent in the stationary phase than in the mobile phase. In contrast to this, scenario 3 is based on a partial dimerization in the stationry phase only, whereas in the mobile phase practically no dimers are allowed to occur[a].

The simulated separations are shown in Figs. 1–4. The separations are due to the different retention behaviour of the homochiral (RR and SS) and the heterochiral (RS) species. This results in different thermodynamic stabilities within at least one phase; in this treatment, the stationary phase. It is then, however, not necessary that the thermodynamic stabilities of the dimers are also different within the mobile phase.

A scenario 4 with partial dimerization to be assumed only in the mobile phase proved to be not suitable under the condition of equal thermodynamic stabilities of RS, RR and SS in the mobile phase (see earlier), as arithmetic examples of the kinetics of dimerization of a mixture of 75% R and 25% S showed that indeed R mainly forms RR and S mainly forms RS, but the degree of dimerization was always exactly equal for R and S. With this, together with an absence of dimerization in the stationary phase, no separation is feasible. A separation which is based on the different thermodynamic stabilities of RS on the one hand and RR and SS on the other hand in the mobile phase is still expected[a].

[a] In scenario 3 the simulation yields strongly asymmetric elution profiles (peak heading). This can be explained as follows: as the dimer formation (second order) is concentration-dependent, the degree of dimerization is larger in the centre of the elution zone than at the periphery. If the dimers have much longer retention times than the monomers, then the centre of the elution zone, which migrates more slowly, is pushed into the rear periphery, whereas the front periphery drifts apart.

[a] In this instance the dimers have almost no retention, and the separation could only be due to one enantiomer spending more of its time in the dimerized form than the other enantiomer; it thus migrates faster. The racemate is eluted *before* the excess enantiomer if the heterodimers RS are more stable. The separation should be largely independent of the choice of the stationary phase [22].

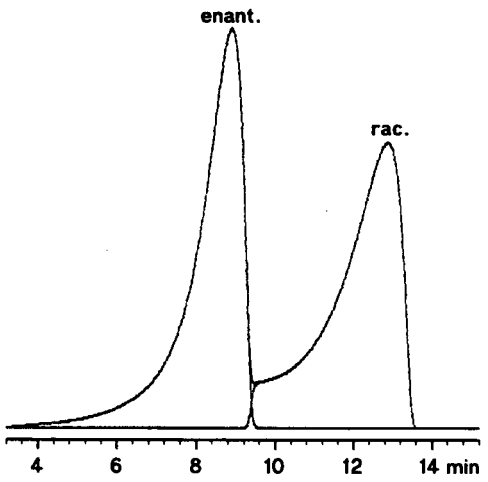

Fig. 3. Simulated chromatogram for scenario 2 (partial dimerization in both phases) with higher retention for RS compared with RR and SS. The total elution curve and the curves for the racemate and the excess enantiomer R are shown. The simulation is based on the following data: total volume of the mobile phase, 5 ml; total volume of the stationary phase, 5 ml; injected amounts, $3 \cdot 10^{-9}$ mol R, $1 \cdot 10^{-9}$ mol S; dead time t_M, 1 min; plate number n, 300; capacity factors k' of RS, SS, R and S, 20, 10, 10, 3 and 3; rate constants of dimerization k_1^m, k_2^m, k_1^s and k_2^s (in 10^{13} l mol^{-1} min^{-1}), 1, 2, 10 and 42.2; rate constants of dissociation of the dimers k_1^m, k_2^m, k_1^s and k_2^s (in min^{-1}), 400, 400, 1778 and 1778. A total of 33% of the monomers R and S injected are eluted in the form of monomers at the column end, the rest in the form of dimers.

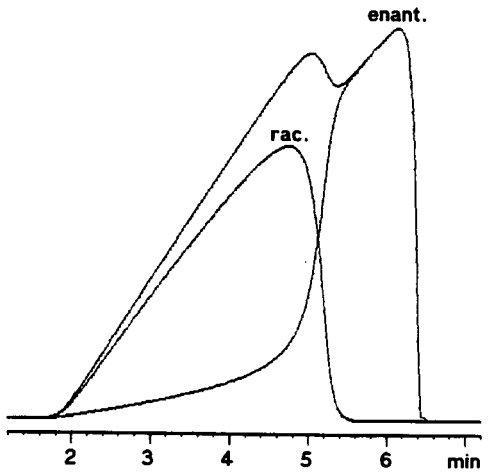

Fig. 4. Simulated chromatogram for scenario 3 (partial dimerization in the stationary phase, negligible dimerization in the mobile phase) with higher retention for RR and SS compared with RS. The total elution curve and the curves for the racemate and the excess enantiomer R are shown. The simulation is based on the following data: total volume of the mobile phase, 5 ml; total volume of the stationary phase, 5 ml; injected amounts, $3 \cdot 10^{-9}$ mol R, $1 \cdot 10^{-9}$ mol S; dead time t_M, 1 min; plate number n, 200; capacity factors k' of RS, RR, SS, R and S, 2 000 000, 4 000 000, 4 000 000, 2 and 2; rate constants of dimerization k_1^m, k_2^m, k_1^s and k_2^s (in l^{-1} min^{-1}), 10^4, $2 \cdot 1^4$, 10^{12}, 10^{12}; rate constants of dissociation of the dimers k_1^m, k_2^m, k_1^s and k_2^s (in min^{-1}); 10 000, 10 000, 25 000 and 25 000. At the column end almost exclusively monomers are eluted. As in this instance no dimers are supposed to exist within the mobile phase, the phase distribution equilibria of the dimer species must be in favour of the stationary phase, *i.e.* the capacity factors of the dimers must be extremely high.

In the simulation of the scenarios 1–3 the elution order, determining whether the racemate or the excess pure enantiomer is eluted first, can freely be chosen in accordance with the retention behaviour of RS, RR and SS. In practice, however, the pure enantiomer is almost exclusively found to elute first [4]. In our theoretical treatment this reflects the fact that the heterochiral dimers RS are more stable than the homochiral dimers RR and SS within the stationary phase. This conclusion is reminescent to the conditions observed in the crystallization of racemic mixtures, where the formation of racemates is favoured whereas that of conglomerates is less often observed [23].

Unfortunately, with so many unknown constants needed for the simulation, the procedure is in this instance not suitable for the simulation of the experimental elution curves or even the determination of kinetic constants (in analogy to the study of enantiomerization during chromatographic separation [16]). However, the program would of course be capable of a correct simulation of the experimental curves if all the constants were known.

CONCLUSIONS

This program successfully simulates elution profiles featuring the separation of non-racemic mixtures into racemate and excess enantiomers by chromatography on achiral stationary phases. The program allows the possibility of studying not only simple interconversions such as enantiomerizations or isomerizations, but also more complicated kinetics by computer simulation of chromatographic elution profiles caused by dynamic reaction chromatography. The program is suitable not only for dimerizations, but can easily be adapted to any kind of chemical transformation.

ACKNOWLEDGEMENTS

This work was supported by the "Deutsche Forschungsgemeinschaft" and the "Fonds der Chemischen Industrie". We thank Professor Dr. E. Gil-Av, Rehovot, Israel, for inspiring and invaluable discussions and Dr. H. Karfunkel, Ciba-Geigy AG, Basle, Switzerland, for very useful advice.

REFERENCES

1 K. C. Kundy and P. A. Crooks, *J. Chromatogr.*, 281 (1983) 17–33.
2 R. Charles and E. Gil-Av, *J. Chromatogr.*, 298 (1984) 516–520.
3 W. L. Tsai, K. Hermann, E. Hug, B. Rhode and A. S. Dreiding, *Helv. Chim. Acta*, 68 (1985) 2238–2243.
4 R. Matusch and C. Coors, *Angew. Chem.*, 101 (1989) 624–626, *Angew. Chem., Int. Ed. Engl.*, 28 (1989) 626–628.
5 R. Noyori and M. Kitamura, *Angew. Chem.*, 103 (1991) 34–55, *Angew. Chem., Int. Ed. Engl.*, 30 (1991) 49–70.
6 L. C. Craig, *J. Biol. Chem.*, 155 (1944) 519.
7 S. H. Langer, J. Y. Yurchak and J. E. Patton, *Ind. Eng. Chem.*, 61 (1969) 11–21.
8 J. Kallen and E. Heilbronner, *Helv. Chim. Acta*, 43 (1960)
9 D. W. Basset and H. W. Habgood, *J. Phys. Chem.*, 64 (1960)
10 H. A. Keller and J. C. Giddings, *J. Chromatogr.*, 3 (1960) 205–220.
11 R. Kramer, *J. Chromatogr.*, 107 (1975) 241–252.
12 W. Melander, H.-J. Lin and C. Horvath, *J. Phys. Chem.*, 88 (1984) 4527–4536.
13 J. Jacobson, W. Melander, G. Vaisnys and C. Horvath, *J. Phys. Chem.*, 88 (1984) 4536–4542.
14 D. E. Henderson and C. Horvath, *J. Chromatogr.*, 368 (1986) 203–213.
15 W. Bürkle, H. Karfunkel and V. Schurig, *J. Chromatogr.*, 288 (1984) 1–14.
16 M. Jung and V. Schurig, *J. Am. Chem. Soc.*, 114 (1992) 529–534.
17 H. Zinner, *Doctoral Thesis*, University of Regensburg, Germany, 1990, Ch. 8.
18 B. Stephan, H. Zinner, F. Kastner and A. Mannschreck, *Chimia*, 44 (1990) 336–338.
19 J. Veciana and M. I. Crespo, *Angew. Chem.*, 103 (1991) 85–88, *Angew. Chem., Int. Ed. Engl.*, 30 (1991) 74–77.
20 E. Gil-Av and V. Schurig, unpublished results.
21 W. H. Press, B. P. Flannery, S. A. Teukolsky and W. T. Vetterling, *Numerical Recipes: The Art of Scientific Computing*, Cambridge University Press, Cambridge, 1986, Ch. 15.
22 E. Gil-Av, personal communication.
23 J. Jacques, A. Collet and S. H. Wilen, *Enantiomers, Racemates and Resolutions*, John Wiley, New York, 1981.
24 M. Jung, Program SIMUL, No. 620, Quantum Chemistry Program Exchange (QCPE), *QCPE Bull.*, 12, No. 3 (1992).

Journal of Chromatography, 605 (1992) 167–174
Elsevier Science Publishers B.V., Amsterdam

CHROM. 24 323

Solute retention in open-tubular liquid chromatography with flowing retentive liquid

K. Šlais, M. Horká and K. Klepárník

Institute of Analytical Chemistry, Czech Academy of Sciences, Veveří 97, CS-611 42 Brno (Czechoslovakia)

(First received February 11th, 1992; revised manuscript received May 5th, 1992)

ABSTRACT

It is suggested that analytes can be separated in the capillary in which the phase adjacent to the internal surface of the capillary is allowed to flow. The analyte retention in such a capillary is described mathematically and verified on the example of the separation of phenols in the reversed-phase system water–cyclohexanol. Using a capillary of 17 μm I.D., the retentions of hydroquinone and phenol relative to the unretained nitrite ion were 1.95 and 4.4, respectively. The term parallel-current open-tubular liquid chromatography is suggested for this type of capillary separation.

INTRODUCTION

Liquid chromatography (LC), similarly to other chromatographic methods, is usually characterizided as a separation method based on the migration of solutes through a system of two phases in contact, a mobile phase and a stationary phase [1–3]. For chromatographic separation, it is essential that the flow along the separation axis is perpendicular to the process of solute enrichment [4,5]. This means that both phases can move relative to the environment, but each with a different speed and, possibly, in different directions. Counter-current chromatography (CCC) [6] and electrokinetic chromatography (EKC) [7] are examples of the chromatographic modes which also fit such a concept.

Liquid–liquid chromatography (LLC) involves partitioning of the solute between the mobile phase and the liquid stationary phase affixed to a solid support [8]. Until now, LLC has not been widely used because of its inconvenience, mainly due to the need for mobile phase presaturation, system thermostating and equilibration and limited use with gradient elution [1–3]. However, the resolving power, wide applicability, predictable solute retention, high column loadability and relative independence of the column selectivity on the nature of the support are advantages in comparison with other modes of LC.

The potential of open-tubular liquid chromatography was theoretically predicted [4,5,9–11] and many practical obstacles (*e.g.*, detection, sampling, pumping) have been overcome. However, the preparation of a capillary of *ca.* 10 μm I.D. with a stable, reasonable content of the stationary phase is still a problem.

Here we propose carrying out the separation in an open capillary, in which the phase adjacent to the internal surface of the capillary (the retentive phase) is allowed to flow. The retention of a solute in such a capillary is described mathematically. The model function and solute retention were verified experimentally using a capillary of 17 μm I.D. and electrochemical detection of phenolic solutes.

Correspondence to: Dr. K. Šlais, Institute of Analytical Chemistry, Czech Academy of Sciences, Veveří 97, CS-611 42 Brno, Czechoslovakia.

0021-9673/92/$05.00

THEORY

Model description

As the retentive phase is allowed to flow, two practical problems must be solved from the point of view of analytical separations. The retentive phase must be continuously renewed at the beginning of the separation capillary to create a retentive layer on the inner wall, and the retentive phase must not be present as a macroscopically heterogeneous component in the liquid entering the detector placed at the end of separation capillary. Owing to the very minute flows and dimensions involved, the phase separation methods used in the past are not acceptable.

Both of the constraints mentioned can be simply met by exploiting the temperature-dependent solubility of the retentive phase in the mobile phase. The experimental set-up of the chromatograph and its function can be described as follows.

The pump delivers a solution of the retentive phase in the mobile phase via a sampling device. The concentration of retentive phase in the mobile phase, s_1, corresponds to saturation at temperature T_1. This saturated, single-phase solution is pumped at temperature T_1. The separation capillary is maintained at a temperature T_2, which is chosen so that the solubility, s_2, of the retentive phase is lower than that at T_1. Hence, at the beginning of the column, the retentive phase separates from the mobile phase. From the practical point of view, it is advantageous to have T_2 higher than T_1. Then, the column is maintained at a temperature elevated relative to the laboratory temperature.

The internal surface of the capillary is modified so that it is wettable by the retentive phase and thus the internal surface of the capillary is covered by the retentive film. The interfacial force between the retentive and mobile phase together with the frictional force due to flow keeps the thickness of the retentive film constant round the internal circumference of the capillary.

When neglecting the volume contractions, the flow of the retentive phase within the capillary, F_r, is given by the product of the flow-rate of the pumped phase, F_p, and the difference between solubilities s_1 and s_2 expressed in volume fractions:

$$F_r = F_p(s_1 - s_2) \tag{1}$$

The flow of the mobile phase within the capillary, F_m, is then

$$F_m = F_p - F_r = F_p(1 + s_2 - s_1) \tag{2}$$

At the end of the capillary column, both the mobile and retentive phases enter the part of the capillary which is maintained at the temperature at which the solubility of the retentive phase is equal to or higher than that at T_1. As a consequence, the retentive phase dissolves completely prior entering the detector.

Calculation of the solute retention

The average velocity of solute i in equilibrium with g moving phases j can be expressed as

$$u_i = \sum_{j=1}^{g} p_{ji} \langle v_j \rangle \tag{3}$$

where $\langle v_j \rangle$ is the average flow velocity of phase j determined by flow-rate F_j of this phase and its cross-section S_j in which it flows under steady-state conditions:

$$\langle v_j \rangle = F_j/S_j \tag{4}$$

and p_{ji} are the probabilities that particle i is found in phase j, defined to be the fraction of particles i in phase j:

$$p_{ji} = n_{ji} / \sum_{j=1}^{g} n_{ji} \tag{5}$$

where n_{ji} is the number of particles i in phase j.

In the case of two phases, the retentive phase r and the mobile phase m, the respective probabilities can be written in terms of distribution constant $K_i = c_{ri}/c_{mi}$, where c_{ri} and c_{mi} are the concentrations of solute i in the retentive and mobile phase, respectively. Then, it holds for the mobile phase

$$p_{mi} = S_m c_{ri}/(S_m c_{mi} + S_r c_{ri}) = S_m/(S_m + S_r K_i) \tag{6}$$

and analogously for the retentive phase

$$p_{ri} = S_r K_i/(S_m + S_r K_i) \tag{7}$$

where S_r is the cross-section of the retentive layer annuli and S_m the cross-section of the mobile phase cylinder.

Now, after the substitution of eqns. 4, 6 and 7 into eqn. 3, the average velocity u_i of solute i in equilibrium with phases r and m is

$$u_i = (F_m + F_r K_i)/(S_m + S_r K_i) \tag{8}$$

In chromatography, it is usual to express the solute retention by the capacity factor, k_i [1–3], which is related both to the solute retention time, t_{ri}, and to the solute distribution constant, K_i. However, k_i is defined for the immobile stationary phase. Therefore, we use here the term reduced retention, k_i^*, which, similarly to k_i, is defined as the ratio of the solute retention time to the dead time, t_0, minus one: $k_i^* = t_{ri}/t_0 - 1$. The relationship between k_i^* and K_i will be shown below.

From the practical point of view, it is useful to define here the dead time as the migration time of a substance which is not absorbed in the retentive phase and migrates through the column dispersed in the mobile phase only, *i.e.*, at the average velocity $\langle v_m \rangle$. Thus, with respect to eqn. 8, k_i^* for the two-phase flow is

$$k_i^* = \frac{\langle v_m \rangle}{u_i} - 1 = \frac{S_r/S_m - F_r/F_m}{1/K_i + F_r/F_m} \quad (9)$$

where the flow-rate ratio, $F_r/F_m = q$, is given from eqns. 1 and 2 as

$$q = F_r/F_m = \frac{s_1 - s_2}{1 - (s_1 - s_2)} \quad (10)$$

The only quantity that is to be found in eqn. 9 is the ratio of cross-sections of both phases, $\phi = S_r/S_m$. The respective volumes of the retentive and mobile phases in the capillary are determined by the difference in the solubilities $s_1 - s_2$ and by the velocity flow profiles of the two phases. In other words, the flow-rates and viscosities of the phases determine the thickness of the retentive layer, $R - R_c$, and the diameter of the mobile phase cylinder, R_c (see Fig. 1).

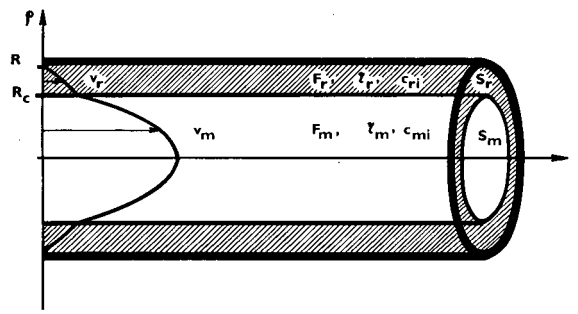

Fig. 1. Flow profiles in open-tubular liquid chromatography with flowing retentive phase. ρ = Radial variable; R = capillary internal radius; R_c = radius of mobile phase cylinder; F_m, F_r = flow-rates of mobile and retentive phase, respectively; η_m, η_r = viscosities of mobile and retentive phase, respectively; c_{mi}, c_{ri} = solute concentrations in mobile and retentive phase, respectively: S_m, S_r = cross-section of mobile and retentive phase, respectively: v_m, v_r = velocities of mobile and retentive phase, respectively, as a function of ρ.

For a two-phase two-dimensional system, the governing differential equations for steady flow velocities are [12]

$$-\frac{\Delta P}{\eta_j L} = \frac{d^2 v_j}{d\rho^2} + \frac{1}{\rho} \cdot \frac{dv_j}{d\rho} \quad j = r, m \quad (11)$$

where η_j is the phase viscosity, ΔP is the pressure drop across the capillary of length L and ρ is the radial distance. This equation gives, after double integration,

$$v_j = \Delta P\, \rho^2/(\eta_j L) + C_j' \ln \rho + C_j'' \quad j = r, m \quad (12)$$

where the integration constants C_j' and C_j'' can be evaluated with the help of the following boundary conditions.

Constant C_m' is zero as v_m does not reach infinity at $\rho = 0$ and because the velocity gradient is zero as a consequence of symmetry:

$$dv_m/d\rho\,|_{\rho=0} = 0 \quad (13)$$

Because of the balance of the friction forces acting at the interface $\rho = R_c$,

$$\eta_r\, dv_r/d\rho\,|_{\rho=R} = \eta_m\, dv_m/d\rho\,|_{\rho=R} \quad (14)$$

constant C_r' is also zero. Constant C_r'' is evaluated with the help of the equality of velocities v_r and v_m at the interface:

$$v_m\,|_{\rho=R_c} = v_r\,|_{\rho=R_c} \quad (15)$$

as $C_r'' = \Delta P\, R^2/(4\eta_r L)$. Zero velocity condition at the inner surface of the capillary,

$$v_r\,|_{\rho=R} = 0 \quad (16)$$

leads to

$$C_m'' = \Delta P/(4L)[R_c^2/\eta_m + (R^2 - R_c^2)/\eta_r]$$

After the substitution of these constants into eqn. 12, the velocity profiles are

$$v_m = \frac{\Delta P}{4L}[(R_c^2 - \rho^2)/\eta_m + (R^2 - R_c^2)/\eta_r] \quad (17)$$

$$v_r = \frac{\Delta P}{4L\eta_r}(R^2 - \rho^2) \quad (18)$$

These equations decribe the velocity profiles of a two-phase flow in a capillary of circular cross-section where the phases create concentric tubes under the action of surface tension. Eqns. 17 and 18 show that the velocity profile of the inner phase is superimposed on the maximum velocity of the outer phase, whereas the profile of the outer phase is unaffected by the inner phase. When $\eta_r = \eta_m$, $R_c = R$ or $R_c = 0$ these equations are transformed into the form of the equation for a one-phase flow.

As stated above, the radius of the mobile phase cylinder R_c is given by the flow-rates of both phases and their velocity profiles. Consequently, R_c can be evaluated by comparing the flow-rate ratio q (eqn. 10) with the ratio of the flow-rates which are obtained by integration of eqns. 17 and 18 over the respective cross-sections. The flow-rates are

$$F_m = \frac{\pi \Delta P}{8\eta_r L}\left(\frac{R_c^4 \eta_r}{\eta_m} - 2R_c^4 + 2R_c^2 R^2\right) \quad (19)$$

$$F_r = \frac{\pi \Delta P}{8\eta_r L}(R_c^2 - R^2)^2 \quad (20)$$

Now, R_c can be found as a solution to the biquadratic equation. The only real and positive root is

$$R_c = R\left(\frac{(q+1) - (q^2 + q\,\eta_r/\eta_m)^{\frac{1}{2}}}{1 - q(\eta_r/\eta_m - 2)}\right)^{\frac{1}{2}} \quad (21)$$

The radius of the mobile phase cylinder is independent of the pumped flow-rate and is controlled only by the physico-chemical parameters of the two phases, *i.e.*, the mutual solubilities at temperatures T_1 and T_2 and viscosities η_r and η_m, respectively.

The phase ratio in the capillary, ϕ, can be expressed as the function of radii R_c and R:

$$\phi = \frac{S_r}{S_m} = \frac{R^2 - R_c^2}{R_c^2} \quad (22)$$

By insertion of eqns. 10 and 21 into eqn. 22 and introducing $t = \eta_r/\eta_m$, and $\Delta s = s_1 - s_2$, we obtain for ϕ

$$\phi = \frac{1 - t + 1/\Delta s}{1/\Delta s - (1 + t(1/\Delta s - 1))^{\frac{1}{2}}} - 1 \quad (23)$$

Based on eqn. 9, the retention of the solute i, expressed in terms of k_i^*, can be calculated by the following equation:

$$k_i^* = (\phi - q)/(1/K_i + q) \quad (24)$$

where the phase ratio, ϕ, is determined by eqn. 23 and the flow ratio, q, is determined by eqn. 10.

EXPERIMENTAL

Capillary preparation

A Simax-type stock glass tube (Kavalier, Sázava, Czechoslovakia) of 7 mm O.D. and 0.6 mm I.D. was drawn using a laboratory-made glass-drawing machine. The capillary obtained, of 0.7 mm O.D. and 17 μm I.D., was hydrophobized by persilylation. The length of the capillary used for chromatographic experiments was 5.670 m.

Chromatograph

The chromatographic system used has been described previously [13]. The pressure source was a VCM 300 micropump (Development Works, Czechoslovak Academy of Sciences, Prague, Czechoslovakia). The sample was injected using a laboratory-made six-port valve with a 20-μl loop and a flow splitter. The splitting ratio was 1:700. The capillary was immersed in a water-bath connected with a U8 thermostat (MLW Prüfgeräte-Werk, Medingen/Sitz Freital, Germany). The capillary was maintained at a constant temperature of 50.0°C. An EMD 10 electrochemical detector (Laboratory Instruments, Prague, Czechoslovakia) was equipped with a thin-layer microcell similar to that described previously [14]. The detector signal was monitored with a TZ 4100 line recorder (Laboratory Instruments).

Mobile phase

The pumped liquid was a 0.1 mol l^{-1} aqueous solution of sodium perchlorate and 1 mmol l^{-1} acetic acid; the solution was saturated with cyclohexanol at 23°C. Based on the interpolation of reported data [15], the difference in the solubilities of cyclohexanol in water between 23 and 50°C was considered to be equal to 0.7 vol.%.

Test solutes

The test solutes were sodium nitrite (dead time marker), gallic acid, 2,5-dihydroxybenzoic acid, hydroquinone, catechol, phenol and 2-nitro-5-aminophenol, purchased from Lachema (Brno, Czechoslovakia).

Viscosity measurement

The viscosities of coexisting liquids in the system cyclohexanol–water at 50°C were measured using a thermostated Ubbelohde viscosimeter. The liquid densities needed were determined pycnometrically. Using reference values for water [16], the densities of the aqueous and organic phases were determined to be 985 and 966 kg m^{-3}, respectively. Further, from ten repetitive measurements, the viscosities η_m and η_r were determined to be 0.57 mN s m^{-2} ± 0.03% and 3.97 mN s m^{-2} ± 0.4%, respectively. Thus, the η_r/η_m ratio was 6.96 at 50.0°C.

Distribution constant determination

The solute K_i was determined by the method described previously [17]. A known amount of analyte was dissolved in the aqueous phase and the absorbance at 288 nm (hydroquinone) or 268 nm (phenol) was determined. The solution was then equilibrated for 2 days at 50°C with a known amount of water-saturated cyclohexanol and the absorbance of the aqueous phase was measured again. The calculated distribution constants for hydroquinone and phenol were 5.0 and 16.7, respectively.

RESULTS AND DISCUSSION

Comparison of theory with experiment

A comparison between the predicted and observed solute retentions can be made from the data summarized in Table I. The values show that the retentions found fit fairly well with the predicted values. Nevertheless, two comments should be made.

Firstly, the ends (about 20 cm in total) of the capillary are maintained at ambient temperature. In this part of the capillary, an appreciable layer of retentive phase should not be present. The negative deviation of the retention from the theory can be up to 3% in the chromatographic configuration used. Second, the calculated retention should be considered as the maximum achievable value. An inhomogeneity in the surface modification can lead to a local decrease in the cross-section of the retentive phase. The role of internal surface modification will be described in detail elsewhere [18].

An example of a chromatogram of phenolic compounds is shown in Fig. 2.

TABLE I

MEASURED AND CALCULATED VALUES FOR REVERSED-PHASE PARALLEL-CURRENT OPEN-TUBULAR LC OF HYDROQUINONE AND PHENOL IN THE SYSTEM WATER–CYCLOHEXANOL

Input values: Δs = 0.007, t = 7.0, $K_{hydroquinone}$ = 5.0, K_{phenol} = 16.7.

Parameter	Hydroquinone	Phenol
q from eqn. 10	0.00705	
ϕ from eqn. 23	0.2293	
k_i^* from eqn. 24	1.072	3.316
k_i^* observed	0.95	3.4
ϕ from eqn. 24 and k_i^* observed	0.204	0.235

Evaluation of the limits of the solute retention

Several interesting features can be concluded from eqn. 24. First, the solute retention is a function only

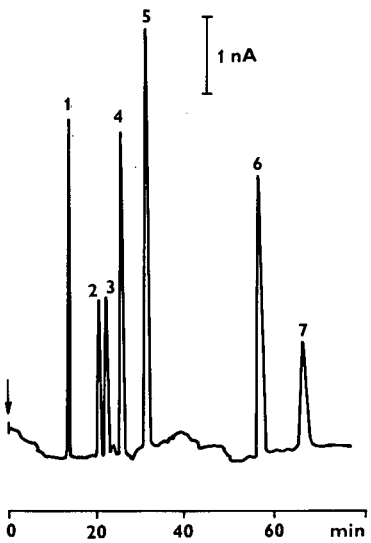

Fig. 2. Chromatogram of separation of phenolic compounds by reversed-phase parallel-current open-tubular liquid chromatography. Capillary: 5.670 m × 17 μm I.D. glass capillary hydrophobized by persilylation; separation temperature, 50°C; mobile phase, 0.1 mol l^{-1} $NaClO_4$–1 mmol l^{-1} acetic acid in water saturated at 23°C with cyclohexanol; detection, amperometric on a platinum electrode; sampling, 20 μl with splitting ratio = 1:700. Peaks: 1 = nitrite ion (dead volume); 2 = gallic acid; 3 = 2,5-dihydroxybenzoic acid; 4 = hydroquinone; 5 = catechol; 6 = phenol; 7 = 2-nitro-5-aminophenol.

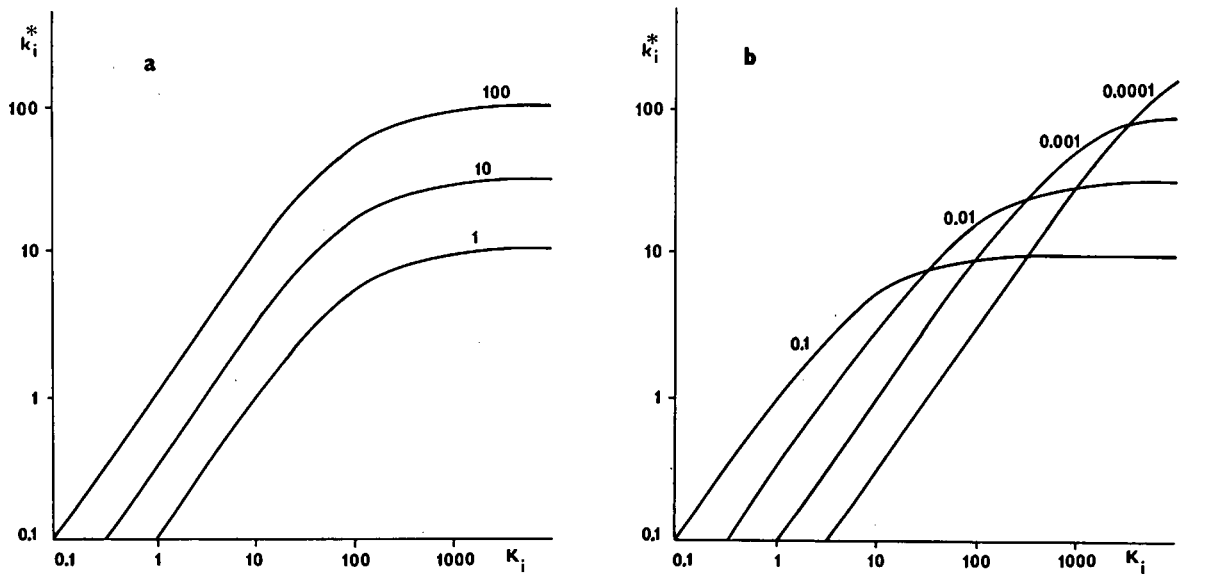

Fig. 3. Plots of dependence of k_i^* on K_i for selected values of Δs and t according to eqn. 24. (a) $\Delta s = 0.01$, t values as shown; (b) $t = 10$, Δs values as shown as a volume fraction of retentive phase in pumped liquid.

of intensive parameters, *i.e.*, temperature, liquid viscosities and component solubilities. No geometrical parameter enters eqn. 24. Hence, as long as eqn. 24 is valid, the capillary dimension can be varied without influencing the solute retention.

It is useful to obtain an idea of the achievable solute retention as a function of Δs, t and K_i. In Fig. 3a, plots of the dependences of k_i^* on K_i for different values of t and a constant $\Delta s = 1\%$ are shown. The examples show that over the whole of the displayed region, an increase in viscosity ratio increases the predicted solute retention. Fig. 3b shows several plots of the dependences of k_i^* on K_i for different values of Δs and a constant $t = 10$. In contrast to Fig. 3a, the influence of the increasing solubility difference is not unambiguous. For low K_i, an increase in Δs predicts a higher k_i^*, whereas for high K_i, the retention should decrease with higher Δs. This can be explained by the retentive phase flow, which increases with increase in Δs (see eqn. 1). To conclude, an increase in retentive phase viscosity is more useful for enhancement of the solute retention than an increase in the difference in retentive phase solubilities between the temperature of the pumped liquid and that of the separation capillary. However, the upper limit of the phase ratio is determined by the retentive film stability. The influence of system parameters on this phenomenon will be discussed elsewhere [18].

If K_i tends to infinity, k_i^* tends to a finite value determined solely by the flow of the retentive phase, F_r. k_i^* of the solute transported exclusively by the retentive phase, $k^*_{i,K\to\infty}$, is

$$k^*_{i,K_i\to\infty} = \phi/q - 1 \tag{25}$$

This equation corresponds to the tangent of the horizontal part of the graphs for eqn. 24 (see Fig. 3a and b). The practical consequence of this property lies in the self-regenerating ability of the capillary, *i.e.*, every sample component which is soluble in at least one of the liquids within the capillary is sooner or later eluted from the capillary.

For small values of Δs ($\Delta s \ll t$, $\Delta s \ll 1$), eqn. 23 can be simplified to

$$\phi \approx (t\Delta s)^{\frac{1}{2}} \tag{26}$$

Such a simplified equation can also be derived under the assumption of a linear profile of velocity within the retentive film and the assumption that the mobile phase cross-section is equal to the capillary internal cross-section. The magnitude of the deviation of eqn. 26 from eqn. 23 is shown in Table II for

TABLE II

RATIO OF ϕ VALUES CALCULATED FROM EQN. 23 TO THOSE CALCULATED FROM EQN. 26 FOR SELECTED VALUES OF Δs AND t

Δs (%, v/v)	t			
	1	7	10	100
0.01	1.0101	1.0038	1.0032	1.0011
0.1	1.0326	1.0124	1.0105	1.0036
1.0	1.1111	1.0438	1.0374	1.0152
10.0	1.4625	1.1952	1.1710	1.0898

TABLE III

RATIO OF k_i^* VALUES CALCULATED FROM EQN. 24 TO THOSE CALCULATED FROM EQN. 27 FOR $t = 10$ AND SELECTED VALUES OF Δs AND K_i

Δs (%, v/v)	K_i			
	0.1	1	10	100
0.01	1.00006	0.99996	0.99905	0.99015
0.1	1.0004	0.9995	0.9905	0.9095
1	1.0049	0.9958	0.9136	0.5004
10	1.147	1.0440	0.5495	0.0958

various values of Δs and t. Here, the ratios of the ϕ values calculated from eqn. 23 to the values calculated from eqn. 26 are given. For $\Delta s < 1$ vol.%, the relative difference between eqns. 26 and 23 is below 5%.

For small Δs ($\Delta s \approx q \ll 1/K_i$), eqn. 24 can also be simplified to

$$k_i^* \approx K_i(t\Delta s)^{\frac{1}{2}} \tag{27}$$

Table III gives selected values of k_i^* ratios calculated by dividing eqn. 24 by eqn. 27 and using $t = 10$. For practical values of Δs and t, k_i^* can be estimated from eqn. 27 within a few percent relative error in comparison with eqn. 24.

CONCLUSION

Because, according to the equations derived, the capillary diameter can be varied without influencing the phase ratio, the suggested method is promising for the use of capillaries with even smaller diameter than used here. Evaluation of the upper limit of the phase ratio in relation to the retentive film stability needs further study.

The temperature dependence of the phase ratio evokes the idea of simple control of solute retention by choice of the capillary temperature. Even more, the temperature programming should be an efficient tool for retention control during the chromatographic separation.

More basically than other liquid–liquid chromatographic methods, the approach presented here substantially reduces problems connected with the interaction of the analyte with solid sorbents, supports or other solid matrices. In comparison with other separation methods that are based on a perpendicular arrangement of liquid flow displacement and relative displacement, and that do not need any solid matrix (*e.g.*, countercurrent chromatography, field-flow fractionation [4,5]) the suggested method offers a much higher number of theoretical plates generated per unit time. In comparison with the modes of open-tubular liquid–liquid chromatography presented up to now, the suggested method simplifies substantially the capillary preparation, which makes open-tubular LC more attractive for the solution of practical analytical problems.

The term parallel-current open-tubular liquid chromatography is suggested for the method presented.

In the near future, the influence of the physical properties of the solvent, modification of the capillary internal surface and the mobile phase velocity will be studied from the point of view of optimization of the performance of the method.

REFERENCES

1 B. L. Karger, L. R. Snyder and Cs. Horváth, *An Introduction to Separation Science*, Wiley, New York, 1973.
2 Z. Deyl, K. Macek and J. Janák, *Liquid Column Chromatography*, Elsevier, Amsterdam, 1975.
3 L. R. Snyder and J. J. Kirkland, *Introduction to Modern Liquid Chromatography*, Wiley, New York, 1979.
4 J. C. Giddings, *Anal. Chem.*, 53 (1981) 945A.
5 J. C. Giddings, *J. Chromatogr.*, 395 (1987) 19.
6 N. B. Mandava and Y. Ito (Editors), *Countercurrent Chromatography*, Marcel Dekker, New York, 1988.
7 S. Terabe, *Trends Anal. Chem.*, 8 (1989) 129.

8 A. J. P. Martin and R. L. M. Synge, *Biochem J.*, 35 (1941) 1358.
9 J. H. Knox and M. T. Gilbert, *J. Chromatogr.*, 186 (1979) 405.
10 J. H. Knox, *J. Chromatogr. Sci.*, 18 (1980) 453.
11 J. W. Jorgenson and E. J. Guthrie, *J. Chromatogr.*, 255 (1983) 355.
12 R. B. Bird, W. E. Stewart and E. N. Lightfoot, *Transport Phenomena*, Wiley, New York, 1965.
13 K. Janák, M. Horká and M. Krejčí, *J. Microcol. Sep.*, 3 (1991) 203.
14 K. Šlais and M. Krejčí, *J. Chromatogr.*, 235 (1982) 21.
15 R. Stephenson and J. Stuart, *J. Chem. Eng. Data*, 31 (1986) 56.
16 R. C. Weast (Editor), *Handbook of Chemistry and Physics*, CRC Press, Boca Raton, FL, 68th ed., 1987–88.
17 J. F. K. Huber, C. A. M. Meijers and J. A. R. J. Hulsman, *Anal. Chem.*, 44 (1972) 111.
18 K. Šlais and M. Horká, in preparation.

Journal of Chromatography, 605 (1992) 175–191
Elsevier Science Publishers B.V., Amsterdam

CHROM. 24 200

Step elution in preparative liquid chromatography

S.-G. Hu, D. D. Do and Md. M. Hossain

Department of Chemical Engineering, University of Queensland, Brisbane, Queensland 4072 (Australia)

(First received October 15th, 1991; revised manuscript received March 24th, 1992)

ABSTRACT

Preparative liquid chromatography with the step elution, in which a sample is loaded into a column at higher binding strength and then eluted at lower binding strength, was numerically simulated with a detailed rate equation model. The model takes into account film mass transfer resistance, pore diffusion, axial dispersion and local equilibrium. The step elution mode was compared with the isocratic elution mode in terms of the preparative performance for a binary mixture having a constant or variable separation factor. The effects of various parameters, such as step height, sample size, solute concentration, feed composition and mobile phase flow-rate, were examined.

INTRODUCTION

Preparative or production-scale liquid chromatography is fundamentally different from analytical chromatography in its purpose. In all preparative and production applications of chromatography, the goal is to separate a desired product with a specified degree of purity and at the lowest cost. Consequently, it is important to seek conditions for the optimum preparative performance, other than conditions for the best resolution between the solute bands.

Fundamental studies of preparative liquid chromatography have been published. These reports discuss theoretically the effects of parameters such as relative retention [1,2], feed composition [3], concentration overload [4], sample size and volume [5], mobile phase flow-rate [6] and column efficiency [7,8]. These investigations allow a better understanding of non-linear preparative liquid chromatography carried out in the isocratic elution mode.

The elution strategy is also important in the optimization of preparative chromatography. Although the linear gradient elution mode is widely used in analytical and preparative chromatography where the components display a broad range of retentivity, only a few reports have described fundamental studies on the gradient elution mode in preparative liquid chromatography. Computer simulations based on the Craig distribution model have been used to examine preparative separations with linear gradient elution for heavily overloaded conditions [9–11]. Antia and Horváth [12] compared isocratic elution with linear gradient elution under preparative conditions. Cox and Snyder [13] reported experimental studies to show that displacement effects occur in the preparative gradient elution chromatography of proteins. Apart from linear gradient elution, non-linear gradients, such as stepwise elution [14–16], are also employed in chromatographic separations in order to take the advantage of the simple apparatus and operating procedure. However, the performance of the preparative liquid chromatography with step elution has not been well understood.

In this paper, we present a comparison of step elution with isocratic elution as a function of sample size on the basis of production rate and yield at a specified purity. In step elution, a sample is loaded into the column with a certain modulator level, such

Correspondence to: Dr. D. D. Do, Department of Chemical Engineering, University of Queensland, Brisbane, Queensland 4072, Australia.

0021-9673/92/$05.00

as salt concentration and pH, so that the binding strength of the solute on the adsorbent in the loading stage is high, and then eluted with a buffer solution having another modulator level to reduce the binding strength. The high loading capacity, the strong compression effect and the short elution time in the step elution mode lead to an improvement in the preparative performance of overloaded liquid chromatography. A detailed rate equation model was used in this work to investigate the preparative performance under the step elution conditions. The effects of various parameters such as step height, sample size, solute concentration, feed composition and mobile phase flow-rate were studied by means of numerical simulation.

THEORY

Model description

We consider a chromatographic process involving a binary mixture taking place in a column of length L. The following assumptions are made in formulating the model: the porous solid adsorbent is spherical and uniform in size; the process is isothermal with no concentration gradient in the radial direction of the column; the pore diffusivity and film mass transfer coefficient are constant; local equilibrium is assumed between the adsorbed species and the free species in the porous particle; and modulator molecules do not adsorb on the stationary phase.

By defining the non-dimensional variables and parameters as in Table I, the following dimensionless equations for solute k can be obtained via mass balance.

The governing equation for the bulk fluid phase is given by

$$\sigma_b(k)\frac{\partial Y_b(k)}{\partial \tau} = \eta(k)\left[\frac{1}{Pe}\cdot\frac{\partial^2 Y_b(k)}{\partial \xi^2} - \frac{\partial Y_b(k)}{\partial \xi}\right] - 3\psi(k)\left.\frac{\partial Y(k)}{\partial X}\right|_1 \quad (1)$$

The initial condition and boundary conditions for eqn. 1 are

$$\tau = 0; \quad Y_b(k) = 0 \quad (2)$$

$$\xi = 0; \quad \frac{1}{Pe}\cdot\frac{\partial Y_b(k)}{\partial \xi} = [Y_b(k) - Y_b^0] \quad (3)$$

$$\xi = 1; \quad \frac{\partial Y_b(k)}{\partial \xi} = 0$$

where

$$Y_b^0 = \begin{cases} 0 & \tau > \tau_{inj} \\ 1 & \tau \leqslant \tau_{inj} \end{cases} \quad (4)$$

TABLE I

DEFINITIONS OF DIMENSIONLESS VARIABLES

$$Y(k) = \frac{C_k}{C_k^0};\ Y_\mu(k) = \frac{C_{\mu k}}{C_{\mu s,k}};\ Y_b(k) = \frac{C_{bk}}{C_k^0};\ \xi = \frac{Z}{L};\ X = \frac{r}{R_0}$$

$$\tau = \frac{t}{t_0};\ t_0 = \frac{L}{V_f}\frac{\sigma_t}{\sum_{l=1}^{NC} C_l^0};\ \sigma_t = [\varepsilon_b + (1-\varepsilon_b)\varepsilon_p]\sum_{l=1}^{NC} C_l^0 + [1-\varepsilon_b(1-\varepsilon_p)]\sum_{l=1}^{NC} C_{\mu s,k}$$

$$\sigma(k) = \frac{(1-\varepsilon_b)\varepsilon_p C_k^0}{\sigma_t};\ \sigma_\mu(k) = \frac{(1-\varepsilon_b)(1-\varepsilon_p)C_{\mu s,k}}{\sigma_t};\ \sigma_b(k) = \frac{\varepsilon_b C_k^0}{\sigma_t}$$

$$\psi(k) = \frac{(1-\varepsilon_b)\varepsilon_p D_{p,k} C_k^0}{\frac{V_f}{L}\sum_{l=1}^{NC} C_l^0};\ \eta(k) = \frac{C_k^0}{\sum_{l=1}^{NC} C_l^0};\ Bi(k) = \frac{k_f R_0}{\varepsilon_m D_{pk}};\ Pe = \frac{LV_f}{D_{ax}}$$

where τ_{inj} is the dimensionless time duration of sample injection.

The governing equation for the particle phase is given by

$$\sigma(k)\frac{\partial Y(k)}{\partial \tau} + \sigma_\mu(k)\frac{\partial Y_\mu(k)}{\partial \tau} = \psi(k)\frac{1}{X^2}\cdot\frac{\partial}{\partial X}\left[X^2\frac{\partial Y(k)}{\partial X}\right] \quad (5)$$

where

$$\frac{\partial Y_\mu(k)}{\partial \tau} = \sum_{l=1}^{NC}\frac{\partial Y_\mu(k)}{\partial Y(l)}\cdot\frac{\partial Y(l)}{\partial \tau}$$

and the term $\partial Y_\mu(k)/\partial Y(l)$ is determined from the isotherm model, described in the next section.

The initial condition and boundary conditions for eqn. 5 are given by

$$\tau = 0; \quad Y(k) = Y_\mu(k) = 0 \quad (6)$$

$$X = 0; \quad \frac{\partial Y(k)}{\partial X} = 0 \quad (7)$$

$$X = 1; \quad \frac{\partial Y(k)}{\partial X} = Bi(k)[Y_b(k) - Y(k)]$$

The film mass transfer coefficient, k_f, used to calculate the Biot number and axial dispersion coefficient, D_{ax}, used to calculate the Peclet number are estimated with the following correlations [17,18]:

$$k_f = (2 + 1.45Re^{0.45}Sc^{1/3})D_{AB}/d_p \quad (8)$$

$$D_{ax} = V_f d_p/(0.2 + 0.11Re^{0.48}) \quad (9)$$

where Sc is the Schmidt number ($Sc = \mu/\rho D_{AB}$), and Re is the Reynolds number ($Re = d_p V_f/\mu$).

In step elution, the rectangular front of elution buffer will be gradually deformed owing to the dispersion. This effect must be taken into account in the model. The mass balance equations for the modulator are basically similar to those for solute except that the term $\partial Y_\mu(k)/\partial \tau$ in eqn. 5 is equal to zero because of the assumption that the modulator molecules do not adsorb on the stationary phase. Unlike analytical chromatography, heavily overloaded elution chromatography generally behaves like the frontal operation in the loading stage. Jandera and Guiochon [19] have observed that the strength of the sample solvent significantly affects the band profile in preparative liquid chromatography. Therefore, the initial conditions of the feed solution, such as pH and ionic strength, play an important role in the preparative performance. For the sake of definition, in this work we assume that the conditions of the feed solution were adjusted prior to injection so that the conditions are the same as those in the initial buffer solution. Accordingly, the initial and boundary conditions for modulator may be written as

$$\tau = 0; \quad Y_m = Y_m^0 \quad (10)$$

$$\xi = 0; \quad Y_m = \begin{cases} Y_m^0, & 0 \leqslant \tau \leqslant \tau_{inj} \\ Y_m^e, & \tau > \tau_{inj} \end{cases} \quad (11)$$

$$\xi = 1; \quad \frac{\partial Y_m}{\partial \xi} = 0 \quad (12)$$

where Y_m is the dimensionless concentration of the modulator and Y_m^0 and Y_m^e are the modulator concentrations in initial and elution buffers, respectively.

Adsorption isotherm

The competitive Langmuir isotherm is the most commonly used isotherm in describing multi-component equilibria. Experimental data for some binary systems are also in reasonable agreement with the predictions from the Langmuir isotherm [12]. For simplicity, therefore, the competitive Langmuir isotherm is chosen as an isotherm model in this work. For multi-component adsorption, the non-dimensional form of the Langmuir isotherm is given by

$$Y_\mu(k) = \frac{\lambda(k)Y(k)}{1 + \sum_{l=1}^{NC}\lambda(l)Y(l)} \quad (13)$$

where $\lambda(k)$ is defined as

$$\lambda(k) = C_k^0 b(k) \quad (14)$$

In order to incorporate the effects of modulator concentration into the isotherm model, the following assumptions are proposed: the saturation capacity, $C_{\mu s}$, is not affected by the modulator concentration; the parameters $b(k)$ are independent of each other; and the types of interaction involved are only electrostatic and hydrophobic.

Depending on the nature and properties of both the solute and stationary phase, various correlations

of $b(k)$ *versus* the modulator concentration can be expected. For the chromatographic systems based on hydrophobic and electrostatic interactions, Melander *et al.* [20] proposed a comprehensive relationship between the retention factor $[= C_{\mu s,k}b(k)(1 - \varepsilon_b)/\varepsilon_b]$ and salt concentration. By separating the $C_{\mu s,k}$ from $b(k)$ and lumping $C_{\mu s,k}$ into the α term in their equation, the following equation can be obtained to express the dependence of $b(k)$ on the modulator concentration, as a Langmuir competitive isotherm with a constant saturation capacity is assumed in this work [20]:

$$\log b(k) = \alpha(k) - \beta(k)\log C_m + \gamma(k)C_m \quad (15)$$

where $\beta(k)$ and $\gamma(k)$ are the electrostatic and hydrophobic interaction parameters, respectively. The parameter $\alpha(k)$ is a constant encompassing all characteristic system parameters and C_m is the molar concentration of the modulator. It is noted that the same form of eqn. 15 was used in the modelling of gradient elution presented by Gu *et al.* [21] and a simplified form was applied by Antia and Horváth [12] in their simulations of linear gradient elution. Although the assumption of the independence of $C_{\mu s}(k)$ on modulator concentration has some experimental support [13], it would be not expected to be valid over a wide range of conditions in multiple solute systems as discussed by Antia and Horváth [12]. However, the influence from the dependence of $C_{\mu s}$ on the modulator concentration can be included in the effect of separation factor as defined by

$$S_f = \frac{b(l)C_{\mu s,l}}{b(k)C_{\mu s,k}} \quad (16)$$

As the separation factor is the foremost factor characterizing the chromatographic separation, the effect of a variable S_f should be equivalent to the effect of a $C_{\mu s}$ dependent on the modulator concentration. Generally, S_f varies with the modulator concentration. In some special cases where the solutes are similar in the molecular structure, S_f may be assumed to be constant. In this study, simulations were carried out for systems with both constant and variable separation factors with changing modulator concentration.

Method for numerical solution

Owing to the non-linearity involved, there is no analytical solution possible for the model equations. Approximate solution by efficient numerical techniques is the only feasible alternative. The model equations are discretized with the method of orthogonal collocation on finite elements [22]. The resulting ordinary differential–algebraic equation set was then solved by using the software DASSL [23].

Definitions of parameters

The load factor, L_f, is given by the ratio of the amount of reference solute in the sample fed into the column to the saturation capacity of the column for that solute. The lesser retained solute A is chosen as the reference in this work.

$$L_f = \frac{V_f C^0 t_0 \tau_{inj}}{L(1 - \varepsilon_b)C_{\mu s}} \quad (17)$$

The production rate, P_k, is the amount of solute k recovered per run at the specified degree of purity per unit column cross-section area divided by the cycle time τ_c, which extends from the start of the run to the point where the last component completes its elution. For simplicity, the following dimensionless form was used for result presentation:

$$P_k = \frac{V_f C_k^0 \int_{\tau_{1,k}}^{\tau_{2,k}} Y_c(k)dt}{V_r C_r \tau_c} \cdot 100 \quad (18)$$

where $Y_c(k)$ is the outlet concentration of solute k at time τ, $\tau_{1,k}$ and $\tau_{2,k}$ are cutting points between which solute k is collected at the desired purity, V_f is the superficial velocity, V_r is a reference superficial velocity, C_k^0 is the concentration of solute k in the feed solution and C_r is the reference concentration. The parameter P_k so defined can be used for comparing the results obtained under different V_f and C_k^0.

It should be pointed out that an actual cycle time τ_c would include any wash and regeneration steps. The influence of column regeneration in step elution on the production rate will be discussed in the next section.

The recovery yield, RY_k, is the fraction of the solute k fed into the column that is recovered at the column outlet as a product with a specified degree of purity. A purity of 98% is chosen in this work.

$$RY_k = \frac{1}{\tau_{inj}} \int_{\tau_{1,k}}^{\tau_{2,k}} Y_c(k)d\tau \quad (19)$$

TABLE II

VALUES OF PARAMETERS IN EQN. 15 FOR SIMULATION

Parameter		Constant S_f			Variable S_f	
		$S_f = 2.41$	$S_f = 1.41$	$S_f = 1.35$	Divergent	Convergent
$\alpha(k)$	A	−3.68	−3.65	−3.03	−3.73	−3.74
	B	−3.30	−3.5	−2.9	−3.38	−3.65
$\beta(k)$	A	3.0	3.0	2.6	3.0	3.0
	B	3.0	3.0	2.6	3.0	2.7
$\gamma(k)$	A	3.0	3.0	1.84	3.09	2.55
	B	3.0	3.0	1.84	3.0	2.6

The enrichment factor, E_k, is defined as the product concentration of solute k divided by its concentration in the feed:

$$E_k = \frac{1}{(\tau_{2,k} - \tau_{1,k})} \int_{\tau_{1,k}}^{\tau_{2,k}} Y_e(k) d\tau \quad (20)$$

RESULTS AND DISCUSSION

Based on the model presented above, the preparative performance in the different elution modes was simulated for various conditions. The parameter values used for simulations are listed in Tables II and III unless mentioned otherwise in the discussion or stated in the figure captions. Parameter values for $\alpha(k)$, $\beta(k)$ and $\gamma(k)$ were selected by reference to some experimental data with proteins [20]. However, these parameters could take any other values, depending on the modulator type and the unit of variables. As the objective of this work was to investigate the effect of the difference in binding strength between the loading stage and elution stage, the important parameter is the binding strength [$b(k)$], which is calculated from eqn. 15. The value of $b(k)$ in this work covers a wide range of 0.02–50. For the parameters given in Table II and the range of modulator concentration (0.5–2.0 M) used in simulations, the binding strength is increased with an increase in the modulator concentration, and also the solute A is the lesser retained component in the binary mixture.

Comparison for the system with constant S_f

Effects of sample size and step height. The simulation results for the system with a constant separation factor of 2.41 are shown in Fig. 1. In the insets in Fig. 1, the values following the hollow symbols are the molar concentrations of the modulator in isocratic elution, while the ranges following the filled symbols are the variations of the modulator concentration in the step elution. The range is thereafter called the step height. The first number of the range is the modulator concentration in the initial buffer and the second is that of the elution buffer.

As shown in Fig. 1a and c, the production rates for both solutes in step elution are considerably higher than those in isocratic elution with a moderate degree of overload. It can also be seen from Fig. 1a and b that with step elution, the optimum load factor for the production rate of solute A is higher than that for solute B. The maximum production

TABLE III

PARAMETER VALUES USED IN SIMULATIONS

$R_0 = 25\ \mu m$	$C_r = 3\ kg/m^3$
$L = 25\ cm$	$\mu = 1.3 \cdot 10^{-3}\ kg/m \cdot s$
$\varepsilon_p = 0.5$	$\rho = 1100\ kg/m^3$
$\varepsilon_b = 0.4$	$D_{AB,k} = 6 \cdot 10^{-11}\ m^2/s$
$V_f = 5 \cdot 10^{-6}\ m/s$	$D_{p,k} = 3.2 \cdot 10^{-12}\ m^2/s$
$V_r = 5 \cdot 10^{-6}\ m/s$	$D_{bm} = 1.59 \cdot 10^{-9}\ m^2/s$
$C_A^0 = 3\ kg/m^3$	$D_{pm} = 3 \cdot 10^{-10}\ m^2/s$
$C_B^0 = 3\ kg/m^3$	$Pe = 2388$
$C_{\mu s,A} = 50\ kg/cm^3$	$Bi_k = 48$
$C_{\mu s,B} = 50\ kg/m^3$	$Bi_m = 11$

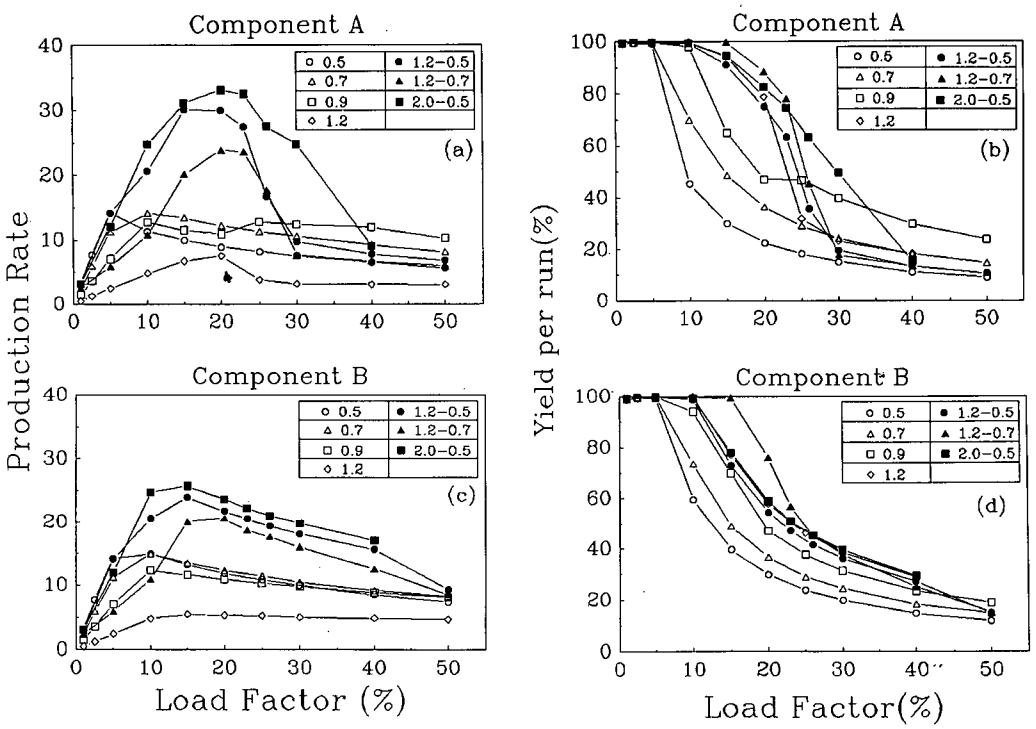

Fig. 1. Production rate and yield as a function of load factor obtained in step elution and isocratic elution. $S_f = 2.41$; 1:1 binary mixture.

rate of solute A is increased more than that of solute B by step elution.

It is also noted from Fig. 1a and c that the improvement in the production rate by using step elution depends greatly on the step height. For a given modulator concentration in the initial buffer, the maximum production rates for both solutes in step elution are decreased with an increase in the modulator concentration in the elution buffer, but the yield is improved to a certain extent as shown in Fig. 1b and d.

A higher initial binding strength allows a greater column loading capacity, which facilitates a larger sample size injected into the column and hence more product recovered in one run. Because of this, the higher the step height, the better is the production rate for the cases in Fig. 1. However, a high loading capacity does not imply a high production rate. It merely provides the possibility of obtaining more products in one run. This is because the production rate is also dependent on the operation time of the process. In isocratic elution, a higher loading capacity always implies a longer elution time. Step elution combines an initial high loading capacity with a short elution time, and this makes it an efficient elution mode in preparative chromatography.

Plots of enrichment factor (defined in eqn. 20) *versus* load factor are shown in Fig. 2. The product concentration of solute A in step elution is more than three times higher than that in isocratic elution for a load factor of 20%. It is clear that the sample size (load factor) favourable to the enrichment (about 20%) is consistent with that for the maximum production rate. Although solute B is not as highly concentrated as solute A in step elution, it is still higher than that in isocratic elution.

The favourable aspects of step elution can be further illustrated by comparing the bed profiles for the two elution modes (Figs. 3 and 4). During the loading stage (Figs. 3a and 4a), the bed profiles are the same for both elution modes because of the same conditions. Under overloaded conditions, the band development in the loading stage clearly resembles that in the frontal adsorption process, which is indicated by the roll-up peaks in Figs. 3a and 4a. In step elution, the difference in binding strength across

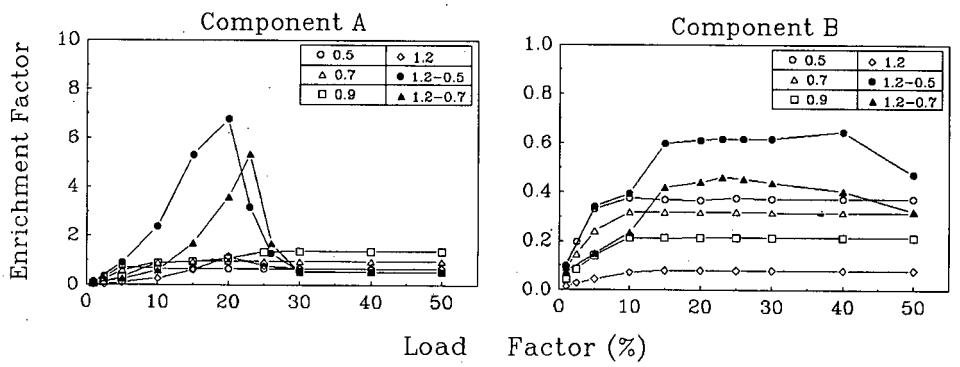

Fig. 2. Enrichment factor as a function of load factor in step elution and isocratic elution. S_f = 2.41; 1:1 binary mixture.

the front of the elution buffer results in the rear portion of both solute bands moving at a higher speed. Hence the bands of both A and B are strongly compressed, as shown in Fig. 3b. The high peak concentration, caused by the compression effect, results in a strong interaction between the bands of both solutes (Fig. 3b and c). The improvement in yield and enrichment with step elution is basically due to such enhanced interactions, especially the displacement effect [24]. On other hand, the "tag-along" effect [25] pulls forward the front of the solute B peak, and hence decreases its maximum concentration (Fig. 3b and c). In isocratic elution, solutes are eluted at the same binding strength as

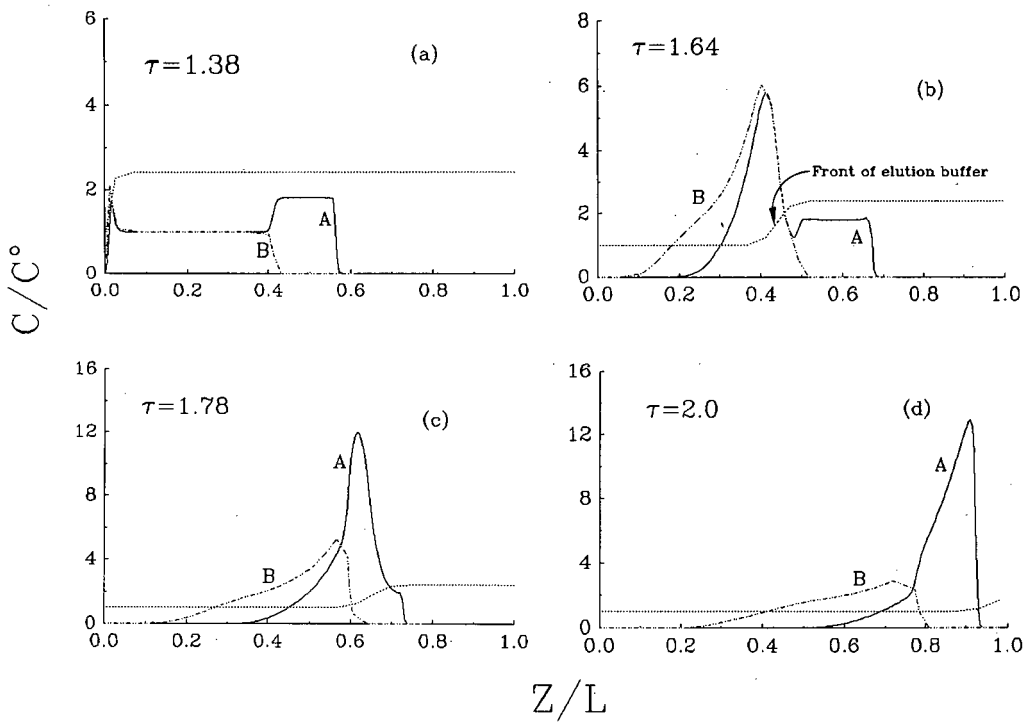

Fig. 3. Bed profiles for the step elution with 1.2–0.5 M variation range of modulator concentration. Load factor = 15%; S_f = 2.41; 1:1 binary mixture. Solid lines, solute A; dot-dashed lines, solute B; dotted lines, modulator.

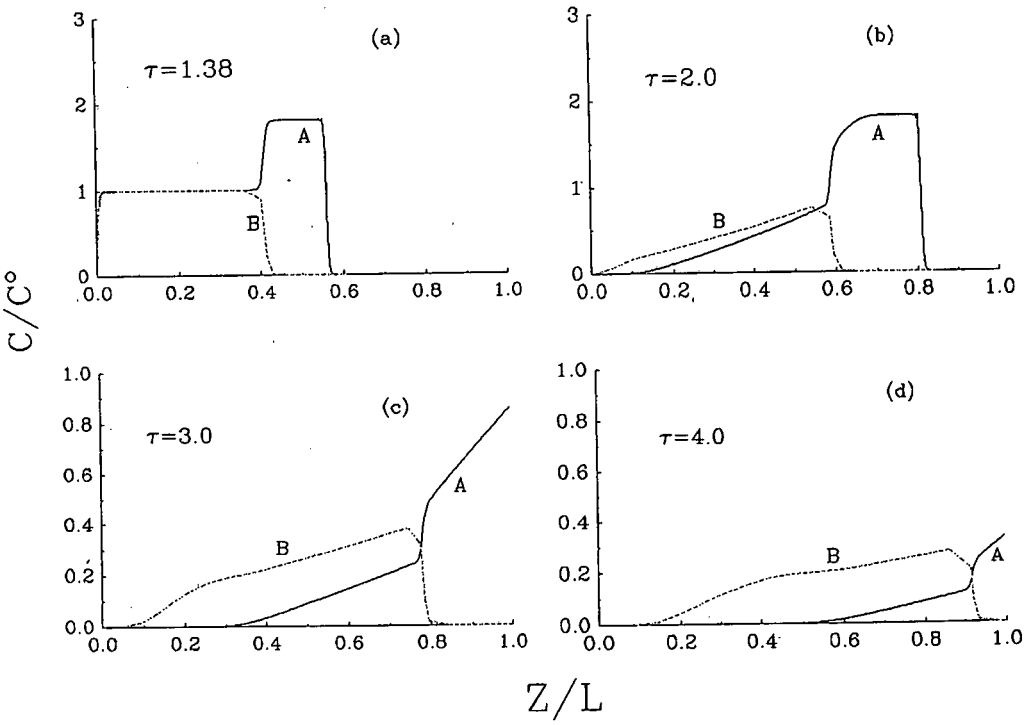

Fig. 4. Bed profiles for the isocratic under 1.2 M modulator concentration. Load factor = 15%; S_f = 2.41; 1:1 binary mixture. Solid lines, Solute A; dot-dashed lines, solute B.

that in the injection stage. The bed profiles in Fig. 4 show that more band spreading occurs as compared with that in Fig. 3, and the elution process takes a longer time to complete.

Unlike isocratic elution where the column is ready to introduce the next sample after the components of the previous sample have left the column, the column with step gradient elution must be returned to its initial conditions (equilibrated with the initial solvent) on completion of each gradient run. Therefore, the increase in production rate in step elution will be offset to some extent by the column regeneration. The regeneration time between successive runs depends largely on the physico-chemical mechanism governing the dependence of solute retention on the modulator. If no slow kinetics are involved in the regeneration process, the time for column re-equilibration is mainly controlled by the mass transfer of modulator between the mobile and stationary phases. This is true for the cases with a salt gradient in hydrophobic interaction and reversed-phase chromatography. As the diffusivity of modulators with small molecules is usually two orders of magnitude greater than those of proteins, the flow-rate used in the regeneration can be much higher than that in the elution stage. The regeneration can also be speeded up in some instances by using a reverse gradient [26]. The regeneration time for a system with a polar stationary phase, such as silica or alumina, could be as long as the elution time [27]. However, such polar packings are rarely used in the separation of proteins. It has been reported that the regeneration time for the reversed-phase chromatography of proteins is much less than the elution time and the initial solvent volume needed for the regeneration is less than the column volume [28]. If the initial solvent volume for regeneration is twice the column volume and the flow-rate for the regeneration is four times higher than that in the elution stage, then the regeneration time would be less than 20% of the elution time for the cases with a retention factor between 0.6 and 3. Because an actual increase in production rate by step elution is affected by the column regeneration, the advantage of step elution

is still significant only for the case where the production rate can be substantially increased by step elution. As we shall see later, the production rate in step elution with a dilute sample could be three times as high as that in isocratic elution. In such a case, step elution would be strongly favoured over isocratic elution even if the column regeneration time is as long as the elution time.

Effect of separation factor. So far our discussion is focused on a system with a separation factor of 2.41. Fig. 5 shows the results for a system with a lower separation factor of 1.41. The curves exhibit trends different from those observed in Fig. 1. The step height effect is significant only when the load factor is greater than 30%. The yield for the solute A also shows a different trend (Fig. 5b). The production rate of solute A (Fig. 5a) passes through a maximum and then decreases with increase in the load factor. Further, the plots in Fig. 5d show no difference in yields obtained by the different elution modes for the system with $S_f = 1.41$. Clearly, there is no significant advantage in using the step elution mode when the separation factor is low. Nevertheless, the situation can be improved for the system with dilute feed solution, as will be illustrated later.

With step elution, there exists a minimum for both the production rate and the yield of solute A, as shown in Fig. 5a and b. This phenomenon can be explained from the observations in Figs. 6 and 7. It is shown in Fig. 6 that the separation achieved during sample injection is not as good as that in Fig. 3 because of a weaker displacement effect resulting from a low value of S_f. The two peaks are simultaneously compressed at the earlier stage of the elution (the same as in Fig. 3), and then the peak of solute A becomes more concentrated owing to the displacement effect by solute B, while the peak of solute B exhibits a strong "tag-along" effect such that the front for solute B catches up with the front for solute A. This "catch-up" phenomenon only takes place for the case of a 20% load factor (Fig. 7b). In this case, the peak fronts are very close to each other as they approach the column exit. Therefore, no more time is available to allow further separation. However, for the case of a 10% load factor (Fig. 7a), a certain degree of separation is obtainable, although

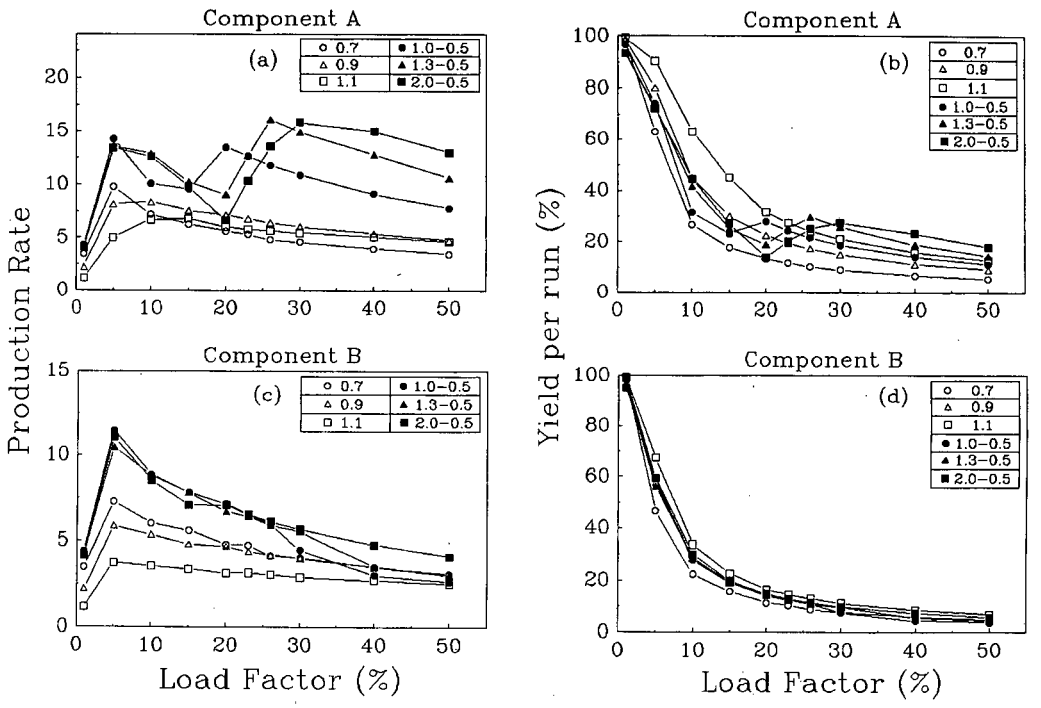

Fig. 5. Production rate and yield as a function of load factor in step elution and isocratic elution. $S_f = 1.41$; 1:1 binary mixture.

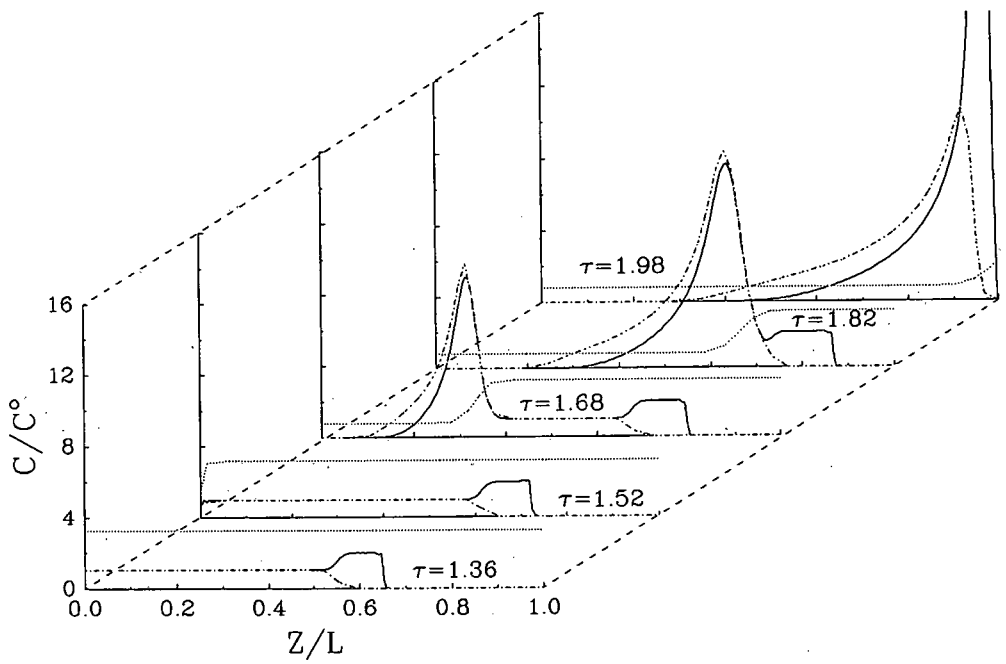

Fig. 6. Bed profiles for the step elution of 2.0–0.5 *M*. Load factor = 20%; S_f = 1.41; 1:1 binary mixture. Solid lines, solute A; dot-dashed lines, solute B; dotted lines, modulator.

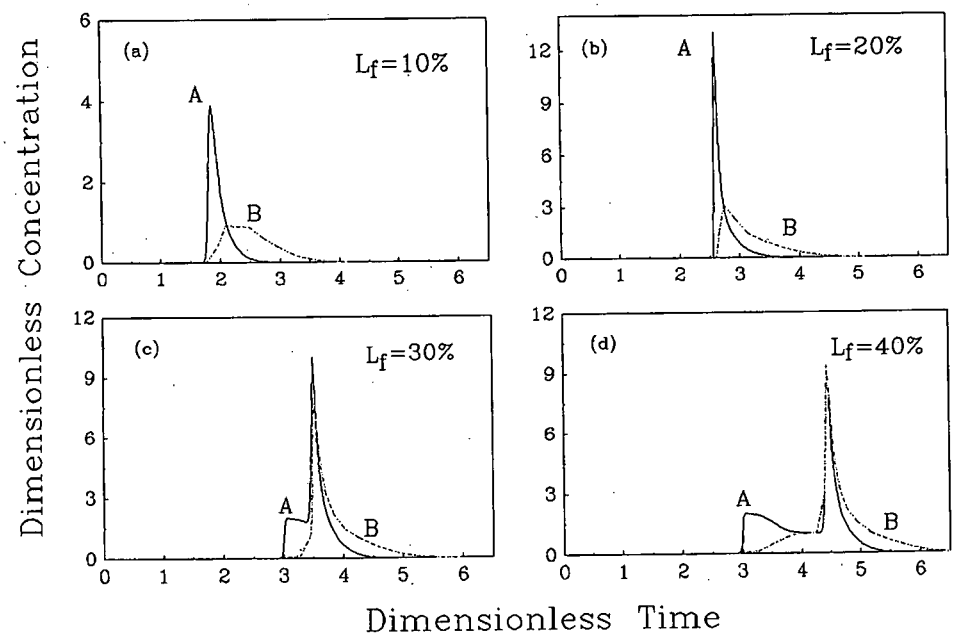

Fig. 7. Elution profiles under different load factors. S_f = 1.35; 1:1 binary mixture.

the fronts might have experienced to some extent the "catch-up" phenomenon. When the load factor is over 20%, the increase in production rate and yield for solute A is due to the result of the "roll up" peak generated by the displacement effect in the injection stage (Fig. 7c and d).

Effect of feed concentration. It is seen from Fig. 8 that step elution is particularly useful for increasing the production rate for the system with dilute feed solution (C_k^0 = 0.6 kg/m). This is also true for a system with a lower separation factor of 1.35, as illustrated in Fig. 9. The maximum production rates are nearly three times as high as those for isocratic elution. The optimum load factors for the maximum production rate (Figs. 8 and 9) are shifted to lower values compared with that in Fig. 1. When the separation factor is higher, the yield for both solutes in step elution with the optimum load factor is better than that in isocratic elution (see Fig. 8b).

It is obvious, by comparing Figs. 1 and 8, that a small volume of concentrated feed solution should be used whichever elution mode is applied. A similar conclusion was reported by Katti and Guiochon [5] in their analysis of preparative chromatography with isocratic elution. However, it is worth pointing out that process broths generally have low product concentrations and, hence, the application of step elution would be preferable. Further, the product can be more concentrated by step elution.

It is well known that for a dilute sample, application of the sample under low solvent strength (high retention) conditions leads to concentration of the sample at the top of the column, so that the band broadening associated with the sample volume is avoided. However, this practice is usually limited to the analytical application of liquid chromatography where the column is not overloaded. As shown in Figs. 8 and 9, the advantage of step elution can be seen only under overloaded conditions and the production rates for both elution modes are nearly the same with a low load factor. This also implies that effect of sample solvent strength is not significant in terms of preparative performance at small sample sizes.

Effect of feed composition. The simulation results for feed compositions (C_A^0/C_B^0) of 6:1 and 1:6 are

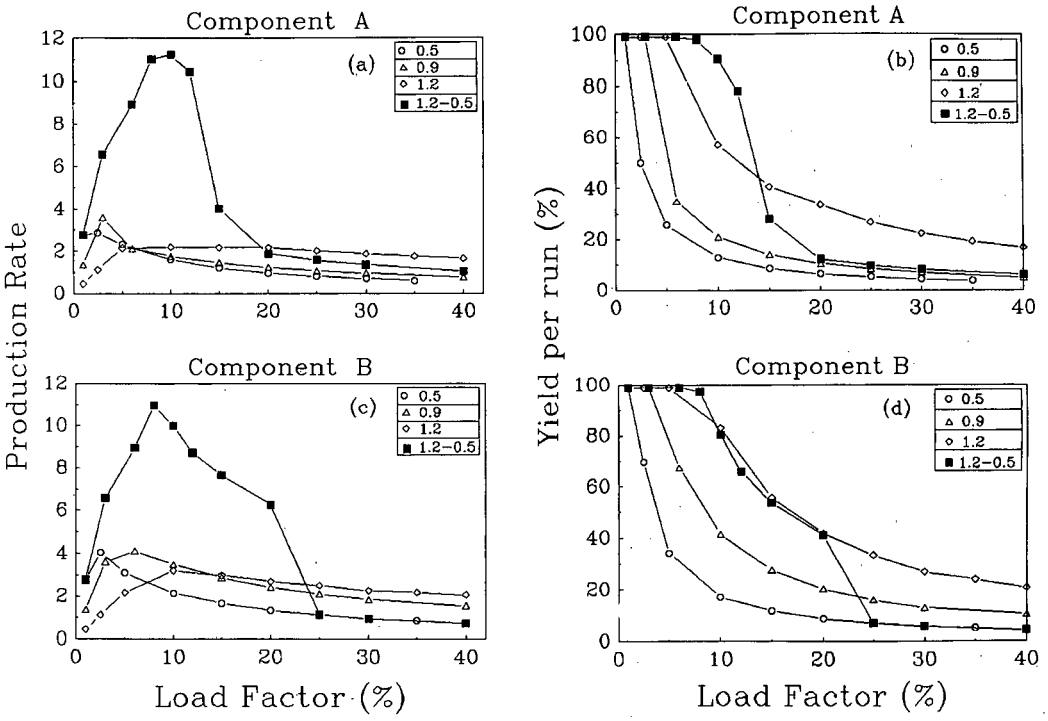

Fig. 8. Production rate and yield for the feed concentration of 0.6 kg/m^3 in solute. S_f = 2.41; 1:1 binary mixture.

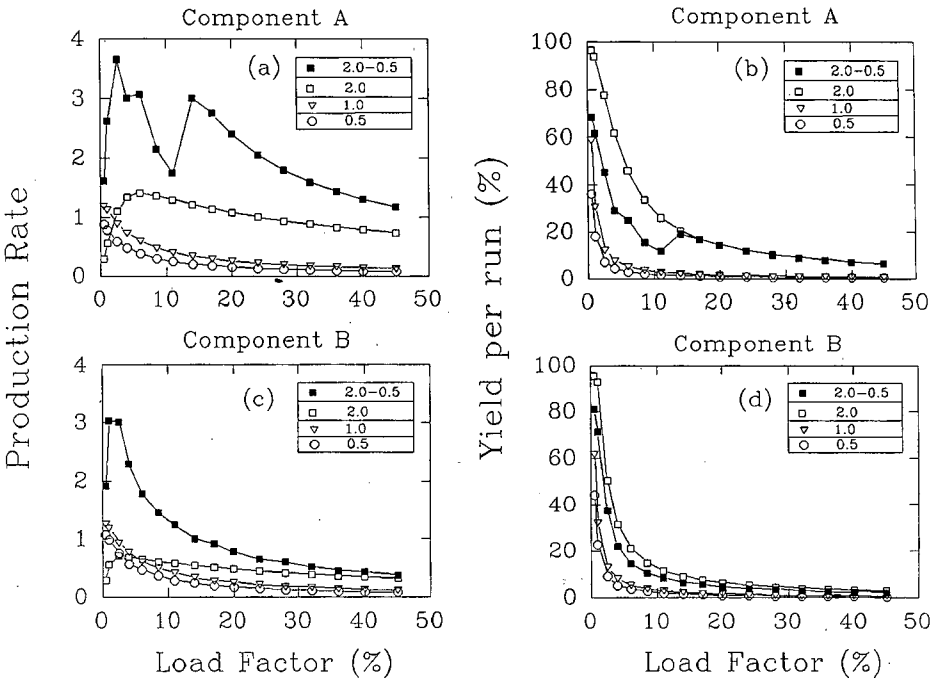

Fig. 9. Production rate and yield for the feed concentration of 0.6 kg/m^3 in solute. S_f = 1.41; 1:1 binary mixture.

shown in Figs. 10 and 11, respectively. It is seen that the improvement in the production rates with step elution is not influenced by the feed composition. The yield (with the optimum load factor for the maximum production rate) is the same as or just slightly lower than that in the corresponding isocratic elution. When the feed solution is rich in solute A (Fig. 10), the maximum production rate for solute A is increased whereas that for solute B is decreased, compared with those for the feed composition of 1:1, as shown in Fig. 1. If the feed solution is rich in solute B (Fig. 11), a trend opposite to that in Fig. 10 is observed.

Effect of mobile phase flow-rate. Simulation results for a superficial velocity of $5.0 \cdot 10^{-5}$ m/s are displayed in Fig. 12. The improvement in the production rate is still significant. It is obvious, by comparing Fig. 12 with Fig. 1, that the optimum sample size for maximum production rate for both solutes is decreased with an increase in the superficial velocity V_f, and the yield at $V_f = 5.0 \cdot 10^{-5}$ m/s is also reduced. Because of the low column efficiency resulting from the increase in V_f, the "catch-up" phenomenon occurs for the case with the step height of 2.0–0.5 M even though the separation factor S_f is 2.41 (Fig. 12a and b).

Comparison for system with variable V_f

Fig. 13 shows the simulation results for the system with a variable separation factor, in which the modulator concentration is varied from 1.3 to 0.5 M, and the corresponding S_f varies from 1.7 to 2.0. Although the separation factor with isocratic elution is higher than that in the loading stage of step elution with a step height of 1.3–0.5 M, it is seen that the curves show a general trend similar to Fig. 1. A significant improvement in the production rate of solute A can be achieved by step elution, whereas the improvement for solute B is relatively modest. The yield with the optimum load factor for the production rate is nearly the same as or better than the best case with isocratic elution.

Fig. 14 shows the simulation results for systems having convergent separation factors. In the case with the filled square symbol, the separation factor (S_f) varies from 1.55 to 1.06, corresponding to modulator concentrations from 1.3 to 0.5 M. For the case with the filled circle symbol, the modulator

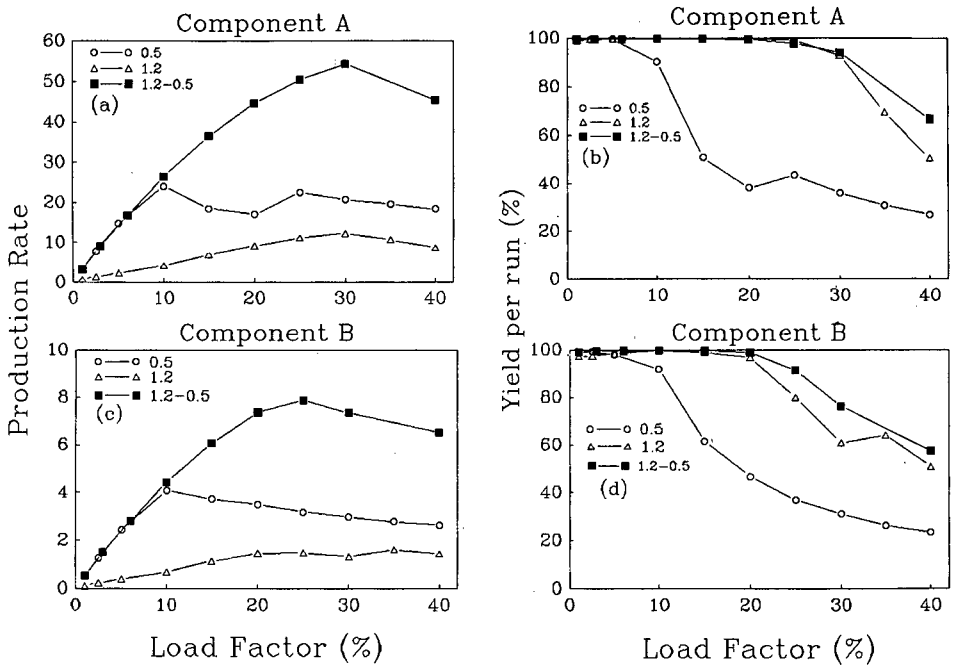

Fig. 10. Production rate and yield for the 6:1 (A:B) binary mixture. S_f = 2.41. Feed concentration: A = 4.2 kg/m^3; B = 0.7 kg/m^3.

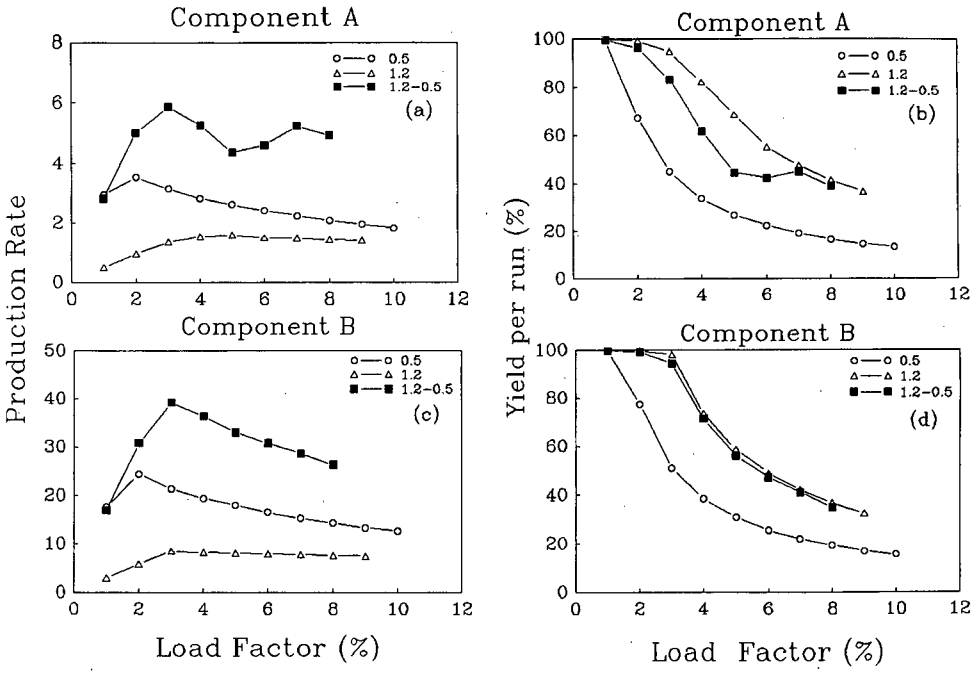

Fig. 11. Production rate and yield for the 1:6 (A:B) binary mixture. S_f = 2.41. Feed concentration: A = 0.7 kg/m^3; B = 4.2 kg/m^3.

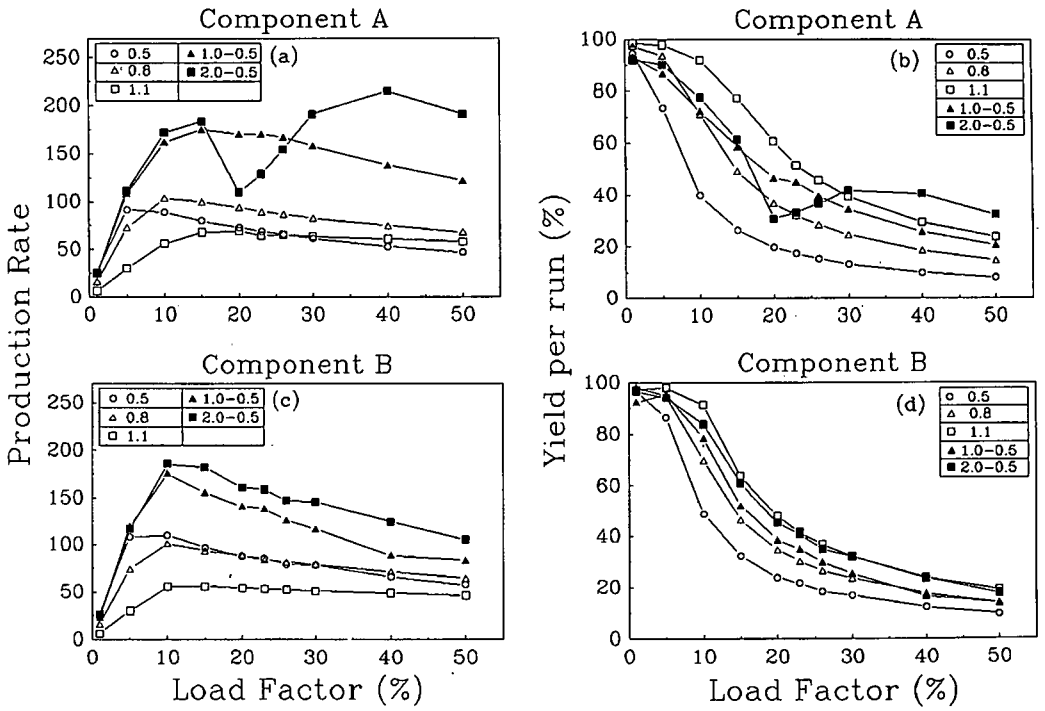

Fig. 12. Production rate and yield calculated at a superficial velocity of $5 \cdot 10^{-5}$ m/s. S_f = 2.41; 1:1 binary mixture.

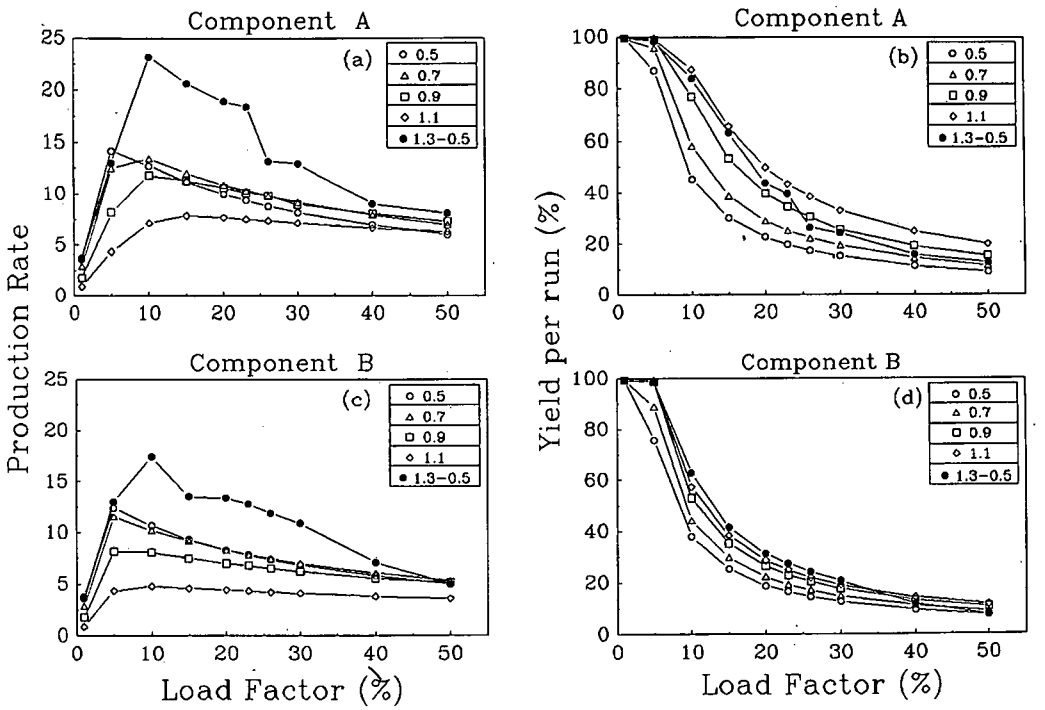

Fig. 13. Production rate and yield for the system having divergent S_f with changing the modulator concentration; 1:1 binary mixture.

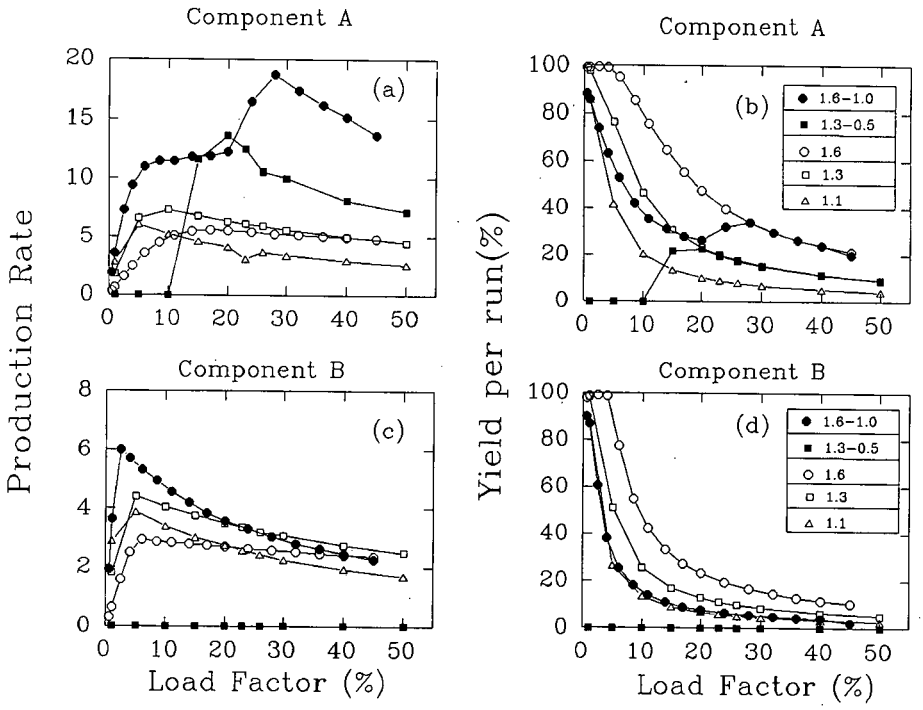

Fig. 14. Production rate and yield for the system having convergent S_f with changing the modulator concentration; 1:1 binary mixture.

concentration is changed from 1.6 to 1.0 M and the corresponding S_f varies from 1.7 to 1.38. Owing to the low S_f of 1.06 in the elution stage for the first case, solute A is not recovered until the column is overloaded to a certain extent. The separation obtained under overloaded conditions results from the front effect. It can be seen that for a low S_f of 1.06 in the elution stage step elution is unfavourable to the production of solute B. However, the improvement in the production rate by step elution is still significant in the second case (S_f = 1.7–1.38). Therefore, when both the initial and terminal S_f are not too low, step elution is superior to isocratic elution whether the separation factor is divergent or convergent with changes in the modulator concentration.

The simulation results reported here are based on the Langmuir competitive isotherm with a saturation capacity independent of modulator concentration, and are also subject to the system without modulator-dependent selectivity reversal. A practical system could follow any type of isotherm, where the separation factor may be dependent on solute and modulator concentrations. As a result, the extension of the conclusion to systems with other isotherms needs to be carefully checked. However, step elution should be still superior to isocratic elution if the following conditions are met by a given practical system: no selectivity inversion due to the changes in solute and /or modulator concentrations is involved; and the separation factor, depending on the solute and modulator concentrations, is not too low during operation.

CONCLUSIONS

A realistic model has been used to simulate step elution in preparative chromatography. In the simulation, a Langmuir competitive isotherm with a saturation capacity independent of modulator concentration has been assumed. The comparison of step elution with isocratic elution, as a function of load factor, shows that the preparative performance of liquid chromatography can be dramatically improved by using step elution for systems having a separation factor that is not too low over the defined range of the modulator concentration. The production rate and enrichment factor for both solutes in

step elution can be higher than those in isocratic elution, and the yield is also slightly improved or is comparable to that in isocratic elution. The maximum production rate achieved in step elution is increased with increase in separation factor. The increases in the production rate and the enrichment factor become significant when the feed solution is dilute. It should be noted that the increase in production rate with step elution would be offset by the column equilibration stage prior to the next run.

The selection of the operational sample size will depend on which solute is the target product and is also dependent on whether a maximum production rate is sought or a compromise between the production rate and the yield is desired. The optimum sample size for maximum production rate is influenced by the separation factor, feed concentration, feed composition and mobile phase flow-rate. With a favourable sample size, the higher the step height the better is the preparative performance of the step elution mode.

SYMBOLS

$b(k)$ Langmuir affinity constant of solute k
C_k^0 Feed concentration of solute k
C_k Concentration of solute k in macropore fluid
$C_{\mu k}$ Concentration of solute k in stationary phase
$C_{\mu s,k}$ Saturation capacity of solute k
$C_{b,k}$ Concentration of solute k in bulk phase
C_m Molar concentration of modulator in macropore fluid
C_r Reference concentration
d_p Particle diameter
$D_{AB,k}$ Molecular diffusivity of solute k
$D_{p,k}$ Effective diffusivity of solute k in particle
D_{bm} Molecular diffusivity of modulator
D_{pm} Effective diffusivity of modulator in particle
D_{ax} Effective axial dispersion coefficient
k_f Film mass transfer coefficient
l Solute l in the mixture.
L Column height
NC Total number of solutes in the mixture
R_0 Particle radius
r Radial coordinate
t Time
t_{inj} Sample loading duration time
t_0 Time scale
V_f Superficial velocity
V_r Reference superficial velocity
X Dimensionless radial coordinate
$Y(k)$ Dimensionless concentration of solute k in macropore fluid
$Y_b(k)$ Dimensionless concentration of solute k in bulk fluid phase
Y_b^0 Dimensionless concentration of feed solution
$Y_e(k)$ Dimensionless outlet concentration of solute k
$Y_\mu(k)$ Dimensionless concentration of solute k in stationary phase
Y_m Dimensionless concentration of modulator
Y_m^0 Dimensionless concentration of modulator in initial buffer
Y_m^e Dimensionless concentration of modulator in elution buffer
Z Axial coordinate

Greek letters

α Coefficient in eqn. 15
β Coefficient in eqn. 15
γ Coefficient in eqn. 15
ε_b Bed void fraction
ε_p Particle porosity
μ Viscosity of fluid
ρ Density of fluid
τ Dimensionless time
τ_c Dimensionless cycle time
τ_{inj} Dimensionless sample loading duration time

ACKNOWLEDGEMENT

M.M.H. acknowledges the support of the Australian NRF in the form of a fellowship.

REFERENCES

1 S. Ghodbane and G. Guiochon, *J. Chromatogr.*, 450 (1988) 27.
2 S. Golshan-Shirazi and G. Guiochon, *J. Chromatogr.*, 523 (1990) 1.
3 S. Ghodbane and G. Guiochon, *J. Chromatogr.*, 440 (1988) 9.
4 S. Ghodbane and G. Guiochon, *J. Chromatogr.*, 444 (1988) 275.
5 A. Katti and G. Guiochon, *Anal. Chem.*, 61 (1989) 982.
6 S. Ghodbane and G. Guiochon, *J. Chromatogr.*, 452 (1988) 209.
7 S. Golshan-Shirazi and G. Guiochon, *Anal. Chem.*, 61 (1989) 1368.

8 G. Cretier, L. Macherel and J. L. Rocca, *J. Chromatogr.*, 590 (1992) 175.
9 L. R. Snyder, J. W. Dolan and G. B. Cox, *J. Chromatogr.*, 484 (1989) 437.
10 L. R. Snyder, J. W. Dolan and G. B. Cox, *J. Chromatogr.*, 540 (1991) 21.
11 L. R. Snyder, G. B. Cox and P. E. Antle, *J. Chromatogr.*, 444 (1988) 303.
12 F. D. Antia and Cs. Horváth, *J. Chromatogr.*, 484 (1989) 1.
13 G. B. Cox and L. R. Snyder, *J. Chromatogr.*, 590 (1992) 17.
14 S. Yamamoto, M. Nomura and Y. Sano, *J. Chromatogr.*, 512 (1990) 89.
15 S. Yamamoto, K. Nakanish and R. Matsuno, *Ion-Exchange Chromatography of Proteins*, Marcel Dekker, New York and Basle, 1988.
16 S. Yamamoto, M. Nomura and Y. Sano, *Chem. Eng. Sci.*, 47 (1992) 185.
17 S. G. Foo and R. G. Rice, *AIChE J.*, 54 (1975) 1149.
18 S. F. Chung and C. Y. Wen, *AIChE J.*, 14 (1968) 857.
19 P. Jandera and G. Guiochon, *J. Chromatogr.*, 588 (1991) 1.
20 W. R. Melander, Z. E. Rassi and Cs. Horváth, *J. Chromatogr.*, 469 (1989) 3.
21 T. Gu, Y.-H. Truei, G.-T. Tsai and G. T. Tsao, *Chem. Eng. Sci.*, 47 (1992) 253.
22 C. F. Carey and B. A. Finlayson, *Chem. Eng. Sci.*, 30 (1975) 587.
23 L. R. Petzold, *A Description of DASSL: a Differential/Algebraic System, Solver,* Technical Report, Sand81-8637, Sandia, CA, 1982.
24 T. Gu, G. T. Tsao, G. Tsao and M. R. Ladisch, *AIChE J.*, 36 (1990) 1156.
25 S. Jacobson, S. Golshan-Shirazi, A. M. Katti, M. Czok, Z. Ma and G. Guiochon, *J. Chromatogr.*, 484 (1989) 103.
26 H. Engelhardt and H. Elgass, *J. Chromatogr.*, 112 (1975) 415.
27 H. Engelhardt and H. Elgass, in Cs. Horváth (Editor), *High-Performance Liquid Chromatography — Advances and Perspectives*, Vol. 2 Academic Press, New York, 1980, pp. 57–111.
28 Y.-B. Yang, K. Harrison and D. Carr, *J. Chromatogr.*, 590 (1992) 35.

Journal of Chromatography, 605 (1992) 193–198
Elsevier Science Publishers B.V., Amsterdam

CHROM. 24 235

Application of colloidal gold for characterization of supports used in size-exclusion chromatography

Martin Holtzhauer

Central Institute of Molecular Biology, Department of Chemistry, Robert Rössle Strasse 10, D(O)-1115 Berlin-Buch (Germany)

Michael Rudolph

Central Institute of Cancer Research, Department of Virology, Robert Rössle Strasse 10, D(O)-1115 Berlin-Buch (Germany)

(First received November 7th, 1991; revised manuscript received March 31st, 1992)

ABSTRACT

Calibration of matrices for size-exclusion (gel permeation) chromatography (SEC) has to be done for the characterization of supports with inert pores and to allow the determination of the molecular masses of macromolecules. It has been shown by several groups that for steric reasons SEC is very sensitive to conformational details of macromolecules (*e.g.*, rods or random coils). Therefore, no set of particles, organic macromolecules or biomacromolecules such as proteins exists which is universally applicable for calibration and characterization of chromatographic supports. It is shown that colloidal gold, which behaves in SEC as macromolecules, offers the advantage of hydrophilic particles with ideally spherical form and easily measured diameters. Therefore, collodial gold can be used for monitoring of the SEC process at the electron microscopic level, for the characterization of supports (determination of pore size) and for the determination of exclusion limits of matrices.

INTRODUCTION

Size-exclusion chromatography (SEC) or gel permeation chromatography is a widely used method in analytical and preparative macromolecular chemistry and biochemistry. In a conventional model the assumption is made that SEC is based on partition of macromolecules (solutes) dissolved in the mobile phase in pores of a macroporous support (stationary phase). In a simplified case, this partition depends only on the sizes of the macromolecule and the pores, respectively.

For the characterization of macromolecules or supports, all the solute particles in the mobile phase should have the same shape and should not interact with the matrix, *e.g.*, by ionic or hydrophobic forces. Further, the pores of the matrix should be tubes or caves of uniform cross-section. However, in reality, these criteria are not fulfilled completely. Especially biomacromolecules differ from spherical geometry, even under denaturing conditions (application of buffers with high concentrations of urea or guanidinium hydrochloride), and can change their structure during interaction with the matrix as a consequence of the flexibility of the chain of their elements. Denaturation of proteins by sodium dodedyl sulphate (SDS) mostly converts the more or less globular proteins into rod-like particles, which have much higher Stokes radii than the non-denatured forms and therefore show lower abolute distribution coefficients (K_D) than the native species [1].

Correspondence to: Dr. Martin Holtzhauer, Max-Delbrück-Centrum für Molekulare Medizin, Robert-Rössle-Strasse 10, D(O)-1115 Berlin-Buch, Germany.

0021-9673/92/$05.00

Several attempts have been made to correlate size parameters such as Stokes radii with chromatographic behaviour in SEC [1–3]. In particular, no universal correlation exists between molecular mass (M_r) and Stokes radius (R_s) or between K_D and R_s. To fit the equation $R_s = aM_r^b$, different coefficient a and b were found for dextrans, polyethylene glycols, polyethylene oxides, spherical proteins [4] and inorganic colloids (aluminosilica sols) [5]. Whereas calibration of SEC columns for M_r determination of synthetic polymers with uniform monomers fulfils the theoretical considerations [6], especially at low polymer concentrations, in the area of biomacromolecules the determination of M_r from SEC data is possible only when the unknown and the calibration standards have the same shape under the distinct experimental conditions.

Values for exclusion limits and pore sizes depend strongly on the (bio)macromolecules used for the determination. Theoretical considerations discriminate between hard-sphere solutes, rods and random-flight chains, which interact differently with the pores of a support [7]. Therefore, for the characterization of SEC gels in aqueous mobile phases, standards which are similar and unchangeable in size and shape and which can be simply monitored would be useful.

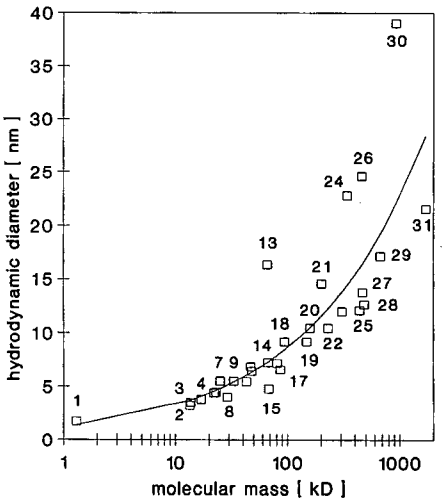

Fig. 1. Plot of hydrodynamic diameter *versus* molecular mass for several macromolecules used in SEC calibration. Macromolecules: 1 = cobalamin; 2 = cytochrome *c*; 3 = RNase II-A; 4 = myoglobin; 5 = trypsininhibitor; 6 = chymotrypsinogen A; 7 = ovomucoid; 8 = carbonic anhydrase; 9 = β-lactoglobulin; 10 = ovalbumin; 11 = Triton X-100 (detergent, micelle); 12 = $C_{12}E_8$ (detergent, micelle); 13 = tropomyosin; 14 = serum albumin; 15 = haemoglobin; 16 = transferrin; 17 = alkaline phosphatase; 18 = tyrosyl-tRNA synthetase; 19 = aldolase; 20 = immunoglobulin G; 21 = α-actinin; 22 = catalase; 23 = aspartate transcarbamylase; 24 = fibrinogen; 25 = ferritin; 26 = spectrin (dimer); 27 = β-galactosidase; 28 = urease; 29 = thyroglobulin; 30 = spectrin (tetramer); 31 = haemocyanin. Data from refs. 1, 2, 8 and 9. kD = kilodalton.

Fig. 1. demonstrates the deviations from a narrow correlation (non-linear regression curve) of molecular mass and hydrodynamic diameter for (bio)macromolecules, frequently used in SEC calibration. These deviations suggest that especially for proteins the M_r determined by SEC should be interpreted very carfully and compared with values obtained by independent methods such as electrophoresis (Ferguson plot analysis), light scattering, viscosimetry, etc.

Application of colloidal gold can overcome some of the disadvantages of organic macromolecules, because the gold particles can be produced as ideal hard-sphere particles, their diameters are easily measurable by electron microscopy, they can be used in aqeuous suspensions and they cannot alter their shape when interacting with the matrix. However, for the determination of molecular masses of biopolymers other standards and distinct correlations are needed.

EXPERIMENTAL

Materials

The supports used were Sepharose 4B (Pharmacia LKB, Uppsala, Sweden) and beaded cellulose Divicell, 80–200 μm (Leipziger Arzneimittelwerk, Leipzig, Germany). A 1% aqueous solution of $HAuCl_4$ was obtained from Feinchemie (Sebnitz, Germany), polyethylene glycol (PEG) 20000, trisodium citrate, tannic acid, bovine serum albumin (BSA) and dinitrophenylalamine (DNP-Ala) were obtained from Serva (Heidelberg, Germany) and Blue Dextran 2000 from Pharmacia (Freiburg, Germany). Chromatography was performed at room temperature in 40 × 1 cm I.D. glass columns using a P1 peristaltic pump and a Uvichord SII UV monitor (Pharmacia). Colloidal gold of different size was prepared according to ref. 10 and was used without further purification.

Methods

Chromatography was done in doubly distilled water containing 0.05% (w/v) PEG 20000 and 0.02% (w/v) of NaN_3, and was monitored at 280 nm. Linear flow-rates were 23.8 cm/h for Divicell and 3.0 cm/h for Sepharose 4B. The sample volume was 1.0 ml, containing 1 absorbance unit of each probe.

For electron microscopy, the beaded cellulose was loaded with the appropriate gold colloid, then it was lyophilized and the spheres were directly embedded in Epon 812. Sections were cut with glass knives on a Ultratome III (LKB). For size determination of colloidal gold, it was spread on 3-mm grids without fixation. Electron microscopic examinations were made on a JEM 100 CX electron microscope (JEOL, Tokyo, Japan).

RESULTS AND DISCUSSION

Fig. 2 shows the electron micrographs of two different colloidal gold preparations. Their photometric properties are given in Table I. Especially the larger material (particle diameter 14 ± 1 nm, Fig. 2A) appears in the electron micrograph as regular spheres. Their homogeneous size distribution is reflected in SEC with both Divicell and Sepharose (Fig. 3A and B, respectively). As shown in Fig. 4, the distribution coefficients (K_{av}) values of gold particles vary linearly with the particle diameter when spheres with diameters from 4 to 14 nm were used. The hydrodynamic diameter and the distribution coefficient of BSA as an example of a globular protein fit this plot of particle diameter *vs.* K_{av} but, as discussed earlier, this cannot be generalized.

The inhomogeneity in size of the gold preparation of 4-nm mean diameter, as shown in the electron micrographs (Figs. 2B and 5B), is reflected in SEC. On both Divicell (Fig. 3A) and Sepharose (Fig. 3B) the relatively large portion of bigger grains appears as an early peak in the chromatograms.

In Fig. 5, the principle of gel filtration becomes visible: exclusion or low penetation of the large gold particles and deep penetration of the smaller particles into the chromatographic matrix (beaded cellulose). As a real SEC matrix contains pores with a non-uniform distribution of diameters and the diffusion rate is inversely proportional to the molecular radius, differently sized particles can penetrate the matrix more or less and prolong the time needed to leave the column.

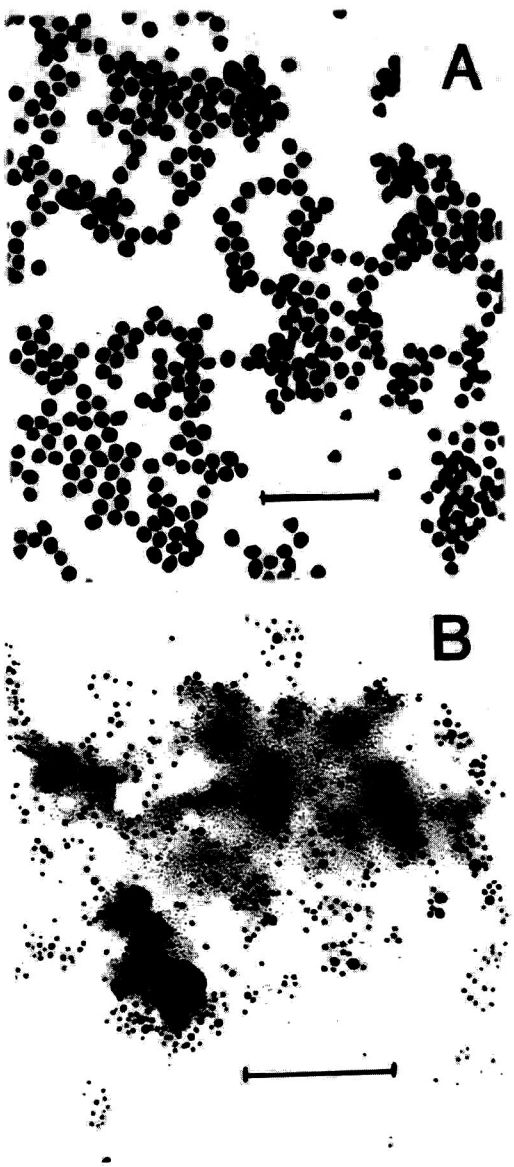

Fig. 2. Electron micrographs of colloidal gold preparations (original magnification × 85 000). (A) Particle diameter 14 ± 1 nm, larger particles up to 28 nm < 5%; (B) particle diameter 4 ± 1.5 nm, larger particles up to 10 nm ≈ 20%. Bars represent 100 nm.

TABLE I

ABSORPTION COEFFICIENTS OF COLLOIDAL GOLD PREPARATIONS

The values obtained are combinations of light absorption and scattering, but registered as absorptions in the two-beam photometer used. Values calculated for 0.1 mg/ml of Au, 1 cm path length.

Sample[a]	$A_{280\ nm}$	$A_{\lambda max}$	λ_{max} (nm)
Au_4	3.505	0.975	515
Au_6	1.841	0.881	526
Au_{10}	1.291	1.133	519
Au_{14}	0.801	0.852	520

[a] Subscripts are mean particle diameters (nm).

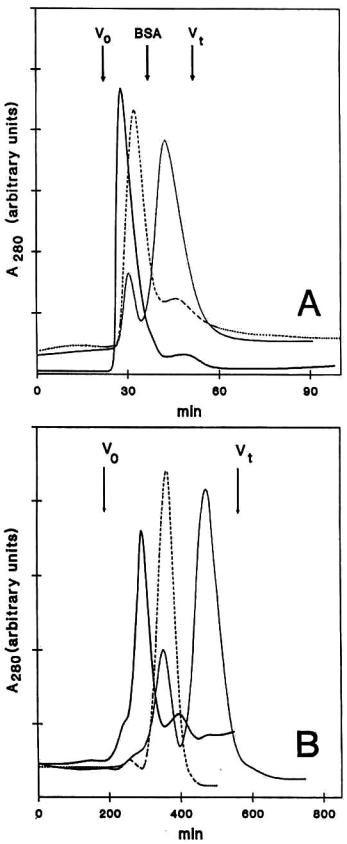

Fig. 3. SEC of colloidal gold on (A) Divicell (beaded cellulose) and (B) Sepharose 4B (beaded agarose). Elution profiles for the respective gold sols: solid lines, Au_{14}; dashed lines, Au_{10}; dotted lines, Au_4 (subscripts represent the mean particle diameters in nm). V_0, elution volume for Blue Dextran 2000 (void volume); BSA, elution volume for bovine serum albumin; V_t, elution volume for DNP-Ala. (total volume).

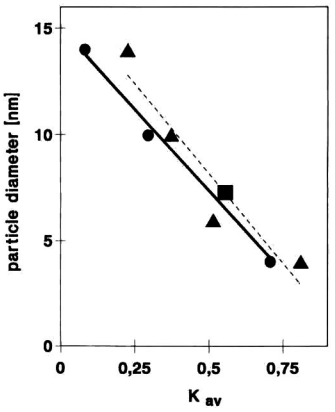

Fig. 4. Plot of K_{av} *versus* particle diameter for colloidal gold, estimated on Divicell (●, solid line) and Sepharose 4B (▲, dotted line). ■ = Respective hydrodynamic and K_{av} values for BSA, run on the same column.

Although, in the uncontrasted electron micrograph, the matrix is only poorly visible, in Fig. 5A it is clearly demonstrated that the large gold particles (Au_{14}) are located at or near the surface. In contrast, the small gold particles (Au_4) are also found in deeper layers of the matrix. Fig. 5C illustrates schematically the principle of the electron micrographs. Hence these figures visualize the principle of gel filtration.

Another interesting effect, first observed in affinity chromatography, can also be seen in Fig. 5B, *viz.*, the density of the gold particles decreases in the direction from the surface to the centre of the cellulose bead. This formation of a "shell" has been found, for instance, when antibodies [11] and enzymes [12] were covalently immobilized on chromatographic supports. Probably this shell may be influenced by the concentration of the solute and/or the flow-rate of the eluent, and its existence could indicate that in a real experiment equilibrium of the solute distribution between the mobile and stationary phases is not reached.

Laboratory-made or commercially available gold particles with diameters ranging from 5 to 30 nm offer the opportunity of determining exact pore size distributions of hydrophilic gels and therefore of true exclusion limits (particle sizes excluded from the matrix). Previously, this was mostly done by using synthetic polymers such as polystyrenes or dextrans [13] or by calibration with globular pro-

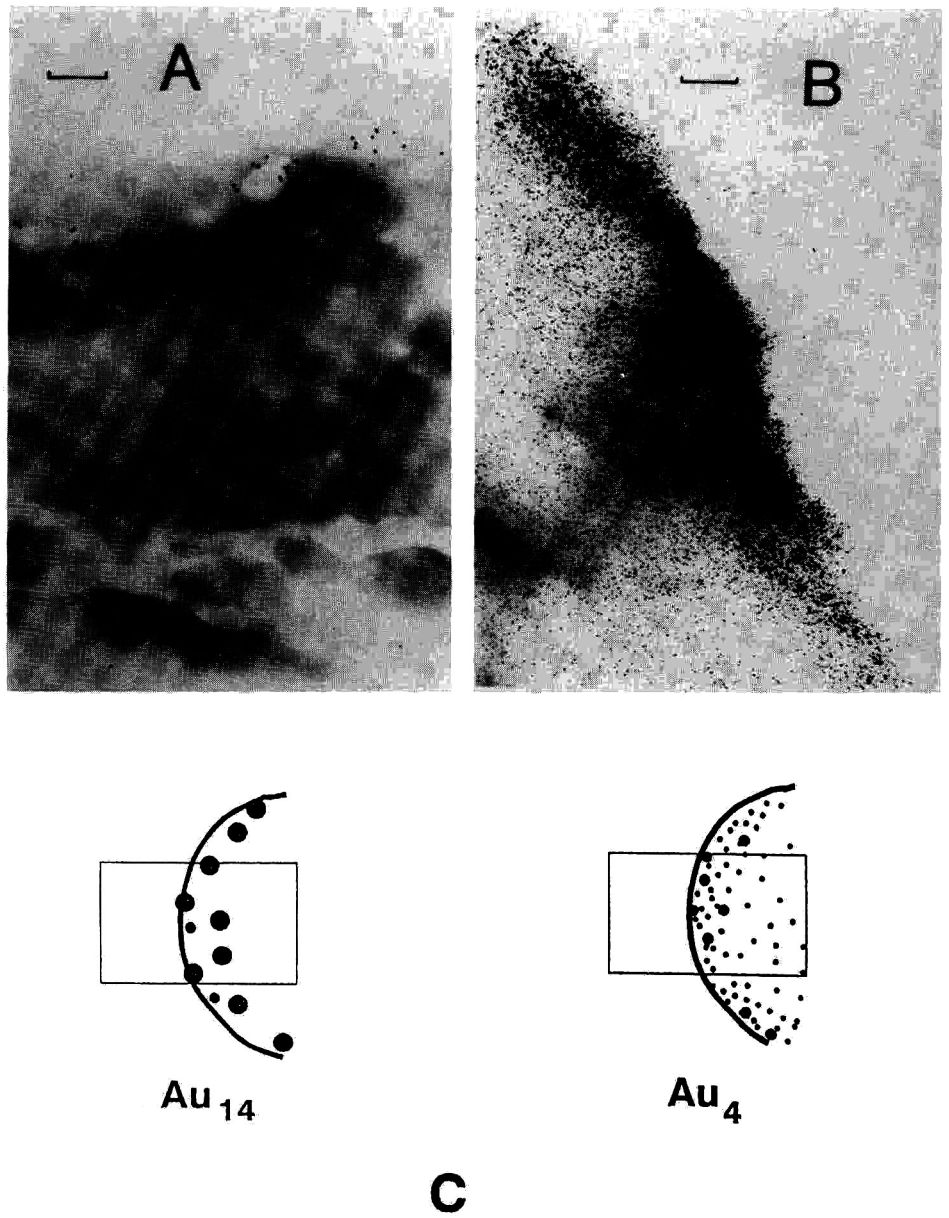

Fig. 5. Transmission electron micrograph (original magnification × 58 000) of partial exclusion of larger particles (mean diameter 14 nm) from Divicell beads (A) and complete penetration of colloidal gold (mean diameter 4 nm) into the matrix (B). (C) Schematic representation of (A) and (B), respectively. The rectangles illustrate the cut of the surface area of cellulose beads as shown in (A) and (B). Bars represent 200 nm.

teins. Calibration with organic macromolecules suffers from the flexibiliy of the macromolecular structures [7], their differing deviations from spherical shape and from several possible types of interactions with the chromatographic matrix. Colloidal metals allow some of these unwanted side-effects to be overcome and the chromatographic behaviour of the colloid and of the matrix can be monitored by (electron) microscopy.

Limitations on the use of colloidal metals are set

by their salt sensitivity, which is a consequence of electrostatic repulsive forces making a sol possible and which requires working at very low ionic strengths. However, as matrices such as beaded cellulose (Divicell) or agarose (Sepharose) contain only very few negatively charged groups, exclusion of (negatively charged) gold sol from pores with diameters in the range of particle diameters is not very probable.

Stabilization of gold colloids by adsorption of proteins or other polar macromolecules is accompanied by an increase in the hydrodynamic diameters [14], which are then not determined as simply as for the pure particles. Further, because this coating is the result of an equilibrium between coated particles and free macromolecules, this macromolecular shell has to be maintained during the whole chromatographic process. Moreover, using a mobile phase as described under Experimental, the simple procedure, the easy monitoring and the general applicability to diverse hydrophilic gels make the use of colloidal metals, especially colloidal gold, recommended for the characterization fo SEC columns, but the problem of calibration for molecular mass determinations of proteins has not been solved, because it is established in the diversity of biopolymers.

CONCLUSIONS

The application of collodial gold for the characterization of SEC supports has advantages and disadvantages compared with other materials used for calibration in SEC. The main disadvantages are chromatographic applicability only at low ionic strengths and the impossibility of determining molecular masses in a simple way from chromatographic data as discussed above. As with other calibration standards, this is possible only if the standard and the unknown sample have the same geometry–molecular mass relationship. The advantages of colloidal gold, which behaves in SEC like a homogenous population of an organic macromolecule, are the easily determined diameter of the gold particles, the homogeneity of the diameter in a given preparation or the possibility of determining the size distribution by electron microscopy, the chemical stability in aqueous solutions and the simple monitoring of the chromatographic process by measuring the optical density in the UV or visible wavelength range.

REFERENCES

1 M. le Maire, A. Viel and J. V. Møller, *Anal. Biochem.*, 177 (1989) 50.
2 M. le Maire, L. P. Aggerbeck, C. Monteilhet, J. P. Andersen and J. V. Møller, *Anal. Biochem.*, 154 (1986) 525.
3 F. Cabré, E. I. Canela and M. Canela, *J. Chromatogr.*, 472 (1989) 347.
4 S. Hagel, in P. L. Dubin (Editor), *Aqueous Size-Exclusion Chromatography*, Elsevier, Amsterdam, 1988, p. 119.
5 J. J. Kirkland, *J. Chromatogr.*, 185 (1979) 273.
6 W. W. Yau, J. J. Kirkland and D. D. Bly, *Modern Size-Exclusion Liquid Chromatography*, Wiley, New York, 1979, pp. 285–313.
7 W. W. Yau, J. J. Kirkland and D. D. Bly, *Modern Size-Exclusion Liquid Chromatography*, Wiley, New York, 1979, pp. 31–42.
8 M. le Maire, A. Ghazi, J. V. Møller and L. P. Aggerbeck, *Biochem. J.*, 243 (1987) 399.
9 M. Potschka, *Anal. Biochem.*, 162 (1987) 47.
10 J. W. Slot and H. J. Geuze, *Eur. J. Cell Biol.*, 38 (1985) 87.
11 E. Sada, S. Katoh, A. Kondo and A. Kiyokawa, *J. Chem. Eng. Jpn.*, 19 (1986) 502.
12 J. Lasch, R. Koelsch, S. Weigel, K. Blana and J. Turková, in T. C. J. Gribnau, J. Visser and R. J. F. Nivard (Editors), *Affinity Chromatography and Related Techniques*, Elsevier, Amsterdam, 1982, p. 245.
13 A. A. Gorbunov, L. Ya, Solovyova and V. A. Pasechnik, *J. Chromatogr.*, 448 (1988) 307.
14 S. R. Simmons, R. M. Albrecht, *Scanning Microsc., Suppl.*, 3 (1989) 27–34.

Journal of Chromatography, 605 (1992) 199–204
Elsevier Science Publishers B.V., Amsterdam

CHROM. 24 133

Application of amino acid-bonded silicas as ion exchangers for the separation of anions by single-column ion chromatography

P. N. Nesterenko

Department of Analytical Chemistry, Lomonosov State University, 119899 Moscow (Russia)

(First received November 21st, 1991; revised manuscript received February 25th, 1992)

ABSTRACT

Different silica-immobilized amino acids were examined for use as stationary phases in single-column ion chromatography. Cation-exchange properties were established for phases with secondary amino groups (L-Arg-SiO_2; L-Val-SiO_2; L-Tyr-SiO_2) and anion-exchange properties for phases with tertiary amino groups (L-Hypro-SiO_2; L-Pro-SiO_2). The correlations between retention times of inorganic anions, concentrations of carboxylic acid (oxalic, citric, acetic, succinic, tartaric) and pH of the eluents were determined.

INTRODUCTION

Although single-column anion-exchange chromatography has been widely used in practice, there are several demands connected with this technique. One constraint is the requirement for further improvements in the efficiency and selectivity of separations. The most progress in this direction has ensued from the application of agglomerated ion exchangers with an opposite charged surface layer [1]. Such an ion-exchange structure provides rapid mass transport and consequently high efficiency, in addition to good selectivity towards anions.

Another promising approach is in the utilization of stationary phases with immobilized zwitterionic molecules on the surface of a suitable matrix, *e.g.*, silica gel. α-Amino acids are the simplest available molecules of this type which are easily attached to a silica surface. Amino acid-bonded silicas are widely used in ligand-exchange [2], metal chelate [3] and affinity chromatography [4]. However, their ion-exchange properties have not been investigated in detail. A detailed study of the use of iminodiacetic acid-bonded silica for the ion-chromatographic separation of alkali, alkaline earth and transition metal ions has been described [5,6]. In a previous paper [7] the ion chromatographic separation of inorganic anions on an L-hydroxyproline-bonded silica gel column was reported. In this study, several silica-based materials were examined for use as stationary phases in anion-exchange chromatography and the eluent variables that affect the retention of anions were also studied.

EXPERIMENTAL

The equipment used included a Beckman Model 114M pump, a Rheodyne Model 7125 injection valve with a 20-μl loop and an LKB conductivity detector. The chromatographic columns (250 × 4 mm I.D.) were all slurry packed. The column packings were L-valine, L-tyrosine- and L-arginine-bonded silica (Silasorb Si 300, 7.5 μm; Lachema, Brno, Czechoslovakia) and L-hydroxyproline- and L-proline-bonded silica (KSK-1, 5 μm; Reakhim, Mos-

Correspondence to: Dr. P. N. Nesterenko, Department of Analytical Chemistry, Lomonosov State University, 119899 Moscow, Russia.

0021-9673/92/$05.00

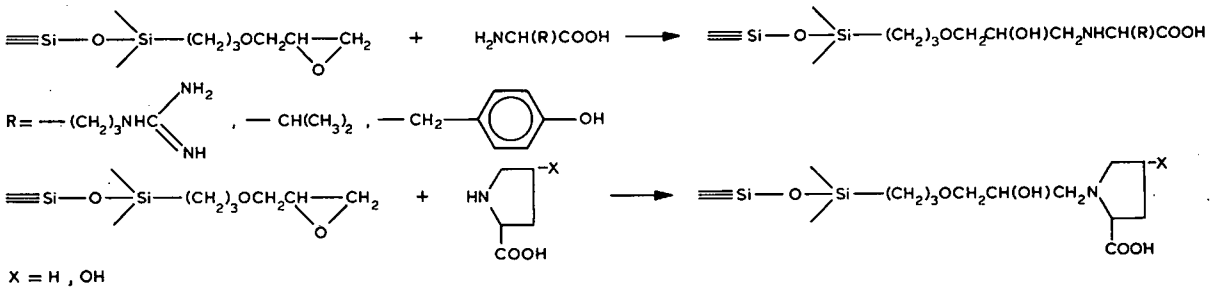

Scheme 1.

cow, Russia). They were prepared via an initial 3-glycidoxypropyltriethoxysilane surface modification followed by amino acid attachment as described [8]. The eluents were citric, oxalic, acetic, succinic and malonic acids; 1 *M* sodium hydroxide was added to adjust the pH.

RESULTS AND DISCUSSION

Ion-exchange properties of amino acid-bonded silicas

It is evident that the main point for consideration of amino acid-bonded silicas as stationary phase in ion chromatography will be the acid–base properties of the ion-exchange sites. Unfortunately, their evaluation is difficult for the following reasons:

(1) It has been established that the basicity of the silica-bound nitrogen-containing ligands decreased drastically in comparison with homogeneous analogues owing to interaction with silanol groups [9].

(2) There is not much difference in protolytic ability between silica-bound carboxylic acids and their homogeneous analogues [10].

(3) The basicity of the α-amino groups in amino acids after amino linkage to a 3-glycidoxypropyl spacer anchored to the silica surface as shown in Scheme 1 can also be altered. The primary amino groups (L-Val, L-Arg, L-Tyr) become secondary and the secondary amino groups (L-Pro, L-Hypro) become tertiary in attached form.

(4) The possible formation of an inner salt be-

TABLE I

p*K* VALUES FOR IONIZABLE GROUPS OF SOME α-AMINO ACIDS

Amino acid	Structure	pK_1	pK_2	pK_3
Arginine	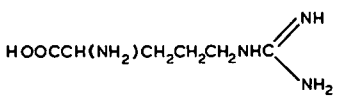	2.18	9.04	12.48
Valine	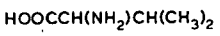	2.32	9.62	
Tyrosine	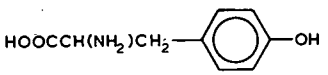	2.20	9.11	
Proline	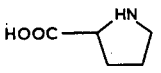	1.93	10.60	
Hydroxyproline	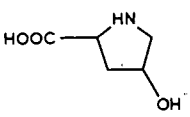	1.92	9.73	

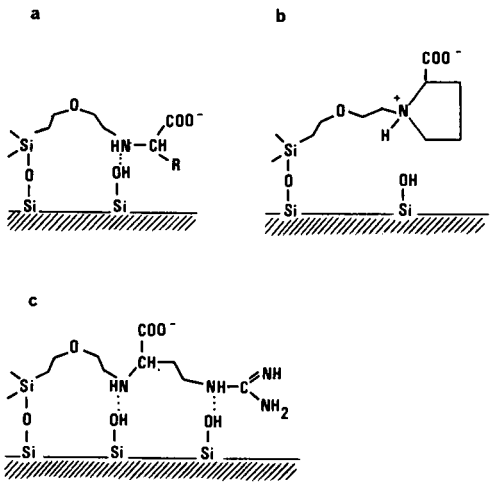

Fig. 1. Possible interaction of bonded amino acids with silanols. (a) L-Val-SiO_2; (b) L-Pro-SiO_2; (c) L-Arg-SiO_2.

tween amino and carboxyl groups can occur in neutral or weakly acidic media at low ionic strength.

L-Valine, L-arginine, L-tyrosine, L-proline and L-hydroxyproline were chosen as ion-exchange sites in accordance with the different acid–base properties of ionogenic groups and side-chain structure (Table I). L-Arginine, L-proline and L-hydroxyproline when bonded to silica can be expected to reveal strong anion-exchange properties owing to the high value of pK_2 for secondary amino groups and pK_3 for a side-chain guanidino functional group. L-Val-SiO_2 and L-Tyr-SiO_2 were used for comparison with the above.

As would be expected, L-Pro-SiO_2 and L-Hypro-SiO_2 confirmed our supposition. On the other hand, it was established that L-Arg-SiO_2 can be considered mainly as a cation exchanger and only a poor separation of chloride, perchlorate and sulphate was achieved with dilute malonic acid as eluent. It was possible to separate alkali metal ions on a column packed with this type of bonded phase. According to our results, L-Val-SiO_2 and L-Tyr-SiO_2 can be characterized as pure cation exchangers. This can be explained from the point of view of the effect of the α-amino group on ion-exchange properties. The main peculiarity of α-amino acids is in the presence of a definite internal acid–base relationship between carboxyl and amino groups: the greater is the protonation constant of the α-amino group in a free amino acid, the lower is the dissociation constant of the carboxyl group. There is one other compensation which may be characterized as "push–pull". The basicity of secondary amino groups after amino acid attachment to the silica surface (L-Arg, L-Val and L-Tyr) is decreased owing to interaction with silanol groups (Fig. 1a and c). Hence some of the carboxyl groups are replaced by intramolecular interaction with α-amino groups by silanols providing cation-exchange properties to L-Arg-SiO_2, L-Val-SiO_2 and L-Tyr-SiO_2. Owing to the same interaction with silanol groups, the effect of the side-chain amino groups on the anion-exchange properties of Arg-SiO_2 can be evaluated as weak but sufficient for the mentioned poor separation of chloride, perchlorate and sulphate.

With bonded L-Pro and L-Hypro we obtained another situation. The tertiary amino group is inaccessible for interaction with silanol groups owing to steric hindrance (Fig. 1b) and provides anion-exchange properties especially in acidic media when the carboxyl group is partially protonated. Hence further investigations were carried out with L-Pro-SiO_2 and L-Hypro-SiO_2.

The retention behaviour of anions in single-column ion chromatography depends on variables of the eluent such as the chemical nature of the carboxylic acid used, its concentration and pH. The chemical nature is determined by the value of the dissociation constant of the carboxyl group and defines the predominant ionic form in the eluent and the eluting power at equal concentration and pH of the eluent. A high percentage of ionization means that a higher concentration of the eluent anion is available to elute sample anions.

Effect of eluent concentration

Oxalic, citric, succinic and acetic acids at concentrations from 1 to 5 mM were used to elute anions without pH adjustment. According to our results (Table II and ref. 7, the elution power decreased in the order oxalic > citric > succinic > acetic acid. The elution order of equal-charged anions was similar for all eluents. As expected, a low concentration of the eluent caused a greater retention of anions than did higher concentrations, but only for L-Hypro-SiO_2 (Fig. 2b). Surprisingly, all the curves (Fig. 2a) for the relationship between log k' and log C_{oxal} contain a maximum in case of L-Pro-SiO_2. This means that the retention of anions was decreased by dilution of the eluent used. This could be caused by

TABLE II

LOG k' OF ANIONS FOR L-Pro-SiO_2 WITH 5 mM CARBOXYLIC ACID ELUENTS

Anion	Oxalic acid	Citric acid	Succinic acid	Acetic acid
Nitrite	0.197	0.436	0.545	0.520
Orthophosphate	0.151	0.386	0.428	0.367
Iodate	0.239	0.502	0.489	0.409
Bromate	0.369	0.663	0.612	0.547
Chloride	–	0.703	0.647	0.569
Bromide	0.601	0.932	0.835	0.713
Nitrate	0.651	0.993	0.874	0.745
Iodide	1.013	–	–	–
Perchlorate	1.270	–	–	–
Sulphate	0.772	>1	0.678	–

the possible formation of an inner salt at low eluent concentrations. It should be noted that as the eluent concentration decreases, the pH at which this interaction occurs increases and promotes inner salt formation. In the inner salt form some sites are not available for ion-exchange interaction with analytes and eluents.

Effect of eluent pH

The pH of the eluent acid should also be expected to affect the retention of various anions. It was demonstrated in an earlier study on L-Hypro-SiO_2 that a pH range of 2.5–4.0 in the eluent was optimum for the separation of singly charged inorganic anions [7]. In this range an increase in pH causes a decrease in retention for all inorganic anions. The effect of the eluent pH on the retention of anions on L-Pro-SiO_2 and L-Hypro-SiO_2 is shownin Fig. 3. The decrease in retention is attributed not only to the change in the degree of ionization of carboxyl groups in the amino acid moiety but also in the carboxylic acid eluent. On the one hand, an increase in the pH of the eluent led to decrease in the number of accessible ion-exchange sites owing to the enhancement of the degree of inner salt formation. The overall positive charge of ion-exchange sites is also reduced owing to dissociation of bonded amino acid carboxyl groups. On the other hand, the concentration and effective negative charge of eluent anions were increased to provide the growing competition with analyte anions for the ion-exchange sites. The elution order did not change for most of

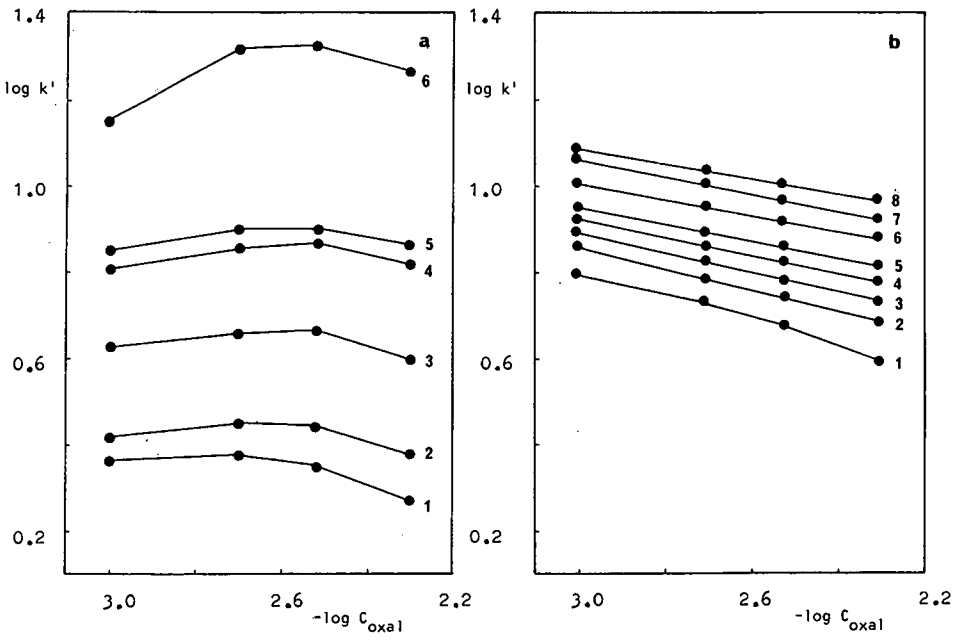

Fig. 2. Influence of oxalic acid concentration on the retention of anions. (a) L-Pro-SiO_2; (b) L-Hypro-SiO_2. Anions: 1 = orthophosphate; 2 = iodate; 3 = chloride; 4 = bromide; 5 = nitrate; 6 = iodide; 7 = perchlorate; 8 = thiocyanate.

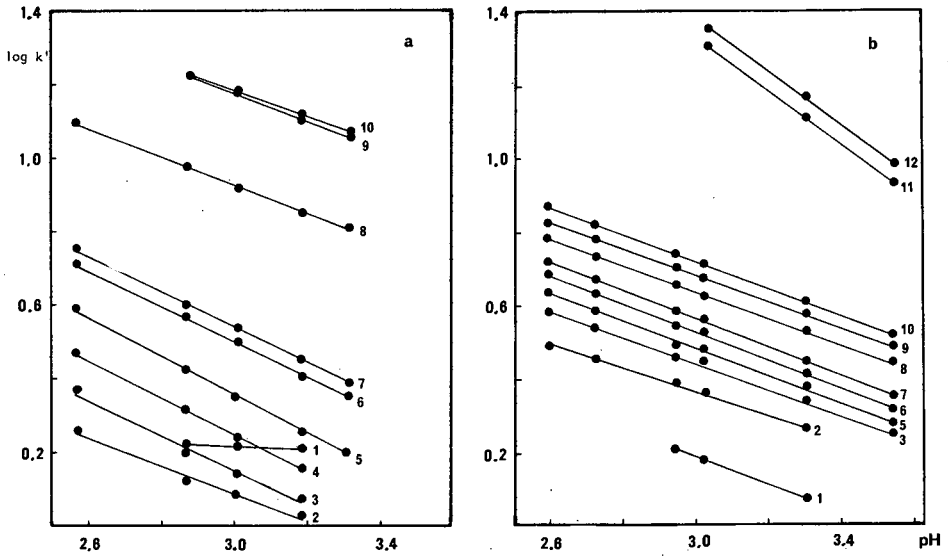

Fig. 3. Influence of pH on the retention of anions. Eluent: 5 m*M* oxalic acid. Columns: (a) L-Pro-SiO_2; (b) L-Hypro-SiO_2. Anions: 1 = nitrite; 2 = orthophosphate; 3 = iodate; 4 = bromate; 5 = chloride; 6 = bromide; 7 = nitrate; 8 = iodide; 9 = perchlorate; 10 = thiocyanate; 11 = sulphate; 12 = thiosulphate.

the anions in the pH range studied. The retention times of divalent anions decreased more rapidly than those of monovalent anions as the eluent pH increased. This may be used for the simultaneous separation of monovalent and divalent anions at high eluent pH. It should be noted, however, that a lower pH would provide a better separation from the point of view interference from the system peak.

The pH stability of silica-based ion exchangers is of great importance. Although the optimum pH range for the separation of anions is between 2.5 and 4.5, the columns studied were used from pH 2 to 7.5 without a noticeable change in performance during at least 1 year. A similar stability has been reported for analogous ligand-exchange chromatographic packings [2].

The concentration and pH of the eluents were optimized to give good separations of different anions tested. Figs. 4 and 5 show examples of the separation of standard anion mixtures on L-Pro-SiO_2 and L-Hypro-SiO_2. It was found that the anion-exchange properties of these bonded amino acids allow a wide variety of separations, including those of common anions such as orthophosphate, chloride, nitrate and sulphate.

The zwitterionic character of L-Pro-SiO_2 and L-Hypro-SiO_2 offers several advantages over traditional anion exchangers. The presence of carboxyl and tertiary amino groups in adjacent ion-exchange sites allows very small values of the ion-exchange capacity to be achieved for these phases by direct

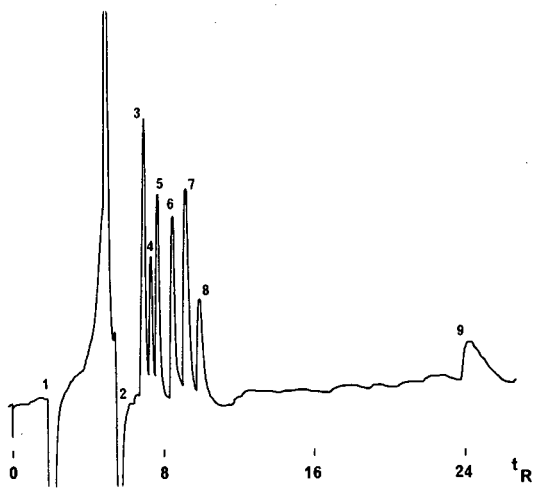

Fig. 4. Chromatogram of mixture of anions. Column: L-Pro-SiO_2, 5 μm (250 × 4 mm I.D.). Eluent: 5 m*M* succinic acid, pH 3.18. Flow-rate: 1.5 ml/min. Detection: conductimetric. Peaks: 1 = alkali metal cations; 2 = system; 3 = chloride; 4 = bromide; 5 = nitrate; 6 = iodide; 7 = perchlorate; 8 = thiocyanate; 9 = sulphate. Concentrations of test anions are: 3 = 5 ppm; 4, 5, 7 = 10 ppm and 6, 8, 9 = 20 ppm. Retention time (t_R) in min.

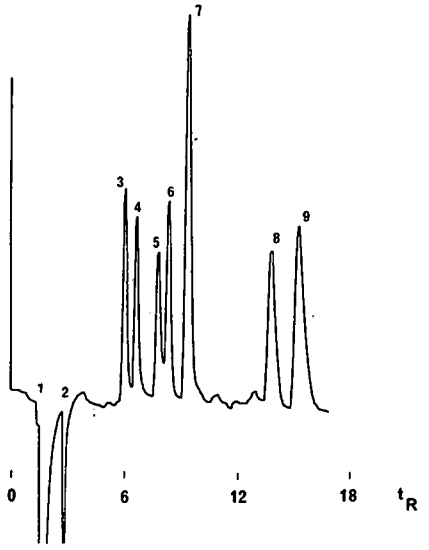

Fig. 5. Chromatogram of mixture of anions. Column: L-Hypro-SiO_2, 5 μm (250 × 4 mm I.D.). Eluent: 5 m*M* oxalic acid. Flow-rate: 1.0 ml/min. Detection: conductimetric. Peaks: 1 = alkali metal cations; 2 = system; 3 = orthophosphate; 4 = iodate; 5 = nitrite; 6 = bromate; 7 = chloride; 8 = bromide; 9 = nitrate. The concentrations of test anions are: 3–6, 8, 9 = 10 ppm and 7 = 5 ppm. Retention time (t_R) in min.

regulation of the eluent pH and concentration. For this reason it is possible to apply dilute eluents with low equivalent conductivity; in practice, this means sensitive detection and the possibility of working in the single-column ion chromatographic mode. Another advantage of the utilization of L-Pro-SiO_2 and L-Hypro-SiO_2 columns is the elution of system peak components before common anions. Finally, the structure of the ion-exchange sites in amino acid-bonded silicas provides good ion-exchange kinetics. The efficiency of the L-Pro-SiO_2 and L-Hypro-SiO_2 columns calculated for nitrate (eluent 5 m*M* oxalic acid) is equal to 7100 and 12 200 theoretical plates, respectively.

CONCLUSIONS

These studies demonstrate that an efficient separation of inorganic anions is possible by using amino acid-bonded silicas. The results confirm the alteration of acid–base properties in amino acids after attachment to the silica surface and demonstrate the dual nature of the bonded phases obtained. Other applications of amino acid-bonded silicas that could be used for cations are being studied.

REFERENCES

1 T. S. Stevens and M. A. Langhorst, *Anal. Chem.*, 54 (1982) 950.
2 G. Gubitz, W. Jellenz and W. Santi, *J. Chromatogr.*, 203 (1981) 377.
3 M. D. Bacold and Z. El Rassi, *J. Chromatogr.*, 512 (1990) 237.
4 A. V. Gaida, V. A. Monastyrskii, Yu. V. Magerovskii, S. M. Staroverov and G. V. Lisichkin, *J. Chromatogr.*, 424 (1988) 385.
5 P. N. Nesterenko and T. A. Bolshova, *Vestn. Mosk. Univ. Ser. Khim. 31 (1990) 167.*
6 G. Bonn, S. Reiffenstuhl and P. Jandik, *J. Chromatogr.*, 499 (1990) 669.
7 P. N. Nesterenko, *J. High Resolut. Chromatogr.*, 14 (1991) 767.
8 V. A. Malinovskii, S. M. Staroverov and G. V. Lisichkin, *Zh. Obshch. Khim.*, 55 (1985) 2767.
9 G. V. Kudryavtsev and G. V. Lisichkin, *Zh. Fiz. Khim.*, 55 (1981) 1352.
10 D. V. Miltchenko, G. V. Kudryavtsev and G. V. Lisichkin, *Teor. Eksp. Khim.*, 27 (1986) 243.

Journal of Chromatography, 605 (1992) 205–213
Elsevier Science Publishers B.V., Amsterdam

CHROM. 24 222

Analytical and micropreparative high-performance gel chromatography of proteins with a short column

Determination of molecular size, rapid determination of ligand binding constant and purification of S-carboxymethylated proteins for microsequencing

Hiromasa Tojo

Department of Molecular Physiological Chemistry, Osaka University Medical School, 2–2 Yamadaoka, Suita, Osaka 565 (Japan)

Kihachiro Horiike, Tetsuo Ishida, Takehiro Kobayashi and Mitsuhiro Nozaki

Department of Biochemistry, Shiga University of Medical Science, Seta, Ohtsu, Shiga 520-21 (Japan)

Mitsuhiro Okamoto

Department of Molecular Physiological Chemistry, Osaka University Medical School, 2–2 Yamadaoka, Suita, Osaka 565 (Japan)

(First received January 10th, 1992; revised manuscript received March 30th, 1992)

ABSTRACT

A short (75-mm) column of TSK-GEL G3000SW (S-column) can be used for both analytical and micropreparative gel chromatography. The elution conditions for the S-column were optimized and thereafter the column was well calibrated under native and denaturing conditions in a manner similar to that with a 600-mm column. The error in the Stokes radii of proteins obtained with the S-column was treated statistically. This S-column has the advantage of the economy in the time taken for analysis and solvent exchange and in the sample amounts required. Hence, it is useful for studying protein–ligand interactions by Hummel–Dreyer gel chromatography and for purifying S-carboxymethylated proteins prepared for microsequencing. These were exemplified by the analysis of the binding of *o*-nitrophenol to catechol 2,3-dioxygenase and of the NH_2-terminal amino acid sequence of rat pancreatic prophospholipase A_2.

INTRODUCTION

High-performance gel chromatography with porous silica- and polymer-based supports has been used to determine molecular weights and Stokes radii, as under suitable conditions the column functions in the size-exclusion mode, and the advantages of higher resolution and speed compared with the usual soft gel columns, have been achieved [1–19]. Because of the superior resolving power of the column, it is possible to perform gel chromatography with a shorter column. Although the reduction in column length more or less sacrifices resolution, the use of a short column may be preferable,

Correspondence to: Dr. Hiromasa Tojo, Department of Molecular Physiological Chemistry, Osaka University Medical School, 2–2 Yamadaoka, Suita, Osaka 565, Japan.

0021-9673/92/$05.00

particularly when economy in time taken for analyses and solvent exchanges and in the sample and solvent amounts required is important, and when dilution of solutes due to axial dispersion should be minimized. These requirements are encountered, for example, in the analysis of protein–protein interactions by gel chromatography [15].

In this paper, we report that a short (75-mm) column of TSK-GEL G3000SW (S-column), which is a commercially available precolumn, has a resolving power sufficient for the determination of molecular weights and Stokes radii of purified proteins using native and denaturing solvent systems. We experimentally determined the random error in gel chromatography with an S-column and examined its effect on the calculated parameters on the basis of a statistical evaluation. Additional utility of the S-column was illustrated by the analysis of protein–ligand interactions by Hummel–Dreyer gel chromatography [20,21] and by the purification of small amounts of reduced and S-alkylated proteins.

EXPERIMENTAL

Materials

The following standards for molecular weight and size determinations were used: cytochrome *c* (horse heart), α-chymotrypsinogen A (bovine pancreas), lactate dehydrogenase (bovine heart), alcohol dehydrogenase (yeast), ovalbumin (egg white), albumin (bovine serum) and urease (jack bean) from Sigma, aldolase (rabbit muscle) from Boehringer and ribonuclease A (bovine pancreas), catalase (bovine liver), ferritin (horse spleen) and blue dextran 2000 from Pharmacia.

Guanidine hydrochloride (GuHCl), sodium dodecyl sulphate (SDS) and sodium iodoacetate of protein chemical grade were obtained from Nacalai Tesque. Lithium dodecyl sulphate (LDS) and *o*-nitrophenol were products of Wako and the latter was recrystallized from ethanol. All other chemicals were of analytical-reagent grade.

Crystalline catechol 2,3-dioxygenase was prepared from *Escherichia coli* W3110 carrying its gene from TOL plasmid according to a previously published method [22], except that Q-Sepharose was used instead of DEAE-cellulose.

Rat pancreatic active phospholipase A_2 and prophospholipase A_2 were purified as reported [23]. To the pancreas homogenate was added 2 m*M* diisopropyl fluorophosphate to prevent activation of the proenzyme.

Small-zone high-performance gel chromatography

Gel chromatography was performed with a Gilson Model 302 liquid delivery module at 25°C. Columns of 600 mm × 7.5 mm I.D. (L-column) and short columns of 75 mm × 7.5 mm I.D. (S-column) of TSK-GEL G3000SW were obtained from Tosoh. The eluents used were (I) 0.05 *M* sodium phosphate containing 0.3 *M* NaCl (pH 7.0), (II) 0.1 *M* sodium pyrophosphate containing 0.3 *M* NaCl (pH 8.3), (III) 6 *M* GuHCl containing 10 m*M* sodium phosphate and 1 m*M* EDTA (pH 6.5) and (IV) 0.1 *M* ammonium acetate (pH 6.8) containing various concentrations of LDS. Protein samples for the experiments with 6 *M* GuHCl and LDS were dissolved in 7 *M* GuHCl (pH 8.5) containing 10 m*M* DL-dithiothreitol and 0.1 *M* Tris–HCl, and 0.1 *M* ammonium acetate containing 0.1% LDS, respectively; otherwise, they were dissolved in the same buffer as for eluent I or II. The effluents were continuously monitored with a Gilson Model 116 detector at 280 and 210/225 nm and/or with a Shodex RI SE-11 differential refractometer.

The distribution coefficients, K_d, of proteins were calculated from the equation $K_d = (V_e - V_0)/(V_t - V_0)$, where V_e, V_0 and V_t are the retention times corresponding to the elution volume of a protein, the void volume and the total available volume, respectively. The V_0 and V_t values were determined from the retention times of blue dextran and water, respectively (see Results and Discussion).

The chromatographic data were analysed by the equation of Ackers [24]:

$$R_e = a_1 + b_1 \mathrm{erf}^{-1}(1 - K_d) \quad (1)$$

where R_e is the Stokes radius, $\mathrm{erf}^{-1}(1 - K_d)$ is the inverse error function of $1 - K_d$ and a_1 and b_1 are empirical constants. The R_e values and molecular weights were taken from the literature [14,25]. The R_e values used for randomly coiled linear polypeptides in 6 *M* GuHCl are the viscosity-based Stokes radii and those for native proteins are the frictional Stokes radii. For native globular proteins the frictional R_e value is virtually identical with the viscosity R_e value over the range of molecular size

used in this study [14,26], and the values for the former are more available [14,18].

In order to relate K_d to the molecular weight (M_r) of a protein, we used eqn. 2 for proteins in 6 M GuHCl, eqn. 3 for globular proteins and eqn. 4 for proteins in 0.1% LDS, which were obtained from eqn. 1 based on the relationships between R_e and M_r [25]:

$$M_r^{0.555} = a_2 + b_2\text{erf}^{-1}(1 - K_d) \quad (2)$$

$$M_r^{1/3} = a_3 + b_3\text{erf}^{-1}(1 - K_d) \quad (3)$$

$$M_r^{0.73} = a_4 + b_4\text{erf}^{-1}(1 - K_d) \quad (4)$$

where a_2, b_2, a_3, b_3, a_4 and b_4 are empirical constants.

Hummel–Dreyer gel chromatography

In order to obtain directly the binding curve of *o*-nitrophenol for catechol 2,3-dioxygenase, Hummel–Dreyer gel chromatography [20,21] was performed at 25°C on an S-column with a Tosoh CCPM computer-controlled dual-pump system. The eluents were *o*-nitrophenol solutions of constant concentrations (2.0–96.6 μM), the ligand being dissolved in 0.05 M sodium phosphate buffer (pH 7.5). The flow-rate was 0.5 ml/min and the absorbance at 410 nm of the effluents was continuously monitored with a Tosoh UV-8000 detector. The injection volume of the mixtures of catechol 2,3-dioxygenase and *o*-nitrophenol was 25 μl and the total concentration of the enzyme as subunit was kept constant.

Preparation of S-carboxymethylated phospholipase A_2

Purified prophospholipase A_2 or phospholipase A_2 (150 pmol each) was reduced under nitrogen with tributylphosphine (150 nmol) in propanol–0.5 M ammonium hydrogencarbonate (pH 8.5) (1:1) for 2 h at room temperature [27], then iodoacetate (900 nmol) in 1 M ammonium hydrogencarbonate (pH 8.5) was added. The mixture was incubated for 30 min at 37°C, then the reaction was stopped by the addition of 1 μl of 2-mercaptoethanol. The sample was dried *in vacuo* and then purified as described below.

Analytical procedures

Amino acid analysis was performed as reported previously [28]. The amino acid sequence was determined with an Applied Biosystems Model 470A gas-phase sequenator and a Model 120A PTH analyser.

RESULTS AND DISCUSSION

Confirmation of convenient determination of V_t values by Himmel and Squire

Low-molecular-weight markers, such as dinitrophenylalanine, usually employed for soft gels to determine the V_t value are inadequate for the G3000SW column, as the gels more or less interact with those molecules. Himmel and Squire [11] reported the convenient determination of V_t with water using an absorption detector, so this was first confirmed here.

When water was injected into the column, a derivative pattern, *i.e.*, a positive peak followed by a negative peak, was recorded with an absorption detector, owing to the difference between the refractive indices of the eluents and water. This signal was reproducibly obtained (Table I). We observed that

TABLE I

RANDOM ERRORS IN RELATIVE RETENTION TIMES AND DISTRIBUTION COEFFICIENTS OBTAINED WITH AN S-COLUMN

Eluent I was used and the flow-rate was 0.2 ml/min. The S.D. was calculated from the data for 8–10 determinations for each sample.

Sample	S.D. · 100		
	r_e	K_d[a]	$\text{erf}^{-1}(1 - K_d)$[b]
Blue dextran	0.20	–	–
Thyroglobulin	0.16	0.44	3.8
Ferritin	0.17	0.31	0.59
Serum albumin	0.23	0.42	0.50
α-Chymotrypsinogen A	0.17	0.30	0.29
Water	0.21	–	–

[a,b] These S.D. values were calculated with the equations

$$\text{S.D.}(K_d) = \left[\left(\frac{K_d}{r_i}\right)^2 \text{var}(r_t) + \left(\frac{1}{r_i}\right)^2 \text{var}(r_e) + \left(\frac{K_d}{r_i} - \frac{1}{r_i}\right)^2 \text{var}(r_0)\right]^{\frac{1}{2}}$$

$$\text{S.D.}[\text{erf}^{-1}(1 - K_d)] = 0.5\pi^{\frac{1}{2}}\text{S.D.}(K_d)\exp\{[\text{erf}^{-1}(1 - K_d)]^2\}$$

respectively, where r is the retention time relative to the $\bar{V}_t$ value (*e.g.*, $r_e = V_e/\bar{V}_t$, $r_i = V_i/\bar{V}_t$), V_i is the internal volume and var and S.D. are the variance and the standard deviation, respectively, of the quantity in parentheses.

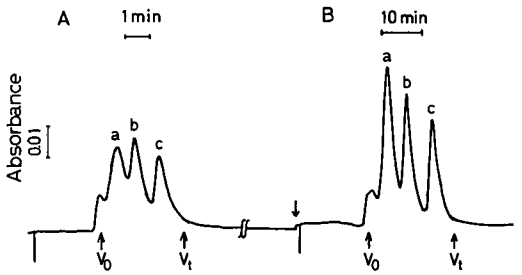

Fig. 1. Elution profiles obtained with the S-column system. Eluent I was used and the flow-rates were (A) 0.5 and (B) 0.08 ml/min. The protein samples used were (a) ferritin, (b) albumin and (c) α-chymotrypsinogen A. The negative deflections indicate the time at which the sample was injected. The flow-rate was changed at the time indicated by the arrow. The chart speeds were (A) 3 cm/min and (B) 10 cm/h.

the retention time of the latter trough obtained with a UV detector coincided with that of water recorded simultaneously with a differential refractometer with a deviation of only 0.2% when the distance between the two detectors connected in series was corrected for the retention times. This deviation was comparable to the random errors and corresponded to an error in K_d of 0.46%. This error was virtually negligible, as discussed below. Therefore, we conveniently determined the V_t value of the column with water, even using an absorption monitor.

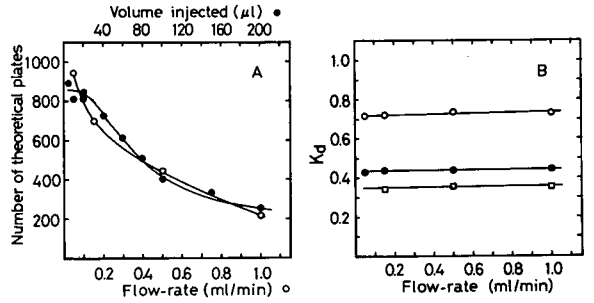

Fig. 2. Characterization of the S-column. Eluent I was used. (A) Effect of the flow-rate and the sample volume on the number of theoretical plates of the S-column with bovine serum albumin. Protein concentration, 3.3 mg/ml. (○) The flow-rate was changed and the sample volume injected remained constant at 10 μl; (●) the sample volume applied was changed at a constant flow-rate of 0.15 ml/min. (B) Dependence of the distribution coefficient, K_d, on flow-rate with the S-column system. The proteins used were (□) aldolase, (●) albumin and (○) α-chymotrypsinogen A. Each sample was injected in a volume of 10 μl.

Performance of the S-column

As Fig. 1 shows, this S-column showed satisfactory resolution for analytical gel chromatography. Its resolution depended on the flow-rate and the sample volume injected (Figs. 1 and 2A), whereas the resolution did not depend on the protein concentration of samples applied up to about 20 mg/ml (data not shown). The resolution increased when the injection volume was decreased, and was no longer improved in a volume of less than about 20 μl at a flow-rate of 0.15 ml/min (Fig. 2A). The S-column had *ca.* 1000 theoretical plates for bovine serum albumin with an injection volume of 10 μl at 0.05 ml/min. The resolving power decreased with an increase in the flow-rate (Fig. 2A). Flow-rates of 0.15–0.5 ml/min suffice for routine analysis, although resolution was sacrificed for a rapid experiment.

The K_d values showed hardly any flow-rate dependence over the range examined (Fig. 2B). These results are consistent with previous observations with an L-column [2]. However, Kakuno *et al.* [8] reported that slightly different V_e values were obtained at 1 and 0.1 ml/min with an L-column (300 mm). The reason for this discrepancy is unknown.

The observed retention times for a given sample were dependent on the injection volume. The time increased with an increase in the volume because it was measured from the moment at which the sample was just injected. This mainly reflected the lag time during which a sample was transferred from the sample loop to the column. Since with a volume below 10 μl the observed values are identical with those extrapolated to zero volume, within experimental error, the sample volume injected remained constant at 10 μl throughout the calibration of the column.

We tested four S-columns and all gave essentially the same K_d values and resolution. The K_d values for given proteins with the S-column were virtually identical with those obtained with an L-column, indicating the homogeneity of the gel matrices [29].

Once the detector baseline had stabilized in our S-column system, baseline drift was not observed even at the range of 0.05 full-scale absorbance when the flow-rate was abruptly changed (Fig. 1). Hence the column was equilibrated at 1.0 ml/min and after about 20 min the flow-rate was changed to the desired value for analysis. In this manner one buffer system was rapidly exchanged with another system.

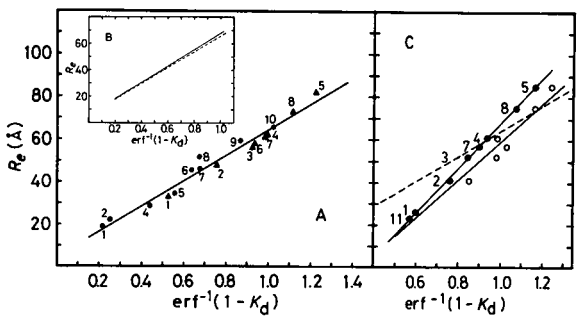

Fig. 3. Correlation between the distribution coefficient, K_d, and Stokes radius, R_e, of proteins with the S-column. Plots of R_e *vs.* $erf^{-1}(1 - K_d)$ for the data obtained under the following conditions; the pairs of values in parentheses are the a_1 and b_1 values in eqn. 1, respectively: (A) 0.15 ml/min, (●) eluent I and (▲) eluent III (4.89, 59.6); (B) dot-dashed line, 0.15 ml/min, eluent I (5.59, 60.3); solid line, 0.5 ml/min, eluent I (5.48, 62.3); dotted line, 0.15 ml/min, eluent II (pH 8.3) (7.42, 58.0); (C) 0.2 ml/min, (○) eluent IV containing 0.1% LDS (−29.5, 88.5) and (●) eluent IV containing 0.03% LDS (−37.6, 105). The dashed line in (C) is the same as the line in (A). As the calibration line for the L-column in eluent I at 1 ml/min (6.79, 58.0) almost coincided with that for the S-column in eluent II at 0.15 ml/min (dotted line), the line for the L-column has been omitted for clarity. The numbers indicate the following proteins: 1 = ribonuclease A; 2 = α-chymotrypsinogen A; 3 = lactate dehydrogenase; 4 = ovalbumin; 5 = albumin; 6 = alcohol dehydrogenase; 7 = aldolase; 8 = catalase; 9 = ferritin; 10 = urease; 11 = cytochrome *c*.

Calibration of the S-column

Fig. 3 shows plots of R_e *vs.* $erf^{-1}(1 - K_d)$ for the S-column. In phosphate buffer (eluent I) and 6 *M* GuHCl (eluent III), these plots were satisfactorily linear (correlation coefficients of 0.987 and 0.991, respectively, although non-linear plots have been reported [16,17]). It is likely that the viscosity-based Stokes radii in both media had the same correlation with K_d irrespective of the hydrodynamic shapes of the standards, so we combined these data and calculated the correlation coefficient to be 0.986 (Fig. 3A). These results were consistent with previous results [6,14,30]. Studies on the mechanism of the separation of macromolecules on gel filtration based on these observations have been reported [14,18]. Under various conditions as shown in Fig. 3A and B, the calibration lines approximately coincided with each other.

However, on chromatography of LDS–protein complexes the plots were almost linear, but did not coincide with those obtained from the combined data in eluents I and III (Fig. 3C). We used LDS in place of SDS because LDS is more soluble than SDS at low temperature, *i.e.*, LDS has a lower Krafft point. The a_1 and b_1 values in eqn. 1 were −29.5 and 88.5, respectively, for 0.1% LDS–gel chromatography. The large negative a_1 value compared with that on chromatography in eluents I and III is notable. These values are consistent with previous results with an L-column equilibrated with 0.1% SDS [7]. This indicated that the columns of TSK-GEL G3000SW do not necessarily function in the size-exclusion mode alone in the presence of the dodecyl sulphate salt [7]. On the other hand, Tanford *et al.* [26] reported that a calibration line with native proteins was superimposable on that with proteins reduced and S-alkylated in 0.1% SDS in gel chromatography on a soft gel (Sephadex G-200) column.

In 6 *M* GuHCl solution, all the proteins used are random coils [31], which have the same hydrodynamic shape, so we can reasonably estimate the molecular weights of the polypeptide chain using eqn. 2 [25]. As Fig. 4A shows, the plot was linear (correlation coefficient 0.991), in agreement with our previous results with an L-column [13].

On the other hand, in order to estimate the molecular weights of native proteins by gel chromatography alone, we must assume that both standards and unknowns have the same shape and partial specific volumes [25,29,32]. The calibration line for native proteins with eqn. 3 was almost linear (correlation coefficient 0.973, Fig. 4A), as the standards used were globular proteins. However, one should use this calibration line with caution in calculating M_r values of proteins of unknown

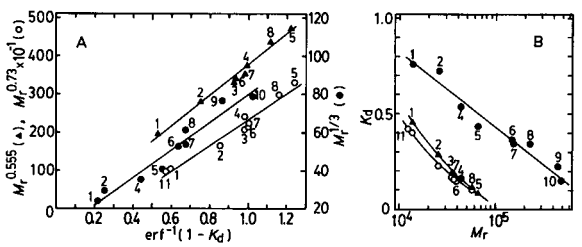

Fig. 4. Correlation between the distribution coefficient, K_d, and the molecular weight, M_r, with the S-column. (A) (▲) Plot of $M_r^{0.555}$ *vs.* $erf^{-1}(1 - K_d)$ for denatured proteins in 6 *M* GuHCl; (●) plot of $M_r^{1/3}$ *vs.* $erf^{-1}(1 - K_d)$ for native proteins; (○) plot of $M_r^{0.73}$ *vs.* $erf^{-1}(1 - K_d)$ for LDS–protein complexes in 0.1% LDS. (B) Plots of K_d *vs.* log M_r. Chromatographic conditions, symbols and numbers as in Fig. 3.

hydrodynamic shape, as has been stressed repeatedly [*e.g.*, 12,14,16–18,25,29,32].

Random errors in gel chromatography on the S-column

We evaluated the random errors in the retention times with several standard samples at a flow-rate of 0.2 ml/min (Table I). The errors were expressed as the standard deviation (S.D.) scaled in terms of a mean V_t value, $\bar{V}_t$. This uncertainty was reported to be mainly due to flow-rate variations [33]. These errors propagate to those in the K_d and $\mathrm{erf}^{-1}(1 - K_d)$ values (Table I).

Although the S.D. values of relative retention time and K_d are almost constant, the error in $\mathrm{erf}^{-1}(1 - K_d)$ showed an unequal distribution on non-linear transformation of K_d (Table I). We therefore performed weighted least-squares analysis with $1/\{\mathrm{var}(R_e) + b_1^2\mathrm{var}[\mathrm{erf}^{-1}(1 - K_d)]\}$ as weights [34], where var is the variance of the quantity in parentheses, assuming that the error in R_e has a constant relative magnitude of 5% [35]. The second term in the denominator in the weights used comes from the random error in gel chromatography. The a_1 and b_1 values obtained without consideration of the second term ($a_1 = 6.32$ and $b_1 = 57.1$) coincided with those obtained with its consideration ($a_1 = 6.31$ and $b_1 = 57.1$). Consequently, the random errors in the raw data for the R_e *vs.* $\mathrm{erf}^{-1}(1 - K_d)$ plot of Ackers do not expand to any significant extent throughout the whole range of K_d values examined.

When the R_e values of proteins with K_d values in the range 0.1–0.75 were estimated from the calibration line in Fig. 3A, the standard deviations of the estimated values were calculated to be at least in the range 0.7–2.0 Å from the following equation:

$$\mathrm{S.D.}(R_e) = \{\mathrm{var}(a_1) + 2\mathrm{erf}^{-1}(1 - K_d)\,\mathrm{cov}(a_1, b_1) + \mathrm{var}(b_1)\mathrm{erf}^{-1}(1 - K_d)^2 + b_1^2\mathrm{var}[\mathrm{erf}^{-1}(1 - K_d)]\}^{\frac{1}{2}} \quad (5)$$

where $\mathrm{cov}(a_1, b_1)$ denotes the covariance between a_1 and b_1. In this instance, we considered the errors in $\mathrm{erf}^{-1}(1 - K_d)$ for a protein in question and in the calibration constants a_1 and b_1, which can approximately be calculated from the weighted least-squares analysis with considering the errors in K_d and R_e for the standard proteins as described above. The uncertainty in $\mathrm{erf}^{-1}(1 - K_d)$ propagates to the R_e value estimated. However, the resulting error in R_e was at most half of the error in R_e obtained by neglecting the random error in K_d. The total error in R_e determined by gel chromatography may depend on the uncertainty in R_e of standard proteins, the error introduced by the use of an empirical relationship between R_e and K_d and/or anomalous elution caused by solute–gel interactions in addition to the minor contribution of the random error in gel chromatography discussed above. This result was consistent with that of a systematic study on the precision of average molecular weights determined by time-based high-performance gel permeation chromatography [33].

Hummel–Dreyer gel chromatography: application to the binding system of catechol 2,3-dioxygenase and o-nitrophenol

Catechol 2,3-dioxygenase catalyses an extra-diol cleavage of catechol to form 2-hydroxymuconate semialdehyde [36]. The enzyme is a homotetramer with a subunit M_r of 35 211 based on the DNA sequence and iron content (one atom per subunit) [22,37]. In order to obtain directly the binding curve of *o*-nitrophenol, a competitive inhibitor [38], we performed Hummel–Dreyer gel chromatography [20,21] because, as described above, the S-column allowed sufficient resolution and rapid separation (Fig. 5).

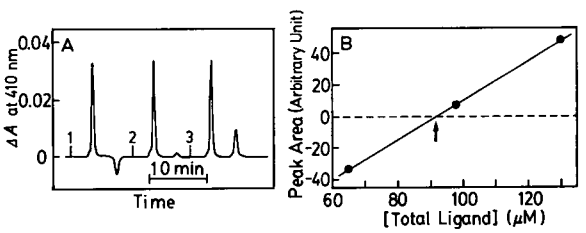

Fig. 5. Hummel–Dreyer gel chromatography for the binding system of catechol 2,3-dioxygenase and *o*-nitrophenol on an S-column at 25°C. The eluent was 14.7 μM *o*-nitrophenol in 50 mM sodium phosphate buffer (pH 7.5). The flow-rate was 0.5 ml/min. (A) Chromatograms. The samples (25 μl) containing various *o*-nitrophenol concentrations (1 = 65.0 μM; 2 = 97.5 μM; 3 = 130 μM) and 141 μM oxygenase per subunit were injected at the times indicated by the positive deflections. (B) Plot of ligand (*o*-nitrophenol) peak area, expressed as positive for the peak or negative for the trough, against the total ligand concentration. The arrow indicates the total *o*-nitrophenol concentration at which the area was zero.

When the free *o*-nitrophenol concentration in the equilibrium mixture of the enzyme and the ligand is equal to that in the eluent, no peak and trough are observed at the elution volume of the ligand on the gel chromatography of the mixture. As the corresponding total ligand concentration can be read from the point at which the area of the plot in Fig. 5B is zero [21], the value of fractional saturation can be easily calculated. To construct a binding curve, several experiments with different ligand concentrations in the eluent are necessary. This method is not time consuming, however, because the times taken for a single run at 0.5 ml/min and for solvent exchange at 1 ml/min were 9 and 20 min, respectively. The binding curve for the enzyme appeared to be nearly hyperbolic, and the dissociation constant was calculated to be 8.1 μM by applying our non-linear least-squares analysis [39].

Determination of the stoichiometry of ligand binding is a prerequisite to investigate the mechanism of protein–ligand interaction. For this, direct methods such as equilibrium dialysis, ultrafiltration [40] and Hummel–Dreyer chromatography [21] are preferable to indirect methods, *e.g.*, spectrometric titration, as the latter cannot detect the presence of the binding sites to which the ligand binding does not induce the spectral change. Further, only the former methods allow us to determine free, not total, ligand concentration directly.

Among the direct methods, the present Hummel–Dreyer method with S-column is more useful and convenient because it is simple, sensitive and not time or sample consuming. In methods using semipermeable membranes, adsorption of samples on the membrane must be considered.

Purification of reduced and S-alkylated proteins for microsequencing: application to phospholipase A_2

With the recent advent of the automated gas-phase sequenator, the amino acid sequences of a protein and its proteolytic digests have been frequently determined to design oligonucleotide probes for cloning of its cDNA. The preparation of reduced and S-alkylated proteins is usually an initial step in protein sequencing strategies. As reduced and S-alkylated proteins are very hydrophobic, special care must be taken to prevent loss due to non-specific adsorption to test-tubes and gels on removing unreacted reagents from a small amount of the polypeptides by column chromatography. Gel chromatography on an S-column in the presence of 0.03% of LDS was found to be suitable for such a purpose.

Takagi *et al.* [7] reported that the resolution of the L-column depended markedly on the salt concentration in the mobile phase containing SDS, and that good separations were obtained over the concentration range 0.05–0.15 M of sodium phosphate; we used 0.1 M ammonium acetate (pH 6.8) or 0.1 M sodium phosphate (pH 7.0), and both solvents were found to be equally effective for the S-column system. We first examined the effect of the LDS concentration on the elution behaviours of standard proteins and phospholipase A_2. With a decrease in the LDS concentration the retention times of S-carboxymethylated proteins increased (Fig. 3C). At LDS concentrations of less than 0.03% (1.1 mM), around the critical micelle concentration [41], the resolution became significantly poorer and the peak of phospholipase A_2 broadened. Therefore, an LDS concentration of at least 0.03% was required for good separation under the conditions employed. As a large excess of LDS may disturb the Edman degradation reaction, we adopted an LDS concentration of 0.03%. We selected a flow-rate of 0.2 ml/min with regard to resolution and speed from the results described above. At this flow-rate an eluted protein could be collected in a volume of 0.2–0.3 ml, and thereby the amount of LDS loaded on a sequenator (less than 0.1 mg) did not affect the Edman reaction.

This method was applied to determine the sequence of the N-terminal extrapeptide of rat pan-

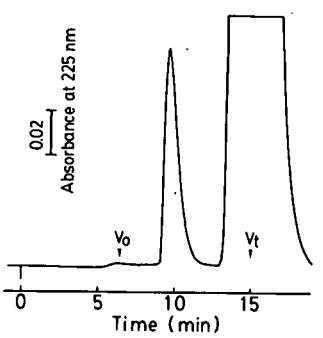

Fig. 6. Elution profile of S-carboxymethylated prophospholipase A_2 on an S-column in 0.03% LDS. The flow-rate was 0.2 ml/min.

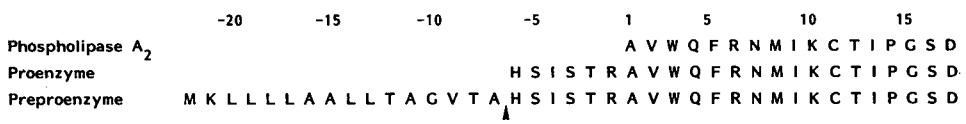

Fig. 7. NH_2-terminal amino acid sequences of rat pancreatic phospholipase A_2 and prophospholipase A_2. The arrowhead indicates a putative signal sequence cleavage site [42].

creatic prophospholipase A_2. The proenzyme was converted into the active enzyme through limited proteolysis of the NH_2-terminal extrapeptide. The phospholipase A_2, prophospholipase A_2 and standard proteins were reduced and S-carboxymethylated as described under Experimental. The dried samples containing a large amount of unreacted reagents were dissolved in 60 μl of 0.1 *M* ammonium acetate in the presence of 0.1% of LDS[a]. The resultant solution was then applied to an S-column as described above. The proenzyme was eluted at the position corresponding to an R_e value of 20.5 Å (Fig. 6). The eluted protein was collected in a 1.5-ml polypropylene tube. The recovery was about 80% as judged by amino acid analysis. The sample was evaporated *in vacuo* over phosphorus pentoxide. As residual ammonium ion may disturb the identification of phenylthiohydantoin-aspartic acid, the sample was further dried after the addition of 100 μl of water. When 0.1 *M* sodium phosphate was used as an elution buffer, this procedure was unnecessary. The dried sample was dissolved in 30 μl of water and then applied to a polybrene-treated glass filter and subjected to automated Edman analysis. The presence of LDS prevented adsorption of the protein on the polypropylene tube.

The NH_2-terminal amino acid sequences of rat pancreatic phospholipase A_2 and prophospholipase A_2 are shown in Fig. 7. The proenzyme has a six-residue long extrapeptide, HSISTR, compared with the active enzyme. The sequence was consistent with processing at a putative signal sequence cleavage site [42] in the amino acid sequence of the preproenzyme deduced from the nucleotide sequence of the phospholipse A_2 cDNA [43].

This method is an alternative to microbore reversed-phase high-performance liquid chromatography (HPLC) [28,44] in microsequencing strategies. Reversed-phase HPLC may be the most powerful technique for the isolation of proteins for microsequencing in many respects, including resolution, sensitivity, speed and the use of volatile organic solvents as mobile phase. Its major drawback, however, is the very low recovery of hydrophobic proteins such as membrane proteins and their low solubility in the organic mobile phase. As the present method utilizes a strong anionic detergent, it may be accommodated to the isolation of membrane proteins of a more hydrophobic nature; the LDS concentration could, if necessary, be adjusted so as to be optimum for the proteins. If proteins are separated by sodium dodecyl sulphate polyacrylamide gel electrophoresis, they can be recovered by electroblotting on to membranes for direct sequencing [45,46]. Although this technique is very useful because of the high resolution of the electrophoresis, it is sometimes hampered by low transfer efficiencies [47]. When a higher resolution than in the present method is desired, S-alkylated proteins separated by 0.03% LDS gel chromatography on an L-column can be similarly handled for microsequencing.

CONCLUSIONS

The short column of TSK-GEL G3000SW is very useul for analytical and micropreparative gel chromatography for the determination of molecular size and weight, the rapid determination of ligand binding parameters and the purification of S-alkylated proteins prepared for microsequencing. Further, it is useful to employ the S-column for analysing the

[a] As the LDS micelles which incorporate low-M_r materials absorbing at 225 nm were eluted just later than the phospholipase A_2 ($M_r \approx 14\,000$), an excess of LDS and low-M_r contaminants may be included in the eluted protein solution when the sample containing an unnecessarily higher concentration of LDS (*e.g.*, 1%) was injected on to the column. A 0.1% LDS solution sufficed for solubilizing S-alkylated phospholipase A_2 and standard proteins used. This method is not suitable for separating proteins of M_r <10 000 because of interference from the LDS micelles eluted and peak broadening of such low-M_r proteins.

protein–protein interactions such as association–dissociation systems as reported previously, *viz.*, a self-associating system of hog kidney D-amino acid oxidase [15].

REFERENCES

1 K. Fukano, K. Komiya, H. Sasaki and T. Hashimoto, *J. Chromatogr.*, 166 (1978) 47.
2 F. E. Regnier and K. M. Gooding, *Anal. Biochem.*, 103 (1980) 1.
3 C. T. Wehr and S. R. Abbott, *J. Chromatogr.*, 185 (1979) 453.
4 N. Ui, *Anal. Biochem.*, 97 (1979) 65.
5 Y. Kato, K. Komiya, H. Sasaki and T. Hashimoto, *J. Chromatogr.*, 190 (1980) 297.
6 T. Imamura, K. Konishi, M. Yokoyama and K. Konishi, *J. Liq. Chromatogr.*, 4 (1981) 613.
7 T. Takagi, K. Takeda and T. Okuno, *J. Chromatogr.*, 208 (1981) 201.
8 T. Kakuno, H. Hiura, O. Ishikawa, M. Umino and Y. Kato, in T. Horio and J. Yamashita (Editors), *Tampakushitsu Koso no Kiso Jikkenho (Basic Experimental Methods for Protein and Enzyme Research)*, Nankodo, Tokyo, 1981, Ch. 2, p. 206.
9 R. A. Jenik and J. W. Porter, *Anal. Biochem.*, 111 (1981) 184.
10 R. C. Montelaro, M. West and C. J. Issel, *Anal. Biochem.*, 114 (1981) 398.
11 M. E. Himmel and P. G. Squire, *Int. J. Pept. Protein Res.*, 17 (1981) 365.
12 K. Horiike, H. Tojo, M. Iwaki, T. Yamano and M. Nozaki, *Biochem. Int.*, 4 (1982) 477.
13 H. Tojo, K. Horiike, K. Shiga, Y. Nishina, R. Miura, H. Watari and T. Yamano, *J. Biochem.*, 92 (1982) 1741.
14 K. Horiike, H. Tojo, T. Yamano and M. Nozaki, *J. Biochem.*, 93 (1983) 99.
15 H. Tojo, K. Horiike, K. Shiga, Y. Nishina, M. Nozaki, H. Watari and T. Yamano, *J. Biochem.*, 95 (1984) 1.
16 M. le Maire, L. P. Aggerbeck, C. Monteilhet, J. P. Andersen and J. V. Møller, *Anal. Biochem.*, 154 (1986) 525.
17 M. le Maire, A. Ghazi, J. V. Møller and L. P. Aggerbeck, *Biochem. J.*, 243 (1987) 399.
18 M. Potschka, *Anal. Biochem.*, 162 (1987) 47.
19 M. le Maire, A. Ghazi, M. Martin and F. Brochard, *J. Biochem.*, 106 (1989) 814.
20 J. P. Hummel and W. J. Dreyer, *Biochim. Biophys. Acta*, 63 (1962) 530.
21 J. M. Andreu, *Methods Enzymol.*, 117 (1985) 346.
22 C. Nakai, K. Hori, H. Kagamiyama, T. Nakazawa and M. Nozaki, *J. Biol. Chem.*, 258 (1983) 2916.
23 T. Ono, H. Tojo, K. Inoue, H. Kagamiyama, T. Yamano and M. Okamoto, *J. Biochem.*, 96 (1984) 785.
24 G. K. Ackers, *J. Biol. Chem.*, 242 (1967) 3237.
25 W. W. Fish, *Methods Membr. Biol.*, 4 (1975) 189.
26 C. Tanford, Y. Nozaki, J. A. Reynolds and S. Makino, *Biochemistry*, 13 (1974) 2369.
27 U. T. Rüegg and J. Rudinger, *Methods Enzymol.*, 47 (1977) 111.
28 H. Tojo, T. Ono, S. Kuramitsu, H. Kagamiyama and M. Okamoto, *J. Biol. Chem.*, 263 (1988) 5724.
29 G. K. Ackers, in H. Neurath and R. L. Hill (Editors), *The Proteins*, Vol. I, Academic Press, New York, 3rd ed., 1975, Ch. 1, p. 1.
30 W. W. Fish, J. A. Reynolds and C. Tanford, *J. Biol. Chem.*, 245 (1970) 5166.
31 S. Lapanje and C. Tanford, *J. Am. Chem. Soc.*, 89 (1967) 5030.
32 K. Kawahara, *Tanpakushitsu Kakusan Koso (Protein, Nucleic Acid and Enzyme)*, 18 (1973) 357.
33 L. Andersson, *J. Chromatogr.*, 216 (1981) 35.
34 W. E. Deming, *Statistical Adjustment of Data*, Wiley, New York, 1943 (Japanese edition, translated by S. Moriguchi, Iwanami Shoten, Tokyo), p. 93.
35 C. Tanford, *Physical Chemistry of Macromolecules*, Wiley, New York, 1961, Ch. 6, p. 356.
36 M. Nozaki, *Top. Curr. Chem.*, 78 (1979) 145.
37 C. Nakai, H. Kagamiyama, M. Nozaki, T. Nakazawa, S. Inouye, Y. Ebina and A. Nakazawa, *J. Biol. Chem.*, 258 (1983) 2923.
38 K. Hori, T. Hashimoto and M. Nozaki, *J. Biochem.*, 74 (1973) 375.
39 H. Tojo, K. Horiike, K. Shiga, Y. Nishina, H. Watari and T. Yamano, *J. Biol. Chem.*, 260 (1985) 12607.
40 A. J. Sophianopoulos and J. A. Sophianopoulos, *Methods Enzymol.*, 117 (1985) 354.
41 K. Kubo and T. Takagi, *Anal. Biochem.*, 156 (1986) 11.
42 G. von Heijne, *Nucleic Acids Res.*, 14 (1986) 4683.
43 O. Ohara, M. Tamaki, E. Nakamura, Y. Tsuruta, Y. Fujii, M. Shin, H. Teraoka and M. Okamoto, *J. Biochem.*, 99 (1986) 733.
44 E. C. Nice, C. J. Lloyd and A. W. Burgess, *J. Chromatogr.*, 296 (1984) 153.
45 S. Yuen, M. W. Hunkapiller, K. J. Wilson and P. M. Yuan, *Anal. Biochem.*, 168 (1988) 5.
46 R. H. Aebersold, D. B. Teplow, L. E. Hood and S. B. H. Kent, *J. Biol. Chem.*, 261 (1986) 4229.
47 R. G. Feick and J. A. Shiozawa, *Anal. Biochem.*, 187 (1990) 205.

Journal of Chromatography, 605 (1992) 215–220
Elsevier Science Publishers B.V., Amsterdam

CHROM. 24 245

Vitamin D determination using high-performance liquid chromatography with internal standard–redox mode electrochemical detection and its application to medical nutritional products☆

Hideo Hasegawa

Medical Nutritional Products Department, Central Research Institute, Meiji Milk Products Co., Ltd., Higashimurayama, Tokyo 189 (Japan)

(First received February 26th, 1991; revised manuscript received March 31st, 1992)

ABSTRACT

The selectivity and sensitivity of high-performance liquid chromatographic analysis for the determination of vitamin D_3 and D_2 content in medical nutritional products were improved with the aid of electrochemical detection in internal standard–oxidation/reduction mode. The relative standard deviation at the 13-nmol level for the analysis of vitamin D in products was 3.6% (n = 5). Recovery rates of added vitamin D_3 were 97.5 ± 3.0% (mean ± S.D.). It is concluded that this method is much more selective and accurate for detection of vitamin D at the nanomolar level than ultraviolet detection methods.

INTRODUCTION

It is well established that vitamin D plays an important role in preventing infantile rickets and adult osteomalacia. The daily requirement of vitamin D in adult humans has been estimated to be in the range 200 to 400 I.U. [1]. In addition, the recommended dietary allowance has been evaluated to be 400 I.U. [2], where one international unit (I.U.) of vitamin D is defined as the activity of 25 ng of *cis*-vitamin D_3 (cholecalciferol). However, a continuous vitamin D intake as low as 50–120 μg per day is known to be toxic [3,4]. Therefore, the contents of vitamin D derivatives in fortified milk and infant formulas should be carefully controlled: they are adjusted to about 400 and 350–500 I.U./l [5], respectively. Thus, estimation of the content of vitamin D in medical nutritional products is very important.

The determination of vitamin D contents in foods has been extensively elaborated by several methods [6,7]. High-performance liquid chromatography (HPLC), for example, has been well established to be useful for evaluating the vitamin D contents of infant formulas [8–11] and milk [5,12–21]. Generally, the usual HPLC methods for vitamin D determination require pretreatments of crude materials. Such HPLC methods involve UV absorbance detection, which is not selective for detecting vitamin D.

Agarwal [21] developed a method in which vitamins D_2 and D_3 are converted into isotachysterols with antimony trichloride and the isotachysterols quantitated using HPLC with UV detection at an absorption maximum of 301 nm. This method has

Correspondence to: Dr. H. Hasegawa, Medical Nutritional Products Department, Central Research Institute, Meiji Milk Products Co., Ltd., Higashimurayama, Tokyo 189, Japan.

☆ Part of this paper was presented at the *44th Annual Meeting of the Japan Society of Nutrition and Food Science, Sendai, May 1990.*

0021-9673/92/$05.00

the advantage that the other components present in the sample do not give any adsorption at this wavelength. The only disadvantage of this method is that it cannot separately determine vitamins D_2 and D_3.

Recently, we found that dual-electrode detection in the electrochemical reduction/reoxidation mode [22] is a selective and sensitive method of detecting hydrophobic vitamins. Vitamin K contained in human milk, for instance, was accurately evaluated by the HPLC method, as reported previously [23].

In this report, we discuss an HPLC–internal standard–redox mode electrochemical detection (ED) method and apply it to the determination of vitamin D in medical nutritional products.

EXPERIMENTAL

Chemicals and materials

Crystalline vitamin D_3 [Japanese Pharmacopoeia (JP) reference standard cholecalciferol] was used as the standard. Crystalline vitamin D_2 (JP reference standard ergocalciferol) was also used as an internal standard. HPLC-grade *n*-hexane, ethanol, isopropanol and acetonitrile were purchased from Wako Pure Chemical Industries (Osaka, Japan). Sodium perchlorate and 60% perchloric acid were purchased from Nakarai Chemicals (Kyoto, Japan). Other reagents were of analytical grade. The test sample was Ensure · liquid. The commercial medical nutritional product, a nutritionally complete liquid-formula diet, was obtained from Meiji Milk Products (Gunma, Japan). It is claimed that the product is fortified with vitamin D_3 at the level of 1.25 μg per can (0.5 μg per 100 ml). The test samples were prepared by adding vitamin D_3 to the nutritional product so as to increase the vitamin D_3 level by about 30%.

Sample preparation

In a 300-ml amber boiling flask, the product sample (40 ml) was mixed with 50 ml of 0.6% ethanolic pyrogallol solution and with 6 g of solid potassium hydroxide. Then, the mixture was saponified by refluxing for 30 min in a boiling water bath. The saponified mixture was transferred to a separatory funnel, and the boiling flask was rinsed with two 25-ml portions of water and with 25 ml of diethyl ether successively. The solution was shaken vigorously in the separatory funnel. The aqueous layer was removed and the extraction procedure was repeated twice with 35 ml of diethyl ether. The diethyl ether layers were combined with those from the first extraction. The diethyl ether extracts were washed with 30-ml portions of water until there was no longer any red colour due to phenolphthalein in the aqueous layer. [When the product contains vitamin D_2, the diethyl ether solution is exactly divided into two parts; the working standard solution (0.25 μg/ml vitamin D_2) is added one of the diethyl ether solutions.] Then a 1-ml volume of the working standard solution (0.25 μg/ml vitamin D_2) was added as an internal standard [24,25] to the extracted ether solution and the solution evaporated in a flask under reduced pressure at 40°C. Then, a 5-ml volume of ethanol was added and re-evaporated to remove any trace of water in the sample. The concentrated extract was diluted with *n*-hexane and transferred to a 10-ml amber sample vial, and again evaporated to dryness under a nitrogen atmosphere. A 0.3-ml volume of *n*-hexane was added to the sample vial and the solution was used for HPLC analysis.

A 100-μl aliquot was injected onto a semipreparative HPLC column. The fraction of D_3 with D_2 was collected and evaporated to dryness under a stream of nitrogen gas. The residue was dissolved in 100 μl of methanol. A 10-μl aliquot was injected onto an HPLC column for quantitative analysis. The working standard solutions in methanol were prepared for calibration. Concentrations of the standard solutions of vitamin D_2 and D_3 were 0.25, 0.50, 0.75 and 1.0 μg/ml.

Semipreparative high-performance liquid chromatography

Generally, preliminary clean-up of the HPLC system in the analysis of vitamin D has employed the reversed-phase mode [26]. However, the highly concentrated residue obtained in saponification is often insoluble in the eluting solvents used for reversed-phase HPLC. Therefore, semipreparative HPLC in normal-phase mode was employed in the first stage.

The semipreparative HPLC system consisted of a Hitachi (Tokyo, Japan) Model L-6000 pump, a Rheodyne (Berkeley, CA, USA) Model 7125 syringe injection valve and a Hitachi Model 638-41 variable-

wavelength UV detector at 265 nm for vitamin D_2 and D_3. A column (Nucleosil 50-5, 5 μm particle size, 25 cm × 4.6 mm I.D.) produced by Macherey-Nagel (Düren, Germany) was used for semipreparation. The eluent was a mixture of *n*-hexane–isopropanol (99.5:0.5) and elution rate was maintained at 4 ml/min.

Quantitative high-performance liquid chromatography

The phase system was optimized in terms of the selectivity between vitamins D_2 and D_3 and co-extracted sample constituents. The quantitative HPLC system consisted of a Hitachi Model L-6200 pump and a Rheodyne Model 7125 sample valve. An ESA 5100A Coulochem system (Bedford, MA, USA) was used for ED of the eluting compounds. The 5100A system was composed of a Model 5011 dual analytical cell and a Model 5020 guard cell. The former dual cell was located in series at the end of the HPLC column; the potentials applied to detectors 1 and 2 in the dual cell were adjusted to +0.65 V and −0.20 V, respectively. The latter guard cell was located between the pump and the sample injector; the potential applied to the guard cell was adjusted to +0.65 V.

An H_2/H^+ (NHE) electrode was used as a reference in our reaction system. All chromatograms from detector 2 were recorded. In our HPLC system, a UV detector as a monitor was also set between the HPLC column and the dual cell. A column (Hitachi Gel 3056 reversed-phase column, 5 μm particle size, 25 cm × 4.0 mm I.D.) for quantitative analysis was purchased from Hitachi. The eluent was acetonitrile–methanol – 50% perchloric acid (970:30:1.2) containing 0.057 *M* sodium perchlorate. The mobile phase was run at a flow-rate of 1.2 ml/min. All experiments were performed at room temperature.

RESULTS AND DISCUSSION

HPLC for semipreparation

Typical chromatograms of a standard solution of vitamin D_2 (2.5 μg/ml) and D_2 (2.5 μg/ml) and an extracted sample are shown in Fig. 1. Vitamins D_3 and D_2 in the sample were eluted at about 6.2 min. It is clear from Fig. 1A that vitamin D_3 is not separated from vitamin D_2, *i.e.*, a single peak is observed at 6.2 min. Therefore, vitamins D_3 and D_2 in the extracted sample should be eluted between 6 and 6.5 min. However, the peak of vitamins D_3 and D_2 in the extracted sample could not be identified on the chromatogram, as shown in Fig. 1B, because of peaks due to contaminants and the relativity low concentration of vitamins in the sample.

Optimization of electrochemical detection

The mean half-peak oxidation potential of vitamin D_3 and D_2 in water containing 25% methanol was estimated to be about 0.95 ± 0.02 V *vs.* Ag/Ag^+ [27]. We found that the oxidation potential of vitamin D_3 and D_2 in acetonitrile–methanol–50% perchloric acid (970:30:1.2) containing 0.057 *M* sodium perchlorate agreed with the above value within the experimental error. The ESA electrochemical detector used here was supposed to either oxidize or reduce 99% of each compound in the sample, depending on the positive or negative potential applied [28,29]. To obtain the optimum potential applied to our HPLC detection system, the

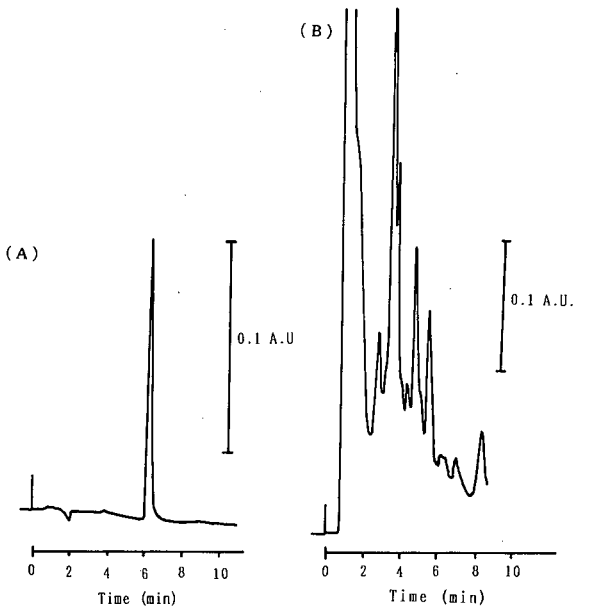

Fig. 1. Profiles of the semipreparative HPLC of the mixture of standard vitamins D_3 and D_2 and the unsaponifiable sample from a medical nutritional product as described in the Experimental section. (A) Chromatogram of an authentic mixture of vitamins D_3 and D_2 in solution (each 2.5 μg/ml); (B) chromatogram of the unsaponifiable sample.

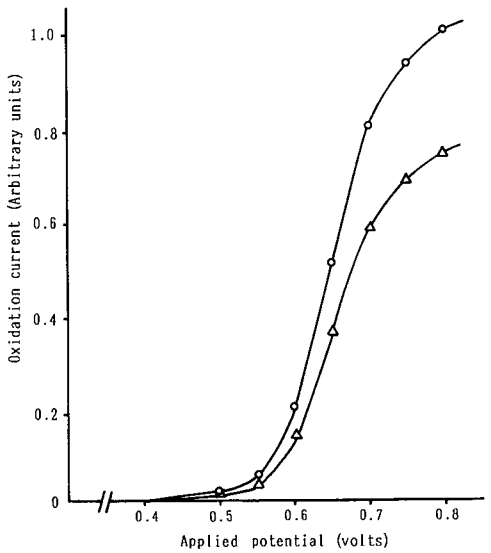

Fig. 2. Hydrodynamic voltammograms of vitamins D_3 and D_2. Hydrodynamic voltammetry was carried out for standard solutions containing vitamins D_3 and D_2: ○ = 1.0 μg/ml cholecalciferol (vitamin D_3); △ = 1.0 μg/ml ergocalciferol (vitamin D_2). The applied potential was variable at the downstream electrode, whereas it was fixed at zero at the upstream electrode.

hydrodynamic voltammetry was carried out for standard solutions containing vitamins D_3 and D_2 (Fig. 2). Fig. 2 shows the hydrodynamic voltammograms of vitamins D_3 and D_2, plots of oxidation currents against the applied potentials to cell 2 (in detector 2) with zero potential to cell 1 (in detector 1). It is apparent from Fig. 2 that vitamins D_3 and D_2 are converted to their oxidized forms by electrochemical oxidation, and that the higher applied potential gives a higher oxidation current for the standard solution. The half-wave potentials for both vitamins are nearly identical, *ca.* +0.65 V. On the basis of the observed noise level, the detection limit for vitamins in the standard solution was estimated to be about 8 pg when an applied potential of +0.65 V was used. Although the sensitivity by this detection mode was much higher than that with the UV method, the chromatograms of the peak fraction from the preparative HPLC were complicated because of strong background due to contaminants. Also, an applied potential higher than about 0.7 V gave rise to greater noise. Another drawback to the electrochemical oxidation method as described above is the problem of recovery of vitamin D. Wilske and Hulthe [30] tried to detect of 25-hydroxyvitamin D_3 in human serum by HPLC–electrochemical oxidation methods. This achieved only a low extraction efficiency (53%) of vitamin D_3.

We have found that the vitamin D was converted to an unidentified oxidated form at the upstream electrode (cell 1) and that it was reconverted to the reduced form at the downstream electrode (cell 2). Keeping a constant potential of +0.65 V at the upstream electrode, the current of the downstream electrode was measured as a function of the downstream electrode potential in the range 0 V to −0.5 V. Fig. 3 shows the plots of reduction current as a function of applied potential. The reduction current is linearly changed as the applied potential is increased from 0 to −0.3 V. A larger current resulted in a more negative potential, but background noise was increased. Thus, the optimum potentials for the oxidation and reduction were +0.65 V and −0.20 V, respectively.

Fig. 4A shows a typical chomatogram of a medical nutritional product obtained under the ED conditions described above. It is remarkable that well resolved peaks of vitamins D_2 and D_3 are observed and that the peaks are also separated from the majority of unsaponifiable compounds. As a result, vitamins D_2 and D_3 can be accurately quantitated by this method. Fig. 4B is a chromatogram of the same sample without vitamin D_2 as an

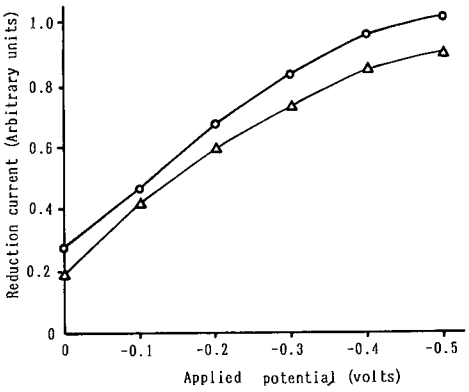

Fig. 3. Hydrodynamic voltammograms of vitamins D_3 and D_2. Hydrodynamic voltammetry was carried out for standard solutions containing vitamins D_3 and D_2: ○ = 1.0 μg/ml vitamin D_3; △ = 1.0 μg/ml vitamin D_2. The applied potential was variable at the downstream electrode, whereas it was fixed at +0.65 V at the upstream electrode.

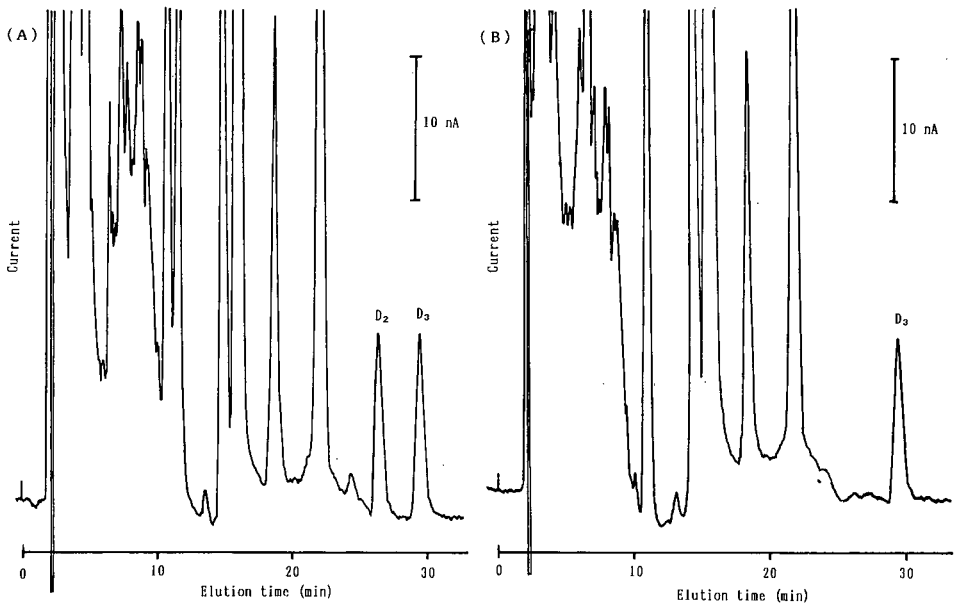

Fig. 4. Typical chromatograms of the extract from a medical nutritional product recorded by ED in the oxidation (+0.65 V)/reduction (−0.20 V) mode. (A) With addition of vitamin D_2 as an internal standard (0.625 μg per 100-ml sample); (B) without addition of vitamin D_2. Peaks D_2 and D_3 were assigned to vitamins D_2 and D_3, respectively.

internal standard. In the absence of vitamin D_2, only one peak due to vitamin D_3 is clearly observed in range 29–30 min. In comparison with the chromatograms observed in the presence and absence of vitamin D_2, the background at peak position is almost at the baseline level.

In conclusion, ED in the redox mode has many advantages over UV detection in terms of both selectivity in the region of elution of vitamins D_2 and D_3 and sensitivity. This method is able to detect both vitamins D_2 and D_3 because the vitamin D_2 and D_3 peaks obtained by UV detection are broad peaks compared with the ED peaks. Therefore, it appears that the UV peaks for vitamins D_2 and D_3 contain co-eluting substances.

Linearity, recovery and precision

Calibration curves for vitamins D_3 and D_2 were obtained based on ED in redox mode. They were found to be linear over the range 0.05–1.0 μg/ml. The peak observed for vitamin D_3 solution at a concentration as low as 50 ng/ml was reproducible and 5 mm in height. Assuming that the detection limit is twice the noise level of the baseline, the limit was estimated to be about 200 pg based on the observed peak height. The amount of vitamin D_3 in a given sample is calculated using internal standard of vitamin D_2.

The relative response factor (R_{rf}) of D_3 is:

$$\frac{\text{Peak height of } D_2}{\text{Concentration of } D_2} \times \frac{\text{concentration of } D_3}{\text{peak height of } D_3}$$

The amount of vitamin D_3 in the product sample (μg per 100 ml) is:

$$\frac{\text{Peak height of } D_3}{\text{Peak height of } D_2} \times \frac{100}{40} \times$$

$$\times \text{ added } D_2 \text{ standard } (\mu g) \times R_{rf} \times F_c$$

where F_c is the conversion factor [31], which was assumed to be 1.25 for pre-vitamin D [32,33].

The precision of our method may be evaluated by its reproducibility in the analysis of medical nutritional products. The results are shown in Table I. When the same sample was analysed five times on different days, a mean value of 5.78 and an S.D. of ±0.21 ng/ml were obtained, meaning that the relative standard deviation from the mean value was 3.6%. Recoveries of added vitamin D_3 were 97.5 ± 3.0% (mean ± S.D.).

TABLE I

REPRODUCIBILITY AND RECOVERY RATE OF VITAMIN D_3 ANALYSIS IN A MEDICAL NUTRITIONAL PRODUCT

Test	Before adding D_3 (μg/100 ml)	After adding 1.5 ng/ml D_3 (μg/100 ml)	Recovery rate	
			μg/100 ml	%
1	0.588	0.736	0.0148	98.7
2	0.585	0.725	0.0140	93.3
3	0.549	0.696	0.0147	98.0
4	0.564	0.708	0.0144	96.0
5	0.602	0.754	0.0152	101.3
Mean	0.578	0.724	0.0146	97.5
S.D.	0.021	0.023	0.0045	3.0

In conclusion, dual ED of vitamin D in the oxidation/reduction mode with an internal standard appears to be much more selective and accurate than UV detection at the nanomolar level for the measurement of vitamin D in medical-nutritional products. Its selectivity can be dramatically improved by converting vitamin D to its oxidized form at the upstream electrode in a dual-electrode system before detecting reduced current at the downstream electrode. The method is applicable to the pharmacokinetic study of vitamin D as well as the analysis of vitamin D in other medical nutritional products, fortified milks and infant formulas.

REFERENCES

1 H. F. DeLuca, in R. B. Alfin-Slater and D. Kritchevsky (Editors), *Human Nutrition*, Plenum Press, New York, 1980, p. 205.
2 *Recommended Dietary Allowances*, National Academy of Sciences, Washington, DC, 1989.
3 Committee on Nutrition, *Pediatrics*, 40 (1967) 1050.
4 H. F. DeLuca, in H. F. DeLuca (Editor), *Handbook of Lipid Research, Vol. 2, Fat. Soluble Vitamins*, Plenum Press, New York, 1978, p. 69.
5 B. Borsje, E. J. De Vries, J. Zeeman and F. J. Mulder, *J. Assoc. Off. Anal. Chem.*, 65 (1982) 1225.
6 D. B. Parrish, *CRC Crit. Rev. Food Sci. Nutr.*, 12 (1979) 29.
7 H. Indyk and D. C. Woollard, *N. Z. J. Dairy Sci. Tech.*, 19 (1984) 1.
8 D. C. Sertl and B. E. Molitor, *J. Assoc. Off. Anal. Chem.*, 68 (1985) 177.
9 W. O. Landen, Jr., *J. Assoc. Off. Anal. Chem.*, 68 (1985) 183.
10 H. Indyk and D. C. Woollard, *J. Micronutr. Anal.*, 1 (1985) 121.
11 J. N. Thompson, G. Hatina, W. B. Maxwell and S. Duval, *J. Assoc. Off. Anal. Chem.*, 65 (1982) 624.
12 J. N. Thompson, W. B. Maxwell and M. L'Abbé, *J. Assoc. Off. Anal. Chem.*, 60 (1977) 998.
13 S. K. Henderson and A. F. Wickroski, *J. Assoc. Off. Anal. Chem.*, 61 (1978) 1130.
14 S. K. Henderson and L. A. McLean, *J. Assoc. Off. Anal. Chem.*, 62 (1979) 1358.
15 T. Okano, A. Takeuchi and T. Kobayashi, *J. Nutr. Sci. Vitaminol.*, 27 (1981) 539.
16 E. J. De Vries and B. Borsje, *J. Assoc. Off. Anal. Chem.*, 65 (1982) 1228.
17 A. F. Wickroski and L. A. McLean, *J. Assoc. Off. Anal. Chem.*, 67 (1984) 62.
18 S. L. Reynolds and H. J. Judd, *Analyst*, 109 (1984) 489.
19 J. T. Tanner, J. Smith, P. Defibaugh, G. Angyal, M. Villalobos, M. P. Bueno, E. T. McGarrahan, H. M. Wehr, J. F. Muniz, B. W. Hollis, Y. Koh, P. Reich and K. L. Simpson, *J. Assoc. Off. Anal. Chem.*, 71 (1988) 607.
20 S. F. O'Keefe and P. A. Murphy, *J. Chromatogr.*, 445 (1988) 305.
21 V. K. Agarwal, *J. Assoc. Off. Anal. Chem.*, 71 (1988) 19.
22 Y. Haroon, C. A. W. Schubert and P. V. Hauschka, *J. Chromatogr. Sci.*, 22 (1984) 89.
23 H. Isshiki, Y. Suzuki, A. Yonekubo, H. Hasegawa and Y. Yamamoto, *J. Dairy Sci.*, 71 (1988) 627.
24 S. L. Reynolds and H. J. Judd, *Analyst*, 109 (1984) 489.
25 H. Indyk and D. C. Woollard, *N. Z. J. Dairy Sci. Tech.*, 20 (1985) 19.
26 *Official Methods of Analysis*, AOAC, Arlington, MA, 15th ed., 1990, Section 980.26.
27 S. S. Atuma, K. Lundström and J. Lindquist, *Analyst*, 100 (1975) 827.
28 K. Hyland, *J. Chromatogr.*, 343 (1985) 35.
29 J. P. Langenberg and U. R. Tjaden, *J. Chromatogr.*, 305 (1984) 61.
30 J. Wilske and B. Hulthe, in A. W. Norman, K. Schaefer, H. G. Grigoleit and D. V. Herrath (Editors), *Vitamin D. A Chemical, Biological and Clinical Update*, Walter De Gruyter, Berlin, 1985, p. 838.
31 *Official Methods of Analysis*, AOAC, Arlington, MA, 15th ed., 1990, Section 981.17.
32 K. H. Hanewald, M. D. Rappoldt and J. R. Roborgh, *Recl. Trav. Chim. Pays-Bas*, 80 (1961) 1003.
33 J. A. K. Buisman, K. H. Hanewald, F. J. Mulder, J. R. Roborgh and K. J. Keuning, *J. Pharm. Sci.*, 57 (1968) 1326.

Journal of Chromatography, 605 (1992) 221–225
Elsevier Science Publishers B.V., Amsterdam

CHROM. 24 152

Determination of gangliosides by high-performance liquid chromatography with photodiode-array detection

Marcello Previti and Francesco Dotta

Department of Endocrinology, University of Rome "La Sapienza", Rome (Italy)

Giuseppe Mario Pontieri

Department of Experimental Medicine, University of Rome "La Sapienza", Rome (Italy)

Umberto Di Mario

Department of Clinical and Experimental Medicine, University of RC-Catanzaro, Catanzaro (Italy)

Luisa Lenti

Department of Experimental Medicine, University of Rome "La Sapienza", Rome (Italy)

(First received December 17th, 1991; revised manuscript received March 3rd, 1992)

ABSTRACT

Mixtures of gangliosides were separated by high-performance liquid chromatography (HPLC) on amino-silica columns according to their negative charge and the length of the carbohydrate portion. The use of an on-line variable wave-length diode-array detector allows the identification of gangliosides on the basis of their UV spectra with maximum absorbance at 196 nm. Accurate analytical data acquired with the diode-array detector allow the qualitative and quantitative determination of gangliosides and therefore eliminate the need for thin-layer chromatography after HPLC separation.

INTRODUCTION

Gangliosides [1], sialic acid-containing glycosphingolipids, are components of the plasma membrane and act as binding sites on the cell surface. In addition, gangliosides can be linked to cytosol- or plasma-specific carrier proteins; however, their possible regulatory functions have only been hypothesized. The hydrophilic part of the ganglioside [2] is represented by a sialo-oligosaccharide, and a sphingosine and a fatty acid are components of the hydrophobic portion (ceramide). The number of sialic acid residues determines the negative charge of the molecule and therefore regulates the physiological capability of gangliosides to react with toxins, growth factors, antibodies and viruses [3–5].

The growing interest in these molecules has improved the methodologies used for their separation and identification. The most common separation by high-performance liquid chromatography (HPLC) generally employs amino-silica columns and a linear gradient at increasing salt concentrations in the eluent [6]. The low selectivity of conventional UV

Correspondence to: Dr. L. Lenti, Department of Experimental Medicine, University of Rome "La Sapienza", Viale R. Elena 324, 00161 Rome, Italy.

0021-9673/92/$05.00

techniques below 200 nm, together with an unfavourable signal-to-noise ratio in the far UV, causes the difficult identification of gangliosides, which are characterized by a lack of chromophores in their molecules. Therefore the identification of gangliosides after separation by HPLC is generally obtained by thin-layer chromatography (TLC) of the UV peaks and subsequent resorcinol staining, which is specific for sialic acid-containing components [7].

The advent of photodiode-array UV detectors in HPLC has provided a valuable tool for solving the analytical problems by greatly improving peak identification, peak purity assessment and quantitation.

In the work reported here anion-exchange chromatography was combined with diode-array detection to separate and identify individual gangliosides. Gangliosides in this paper are named according to the Svennerholm nomenclature [1].

EXPERIMENTAL

Chemicals

Pre-coated high-performance thin-layer chromatography (HPTLC) plates with silica gel 60 and a LiChrosorb NH_2 HPLC column (250 × 4 mm I.D., 5 μm particle size) were obtained from Merck (Darmstadt, Germany). Ganglioside standards GM3, GM1, GD1a, GD1b and GT1b were purchased from Sigma (St. Louis, MO, USA); GM2 was the kind gift of Fidia Research Labs. (Abano Terme, Italy). Phosphatidylcholine, phosphatidylethanolamine, phosphatidylserine, phosphatidylinositol and asialo GM1 were purchased from Sigma; lactosylceramide was purchased from BioCarb (Lund, Sweden). Water and acetonitrile were of HPLC grade (Merck). All other chemicals were of analytical-reagent grade.

Equipment

A Perkin-Elmer (Norwalk, CT, USA) Series 410 LC pump equipped with a SEC-4 solvent environmental control and a Rheodyne sampling valve with a 50-μl sample loop were used as the chromatographic system. The detector was a Perkin-Elmer LC-95 variable wavelength UV–visible spectrophotometer interfaced to an Epson PCAX2e computer for system control, data acquisition and report generation; the installed hardware and software were PE OMEGA. The HPLC system included an on-line Perkin-Elmer LC-235 photodiode-array detector equipped with a GP-100 graphics printer.

A Perkin-Elmer Lambda 4B UV–visible spectrophotometer was used to determine the UV spectra of all the gangliosides studied.

Chromatographic conditions

HPTLC. A standard ganglioside mixture and ganglioside-containing fractions collected during HPLC separation were assayed on HPTLC plates developed with chloroform–methanol–0.25% aqueous KCl (5:4:1, v/v/v). Gangliosides were detected with the resorcinol spray reagent [7].

HPLC. Gangliosides were chromatographed according to the method of Gazzotti *et al.* [8]. The eluent consisted of (A) acetonitrile–5 m*M* disodium phosphate buffered at pH 5.6 by phosphoric acid (83:17, v/v) and (B) acetonitrile–20 m*M* disodium phosphate buffered at pH 5.6 by phosphoric acid (1:1, v/v). The gradient elution programme used was: 7 min with A, 53 min linear gradient from A to A–B (66:34, v/v), 20 min linear gradient from A–B (66:34, v/v) to A–B (36:64, v/v). The flow-rate was 1 ml/min. All the eluents were filtered before use and degassed with helium during chromatography. A 5-μg amount of each ganglioside or 10 μg of a ganglioside mixture from bovine brain (GM1 21%, GD1a 40%, GD1b 16% and GT1b 19%) with the addition of 2 μg of GM3 and GM2 was dissolved in 50 μl of solvent A and injected. The detection wavelength was fixed at 215 nm.

Diode-array detector parameters. Using a pilot signal at 200 nm, spectra were acquired in the range 195–370 nm on the apex and on the ascending and descending part of each peak and were overlapped to determine the peak purity. In parallel, the elution profiles were acquired at 215 nm. The detection limit of the system was determined by injecting scalar concentrations of each ganglioside in the range 2.5–0.078 μg. The working *y*-axis value was fixed at 0.05 a.u.f.s.

Spectrophotometric analysis. The HPLC peaks were collected and their UV spectra recorded in the range 190–220 nm by a PE Lambda 4B UV–visible spectrophotometer. Subsequently the solvents were evaporated under nitrogen and the residues chro-

matographed on HPTLC plates as described previously.

RESULTS AND DISCUSSION

Chromatographic analysis of gangliosides

GM3, GM2, GM1, GD1a, GD1b and GT1b were injected separately and mixed to determine the retention times. In our system, gangliosides were separated according to their negative charge (mono-sialogangliosides precede di- and tri-sialogangliosides) and the length of the carbohydrate portion. The presence of a single ganglioside in each detected UV peak was confirmed by HPTLC. The resorcinol stained the bands containing the ganglioside blue–purple (Fig. 1).

Diode-array detector analysis

HPLC of the standard gangliosides was carried out with the on-line photodiode-array detector. All the gangliosides detected showed the same UV spectrum with maximum absorbance at 196 nm. Data on the peak purity of the standard gangliosides used were obtained by comparing the spectra in the ascending, apex and descending portion of each ganglioside containing peak. For standard gangliosides the three spectra were superimposable, indicating the absence of impurities and that the corresponding purity index was 1.0 (Fig. 2). Other experiments carried out on glycolipid extracts obtained from tissues (data not shown) suggested that the peak purity is acceptable if the purity index is between 1.0 and 1.5. In our system, ganglioside identification was addressed by taking into account the retention times and absorbance spectra. With regard to the detection limit, it was found to be as low as 78.125 ng. Linearity was observed up to 2.5 μg (correlation coefficient $r = 0.9866$).

Spectrophotometric analysis

The maximum absorbance characteristic of gan-

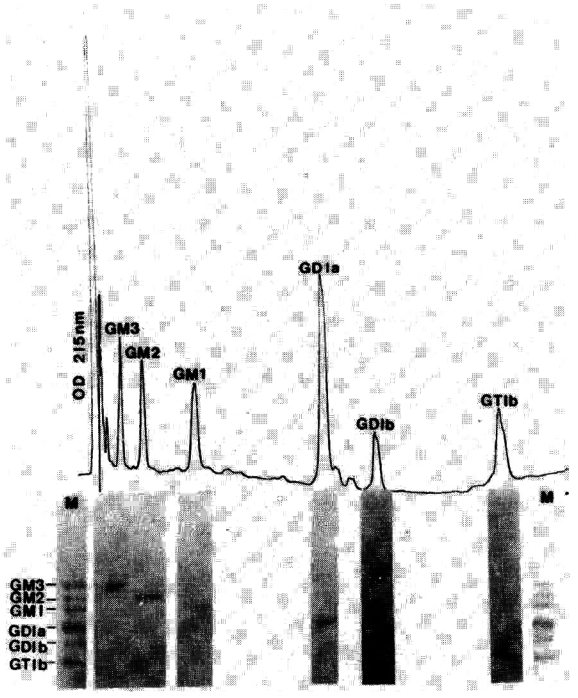

Fig. 1. HPLC and TLC analysis of a standard ganglioside mixture (GM3, 2 μg; GM2, 2 μg; GM1, 2.1 μg; GD1a, 4 μg; GD1b, 1.6 μg; GT1b, 1.9 μg). HPLC separation of standard ganglioside mixture obtained using a LiChrosorb NH_2 column; the elution profile was monitored by UV absorbance at 215 nm. Each UV peak was collected, chromatographed on silica gel 60 HPTLC plates and visualized by resorcinol staining. M = markers.

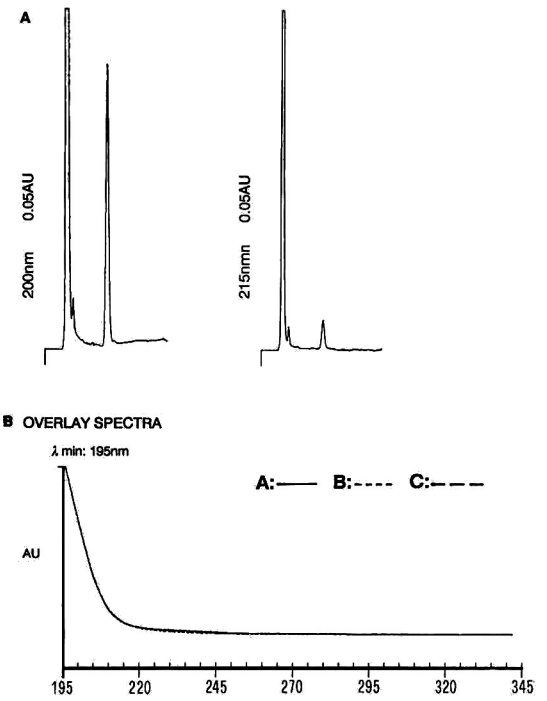

Fig. 2. (A) Chromatograms of standard GM3 detected by diode-array detector at 200 and 215 nm. (B) Peak purity of standard GM3 determined by diode-array detector. UV spectra acquired in the ascending (A), apex (B) and descending (C) portion of the peak were superimposable, indicating the absence of impurity.

gliosides corresponded in our diode-array detector system to the start of the UV acquisition data range (195–370 nm). Therefore it was planned to confirm the diode-array detector results using the Lambda 4B spectrophotometer adjusted in the range 190–220 nm. UV absorbance spectra of all the standard gangliosides, dissolved in the corresponding HPLC eluent fractions, were determined before HPLC analysis. All of them showed a characteristic spectrum with maximum absorbance at 195.8 nm (Fig. 3A). Furthermore, during HPLC separation, all the UV peaks eluting from diode-array detector system were collected. These fractions, when analysed using the spectrophotometer, confirmed the maximum absorbance at 195.8 nm obtained with diode-array detector system, thus suggesting that our HPLC conditions do not interfere with the spectrophotometric properties of ganglioside molecules. The same fractions, when dried and chromatographed on HPTLC plates, gave positive results on resorcinol staining, confirming the presence of gangliosides.

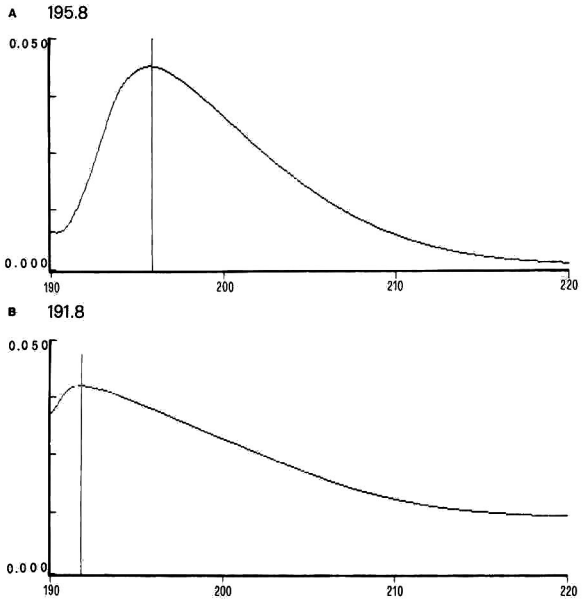

Fig. 3. Absorbance spectrum in the range 190–220 nm of (A) standard GM3 and (B) a collected unretained peak (*i.e.* phosphatidylethanolamine). *x*-Axis, wavelength expressed in nm; *y*-axis, UV absorbance expressed in a.u.f.s. The maximum absorbance is at the top of the *y*-axis.

HPLC analysis of non-ganglioside glycolipids

As highly polar lipids can be extracted with gangliosides and can co-elute with gangliosides during HPLC analysis, the retention times of non-sialic acid-containing glycolipids and phospholipids were determined. Under these chromatographic conditions, non-sialic acid-containing glycolipids (asialo GM1 and lactosylceramide) and phospholipids (phosphatidylcholine and phosphatidylethanolamine) were not retained, whereas phosphatidylserine and phosphatidylinositol had retention times of 3.5 and 3.9 min, respectively. All phospholipids tested had a maximum absorbance at 191.8 nm (Fig. 3B). In addition, a chromatographic separation of a mixture of phosphatydilinositol and GM3 (the last phospholipid and the first ganglioside to be eluted) showed two very distinct peaks, the first with the expected retention time (3.9 min) of phosphatydilinositol, the second with expected retention time (6.9 min) of GM3 (data not shown). These data show that under these chromatographic conditions phospholipids do not interfere with ganglioside seperation.

These data on the diode-array detection of gangliosides suggest that the difficulties associated with traditional UV detection at 215 nm can be avoided by the use of the variable-wavelength detector. Analytical data acquired with the diode-array detector make accurate qualitative and quantitative analyses possible. Furthermore, its high sensitivity eliminates the need for subsequent HPTLC analysis (which has until now been used for the identification of gangliosides after HPLC separation), thereby avoiding the accompanying problems of that analysis and the large sample sizes that it requires.

ACKNOWLEDGEMENTS

This work was supported by grants from the Italian Ministry of Education, National Research Council and Centro Internazionale Studi Diabete. The authors gratefully acknowledge the excellent technical assistance of P. Zoppitelli and the editorial assistance of C. Caputi and S. Salvati.

REFERENCES

1 L. Svennerholm, *J. Neurochem.*, 10 (1963) 613.
2 R. W. Leeden and R. K. Yu, *Methods Enzymol.*, 83 (1982) 139.

3 W. van Heyningen, *J. Gen. Microbiol.*, 20 (1959) 291.
4 S. Hakomori, *Proc. Natl. Acad. Sci. U.S.A.*, 67 (1970) 1741.
5 S. Spiegel and P. Fishman, *Proc. Natl. Acad. Sci. U.S.A.*, 84 (1987) 141.
6 R. Kannagi, K. Watanabe and S. Hakomori, *Methods Enzymol.*, 138 (1987) 3.
7 G. W. Jourdian, L. Dean and S. Roseman, *J. Biol. Chem.*, 246 (1971) 430.
8 G. Gazzotti, S. Sonnino and R. Ghidoni, *J. Chromatogr.*, 348 (1985) 371.

Journal of Chromatography, 605 (1992) 227–240
Elsevier Science Publishers B.V., Amsterdam

CHROM. 24 233

Determination of the explosive 2,4,6-trinitrophenylmethylnitramine (tetryl) and its transformation products in soil

S. D. Harvey, R. J. Fellows, J. A. Campbell and D. A. Cataldo

Pacific Northwest Laboratory, P.O. Box 999, Richland, WA 99352 (USA)

(First received October 4th, 1991; revised manuscript received April 2nd, 1992)

ABSTRACT

Soils amended with uniformly ring-labeled [^{14}C]-2,4,6-trinitrophenylmethylnitramine (tetryl) were subjected to exhaustive Soxhlet extraction followed by high-performance liquid chromatographic analysis immediately after amendment and at 11, 30, and 60 days post-amendment. Transformation of tetryl was found to be extremely rapid. Tetryl was below the detection limit in soil extracts by 30 days post-amendment. Radiochromatographic profiles revealed the presence of a variety of transformation products. The primary transformation product appeared in soil extracts immediately after amendment and was subsequently identified as N-methyl-2,4,6-trinitroaniline. A minor transformation pathway was identified that involved direct ring nitro reduction of tetryl, resulting in the production of an aminodinitrophenylmethylnitramine isomer. The mass balance of the soil system was greater than 79% over the 60-day study, with 43% of the amended radiolabeled found to be non-extractable at the conclusion of the study.

INTRODUCTION

The explosive 2,4,6-trinitrophenylmethylnitramine, commonly referred to as tetryl (structure given in Fig. 7), detonates with more force and less shock or frictional provocation than either 2,4,6-trinitrotoluene (TNT) or hexahydro-1,3,5-trinitrotriazine (RDX). As such, tetryl has found its primary use as either a booster explosive or a base charge in blasting caps and detonators. Substitution of more stable high explosives, such as RDX, for uses traditionally dominated by tetryl has been a recent trend that has culminated in discontinuation of tetryl production within the United States [1].

Munitions manufacturing, packing and decommissioning facilities produce large quantities of waste waters containing explosives residues. In the past, these manufacturing rinse waters were directed to lagoons for primary settling before being discharged to rivers and streams. For environmental reasons, this practice has long been abandoned; however, environmental concerns persist because evaporation of lagoons has resulted in localized areas of severe contamination. Although TNT and RDX were the primary contaminants contained in discharge waste waters, significant amounts of other explosives residues, including tetryl, were released. The potential pollution problem becomes apparent when one considers that tetryl production resulted in daily release of an estimated 16 kg of tetryl from a single manufacturing plant [2]. As the toxic parent munitions and their soil transformation products are available for plant uptake, it becomes imperative to delineate soil transformation pathways, the propensity for plant uptake of these compounds and further plant metabolic alteration of the munitions residues. Such studies will ultimately result in understanding the impact of lagooning practices on food-chain transfer of munitions residues.

Correspondence to: Dr. S. D. Harvey, Pacific Northwest Laboratory, P.O. Box 999, Richland, WA 99352, USA.

The toxicity of tetryl has been documented. Acute toxic effects of tetryl exposure include skin irritation and dermatitis [3,4]. These symptoms were commonly manifested by munitions workers in early production facilities that lacked vigorous hygiene precautions. Tetryl has also been found to be mutagenic in several different bacterial assays [5].

Although studies elucidating the environmental fate of tetryl are absent from the literature, the toxicity of the possible transformation products is sufficient for concern. The related polynitro aromatic explosive TNT is known to undergo bacterial metabolism to nitroso metabolites [6]. Further reduction of the nitroso group to an amino functionality is a transformation pathway that also is well documented for TNT [6]. Transformation of tetryl could proceed in an analogous manner by reduction at either the aniline nitro group or the aromatic nitro positions resulting in formation of N-nitroso or nitroso transformation products, respectively. The mutagenicity of both these classes of compounds is well established.

A survey of the analytical literature pertaining to tetryl reveals that gas chromatographic analysis of water exracts with electron-capture detection can achieve detection limits ranging from *ca.* 1000 to 20 parts per 10^{12} (ppt) [7,8]. However, the thermal lability of this explosive would seem to indicate an obvious advantage for the use of condensed-phase over gas chromatographic separation techniques. A number of researchers have described high-performance liquid chromatographic (HPLC) methods utilizing ultraviolet absorption detection for the determination of tetryl [9–11]. Several of these methods have been applied to the determination of explosives in soil extracts [10–13].

The aim of this study was to investigate the environmental fate of tetryl in soil with the primary objective of gaining a clear understanding of the products available for plant uptake. Uniformly ring-labeled tetryl was utilized to evaluate the soil system for a mass balance of amended analyte and to allow for unambiguous identification of transformation products.

EXPERIMENTAL

Uniformly ring-labeled [^{14}C]tetryl, having a specific activity of 14.64 mCi/mmol, was obtained from New England Nuclear (DuPont, Boston, MA, USA). Radio-HPLC was utilized to assess the purity of [^{14}C]tetryl. During the chromatographic analysis (conditions described below), successive 0.5-ml increments of the column eluate were collected. After the addition of 15.0 ml of Ready-Solv EP cocktail (Beckman Instruments, San Ramon, CA, USA), the individual fractions were assayed for radiocarbon by liquid scintillation spectrometry. The purity of [^{14}C]tetryl was determined to be 98.70%. This purity was judged adequate for subsequent environmental fate studies and the material was used without further purification. Bulk tetryl was obtained from the US Biomedical Research and Development Laboratory (Fort Detrick, Frederick, MD, USA). A small amount of authentic tetryl was obtained from the US Army Toxic and Hazardous Materials Agency (Aberdeen Proving Ground, MD, USA) and served as a standard analytical reference material (SARM). HPLC co-injection experiments with the SARM provided verification of the identity of radiolabeled and bulk tetryl.

Soil amendment and incubation conditions

Palouse soil, a typical Washington State agricultural soil, was used for most studies. Palouse is a silt-loam, mixed Pachic Ultic Haploxeroll. The sample was collected at Pullman, WA, USA, and consisted of the Ap horizon [14]. This soil is 77% silt and 21% clay, contains 2% organic matter, has a cation-exchange capacity of 23.8 mequiv. per 100 g and a pH of 5.4. For comparison to Palouse soil, Burbank (a sandy loam having a pH of 7.4) and Cinebar (a silt loam having a pH of 5.6) soils were also studied. Solutions containing appropriate proportions of non-radiolabeled and ^{14}C-labeled tetryl were prepared in 2.0 ml of methanol and amended to 400 g of air-dried soil to give a final concentration of 60 ppm tetryl containing 10 μCi of radiolabeled tetryl. Uniform amendment was facilitated by thoroughly cutting the tetryl solution into the soil for 15 min with a spatula prior to packing the soil into a plastic-lined carton. Amended soils were immediately brought to and maintained at 66% field capacity with water. Soils were incubated in a growth chamber environment that simulated the luminous intensity and spectral dispersion of sunlight during the 16-h light period. The chamber was maintained at a day/night temperature of 26/22°C and a relative humidity of 50%.

Analytical separations

Analytical separations were performed on a system consisting of a Waters Model 600E controller and pump and a Waters Model 490E detector (Waters Assoc., Milford, MA, USA). Injections (20 μl) were provided to a Beckman Ultrasphere ODS (5 μm) (24 cm × 4.6 mm I.D.) column by a Waters WISP Model 710 automatic injector. The absorbance maximum of tetryl in acetonitrile was determined to be 264 nm (Beckman DU-7 spectrophotometer). This wavelength was utilized at a detector sensitivity of 0.008 a.u.f.s. for all chromatographic profiles generated in this study. Separations were effected by solvent programming the acetonitrile–water mobile phase from 35 to 100% acetonitrile over 30 min and maintaining the final mobile phase composition for an additional 10 min. HPLC-grade solvents, obtained from J. T. Baker (Phillipsburgh, NJ, USA), were used throughout these studies. Integrated peak areas, provided by a Hewlett-Packard (Avondale, PA, USA) Model 3390A integrator, formed the basis for quantification.

Representative soil extracts were further analyzed by radiochromatography in order to identify unambiguously tetryl transformation products. Once incorporation of radiolabel had been verified by radiochromatography, soil transformation products were further characterized by determining their alkylphenone retention indices [15,16].

Ancillary techniques

The column eluate corresponding to the elution of tetryl transformation products was collected during repetitive chromatographic runs to collect sufficient material for further chemical characterization. Fourier transform infrared (FT-IR) spectra were obtained on NaCl pellets by use of an IR microscope (IR-Plan advanced analytical microscope, Spectra-Tech, Stamford, CT, USA) interfaced to a Nicolet (Fremont, CA, USA) Model 740 spectrometer. Analysis by gas chromatography–mass spectrometry (GC–MS) of the HPLC-purified transformation products was conducted on a Hewlett-Packard Model 5890 gas chromatograph interfaced to a Hewlett-Packard Model 5970 mass-selective detector. Samples were introduced to a 30 m × 250 μm I.D. DB-5 (d_f = 1.0 μm) column (J & W Scientific, Folsom, CA, USA) by on-column injection, at which time the column was programmed from 110 to 300°C at 10°C/min. Direct insertion probe analyses were performed on a Hewlett-Packard Model 5985 mass spectrometer operated at a source temperature of 200°C in either the 70-eV electron impact or the chemical ionization mode. For chemical ionization experiments, isobutane reagent gas delivery was adjusted to achieve $1.8 \cdot 10^{-4}$ Torr as measured external to the source.

Extraction of soils

Soils were sampled (10.00 g) in triplicate immediately after amendment and at 11, 30 and 60 days post-amendment. Samples were placed in preweighed glass extraction thimbles and subjected to exhaustive Soxhlet extraction with 200 ml of methanol for 48 h. The first soil extractions (t = 0) were initiated within 30 min of amendment. The Soxhlet apparatus was wrapped with aluminum foil during extractions to minimize photodecomposition of tetryl. After extraction, the methanol extract was filtered through a 0.45-μm nylon 66 filter (Alltech, Deerfield, IL, USA) and reduced in volume to *ca.* 20 ml by rotary evaporation. The concentrated extract was then filtered through a 0.45-μm nylon 66 filter and the final volume adjusted to 25.0 ml. Samples of the final extract were removed for liquid scintillation spectrometry and HPLC analysis. The methanol distillates resulting from rotary evaporation and spent filters were assayed for radioactivity by liquid scintillation spectrometry.

Residual methanol contained in the soils after extraction was removed under vacuum (*ca.* 10^{-4} Torr) for 14 h. Accurate soil dry weights were then obtained and sub-samples removed for oxidation. Oxidation of the extracted soils, performed on a Packard (Downers Grove, IL, USA) Model 306 oxidizer, allowed the determination of the non-extractable radiolabel that was associated with the soil matrix.

Room-temperature methanol extraction was performed on tetryl-amended Palouse soil for comparison with extracts generated by the Soxhlet extraction procedure. Extraction was effected by agitating 6.0 g of soil with 10 ml of methanol on a vortex mixer for 15 min. After centrifugation, the supernatant was decanted and the extraction repeated with two additional portions of methanol. The methanol extracts were then pooled, filtered and reduced to dryness with a stream of dry nitrogen. The

residue was reconstituted with 15.0 ml of methanol prior to analysis by HPLC.

Determination of $^{14}CO_2$ and volatile organic emissions

The emission of volatile organics and $^{14}CO_2$ from tetryl-amended soil was monitored by a previously described technique [17]. Briefly, soil pots were enclosed within a sealed canister through which air was drawn by vacuum at a rate of 500 ml/min. Air passed successively over the soil, through a column containing XAD-2 resin which sorbed volatile organics and finally through three consecutive bubbler traps containing 3 *M* NaOH to trap $^{14}CO_2$. After collection, the organics were eluted from the XAD column with methanol. Liquid scintillation spectrometry was utilized to determine radiocarbon present in the NaOH and the methanol eluate from the XAD column.

RESULTS AND DISCUSSION

The chemical integrity of the radiolabeled and bulk tetryl was verified by chromatographic co-elution experiments with the SARM standard under

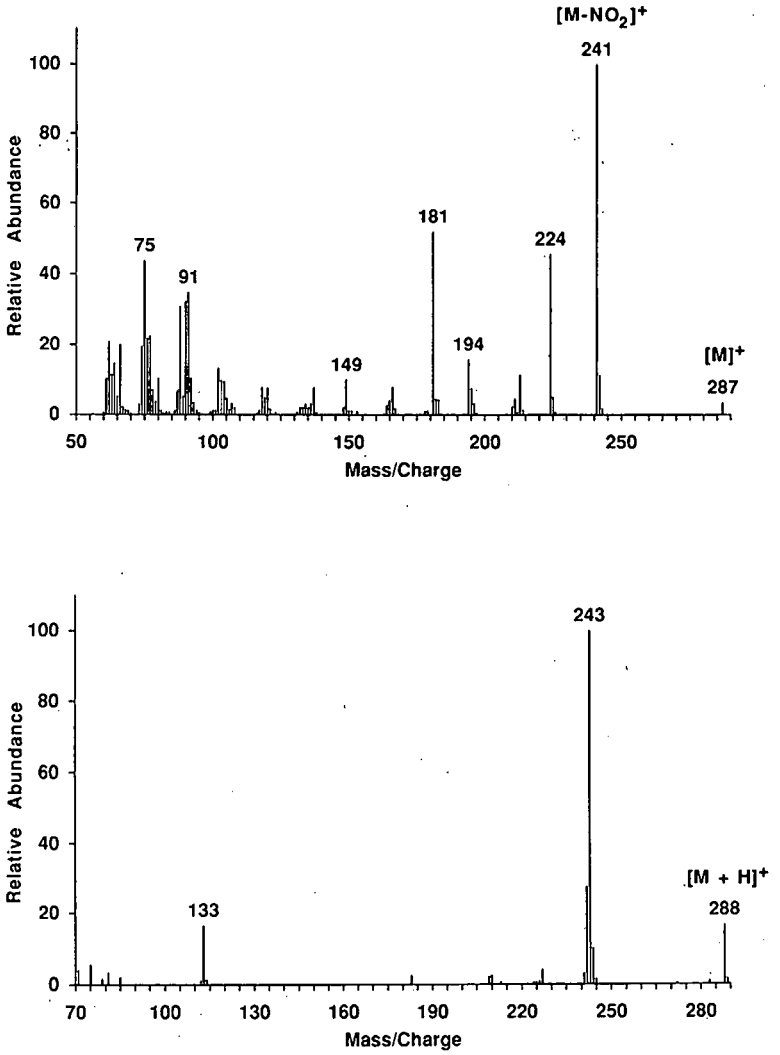

Fig. 1. Direct insertion probe electron impact (top) and isobutane chemical ionization (bottom) mass spectra of tetryl.

the HPLC conditions described above. Analysis of the SARM tetryl (molecular weight 287) by GC–MS yielded a single peak with a retention time of 19.9 min. The corresponding mass spectrum gave an apparent molecular ion at m/z 242 with a base fragment of 194, indicating that tetryl had undergone thermal decomposition on GC analysis. A possible thermal degradation mechanism would involve the cleavage of the aniline nitro group, resulting in the formation of N-methyl-2,4,6-trinitroaniline (molecular weight 242). Artifactitious formation of N-methyl-2,4,6-trinitroaniline, resulting from thermal decomposition of tetryl on GC analysis, has been described previously [18]. Further efforts to verify the identity of the SARM standard centered on direct insertion probe mass spectrometry due to the more thermally mild analytical conditions. Direct introduction of the standard material into the mass spectrometer source gave the electron impact and isobutane chemical ionization mass spectra shown in Fig. 1. These spectra match those previously reported for tetryl [19,20]. The spectra in Fig. 1 are presented here for comparison with subsequent mass spectral studies of tetryl transformation products that were conducted under identical source pressure and temperature conditions.

Tetryl transformation products in soil extracts

The stability of tetryl under the extraction conditions was examined by refluxing triplicate 200-ml methanol solutions containing 15 ppm of tetryl for 48 h. After this reflux period, the solutions had a distinct greenish hue, indicating that decomposition of the parent explosive had occurred. Chromatographic recovery of tetryl in the heated solutions

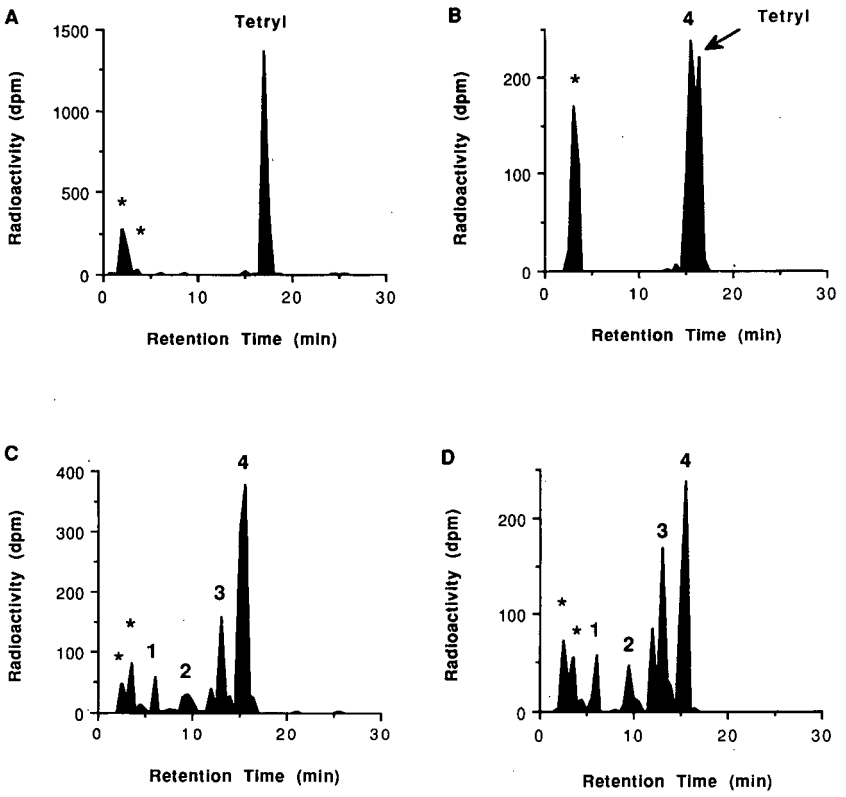

Fig. 2. Representative radio-HPLC profiles of (A) a methanolic solution of tetryl after 48 h of reflux, and extracts of tetryl-amended soil performed (B) immediately after amendment, (C) 11 days post-amendment and (D) 30 days post-amendment. Peaks labeled 1–4 correspond to tetryl soil transformation products. Peaks marked with asterisks elute in a retention window that contains tetryl decomposition products that arise from the Soxhlet extraction procedure.

was determined to be 82.46 ± 1.68%. A radiochromatogram of the refluxed tetryl solution is shown in Fig. 2A. This radiocarbon profile indicates that all tetryl decomposition products (18% of the radiolabel) are contained in two peaks that eluted immediately after the column dead volume. These extraction artifacts are labeled with asterisks in Fig. 2A. Although the extraction conditions induced a limited amount of tetryl decomposition, the utility of this technique was evident as tetryl transformation products could be determined, provided that elution is not coincident with the column void volume.

A variety of tetryl transformation products were observed in the chromatograms of the soil extracts. Radiochromatographic analysis of extracts from tetryl-amended soils aged for 0, 11 and 30 days are shown in Fig. 2B, C and D, respectively. Fig. 2B shows the presence of a primary tetryl transformation product (peak 4) that appeared in extracts initiated immediately after amendment. Tetryl and transformation product 4 are not fully resolved in Fig. 2 owing to the loss of chromatographic resolution that occurs when assaying individual 0.5-ml fractions for radiocarbon. These compounds were, however, baseline resolved in chromatograms utilizing UV absorption detection. Chromatograms of extracts from the 11- and 30-day periods show the persistence of peak 4 and the appearance of several additional transformation products of higher polarity (peaks 1–3). The same transformation products were observed in extracts from tetryl-amended Burbank and Cinebar soils. The first-eluting peaks in these chromatograms (labeled with asterisks) appear at the same retention time as the artifacts formed from tetryl during the reflux period.

The soil transformation products observed in this study were further characterized by their alkylphenone retention indices [15,16]. Calculations were based on a co-injection of alkylphenone standards with an extract of Palouse soil that had been incubated with tetryl for 11 days. The retention indices were determined to be 714, 813, 872 and 922 for transformation products 1, 2, 3 and 4, respectively. An alkylphenone retention index of 946 was calculated for tetryl.

Identification of the primary tetryl transformation product (transformation product 4)

Interestingly, GC–MS analysis of the HPLC-purified transformation product 4 gave a single peak with a retention time and mass spectrum that were identical with those previously observed during GC–MS studies of tetryl. The most plausible explanation of this result is that soil transformation product 4 is actually the same product formed by the thermal decomposition of tetryl during GC analysis. Alternatively, the transformation product could contain an alteration of the aniline nitro group that decomposes in a manner similar to that hypothesized for tetryl when subjected to the temperatures necessary for GC.

Additional information about the identity of transformation product 4 was provided by FT-IR and UV–VIS spectrometry. The FT-IR spectrum of transformation product 4 featured an absorbance at 3332 cm^{-1} that was absent from the spectrum of tetryl. This spectral feature suggests the presence of an N–H bond in transformation product 4. The UV–VIS spectrum of transformation product 4 contained maxima at 344 and 415 nm. These absorbance maxima, and their relative absorption intensities, are in good agreement with a UV–VIS spectrum of N-methyl-2,4,6-trinitroaniline reported by Dubovitskii *et al.* [21].

A direct insertion probe electron impact mass spectrum of the HPLC-purified transformation product 4 was acquired to evaluate whether the spectrum obtained during GC–MS studies was due to a thermal decomposition product. The resulting mass spectrum is presented at the top of Fig. 3. This spectrum is identical with those previously obtained during GC–MS analysis of both transformation product 4 and tetryl. It appears, therefore, that transformation product 4 remains intact during GC analysis. Further mass spectral studies centered on isobutane chemical ionization to verify the molecular weight of transformation product 4. The chemical ionization mass spectrum of HPLC-purified transformation product 4 is presented at the bottom of Fig. 3. The prominent $[M + H]^+$ ion at m/z 243 indicates a molecular weight of 242. The studies described above strongly implicate N-methyl-2,4,6-trinitroaniline as the identity of transformation product 4.

Final structural verification of the identity of transformation product 4 involved the synthesis of N-methyl-2,4,6-trinitroaniline by the nucleophilic aromatic substitution reaction of picryl chloride

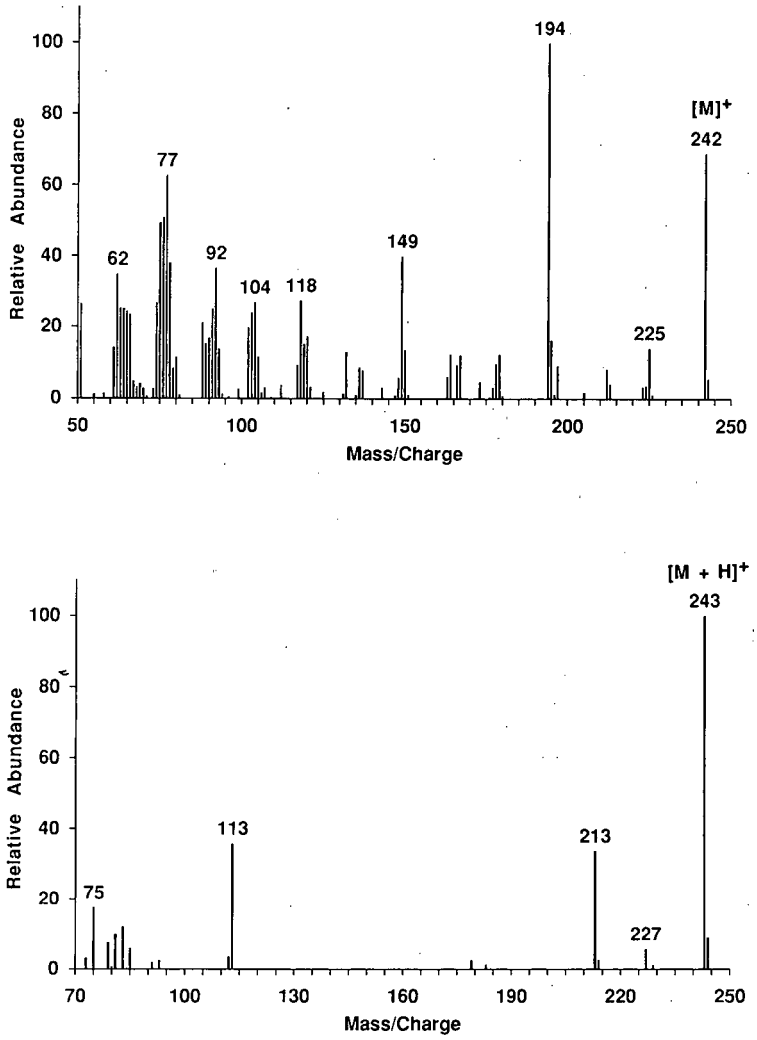

Fig. 3. Direct insertion probe electron impact (top) and isobutane chemical ionization (bottom) mass spectra of tetryl transformation product 4.

with excess of methylamine. The reaction proceeded quantitatively to the expected product at room temperature in methylene chloride solvent. HPLC co-elution of synthetic N-methyl-2,4,6-trinitroaniline with transformation product 4 is illustrated in Fig. 4. The top chromatogram is a profile of an extract from soil incubated with tetryl for 30 days; the bottom chromatogram resulted from co-injection of the same extract with synthetic N-methyl-2,4,6-trinitroaniline. The bottom chromatogram illustrates an increased relative area of peak 4 due to co-elution of synthetic N-methyl-2,4,6-trinitroaniline and transformation product 4. The synthetic product also exhibited mass spectral and chromatographic properties identical to the primary tetryl transformation product when analyzed by GC–MS, thereby verifying the structural assignment of transformation product 4 as N-methyl-2,4,6-trinitroaniline.

At room temperature, tetryl is stable and may be stored for years without indications of decomposition [9]. However, at temperatures above 120°C,

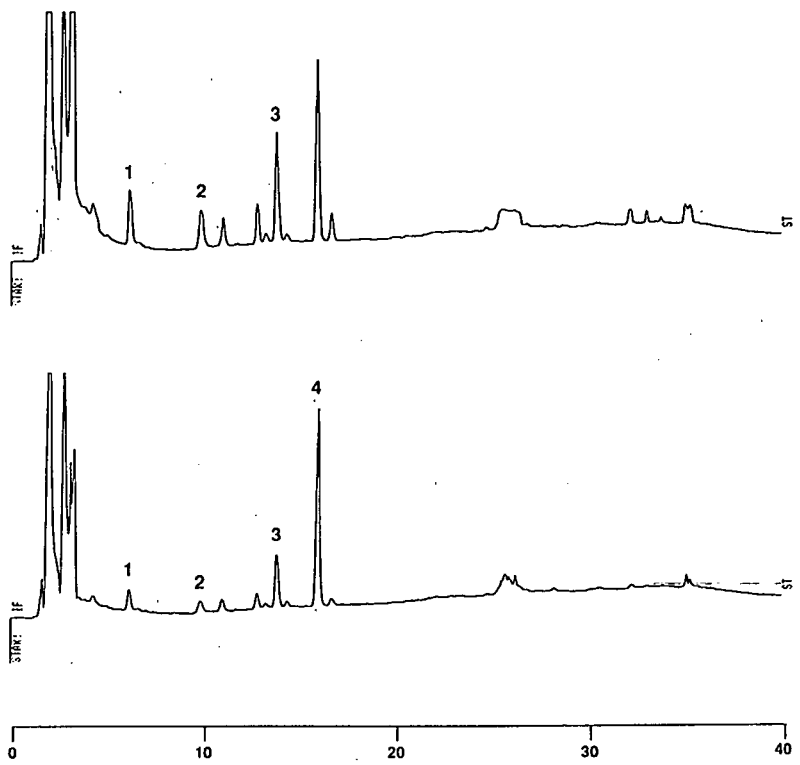

Fig. 4. HPLC profile of an extract of tetryl-amended soil performed 11 days after amendment (top) and a co-injection of the same extract with synthetic N-methyl-2,4,6-trinitroaniline (bottom). Peaks labeled 1–4 correspond to tetryl soil transformation products identified by radiochromatography (Fig. 2). This co-elution experiment establishes N-methyl-2,4,6-trinitroaniline as the identitity of tetryl transformation product 4.

thermal decomposition of tetryl readily occurs. Several studies have focused on the identification of residual components remaining after heating tetryl. Inevitably, N-methyl-2,4,6-trinitroaniline was observed in tetryl samples subjected to prolonged heating [9,21,22]. It should be emphasized that the N-methyl-2,4,6-trinitroaniline observed in this study was a true soil transformation product and did not arise as an extraction or analysis artifact.

Tentative identification of transformation product 3

HPLC-purified tetryl transformation product 3 was examined by GC–MS and direct insertion probe mass spectrometry. GC–MS analysis of HPLC peak 3 resulted in the total ion current chromatogram shown at the top of Fig. 5. The mass spectrum corresponding to the peak eluting at 20.2 min is presented at the bottom of Fig. 5. The results from this study suggest that transformation product 3 has a molecular weight of 212; however, direct insertion probe mass spectrometry resulted in an electron impact mass spectrum of transformation product 3 that differed from that obtained during the GC–MS study. The direct insertion probe mass spectrum of transformation product 3 is shown at the top of Fig. 6. The differences between spectra obtained by GC–MS and direct insertion probe analysis are attributable to thermal decomposition of transformation product 3 during GC analysis to yield a product with a molecular weight of 212.

Isobutane chemical ionization mass spectrometry of transformation product 3 resulted in the spectrum shown at the bottom of Fig. 6. The $[M + H]^+$ ion at m/z 258 indicates that transformation product 3 has a molecular weight of 257. This molecular weight (30 less than for tetryl) suggests that trans-

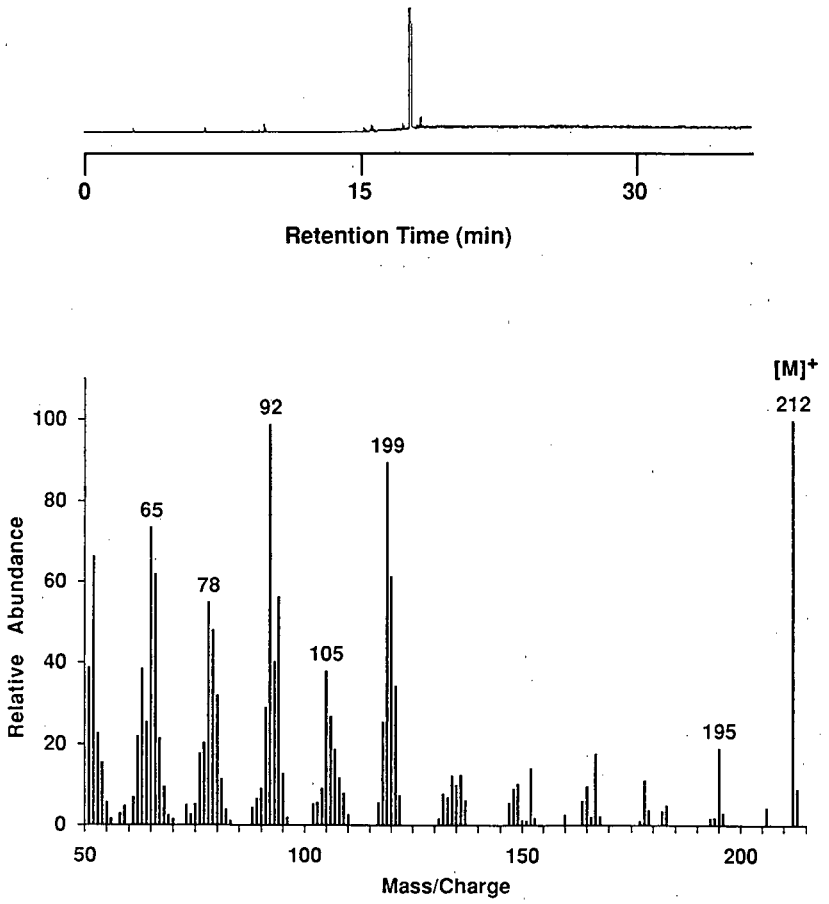

Fig. 5. Total ion current gas chromatogram (top) and corresponding mass spectrum (bottom) of transformation product 3.

formation product 3 is a nitro reduction product of the parent munition. By examination of the electron impact mass spectrum, it is possible to assign the site of nitro reduction. The base ion at m/z 211 results from cleavage of the aniline nitro group in a manner analogous to that previously observed for tetryl (see top of Fig. 1 for the spectrum of tetryl). The site of nitro reduction must therefore be at a ring position. Thermal decomposition of both tetryl and transformation product 3 occurred on GC analysis and proceeded by cleavage of the aniline nitro group. The mass spectrum of the thermal decomposition product of transformation product 3 (Fig. 5) further serves to localize the site of nitro reduction at a ring position. These data strongly suggest that transformation product 3 is a dinitroaminophenylmethylnitramine isomer. Nitro reduction products have been identified as the primary soil transformation products of the chemically related explosive TNT [12].

Thermal stability of transformation products and tentative tetryl transformation pathway

A methanol solution containing 16.8 ppm of N-methyl-2,4,6-trinitroaniline was subjected to reflux conditions for 48 h. The chromatographic recovery

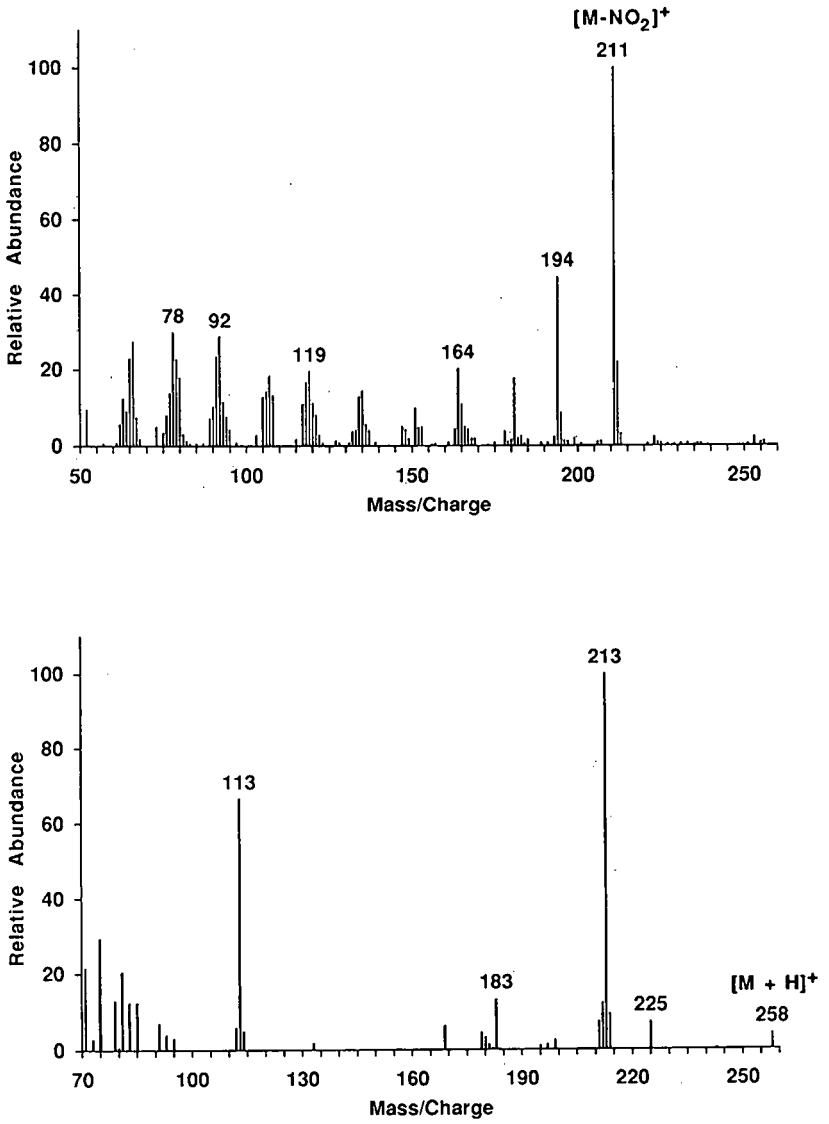

Fig. 6. Direct insertion probe electron impact (top) and isobutane chemical ionization (bottom) mass spectra of tetryl transformation product 3.

in the heated methanol solution was 95.2%. This high recovery indicated that N-methyl-2,4,6-trinitroaniline was sufficiently stable under the conditions employed for Soxhlet extraction.

A room-temperature methanol extraction was performed on Palouse soil that had been incubated with non-radiolabeled tetryl for 11 days to investigate whether Soxhlet extraction promoted decomposition of labile tetryl soil transformation products. HPLC analysis of this soil extract revealed the presence of tetryl and transformation products 1–4. Additionally, a previously unobserved transformation product (retention index of 894) was present in the room-temperature extract. The peak areas of the unknown transformation product and transformation product 3 were approximately equal. Subsequent heating of the room-temperature extract in a sealed vial at 65°C for 48 h resulted in the com-

plete destruction of the unknown tetryl transformation product. In an attempt to delineate products arising from thermal decomposition of this material, a methanol solution of HPLC-purified transformation product was heated at 65°C for 48 h. Although chromatographic studies of the heated solution confirmed rapid thermal decomposition of the unknown transformation product, the appearance of decomposition products absorbing at 246 nm was not observed.

From these studies, it is possible to postulate a tentative tetryl transformation pathway in soils as summarized in Fig. 7. The transformations proceed by two independent pathways. The most prominent tetryl transformation involves conversion of tetryl into N-methyl-2,4,6-trinitroaniline. A minor transformation pathway involves ring nitro reduction of the parent explosive, resulting in the formation of a dinitroaminophenylmethylnitramine isomer. The role of the thermally labile transformation product (retention index 894) in the tetryl transformation pathway remains uncertain. Further studies are necessary to elucidate the structure of this compound. Other more highly polar transformation products were observed in this study by radiochromatography (see peaks 1 and 2 in Fig. 2). These compounds are possible further reduction products of N-methyl-2,4,6-trinitroaniline (transformation product 4) and dinitroaminophenylmethylnitramine (transformation product 3).

Mass balance of tetryl in soil

Table I presents the mass balance of tetryl in Palouse soil that was obtained over the 60-day study. The second column is the percentage of radiolabel that was recovered in the methanol extracts, as de-

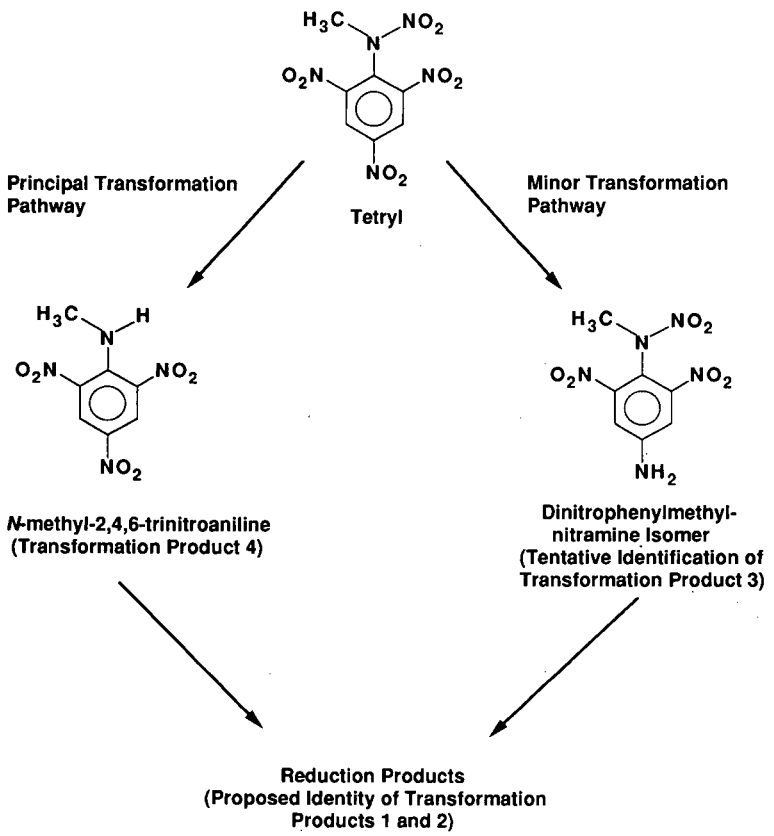

Fig. 7. Transformation pathway of tetryl in soils.

TABLE I

MASS BALANCE OF PALOUSE SOIL CONTAINING 60 ppm OF TETRYL

Time (days)	Radiolabel in methanol extract (%)	Unaltered tetryl (%)	Radiolabel in soil after extraction (%)	Mass balance deficit (%)
0	95 ± 21[a]	46 ± 9[a]	2.8 ± 0.2[a]	2 ± 21[a]
11	67 ± 5[a,b]	8 ± 4[b]	32.4 ± 0.8[b]	1 ± 5[a]
31	45 ± 4[b]	<0.5	40.2 ± 1.8[c]	15 ± 4[a]
60	36 ± 3[b]	<0.5	43.3 ± 2.3[c]	21 ± 3[a]

[a,b] Significant differences within each column are denoted by different superscripts (one-factor ANOVA for repeated measures with subsequent comparison by Scheffe F-test, $p < 0.05$). Values of <0.5% are below the chromatographic detection limit.

termined by liquid scintillation spectrometry. The third column lists the amount of the parent explosive that was speciated as tetryl, as determined by HPLC analysis. The amount of radiolabel that was not extractable in methanol is listed in column 4. These values were determined by oxidation of the extracted soils. Finally, the mass balance deficit [100 − (column 2 + column 4)] is listed in the last column. The mass balance deficit does not take into account radiolabel that was volatilized from the soils during the course of the study.

The filters used for the preparation of the final extracts and the methanol distillate resulting from rotary evaporation were found to contain negligible amounts of radiolabel. Initially, most of the radiolabel was extracted and present in the methanol extracts. It is noteworthy that only 46% of the radiolabel was speciated as tetryl in extracts initiated immediately after amendment. This indicates that transformation of tetryl was an extremely rapid process. Transformations continued at a rapid rate with less than 8% of the amended radiolabel speciated as tetryl in extracts from soils aged for 11 days. By 30 days post-amendment, the concentration of tetryl was below the chromatographic detection limit of 0.1 ppm. This detection limit corresponds to *ca.* 0.5% recovery of the amended tetryl. Immobilization of radiolabel was initially rapid, with 32% of the amended radiolabel irreversibly bound to the soil by 11 days post-amendment. Binding to the soil matrix continued at a slower rate throughout the remainder of the study. By the end of the 60-day study, 43% of the radiolabel was non-extractable. The mass balance deficits were found to be statistically equivalent throughout the study. At the end of the 60-day study, over 79% of the radiolabel initially amended to the soil was recovered in either the methanol extracts or the extracted soils.

Tetryl-amended soil was allowed to equilibrate for 21 days prior to monitoring the emission of volatile products for three consecutive days. A moderate amount of $^{14}CO_2$ was evolved from the soils. Assuming a constant rate of $^{14}CO_2$ evolution throughout the 60-day study, an amount equal to 9% of the amended radiolabel was mineralized to $^{14}CO_2$. Emission of volatile organic compounds was not observed for tetryl-amended soils.

The fate of tetryl in soil can be compared with results previously obtained for the explosives RDX and TNT [12,13]. Valid comparisons are possible because the same Palouse soil and post-amendment incubation conditions were utilized for all three munitions fate studies. Additionally, the soil extraction and analytical conditions were similar for all three explosives, with the exception that RDX was extracted with acetonitrile rather than methanol. TNT showed rapid soil transformation to 2- and 4-aminodinitrotoluene isomers; however, transformation was less rapid than observed for tetryl. For example, 88 ± 1 and 36 ± 3% of the amended TNT were recovered as the parent compound immediately after amendment and at the end of the 60-day study, respectively. Although TNT displayed substantial irreversible binding to the soil constituents (30 ± 1% after 60 days of incubation), this process was more pronounced for tetryl. The fates of both TNT and tetryl contrast sharply with that of RDX. RDX did not undergo transformations within the soil and only 1.10 ± 0.26% was non-extractable at the end of the 60-day study. Ad-

ditionally, moderate amounts of $^{14}CO_2$ were evolved from both TNT and tetryl-amended soils. Mineralization to $^{14}CO_2$ accounted for 4 and 9% of the amended TNT and tetryl, respectively, over the 60-day study. The amount of RDX that was oxidized to CO_2 (0.31%) was small in comparison with the aromatic explosives.

CONCLUSIONS

A method based on exhaustive Soxhlet extraction and subsequent HPLC analysis of tetryl was developed and applied to study the fate of this explosive in the soil environment. Tetryl was found to undergo extremely rapid transformation. Two independent tetryl transformation pathways were identified. The first and principal pathway resulted in the formation of N-methyl-2,4,6-trinitroaniline. The second, less prominent transformation pathway resulted in the formation of an aminodinitrophenylmethylnitramine isomer. Other, more polar transformation products were identified by radiochromatography and characterized by their alkylphenone retention indices. These products were likely reduction products of N-methyl-2,4,6-trinitroaniline and aminodinitrophenylmethylnitramine. Transformation of tetryl was so extensive that the parent compound was below the detection limit in soil extracts by 30 days post-amendment. Progressive binding of radiolabel to the soil constituents occurred throughout the study and was particularly rapid during the first 10 days of incubation. The mass balance of radiolabel in amended soil was better than 79% throughout the 60-day study.

It is clear that a broad range of compounds are available for uptake by plants grown in tetryl-contaminated soils. A large proportion of tetryl-derived residues will eventually become immobilized by binding to the soils. Although binding with the soil matrix precludes dispersal of contamination by leaching, it must be emphasized that the bound residues may still be available for plant uptake and further metabolism.

This study clearly emphasizes the advantages of HPLC for the analysis of tetryl and tetryl soil transformation products. Had our study drawn exclusively on gas-phase separation techniques, tetryl transformation product 4 could not have been distinguished from the parent munition. Additionally, tetryl transformation product 3 would have been erroneously assigned a molecular weight of 212. The studies described here provide independent verification that previously described GC methods for the determination of tetryl [7,8] have resulted in the separation and detection of the thermal decomposition product of tetryl, N-methyl-2,4,6-trinitroaniline [18].

ACKNOWLEDGEMENTS

This research was supported by the US Army Biomedical Research and Development Laboratory under a Related Services Agreement with the US Department of Energy under Contract DE-AC06-76RLO 1830. Pacific Northwest Laboratory is operated for the US Department of Energy by Battelle Memorial Institute. The views, opinions and/or findings contained in this paper are those of the authors and should not be construed as an official Department of the Army position, policy or decision, unless so designated by other documentation.

REFERENCES

1 J. Yinon, *Toxicity and Metabolism of Explosives*, CRC Press, Boca Raton, FL, 1990, pp. 69–80.
2 M. J. Small and D. H. Rosenblatt, *Munitions Production Products of Potential Concern as Waterborne Pollutants. Phase II, Technical Report No. 7404 (AD-919031)*, US Army Medical Bioengineering Research and Development Laboratory, Aberdeen Proving Ground, MD, 1974.
3 L. J. Witkowski, C. N. Fisher and H. D. Murdock, *J. Am. Med. Assoc.*, 119 (1942) 1406.
4 H. B. Troup, *Br. J. Ind. Med.*, 3 (1946) 20.
5 W.-Z. Whong, N. D. Speciner and G. S. Edwards, *Toxicol. Lett.*, 5 (1980) 11.
6 N. G. McCormick, F. E. Feeherry and H. S. Levinson, *Appl. Environ. Microbiol.*, 31 (1976) 949.
7 F. Belkin, R. W. Bishop and M. V. Sheely, *J. Chromatogr. Sci.*, 24 (1985) 532.
8 J. C. Hoffsommer and J. M. Rosen, *Bull. Environ. Contam. Toxicol.*, 7 (1972) 177.
9 M. G. Farey and S. E. Wilson, *J. Chromatogr.*, 114 (1975) 261.
10 T. F. Jenkins and M. E. Walsh, *Development of an Analytical Method for Explosive Residues in Soil*, Rep. No. CRREL 87-7, US Army Cold Regions Research and Engineering Laboratory, Hanover, NH, 1987.
11 R. Bongiovanni, G. E. Podolak, L. D. Clark and D. T. Scarborough, *Am. Ind. Hyg. Assoc. J.*, 45 (1984) 222.
12 S. D. Harvey, R. J. Fellows, D. A. Cataldo and R. M. Bean, *J. Chromatogr.*, 518 (1990) 361.
13 S. D. Harvey, R. J. Fellows, D. A. Cataldo and R. M. Bean, *Environ. Toxicol. Chem.*, 10 (1991) 845.

14 R. L. Guthrie and J. E. Whitty, *Soil Sci. Soc. Am. J.*, 46 (1982) 443.
15 R. M. Smith, *J. Chromatogr.*, 236 (1982) 313.
16 D. W. Hill, T. R. Kelley, K. J. Langner and K. W. Miller, *Anal. Chem.*, 56 (1984) 2576.
17 R. J. Fellows, R. M. Bean and D. A. Cataldo, *J. Agric. Food Chem.*, 37 (1989) 1444.
18 T. Tamiri and S. Zitrin, *J. Energ. Mater.*, 4 (1986) 215.
19 *Eight Peak Index of Mass Spectra*, Vol. 1, Part 2, Mass Spectrometry Data Centre, Royal Society of Chemistry, Nottingham, 3rd ed., p. 819.
20 J. Yinon, in J. Yinon (Editor), *Forensic Mass Spectrometry*, CRC Press, Boca Raton, FL, 1987, pp. 105–129.
21 F. I. Dubovitskii, G. B. Manelis and L. P. Smirnov, *Russ. J. Phys. Chem.*, 35 (1961) 255.
22 S. K. Yusada, *J. Chromatogr.*, 50 (1970) 453.

Journal of Chromatography, 605 (1992) 241–249
Elsevier Science Publishers B.V., Amsterdam

CHROM. 24 229

Capillary gas chromatography of protein amino acids as N(O,S)-isobutyloxycarbonyl *tert.*-butyldimethylsilyl derivatives in aqueous samples

Kyoung-Rae Kim

College of Pharmacy, Sungkyunkwan University, Suwon 440-746 (South Korea)

Jung-Han Kim and Chang-Hwan Oh

Department of Food Engineering, Yonsei University, Seoul 120-749 (South Korea)

Tom J. Mabry

Department of Botany, University of Texas at Austin, Austin, TX 78713-7640 (USA)

(First received September 23rd, 1991; revised manuscript received March 31st, 1992)

ABSTRACT

A method for the quantitative determination of the nineteen protein amino acids by gas chromatography is described. The amino acids were allowed to react with isobutyl chloroformate in a basic aqueous medium and the resulting N(O,S)-isobutyloxycarbonyl (isoBOC) amino acids were extracted into an organic solvent after acidification. The isolated N(O,S)-isoBOC amino acids were then converted to stable *tert.*-butyldimethylsilyl (TBDMS) derivatives, which were analyzed by gas chromatography and gas chromatography–mass spectrometry. The characteristic [M − 57], [M − 113], [M − 159], [M − 174], etc. ions in the mass spectra of N(O,S)-isoBOC TBDMS derivatives enabled rapid confirmation of the amino acids. Temperature-programmed retention index (I) sets measured on DB-5 and DB-17 capillary columns were characteristic of each amino acid thus being useful for the quick identification by computer I matching. The overall extraction and derivatization yields of the amino acids studied were linear in the range of 20–80 μg.

INTRODUCTION

High-resolution capillary gas chromatography (GC) of amino acids requires blocking of the active protons on the amino, carboxyl, hydroxyl and thiol groups. The preparation of volatile, yet stable derivatives by a single-step procedure is most desirable and the silylation is the closest approach to this goal. When the trimethylsilyl (TMS) function was used for the silylation of amino acids, the inherent instability of the resulting TMS derivatives toward hydrolysis and the excessive silylation of the nitrogen atoms led to the formation of multiple derivatives for some amino acids [1–3].

The *tert.*-butyldimethylsilyl (TBDMS) function first employed as a more moisture stable alternative to the TMS group [4] is now widely used for the silylation of hydroxyl and carboxyl groups using N-methyl-N-(*tert.*-butyldimethylsilyl)trifluoroacetamide (MTBSTFA) [5] as the silylating reagent. The TBDMS derivatives were found to have superior GC and mass spectral (MS) properties [6,7]. In a previous report, we demonstrated that multifunctional organic acids were quantitatively converted to their TBDMS derivatives, yielding a single

Correspondence to: Dr. Tom J. Mabry, Department of Botany, University of Texas at Austin, Austin, TX 78713-7640, USA.

0021-9673/92/$05.00

peak for each organic acid [8]. In recent years, the TBDMS derivatization has been successfully extended to amino acids [9–16]. However, a painstaking step for the moisture removal from the hydrochloride salts of amino acids is prerequisite.

Prior to conversion to suitable volatile derivatives, amino acids are isolated from complex aqueous samples mainly by the multi-step ion-exchange technique though its inherent drawbacks are well known [17]. There appears to be a need for improvement of sample purification. In the literature, as a different approach, Makita and co-workers [18–21] demonstrated that amino acids were quantitatively extracted with diethyl ether from aqueous media after selective blocking of the active hydrogens on the amino, thiol, imidazole, and phenolic hydroxyl groups by reaction with isobutyl chloroformate (isoBCF). The remaining carboxyl groups of the resulting N(O,S)-isobutyloxycarbonyl (-isoBOC) amino acids were then methylated with diazomethane.

It occurred to us that by combining Makita's N(O,S)-isoBOC procedure for the selective purification of amino acids from aqueous samples and the TBDMS derivatization of the carboxyl and remaining amide or alcoholic hydroxyl groups in the N(O,S)-isoBOC amino acids would give a better result for the GC analysis of amino acids. The present work describes a method for the GC analysis of amino acids in aqueous samples as their N(O,S)-isoBOC TBDMS derivatives. The structures of the derivatives were confirmed by GC–MS.

EXPERIMENTAL

Materials

All of the amino acids used in this study, isobutyl chloroformate (isoBCF), and *tert.*-butyldimethylchlorosilane (TBDMCS) were purchased from Sigma (St. Louis, MO, USA); dimethylformamide (DMF), acetonitrile, pyridine and N-methyl-N-(*tert.*-butyldimethylsilyl)trifluoroacetamide (MTBSTFA) of silylation grade from Pierce (Rockford, IL, USA). Diethyl ether purchased from Oriental Chemical Industry (Seoul, Korea) was distilled over potassium hydroxide in an all-glass apparatus and stored in an amber screw-cap bottle in the presence of anhydrous sodium sulfate at 4°C. Sodium chloride was purchased from Junsei (Tokyo, Japan), sodium carbonate and hydrogen chloride from Duksan (Seoul, Korea), and *n*-hydrocarbon standards (C_{12}–C_{36}, even numbers only) from Polyscience (Niles, IL, USA).

Amino acid solutions

The amino acid solution containing nineteen amino acids, 0.5 μg each per μl in 0.1 *M* HCl was used as the working solution. Arginine was excluded from this study. 3,4-Dimethoxybenzoic acid (Aldrich, Milwaukee, USA) used as the internal standard was dissolved in methanol at a concentration of 5 μg/μl.

N(O,S)-isoButyloxycarbonylation of amino acids

According to the procedure of Makita *et al.* [18], the internal standard solution (20 μg), distilled water (1.5 ml) and 5% sodium carbonate solution (0.5 ml) and isoBCF (0.1 ml) were added to an aliquot (100 μl) of the amino acid solution. The mixture was shaken for 10 min at room temperature and washed with diethyl ether (4 × 2 ml). The aqueous mixture was then adjusted to pH 1–2 (10% hydrochloric acid), saturated with sodium chloride, and was extracted with diethyl ether (4 × 1 ml).

tert.-Butyldimethylsilylation of N(O,S)-isoBOC amino acids

The ether extract containing N(O,S)-isoBOC amino acids was evaporated to dryness under gentle stream of nitrogen at 50°C. To the residue were added 10 μl of acetonitrile and 50 μl of MTBSTFA. The mixture was heated to 60°C for 20 min to form TBDMS derivatives. The reaction mixture was directly examined by GC and GC–MS. The calibration samples for precision tests of the overall procedure were prepared with amino acid solutions containing 20, 40 or 80 μg of each amino acid and 20 μg of internal standard. In place of acetonitrile, dimethylformamide and pyridine were investigated as solvent and also 1% TBDMCS in the MTBSTFA as catalyst. The effect of varying temperature (room temperature to 90°C) and heating time on the derivative yields was also investigated.

Gas chromatography

GC analyses were performed with Hewlett-Packard HP 5890A gas chromatograph, equipped with a split/splitless capillary inlet system, and two

flame ionization detectors, an HP 3392A integrator, and interfaced to an HP 5895A GC Chemstation on a 25 m × 0.32 mm I.D. fused-silica Ultra-1 capillary column (film thickness, 0.17 μm; Hewlett-Packard, Avondale, PA, USA). Nitrogen at a flow-rate of 1.03 ml/min was used as the carrier gas, and *ca.* 1-μl aliquots of samples were injected with a split ratio of 30:1. After an initial hold time of 2 min at 120°C, oven temperature was programmed to 280°C at a rate of 5°C/min. The injector and detector temperatures were 280 and 300°C, respectively. DB-5 (30 m × 0.25 mm I.D., 0.24 μm d_f) and DB-17 (30 m × 0.25 mm I.D., 0.25 μm d_f) fused-silica capillary columns (J. & W. Scientific, Rancho Cordova, CA, USA) were used for the retention index (*I*) measurement. A DB-1701 (30 m × 0.25 mm I.D., 0.25 μm d_f) fused-silica capillary column was also investigated as a potential column for *I* measurement. For the *I* measurement, after an initial hold time of 2 min at 150°C, oven temperature was programmed to 280°C at a rate of 3°C/min. A standard solution of *n*-hydrocarbons (C_{12}–C_{36}, even numbers only) in isooctane was co-injected with the samples in the split mode (30:1). Samples were analyzed in triplicate.

Gas chromatography–mass spectrometry

A Hewlett-Packard HP 5890A gas chromatograph, interfaced to an HP 5970B MSD (70 eV, EI mode) which was on-line to a HP 59940A MS Chemstation system, was used with an HP-1 cross-linked capillary column (12 m × 0.20 mm I.D., 0.33 μm film thickness) to obtain mass spectra. Samples were introduced in the split-injection mode (30:1) at 260°C, and the oven temperature was initially 100°C then programmed to 280°C at a rate of 15°C/min. The interface temperature was 300°C. The mass range scanned was 60–500 a.m.u. at a rate of 1.29 scan/s.

RESULTS AND DISCUSSION

As an alternative to the conventional ion-exchange clean-up for protein amino acids from aqueous samples prior to the TBDMS derivatization, we adopted Makita's N(O,S)-isobutyloxycarbonyl (-isoBOC) reaction method [18] with minor modifications. Prior to extraction with diethyl ether, the reaction mixture was acidified by HCl solution rather than H_3PO_4 since the large TBDMS triester of the extracted H_3PO_4 interfered in the GC analysis of the amino acid derivatives. The N(O,S)-isoBOC reaction readily transforms the zwitterionic amino acids into the corresponding organic extractable carboxylic acids by blocking the basic amino functions with isoBCF in a basic aqueous medium. Thiol, phenolic hydroxyl and imidazole functions, if present, are blocked too. Arginine was excluded from the present study as it was shown not to be amenable directly to the Makita method [18].

The TBDMS derivatization of the resulting N(O,S)-isoBOC amino acids offers advantages over the Makita methylation [18], since polar hydroxyl and amide functions as well as the carboxyl group are converted to TBDMS derivatives which generate diagnostically useful [M − 57] ions in their mass spectra. With the exception of glutamine, asparagine, serine and threonine, the TBDMS derivatization of the N(O,S)-isoBOC amino acids in acetonitrile (10 μl) was completed when mixed with MTBSTFA (50 μl) at room temperature. Serine with a hydroxyl function required longer reaction time at room temperature for complete conversion to di-TBDMS derivative. Threonine, due to the steric hindrance of the β-hydroxyl group toward the bulky TBDMS moiety, gave mono- and di-TBDMS derivatives even after extended heating at 60°C. Basic amino acids such as lysine, asparagine and glutamine when heated at 90°C or higher produced diminished responses. At a higher temperature and with extended heating the responses of all the amino acid derivatives generally were reduced, especially those of alanine and glycine. The addition of 1% (w/w) TBDMCS to MTBSTFA did not improve the derivative yields.

When the reaction in DMF was conducted at 75°C for 2 h, the responses of amino acids except for proline were significantly reduced and also in pyridine, cysteine, lysine, histidine and tyrosine were observed to give smaller responses. On the other hand, when the reaction was performed directly in MTBSTFA without any added solvent, good results were produced although the stability of the derivatives was not very good.

In general, the condition producing optimal overall derivatization was heating at 60°C for 15 min in acetonitrile and MTBSTFA.

The three combined procedures including N(O,

S)-isoBOC reaction, solvent extraction and TBDMS derivatization were examined for the overall precision and linearity of the calibration plots. A linear response in the range of 20–80 μg was obtained for most amino acids with the correlation coefficients approaching 0.99 as listed in Table I. For serine and threonine, each combined peak area of mono- and di-TBDMS peaks was used. Typically, the relative standard deviation (n = 3) was lower than 5% on the average except for lysine, histidine, tryptophan and tyrosine which gave higher R.S.D. but within 8%. Considering the method consists of three independent steps, its overall reproducibility is satisfactory for the quantitation of amino acids.

The separation of the nineteen amino acid derivatives on three different fused-silica capillary columns is presented in Fig. 1. Each amino acid derivative displayed a single symmetrical peak with the exception of serine and threonine which exhibited two peaks due to mono- and di-TBDMS derivatives, labeled serine-1, serine-2, threonine-1, and threonine-2, respectively. Serine-2 and threonine-2 were not adequately resolved on Ultra-1, DB-5 and DB-17 columns. Temperature-programmed retention index sets for each derivative measured on DB-5 and DB-17 columns are given in Table II. The I sets were characteristic of each amino acid, thus being useful for the quick identification by the computer I library matching as described in our organic acid profiling works [22,23].

When a DB-1701 column was used, no peaks were obtained from the derivatives of glutamine and asparagine. Their labile N-TBDMS bonds appear to be decomposed by the polar cyanopropyl functions of the DB-1701 column.

Most N(O,S)-isoBOC TBDMS derivatives of

TABLE I

LINEAR REGRESSION ANALYSIS OF RELATIVE RESPONSE AGAINST RELATIVE WEIGHT OF AMINO ACID AS THEIR N(O,S)-isoBOC TBDMS DERIVATIVES

Amino acid	Mean AR ± S.D. (%R.S.D.)[a]			Regression line		
	20 μg	40 μg	80 μg	m[b]	b[c]	r[d]
Alanine	1.610 ± 0.059 (3.7)	3.610 ± 0.074 (2.0)	7.358 ± 0.194 (2.6)	1.910	−0.264	0.999
Glycine	1.705 ± 0.071 (4.2)	3.929 ± 0.067 (1.7)	7.769 ± 0.133 (1.7)	2.007	−0.215	0.999
Valine	1.497 ± 0.034 (2.3)	3.309 ± 0.033 (1.0)	6.550 ± 0.114 (1.7)	1.675	−0.124	0.999
Leucine	1.332 ± 0.026 (2.0)	2.892 ± 0.056 (1.9)	5.607 ± 0.163 (2.9)	1.415	−0.026	0.999
Isoleucine	1.303 ± 0.018 (1.4)	2.808 ± 0.043 (1.5)	5.475 ± 0.111 (2.0)	1.383	−0.031	0.999
Proline	1.501 ± 0.006 (0.4)	3.197 ± 0.028 (0.9)	6.159 ± 0.038 (0.6)	1.542	0.020	0.999
Methionine	0.872 ± 0.038 (4.4)	1.942 ± 0.078 (4.0)	3.835 ± 0.183 (4.8)	0.982	−0.075	0.999
Serine	1.319 ± 0.031 (2.4)	2.775 ± 0.032 (1.2)	4.966 ± 0.240 (4.8)	1.199	0.224	0.997
Threonine	0.648 ± 0.021 (3.2)	1.421 ± 0.031 (2.2)	2.731 ± 0.121 (4.4)	0.688	−0.007	0.999
Phenylalanine	1.385 ± 0.021 (1.5)	2.556 ± 0.126 (4.9)	5.172 ± 0.211 (4.1)	1.269	0.077	0.999
Aspartic acid	1.538 ± 0.043 (2.8)	2.853 ± 0.095 (3.3)	5.600 ± 0.238 (4.3)	1.357	0.165	0.999
Cysteine	1.118 ± 0.053 (4.7)	2.315 ± 0.116 (5.0)	4.289 ± 0.212 (4.9)	1.047	0.131	0.999
Glutamic acid	0.714 ± 0.021 (2.9)	1.237 ± 0.056 (4.5)	2.432 ± 0.096 (3.9)	0.576	0.117	0.999
Asparagine	0.175 ± 0.007 (4.0)	0.432 ± 0.021 (4.9)	0.846 ± 0.036 (4.3)	0.221	−0.032	0.998
Glutamine	0.345 ± 0.015 (4.3)	0.579 ± 0.027 (4.7)	1.257 ± 0.006 (0.5)	0.309	0.006	0.996
Lysine	0.519 ± 0.007 (1.3)	0.851 ± 0.037 (4.3)	1.794 ± 0.121 (6.7)	0.432	0.048	0.997
Histidine	0.213 ± 0.012 (5.6)	0.458 ± 0.034 (7.4)	0.826 ± 0.058 (7.0)	0.201	0.029	0.997
Tryptophan	0.869 ± 0.026 (3.0)	1.354 ± 0.084 (6.2)	2.862 ± 0.106 (3.7)	0.677	0.115	0.995
Tyrosine	0.185 ± 0.014 (7.6)	0.603 ± 0.032 (5.3)	1.098 ± 0.087 (7.9)	0.296	−0.063	0.990

[a] AR = Peak area ratio relative to internal standard (I.S.); S.D. = standard deviation for n = 3.
[b] m = Slope = relative weight response = mean AR × weight of I.S./weight of amino acid.
[c] b = y-intercept.
[d] Correlation coefficient.

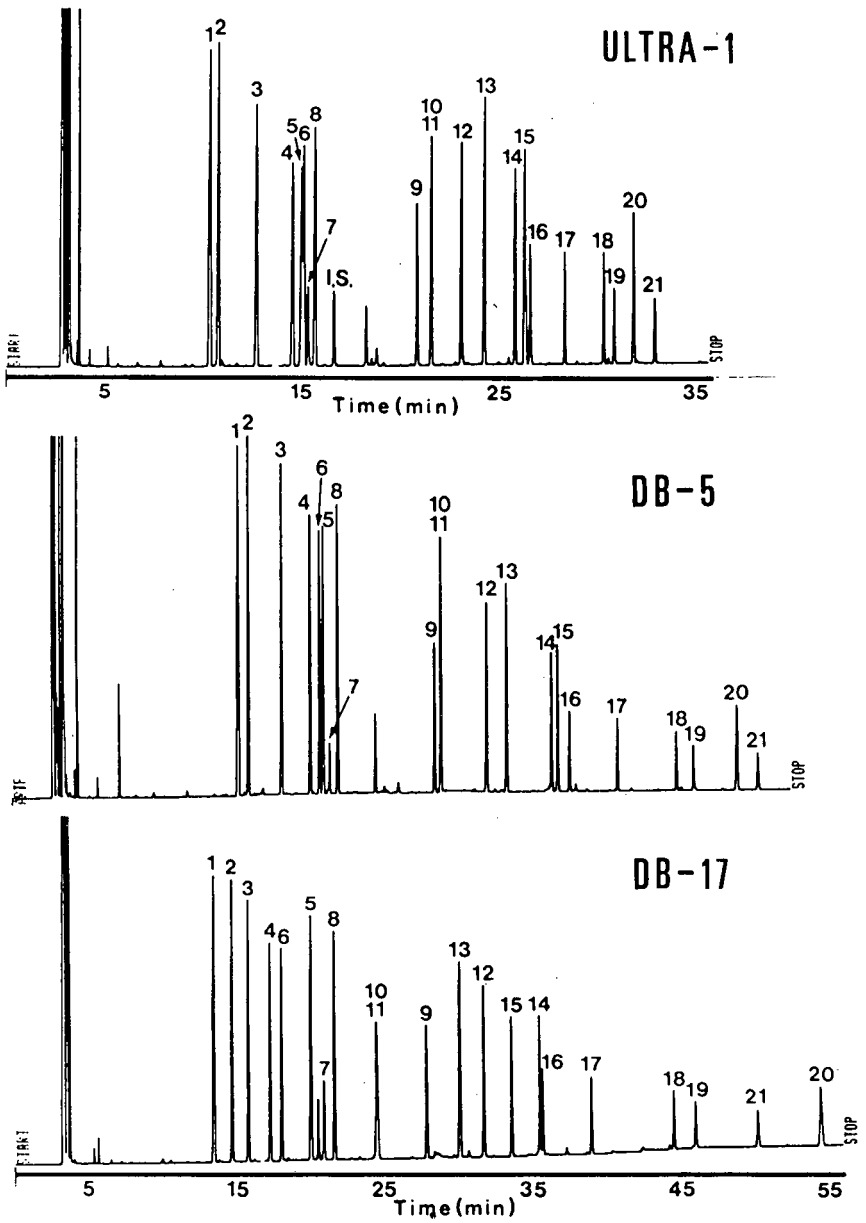

Fig. 1. Chromatograms of the nineteen amino acid mixture as their N(O,S)-isoBOC TBDMS derivatives separated on Ultra-1 (25 m × 0.32 mm I.D.), DB-5 (30 m × 0.25 mm I.D.) and DB-17 (30 m × 0.25 mm I.D.) fused-silica capillary columns. GC conditions are in the text. Peaks: 1 = alanine; 2 = glycine; 3 = valine; 4 = leucine; 5 = threonine-1; 6 = isoleucine; 7 = serine-1; 8 = proline; 9 = methionine; 10 = serine-2; 11 = threonine-2; 12 = phenylalanine; 13 = aspartic acid; 14 = cystein; 15 = glutamic acid; 16 = asparagine; 17 = glutamine; 18 = lysine; 19 = histidine; 20 = tryptophan; 21 = tyrosine (peak numbers correspond to those in Table II).

TABLE II

GAS CHROMATOGRAPHIC AND MASS SPECTRAL DATA OF N(O,S)-isoBOC TBDMS DERIVATIVES OF AMINO ACIDS

Amino acid	GC I^a data set		Mol. wt.	Mass spectral data set						
	DB-5	DB-17		[M − 57]	[M − 15]	[M − 113]	[M − 131]	[M − 159]	[M − 174]	Other ion
1 Ala	1702.2	1854.8	303	246 (33)	288 (1)	190 (100)	172 (2)	144 (23)	129 (2)	
2 Gly	1724.9	1901.1	289	232 (26)	274 (0)	176 (100)	158 (8)	130 (4)		
3 Val	1800.0	1942.9	331	274 (35)	316 (1)	218 (100)	200 (2)	172 (28)	157 (3)	
4 Leu	1860.1	2000.0	345	288 (38)	330 (1)	232 (100)	214 (2)	186 (36)	171 (3)	
5 Thr-1	1887.3	2094.6	333	276 (11)	318 (1)	220 (64)	202 (100)	174 (9)	159 (4)	
6 Ile	1879.8	2026.7	345	288 (39)	330 (1)	232 (100)	214 (2)	186 (35)	171 (3)	
7 Ser-1	1900.8	2127.8	319	262 (12)	304 (1)	206 (46)	188 (100)	160 (15)	145 (5)	
8 Pro	1917.9	2152.0	329	272 (50)	314 (1)	216 (100)	198 (0)	170 (56)	155 (0)	
9 Met	2133.5	2372.1	363	306 (65)	348 (3)	250 (40)	232 (28)	204 (21)	189 (5)	178 (100)
10 Ser-2	2146.8	2252.7	433	376 (100)	418 (4)	320 (14)	302 (33)	274 (11)	259 (4)	
11 Thr-2	2146.8	2255.2	447	390 (100)	432 (4)	334 (7)	316 (28)	288 (17)	273 (5)	
12 Phe	2251.9	2515.6	379	322 (82)	364 (2)	266 (100)	248 (14)	220 (18)	205 (57)	
13 Asp	2299.0	2454.9	461	404 (100)	446 (2)	348 (3)	330 (12)	302 (15)	287 (49)	
14 Cys	2405.8	2663.7	435	378 (100)	420 (3)	322 (23)	304 (6)	276 (16)	261 (25)	
15 Glu	2421.2	2588.8	475	418 (100)	460 (3)	362 (2)	344 (89)	316 (58)	301 (2)	
16 Asn	2450.9	2671.6	460	403 (100)	445 (5)	347 (4)	329 (19)	301 (3)	286 (27)	
17 Gln	2572.3	2791.0	474	417 (100)	459 (4)	361 (2)	343 (33)	315 (24)	300 (2)	
18 Lys	2729.0	3050.2	460	403 (44)	445 (3)	347 (6)	329 (15)	301 (2)	286 (0)	184 (100)
19 His	2772.6	3111.4	469	412 (93)	454 (9)	356 (3)	338 (42)	310 (91)	295 (100)	
20 Trp	2866.9	3404.8	418	361 (8)	403 (1)	305 (1)	287 (4)	259 (3)	244 (23)	130 (100)
21 Tyr	2911.5	3269.2	495	438 (12)	480 (1)	382 (9)	364 (6)	336 (3)	321 (100)	

[a] R.S.D. ranged from 0.01–0.05% from three measurements.

amino acids were stable for at least two months at 4°C kept in tightly closed Teflon-lined screw-cap reaction vials, indicating that they are more stable than the corresponding N(O,S,COO)-TBDMS derivatives [9–15].

The amino acid derivatives were subjected to GC–MS analysis. The electron-impact MS data are summarized in Table II. As is characteristic of the TBDMS derivatives [6–16], the intense [M − 57] ions formed by the loss of the labile *tert.*-butyl function, together with weak [M − 15], and prominent [M − 131] and [M − 159] ions generated by the loss of CH_3, OTBDMS, and COOTBDMS from molecular ions, respectively, were useful for the structure confirmation of each amino acid.

[M − 57] ions constitute the base peaks for the amino acids having O- or COO-TBDMS derivatized side chains such as serine-2, threonine-2, aspartic acid, glutamic acid, asparagine and glutamine, and for cysteine with a S-isoBOC side chain as exemplified by the glutamine mass spectrum (Fig. 2A). For serine-1 and threonine-1, [M − 131] ions were the base peaks.

In amino acids with simple side chains such as alanine, glycine, valine, leucine, isoleucine, proline and phenylalanine the base peaks were [M − 113] ions representing the loss of $CHCH(CH_3)_2$ from [M − 57] ions as shown in the proline mass spectrum (Fig. 2B).

The base peaks of histidine and tyrosine having N-isoBOC derivatized side chains are [M − 174] ions which appear to be formed either by the loss of NH_2isoBOC from [M − 57] ions or by the loss of OTBDMS and $CH(CH_3)_2$ from molecular ions as demonstrated in the mass spectrum of histidine (Fig. 2C).

For tryptophan the ion at *m/z* 130 formed by the preferential benzylic cleavage constitutes the base

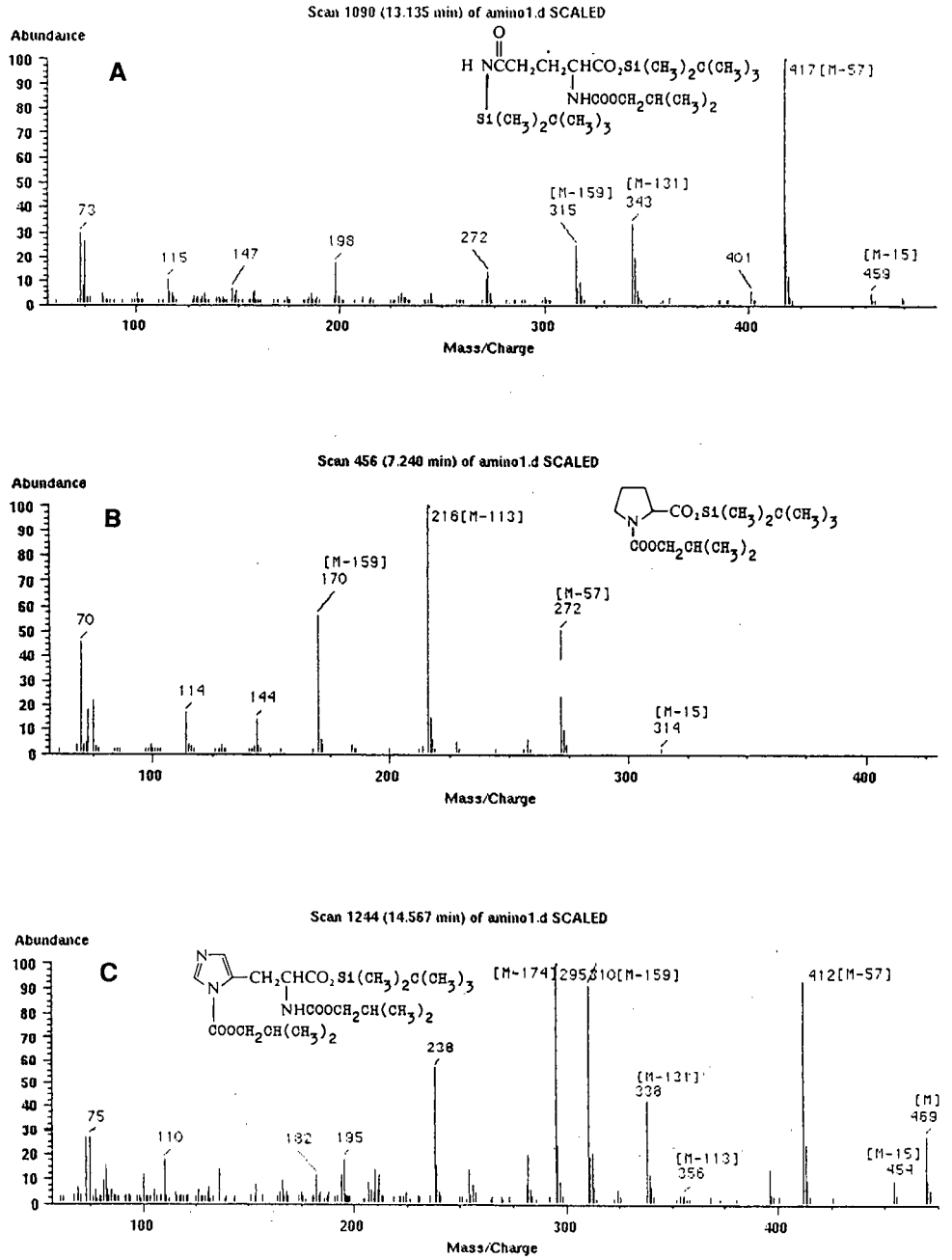

Fig. 2. Electron-impact mass spectra of N(O,S)-isoBOC TBDMS derivatives of glutamine (A), proline (B) and histidine (C).

peak while the base peaks at m/z 184 of lysine and at m/z 178 of methionine appear to represent the loss of $HCOOCH_2CH(CH_3)_2$ from [M − 174] ion, and the consecutive losses of CO and $COOCHCH(CH_3)_2$ from [M − 57] ion, respectively, as shown in Fig. 3.

CONCLUSIONS

A significant advantage of the present method is that the isobutyloxycarbonylation of the amino functions is performed in basic aqueous media for

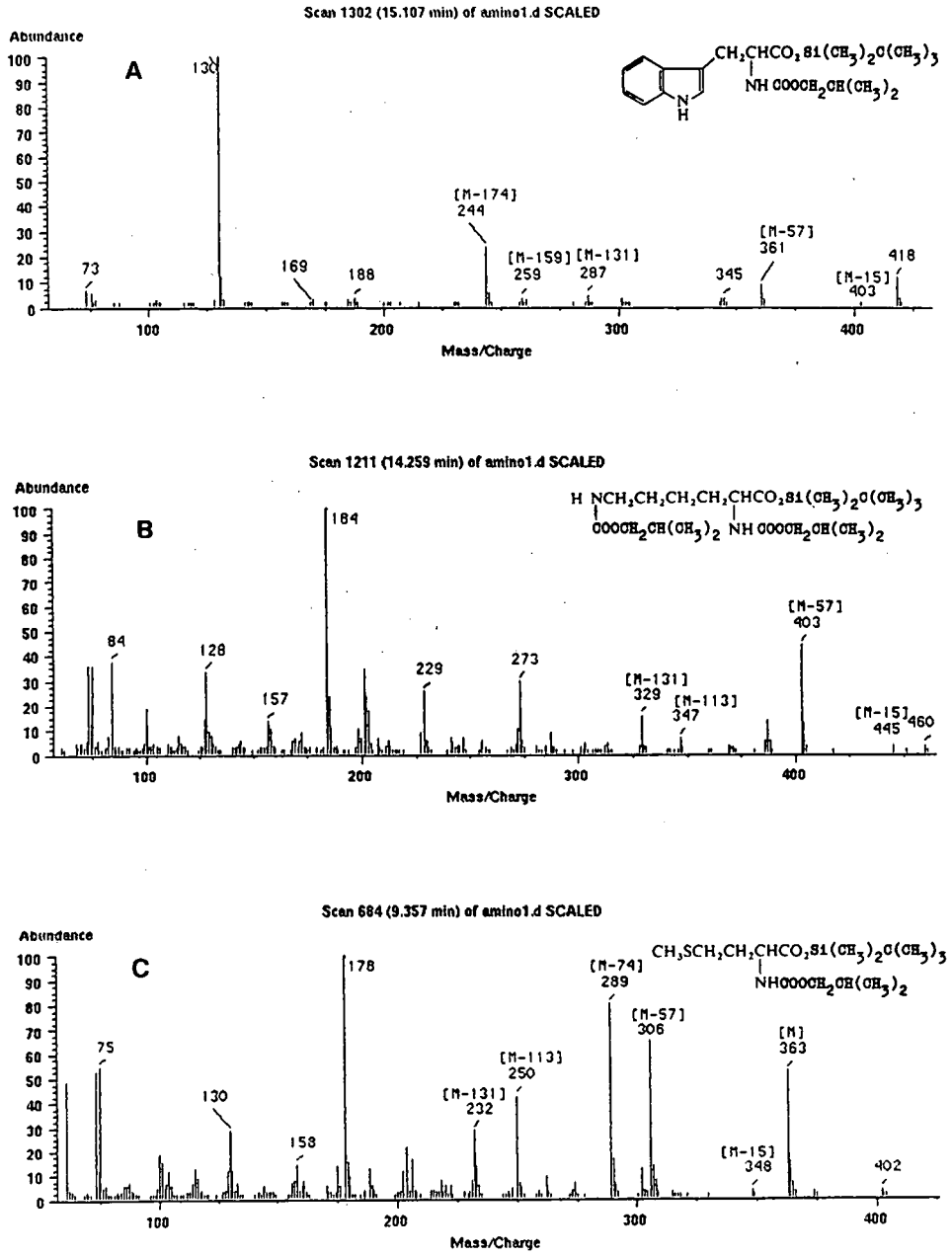

Fig. 3. Electron-impact mass spectra of N(O,S)-isoBOC TBDMS derivatives of tryptophan (A), lysine (B) and methionine (C).

the selective clean-up for zwitterionic amino acids prior to conversion to the corresponding stable TBDMS derivatives. The simple clean-up step and rapid derivatization process make this method suitable for the routine amino acid profiling works. This method was successfully applied to various food samples for the amino analysis as reported elsewhere [24]. Further investigation on the satisfactory deri-

vatization of arginine is in progress. The extension of the present method to protein and non-protein amino acid profiling analyses are under way.

ACKNOWLEDGEMENT

This work was supported by the Korea Science & Engineering Foundation (1991 project number: 911-0304-044-2).

REFERENCES

1 C. W. Gehrke and K. Leimer, *J. Chromatogr.*, 57 (1971) 219.
2 G. Eisenbrand, C. Janzowski and R. Preussmann, *J. Chromatogr.*, 115 (1975) 602.
3 E. Gajewski, M. Dizdaroglu and M. G. Simic, *J. Chromatogr.*, 249 (1982) 41.
4 E. J. Corey and A. Venkateswarlu, *J. Am. Chem. Soc.*, 94 (1972) 6190.
5 T. P. Mawhinney and M. A. Madson, *J. Org. Chem.*, 47 (1982) 3336.
6 A. C. Bazan and D. R. Knapp, *J. Chromatogr.*, 236 (1982) 201.
7 T. P. Mawhinney, *J. Chromatogr.*, 257 (1983) 37.
8 K. R. Kim, M. K. Hahn, A. Zlatkis, E. C. Horning and B. S. Middleditch, *J. Chromatogr.*, 468 (1989) 289.
9 S. L. MacKenzie and D. Tenaschuk, *J. Chromatogr.*, 322 (1985) 228.
10 C. J. Biermann, C. M. Kinoshita, J. A. Marlett and R. D. Steele, *J. Chromatogr.*, 357 (1986) 330.
11 T. P. Mawhinney, R. S. R. Robinett, A. Atalay and M. A. Madson, *J. Chromatogr.*, 358 (1986) 231.
12 G. Fortier, D. Tenaschuk and S. L. MacKenzie, *J. Chromatogr.*, 361 (1986) 253.
13 S. L. MacKenzie, D. Tenaschuk and G. Fortier, *J. Chromatogr.*, 387 (1987) 241.
14 H. J. Chaves das Neves and A. M. P. Vasconcelos, *J. Chromatogr.*, 392 (1987) 249.
15 R. J. Early, J. R. Thomson, G. W. Sedgwick, J. M. Kelly and R. J. Christopherson, *J. Chromatogr.*, 416 (1987) 15.
16 H. J. Chaves das Neves, A. M. P. Vasconcelos, J. R. Tavares and P. N. Ramos, *J. High Resolut. Chromatogr. Chromatogr. Commun.*, 11 (1988) 12.
17 D. Labadarios, I. M. Moodie and G. S. Shephard, *J. Chromatogr.*, 310 (1984) 223.
18 M. Makita, S. Yamamoto and M. Kono, *J. Chromatogr.*, 120 (1976) 129.
19 M. Makita, S. Yamamoto, K. Sakai and M. Shiraishi, *J. Chromatogr.*, 124 (1976) 92.
20 S. Yamamoto, S. Kiyama, Y. Watanabe and M. Makita, *J. Chromatogr.*, 233 (1982) 39.
21 M. Makita, S. Yamamoto and S. Kiyama, *J. Chromatogr.*, 237 (1982) 279.
22 K. R. Kim, M. K. Hahn, J. H. Kim and H. K. Park, *Proceedings of the Third Korea–Japan Joint Symposium on Analytical Chemistry, Daeduck, Korea, April 19–21, 1989*, 1989, p. 119.
23 K. R. Kim, J. H. Kim, H. K. Park and C. H. Oh, *Bull. Korean Chem. Soc.*, 12 (1991) 87.
24 K. R. Kim, J. H. Kim and C. H. Oh, *Anal. Sci.*, 7, Suppl. (1991) 231–234.

Journal of Chromatography, 605 (1992) 251–255
Elsevier Science Publishers B.V., Amsterdam

CHROM. 24 185

Evaluation of the liquid–liquid extraction technique and application to the determination of volatile halo-organic compounds in chlorinated water

C. García, P. G. Tiedra, A. Ruano, J. A. Gómez and R. J. García-Villanova

Departamento de Química Analítica, Nutrición y Bromatologia, Facultad de Farmacia, Universidad de Salamanca, Avenida Campo Charro S/N, E-37007 Salamanca (Spain)

(First received January 2nd, 1992; revised manuscript received March 17th, 1992)

ABSTRACT

The experimental conditions of a simple liquid–liquid extraction method for the determination of sixteen volatile halo-organic compounds, including the main trihalomethanes (THMs), in water were evaluated. The volatile halo-organic compounds were extracted with *n*-pentane and analysed by gas chromatography using a semi-capillary column and an electron-capture detector. The extraction recoveries for the four THMs were almost complete and the detection limits were lower than 1 μg/l. The method was applied to the analysis of raw and chlorinated water from the river Tormes for distribution in the city of Salamanca (Spain). Chloroform and bromodichloromethane were detected in all the chlorinated water samples; the mean concentrations determined in the finished water were 9.59 and 2.58 μg/l, respectively, from February to July, 1991.

INTRODUCTION

Disinfection of water destined for human consumption by chlorination has the drawback that substances potentially harmful to health may be formed [1,2]. Of the organic halogen derivatives that may be formed in chlorinated water, the compounds known as trihalomethanes (THMs) occur frequently; these mainly include chloroform, bromodichloromethane, chlorodibromomethane and bromoform.

As the toxicity and carcinogenic potential of chloroform depends on the breed, species, sex and age of experimental animals, controversy exists with respect to its toxic and mutagenic effects [3–6]. Despite this, the concentrations of chloroform detected in treated water may cause hepatotoxicity and nephrotoxicity [7]. The other three THMs show mutagenicity according to the Ames assay and genetotoxicity in *in vitro* experiments [8,9].

As a result of the possible risks to health, the World Health Organization has recommended a limit of 30 μg/l of chloroform [10] and US legislation has established a limit of 100 μg/l for total THMs [11]. Like the EEC report [12], Spanish technical-sanitary legislation [13] for the supply and quality of public drinking water does not establish maximum admissible concentrations of organochlorinated compounds and the limit for THMs is not clear.

Among the numerous methods used for the determination of volatile halo-organic compounds in water, the technique used for the separation and quantification of each of the different compounds is gas chromatography (GC). The compounds can be determined by direct injection [14] or, more commonly, following isolation or preconcentration, or

Correspondence to: Dr. C. García, Departamento de Química Analítica, Nutrición y Bromatología, Facultad de Farmacia, Universidad de Salamanca, Avenida Campo Charro S/N, E-37007 Salamanca, Spain.

0021-9673/92/$05.00

both, of the organic compounds from the aqueous sample, adsorption onto solid materials [15], gas extraction (head space [16,17] purge and trap [18,19] and closed-loop stripping [20]), permeability through membranes [21] and liquid–liquid extraction [22–24]. The two methods used by the US. Environmental Protection Agency are the purge and trap method and the liquid–liquid extraction method. Comparison of these two methods shows that extraction-based procedures offer two primary advantages: analysis times can be significantly reduced, and the recovery and precision for all four THMs are better by liquid–liquid extraction. These advantages are especially important in the routine analysis of large numbers of samples.

In this work the application of a simple extraction step with *n*-pentane was applied to the analysis of sixteen halo-organic compounds, including the THMs, by GC with a capillary column. The proposed procedure was applied to the identification and quantification of these organic compounds in raw and supply water of the city of Salamanca (Spain), studying the effect of the different treatments (chlorination, flocculation and filtration) applied in the two town drinking water treatment plants on the formation of halo-organic compounds.

EXPERIMENTAL

Apparatus

The analyses were performed on a Varian Model 3700 gas chromatograph equipped with a ^{63}Ni electron-capture detector and a VOCOL fused-silica semi-capillary 30 m × 0.53 mm I.D. column with a 3.0-μm film.

The carrier and make-up gases were N-52 nitrogen at flow-rates of 5 and 20 ml/min, respectively.

After each 1-μl injection the column temperature was kept at 30°C for 8 min, then increased to 90°C at a rate of 2°C/min.

The temperatures of the electron-capture detector and the injector were 300 and 150°C, respectively.

The gas chromatograph was coupled to a Varian Model 9176 recorder and a Varian CDS Model 111 integrator.

Reagents

The extraction solvent was *n*-pentane, residues grade (Merck). Na_2SO_3 [analytical grade (Panreac)] was used as a sample preservative.

The individual standards of the halo-organic compounds were of analytical standards stockroom quality supplied by Kromxpek Analítica. The concentrations were 0.1 mg/ml in methanol.

The working solutions used for the qualitative and quantitative analyses and for control of the results (reagent purity, extraction recovery and detection limit) were prepared immediately before use by dilution of the standards with *n*-pentane.

Sample collection

Samples were collected in 120 ml amber-coloured glass vials previously washed with special detergents and dried at 110°C. As a preservative, 10 mg of Na_2SO_3 were added, without headspace in the vials, which were sealed hermetically by a septum and an aluminium cap.

Extraction technique

Aliquots of 5.0 ml of *n*-pentane were injected through the septum. These displaced an equal volume of water which was collected in another syringe. Both phases were shaken for 120 s and when equilibrium was reached 1 μl of the organic phase was injected into the chromatograph.

Quantification

The concentrations of the halo-organic compounds were determined by the addition to the samples of *cis*-1,3-dichloropropene as an internal standard before extraction at a concentration at which the height of the peak was similar to that of the halo-organic compounds present in the samples.

For control of the results, periodic calibration graphs were obtained of the compounds identified in the samples in the working concentration zone.

RESULTS AND DISCUSSION

Optimization of the method

Using standard working solutions, the optimum chromatographic conditions for the detection and quantification of the sixteen halo-organic compounds were determined (Table I).

n-Pentane was chosen as the extraction solvent

TABLE I

VOLATILE HALO-ORGANIC COMPOUNDS DETERMINED IN THIS STUDY

Compound	Retention time (min)	Detection limit (μg/l)
Methylene chloride (**a**)	4.3	4.3
1,1-Dichloroethane (**b**)	6.0	5.2
Chloroform (**c**)	8.0	0.9
Carbon tetrachloride (**d**)	9.9	0.4
1,2-Dichloroethane (**e**)	11.2	2.6
Trichloroethylene (**f**)	13.7	1.7
1,2-Dichloropropane (**g**)	14.7	3.5
Bromodichloromethane (**h**)	16.0	0.4
2-Chloroethylvinylether (**i**)	18.3	4.3
cis-1,3-Dichloropropene (**j**)	18.9	1.7
trans-1,3-Dichloropropene (**k**)	22.0	2.6
1,1,2-Trichloroethane (**l**)	22.6	2.6
Tetrachloroethylene (**m**)	23.5	1.7
Chlorodibromomethane (**n**)	25.3	0.4
Bromoform (**o**)	34.7	0.9
1,1,2,2-Tetrachloroethane (**p**)	36.7	0.9

because it induces fewer interferences in the response of the electron-capture detector (Fig. 1).

Extraction rate. The extraction rate with *n*-pentane was determined by shaking 120 ml of ultrapure water containing the four main THMs at three concentration levels: 2.0, 5.0 and 9.0 μg/l. The two phases were in equilibrium after 120 s (Fig. 2). The

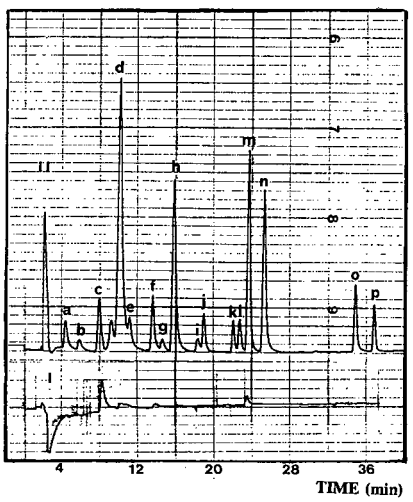

Fig. 1. (I) Chromatogram of *n*-pentane; (II) chromatogram of the multicomponent solution.

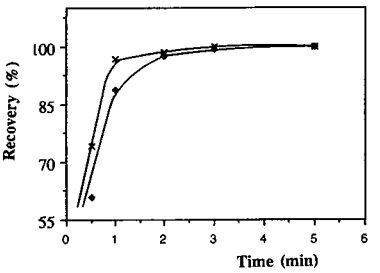

Fig. 2. Extraction rate for: (◆) chloroform and (×) bromoform at concentrations of 5.0 μg/l.

graphs obtained at the other concentrations and for the four THMs are similar to those shown here.

Extraction efficiency. Extraction efficiency was determined by shaking 120 ml of ultrapure water containing the sixteen halo-organic compounds at three concentrations ranging between 2.0 and 9.0 μg/l. The shaking time was 120 s and the concentrations of the compounds in the extracts were compared with standards prepared directly in *n*-pentane. Table II gives the recoveries obtained for the THM compounds; it is seen that they do not depend on concentration (small standard deviation) and are almost complete.

Detection limit. To determine the detection limits, ten different blank assays were performed, the interferences being negligible except for chloroform, an impurity of *n*-pentane, which was taken into account to obtain the detection limit of this compound.

The detection limit (Table I) ranged from 0.4 to 5.2 μ/l; for chloroform and bromoform it was 0.9 μg/l and for bromodichloromethane and chlorodibromomethane it was 0.4 μg/l.

Precision. By applying the optimum experimental conditions to eight vials containing 5.0 μg/l of the four main THMs and *cis*-1,3-dichloropropene as an internal standard a standard deviation ranging between 0.32 and 0.78 was obtained, together with a relative standard deviation in the range 8.7–18%.

Application of method

The method was applied to the determination of halo-organic compounds in raw water and in treated water in the city of Salamanca. The treated water is a mixture of water treated in two different plants (the "old" and "new" plants) and the water in each

TABLE II

EXTRACTION EFFICIENCY AT 2.0, 5.0 AND 9.0 μg/l

Compound	Extraction efficiency (%)			
	2.0 μg/l	5.0 μg/l	9.0 μg/l	Mean ± S.D.
Chloroform	90	98	97	95 ± 4
Bromodichloromethane	106	95	94	98 ± 6
Chlorodibromomethane	110	99	113	107 ± 7
Bromoform	108	105	106	106 ± 1

is treated in a slightly different way. To study the effect of the different treatments and processes on the formation of the halo-organic compounds samples were taken at different points, the locations of which in the different plants are shown in Fig. 3.

Eighty-eight duplicate analyses were made. These were raw (eleven) and treated (eleven) water samples, as well as samples from six selected steps (sixty-six) during the plant treatments from February

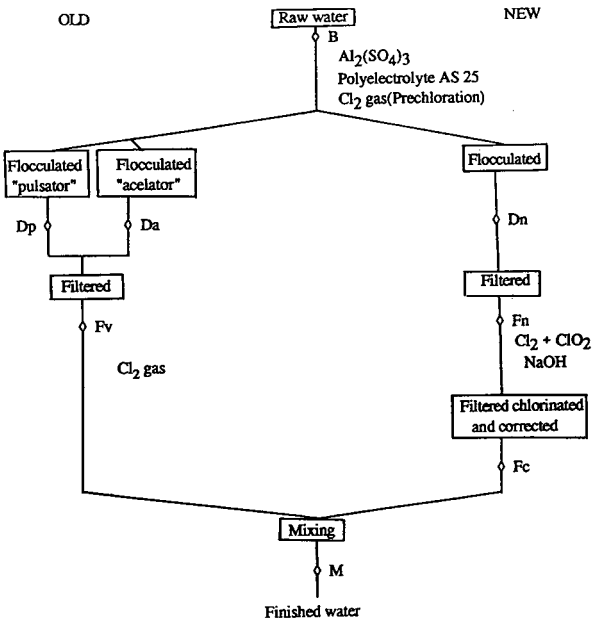

Fig. 3. Location of sampling points in the water treatment plants of the city of Salamanca. B = Raw water; Dp, Da = water treated with gaseous Cl_2 and flocculated with the "pulsator" or "acelator" in the "old" plant; Fv = water filtered in "old" plant after prechlorination step; Dn = water treated with gaseous Cl_2 and flocculated in the "new" plant; Fn = water filtered in "new" plant after prechlorination step; Fc = water treated with Cl_2 and ClO_2, filtered and pH corrected with NaOH in "new" plant; M = mixing point for Fc and Fv treated again with Cl_2.

to July 1991. The sampling frequency was fortnightly.

None of the sixteen halo-organic compounds was detected in any of the raw water samples. Chloroform and bromodichloromethane were formed in all the samples of treated water, whereas dichlorobromomethane and 1,1,2-trichloroethane were detected in 98.7 and 23.4%, respectively. Chloroform was always formed at the highest concentrations and chlorodibromomethane and 1,1,2-trichloroethane were present at values lower than the detection limit in most instances.

The concentrations of chloroform and bromodichloromethane were higher at the sampling points (Dn, Fn and Fc) in the "new" plant than in those corresponding to the "old" plant (Da, Dp and Fv) (Table III) because although the chlorination levels are similar in both plants (5–6 g Cl_2 per m^3), the greater efficiency of the flocculation and filtration processes in the "old" plant produces smaller amounts of organic matter (absorbance measurement at 254 nm). Additionally, it is seen that in sample Fc the maximum concentrations of both compounds are detected (a new treatment with Cl_2 and ClO_2 is performed) and that filtration does not significantly affect the level of formation of chloroform and bromodichloromethane in this plant (Student's t-test applied to Dp and Fv, and to Dn and Fv).

In the treated water, point M, an increase is seen in the concentration of chloroform during the sampling period, probably due to the increase in the temperature of the raw water between February and July, whereas the concentration of bromodichloromethane remained almost constant (Table IV). However, the mean respective concentrations, 9.59 and 2.58 μg/l, during the period from February

TABLE III

MEAN, MAXIMUM AND MINIMUM CONCENTRATIONS OF HALO-ORGANIC COMPOUNDS AT SAMPLING POINTS OF THE WATER TREATMENT PLANTS IN SALAMANCA (SPAIN)

Values given are mean ± standard deviation of eleven determinations with maximum and minimum concentrations during sampling in parentheses.

Sampling point	Concentration (μg/l)	
	Chloroform	Bromodichloromethane
Da	4.38 ± 2.05 (1.4–7.8)	0.99 ± 0.32 (0.5–1.4)
Dp	6.00 ± 2,31 (2.0–9.5)	1.31 ± 0.36 (0.8–1.8)
Fv	6.51 ± 3.08 (2.0–12.7)	1.54 ± 0.59 (1.0–2.6)
Dn	9.18 ± 4.35 (4.3–17.6)	1.96 ± 0.40 (1.4–2.7)
Fn	9.14 ± 4.49 (3.6–15.8)	1.99 ± 0.70 (1.0–3.2)
Fc	11.81 ± 5.89 (4.0–25.2)	2.61 ± 0.89 (1.5–4.1)

TABLE IV

VARIATION IN CONCENTRATIONS OF CHLOROFORM AND BROMODICHLOROMETHANE IN THE TREATED WATER IN SALAMANCA (SPAIN)

Sampling point	Concentration (μg/l)	
	Chloroform	Bromodichloromethane
1	5.3	2.8
2	3.1	1.9
3	7.3	3.0
4	7.2	1.7
5	17.2	2.8
6	7.1	1.8
7	10.6	2.4
8	15.4	2.3
9	15.8	2.8
10	6.5	2.5
11	10.0	4.3
Mean	9.59	2.58
Standard deviation	4.69	0.81
Relative standard deviation (%)	49	32

to July, 1991, are lower than the limits established by the World Health Organization.

REFERENCES

1 J. J. Rook, *Water Treat. Exam.*, 23 (1974) 234.
2 T. A. Bellar and J. J. Lichtenberg, *J. Am. Wat. Works Assoc.*, 66 (1974) 739.
3 J. E. Smith, W. R. Hewitt and J. B. Book, *Toxicol. Appl. Pharmacol.*, 79 (1985) 166.
4 C. F. Tumasonis, D. N. McMartin and B. Bush, *Ecotoxicol. Environ. Safety*, 9 (1985) 233.
5 R. J. Bull, J. Brown, T. A. Jorgerson, E. A. Meierhenry, M. Robinson and J. A. Stober, *Fundam. Appl. Toxicol.*, 5 (1985) 760.
6 R. L. Rosenthal, *Environ. Molec. Mutagen.*, 10 (1987) 211.
7 T. A. Jorgenson, E. F. Meierhenry, C. F. Rusmbrook, R. J. Bull, M. Robinson and C. E. Whitmire, *Fundam. Appl. Toxicol.*, 5 (1985) 760.
8 K. Marimoto and A. Koizumi, *Environ. Res.*, 32 (1983) 72.
9 R. C. Woodruff, J. M. Mason, R. Valencia and S. Zimmering, *Environ. Mutagenesis*, 7 (1985) 677.
10 *Guidelines for Drinking Water Quality, Recommendations*, Vol. 1, World Health Organization, Geneva, 1984, p. 77.
11 National Interim Primary Drinking Water Regulations: Control of Trihalomethanes in Drinking Water, *Fed. Regist.*, 44 (231) (Nov. 1979) 68 624.
12 *EEC rapport, Quality of water destined for human consumption, DO No. L 229*, Brussels, 15 July 1980, p. 174.
13 *B.O.E. 20 September 1990 (R.D. 1138/1990 14 September)*, Spanish Technico-Sanitary Legislation, Madrid.
14 D. Carmichael and W. Holmes, *J. High Resolut. Chromatogr.*, 13 (1990) 267.
15 I. Maier and M. Fieber, *High Resolut, Chromatogr. Chromatogr. Commun.* 11 (1988) 566.
16 D. Gryder-Boutet and J. Kennish, *J. Am. Wat. Works Assoc.*, 80 (1988) 52.
17 D. Herzfeld, K. van der Gun and R. Louw, *Chemosphere*, 18 (1989) 1425.
18 M. Mehran, M. Nickelsen, N. Golkar and W. Cooper, *J. High Resolut. Chromatogr.*, 13 (1990) 429.
19 L. S. Clesceri, A. E. Greenberg and R. R. Trussell (Editors), *Standard Methods for the Examination of Water and Wastewater*, APHA, AWWA, WPCF, Washington, 1989.
20 P. Buszka, S. Zangg and M. Werner, *Bull Environ. Contam. Toxicol.*, 45 (1990) 507.
21 R. D. Blanchard and J. K. Hardy, *Anal. Chem.*, 58 (1986) 1529.
22 K. Abrahamsson and S. Klick, *J. Chromatogr.*, 513 (1990) 39.
23 R. C. Graham and J. K. Robertson, *J. Chem., Educ.*, 65 (1988) 8.
24 Y. A. Mahmood and J. P. Riley, *Wat. Res.*, 24 (1990) 533.

Journal of Chromatography, 605 (1992) 257–262
Elsevier Science Publishers B.V., Amsterdam

CHROM. 24 260

Speciation of arsenic-containing chemical warfare agents by gas chromatographic analysis after derivatization with thioglycolic acid methyl ester

K. Schoene, J. Steinhanses, H.-J. Bruckert and A. König

Fraunhofer-Institut für Umweltchemie und Ökotoxikologie, D-5948 Schmallenberg (Germany)

(First received February 6th, 1992; revised manuscript received April 13th, 1992)

ABSTRACT

Various organoarsenic halogenides, oxides and hydroxides were converted into the corresponding thioarsenites by reaction with thioglycolic acid methyl ester (TGM). The yields and the chemical structures of the TGM derivatives were evaluated by gas chromatography coupled with mass spectrometry and atomic emission spectrometry.

INTRODUCTION

During World Wars I and II, chemical warfare agents were produced in large amounts. After 1945, in Germany, the plants were destroyed and the stockpiles were sunk in the sea or deposited in dumping grounds, floated gravel pits and other places. These deposits still pose a serious risk today. For mapping out contaminated areas, monitoring the groundwater, etc., appropriate an alytical methods are required. One important group within these hazardous chemicals are the organoarsenic halogenides [1]. Representative substances, as far as available for this study, are listed in Table I, together with some presumable decomposition products. The objective of our work was to find a suitable method for detecting, identifying and quantifying such arsenic contaminants.

As it was thought to be the best choice, we decided to apply the gas chromatographic (GC) separation technique, coupled with mass spectrometry (MS) and atomic emission spectrometric detection (AED): by means of AED the elemental composition of the GC peak can be determined [2,3] which complements the MS identification in an ideal manner; furthermore, AED should enable us to quantify the analytes even in cases where authentic reference substances are not available.

However, thermally labile substances such as IV, V and VI (see Table I) cannot be gas chromatographed reliably as the precursor II and the hydrolysis products I and VIII–XI are totally inaccessible to GC [4]. Consequently, in the literature various methods are described for converting such substances into chromatographable derivatives: trimethylsilylation [5,6] (leading to rather unstable products [7]), reduction to hydrides [8,9] (not applicable for aryl arsenic compounds [10] and conversion into iodides [6] and thioarsenites [7,11–14]. In each case, however, the authors applied their procedures only to distinct groups of substances, mostly arsinic acids, or single compounds such as Lewisite (V).

As the most promising alternative with respect to general applicability, we opted for conversion into thioarsenites using thioglycolic acid methyl ester

Correspondence to: Dr. K. Schoene, Fraunhofer-Institut für Umweltchemie und Ökotoxikologie, D-5948 Schmallenberg, Germany.

0021-9673/92/$05.00

TABLE I

ARSENIC COMPOUNDS SUBJECTED TO DERIVATIZATION

	Compound	Formula	CA-RN	Source	Purity (%)	Stock solution (μmol/ml)
I	Sodium arsenite	$NaAsO_2$	7784-48-5	Merck	p.a.	0.05 *M*
II	Arsenic trichloride	$AsCl_3$	7784-34-1	Merck	Supra-pur	3.06
III	Methylarsin dibromide	H_3CAsBr_2	676-70-0	K&K Lab.	93	2.12
IV	Ethylarsin dichloride	$H_5C_2AsCl_2$	598-14-1	–[a]	?	3.40[b]
V	2-Chlorovinylarsin dichloride	$ClCH=CHAsCl_2$	541-25-3	–[a]	96	2.56
VI	Phenylarsin dichloride	$C_6H_5AsCl_2$	696-28-6	–[a]	~90[c]	3.69
VII	Diphenylarsin chloride	$(C_6H_5)_2AsCl$	712-48-1	–[a]	94[d]	3.53
VIII	Dimethylarsinic acid	$(CH_3)_2As(O)OH$	75-60-5	Aldrich	98	3.44
IX	Phenylarsinic acid	$C_6H_5AsO(OH)_2$	98-05-5	Aldrich	98	2.88
X	Phenylarsin oxide	C_6H_5AsO	637-03-6	Aldrich	97	2.76
XI	Diphenylarsinic acid	$(C_6H_5)_2As(O)OH$	4656-80-8	–[a]	?	1.25[b]
XII	Bis(diphenylarsin)oxide	$[(C_6H_5)_2As]_2O$	2215-16-9	–[a]	93	0.96

[a] Analytical samples were made available by the Bundesministerium Verteidigung, Bonn, Germany, via the Wehrwissenschaftliche Dienststelle der Bundeswehr, Munster, Germany.
[b] Assuming 100% purity.
[c] Contained 4% compound VI.
[d] Contained 5% compound V.

(TGM). According to refs. 7, 12 and 13, TGM reacts in acidic aqueous solution with monomethylarsinic acid (MMA), dimethylarsinic acid (DMA), inorganic arsenite and arsenate in the following way to yield derivatives detectable by GC:

$$\underset{\text{DMA}}{(H_3C)_2As(O)OH} + 3\,\underset{\text{TGM}}{HSCH_2C(O)OCH_3} \rightarrow$$

$$\underset{\text{DMA-SGM}}{(H_3C)_2As\text{-}SCH_2C(O)OCH_3} +$$

$$H_3CO(O)CCH_2S\text{–}SCH_2C(O)OCH_3 + 2\,H_2O$$
$$(SGM)_2$$

According, MMA yields $H_3CAs(SGM)_2$, and from inorganic arsenicals $As(SGM)_3$ is formed [12,13]. The derivatives contain the arsenic exclusively in the trivalent state; arsenic(V) compounds are reduced by the thiol, which in turn is oxidized to the disulphide.

After some procedural modifications, this derivatization reaction can now be applied to all the substances listed in Table I. Using GC–MS and GC–AED analysis, the chemical structures of the reaction products and their overall yields were evaluated.

EXPERIMENTAL

Chemicals

The following chemicals were used: dichloromethane, nanograde (Promochem), redistilled; *n*-hexane, nanograde (Promochem); thioglycolic acid methyl ester (TGM, CA-RN 2365-48-2), 98% (Aldrich), stored under argon to prevent oxidation; 0.005 *M* sulphuric acid, Titrisol (Merck); triphenylarsine, 97% (Aldrich); 1.4-dithiane, 97% (Aldrich); 1,2,4-trichlorobenzene, 99%+ (Aldrich); *n*-pentadecane, 99+% (Aldrich). The extraction solution contained 5 μg (23.54 nmol) of pentadecane per ml of *n*-hexane. The arsenic compounds used for the derivatization experiments are listed in Table I. The purities of V, VII and XII were determined by GC–AED analysis; the value given for VI is an estimate, because this compound was not reliably chromatographable; IV and IX could not be gas chromatographed at all.

Gas chromatographic equipment and conditions

Gas chromatography–mass spectrometry. An HP 5890 II gas chromatograph with an on-column injection port, an HP 7673 autosampler, and an HP 5970 B mass-selective detector (Hewlett Packard)

were used. The conditions were as follows: retention gap, WCOT FS deactivated, 2 m × 0.53 mm I.D. ("methyl", Chrompack 8009 3552); GC column HP 1, cross-linked methylsilicone, 25 m × 0.17 mm I.D. (Hewlett-Packard); helium, 55 kPa (0.6 ml/min); oven, 40°C (2 min), 10°C/min to 250°C (40 min); injection volume, 1 μl.

Gas chromatography–atomic emission spectrometry. The gas chromatograph, autosampler, retention gap and oven programme were as above. The conditions were as follows: atomic emission detector, HP 5921 A with ChemStation 5895 A (Hewlett Packard); the GC column was as described above but 25 m × 0.31 mm I.D.; helium 150 kPa; AED, ferrule purge 30.4, cavity vent 76.4 ml/min; nitrogen 2 l/min; oxygen 140, helium 350, helium 200, nitrogen/methane 450 kPa; injection volume, 1 μl.

Calibration of GC–AED

The GC–AED system was calibrated for the elements carbon, hydrogen, arsenic, chlorine and sulphur using four different concentrations of standard solutions in iso-octane, containing mixtures of the following compounds (concentration range in brackets): triphenylarsine (4–40 nmol/ml), 1,4-dithiane (15–150 nmol/ml), 1,2,4-trichlorobenzene (30–300 nmol/ml), pentadecane (6–60 nmol/ml); the concentrations of the first two solutions were corrected for the 97% purity indicated by the supplier.

Using oxygen as the reagent gas, carbon, hydrogen and chlorine were measured at 495.724, 486.133 and 480.192 nm, respectively; with oxygen and hydrogen as the reagent gas, carbon was determined at 193.031 and sulphur 181.379 nm; arsenic was measured at 189.042 nm applying hydrogen as the reagent gas and an increased make-up flow.

Using three GC injections per standard solution at each of the three reagent gas settings, linear calibration functions were obtained in each case. From these, the individual response factors were derived. With the lowest concentrations of solutions, the highest standard deviations were found as follows: 5% (carbon, 193 nm); 2% (carbon, 496 nm); 17% (hydrogen); 2% (arsenic); 4% (chlorine); 3% (sulphur). Under the conditions applied, the detection limits (pg/s) were for carbon 193, 3; carbon 496, 65; hydrogen, 5; arsenic, 56; chlorine, 181; sulphur, 17.

Derivatization and analysis

From one of the individual stock solutions, 10 μl were pipetted into a 1.8-ml crimp-top vial containing 500 μl of 0.05 *M* sulphuric acid. After flushing the headspace with argon, 10 μl (106 μmol) of TGM were added and the vial closed with a septum (PTFE/butyl rubber) and kept for 30 min in an ultrasonic bath at 60–70°C. After cooling to room temperature, the vial was opened, 400 μl of extraction solution (see above) were added and the vial was closed and shaken for 2 min. From the organic phase, 250 μl were transferred into an autosampler vial with a 250-μl insert and analysed by GC–MS and GC–AED (injection volume 1 μl). The experiments were carried out in duplicate.

Evaluation of results

The peak areas, obtained from the AED signals (Fig. 1), were converted into pg atoms (1 pg atom = $1 \cdot 10^{-12}$ g atoms) of the respective element. Taking the lowest number of pg atoms (here generally that of arsenic) as unity, an approximate empirical formula and presumable molecular weight were calculated. This was compared with the information given by the mass spectrum, to confirm the structure of the reaction product. The empirical formula was then recalculated on the basis of the number of carbon atoms (theoretically) present in the molecule (with respect to the calibration procedure, the carbon data should be most reliable).

Knowing the empirical formula and the pg atoms of carbon and of any other element) present in the GC peak, the picomoles which had reached the detector could be calculated. A similar calculation for the internal standard gave the procedural recovery ratio (pentadecane introduced/found). After correcting the picomoles of analyte in the same way, the overall yield was calculated by relating the picomoles of analyte found to the amount of starting compound which had been introduced into the assay.

RESULTS AND DISCUSSION

From each of the compounds listed in Table I, a thioarsenite derivative could be obtained. In addition, several attempts were made to derivatize 5,10-dihydrophenarsazin chloride (adamsite, CA-RN 578-94-9) in this way but were unsuccessful. It is

TABLE II

TGM DERIVATIVES OF ARSENIC COMPOUNDS

Key fragments[a] in the mass spectra ("SGM" = $-SCH_2COOCH_3$).

Starting compound[a]	Derivative (mol. mass)	M^+ (%)	M^+-15 (%)	M^+-73 (%)	M^+-105 (%)	285 (%)	180 (%)	107 (%)
I, II	$As(SGM)_3$ (390)	–	–	3	100	(100)	8	18
III	$H_3CA_s(SGM)_2$ (300)	–	96	3	100	(96)	1	30
IV	$H_5C_2As(SGM)_2$ (314)	–	20	5	18	100	4	32
V	$ClC_2H_2As(SGM)_2$ (346)	–	–	1	22	1	100	20
VI, IX, X	$C_6H_5As(SGM)_2$ (362)	5	–	6	100	1	22	18
VII, XI, XII	$(C_6H_5)_2AsSGM$ (334)	30	–	100	28	–	12	10
VIII	$(H_3C)_2AsSGM$ (210)	38	100	35	25	–	–	23

[a] Tentative interpretation: M^+-15 = M^+-CH_3; M^+-73 = M^+-$CH_3C(O)OCH_2$; M^+-105 = M^+-$SCH_2C(O)OCH_3$; 285 = $As(SGM)_2$; 180 = AsSGM; 107 = AsS.

not clear whether the product formed could not be gas chromatographed or whether adamsite did not react at all.

The results obtained from the GC–MS runs are given in Table II. As expected, the products obtained from phenylarsin dichloride, phenylarsin oxide and phenylarsinic acid exhibited identical mass spectra, as did those from the corresponding diphenylarsinic compounds VII, XI and XII. Molecular ions appeared only in the spectra of thioarsenites containing either one SGM group or a phenyl moiety attached to the arsenic atom. The formation of $M^+ - 15$ fragments was confined to methyl- and ethylarsenic compounds. $M^+ - 105$ represents the structure-related key fragment, in each case accompanied by the mass 107 (arsenic sulphide [11]).

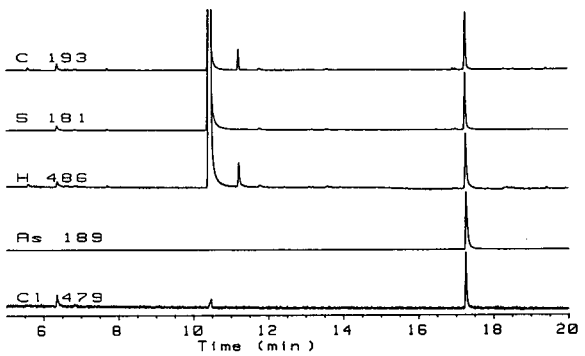

Fig. 1. GC–AED chromatogram of a sample (diluted 1:5 with hexane) containing the TGM derivative of compound V (Lewisite): 6.8 min, unknown; 10.9 min, disulphide $(SGM)_2$ (impurity from the reagent); 11.2 min, pentadecane, 4.7 pmol; 17.3 min, $ClC_2H_2As(SGM)_2$, 44 pmol.

The empirical formulae resulting from the GC–AED analysis are given in Table III, together with the overall yields and the relative retention times (RRT = retention time of analyte/retention time of pentadecane). The elemental compositions found are consistent with the formulae derived from the mass spectra. In the empirical formulae, the deviations from the theoretical values amount to 20%. The source of these errors is not yet clear; with growing experience in handling this analytical system, which is relatively new in our laboratory, a somewhat better performance will probably be achievable.

Regarding the reactivity towards TGM, the twelve test substances behaved differently. For example, DMA could be derivatized completely even at room temperature within a few minutes,

TABLE III

TGM DERIVATIVES OF ARSENIC COMPOUNDS

Relative retention times (RRT), empirical formulae and overall yields ("SGM" = $-SCH_2COOCH_3$).

Starting compound	Derivative, empirical formula	RRT[a]	Empirical formula found[b]					Overall yield	
			C	H	As	Cl	S	Pmol found[c]	%
I	$As(SGM)_3$	1.82							
	$C_9H_{15}AsO_6S_3$		9	12.4	0.9	–	3.1	10	40
II	$As(SGM)_3$	1.82							
	$C_9H_{15}AsO_6S_3$		9	13.9	1.1	–	3.0	29	37
III	$H_3CAs(SGM)_2$	1.31							
	$C_7H_{13}AsO_4S_2$		7	11.1	0.8	–	1.9	40	81
IV	$H_5C_2As(SGM)_2$	1.38							
	$C_8H_{15}AsO_4S_2$		8	12.8	0.9	–	2.1	45	53[d]
V	$ClC_2H_2As(SGM)_2$	1.55							
	$C_8H_{12}AsClO_4S_2$		8	11.2	1.1	0.9	2.1	44	66
VI	$C_6H_5As(SGM)_2$	1.77							
	$C_{12}H_{15}AsO_4S_2$		12	16.1	1.0	–	2.2	68	~80
VII	$(C_6H_5)_2AsSGM$	1.69							
	$C_{15}H_{15}AsO_2S$		15	14.5	0.9	–	1.1	85	103
VIII	$(H_3C)_2AsSGM$	0.61							
	$C_5H_{11}AsO_2S$		5	12.7	1.0	–	0.9	87	102
IX	$C_6H_5As(SGM)_2$	1.77							
	$C_{12}H_{15}AsO_4S_2$		12	12.5	0.9	–	2.0	56	80
X	$C_6H_5As(SGM)_2$	1.77							
	$C_{12}H_{15}AsO_4S_2$		12	15.6	0.8	–	2.2	55	81
XI	$(C_6H_5)_2AsSGM$	1.69							
	$C_{15}H_{15}AsO_2S$		15	16.9	1.1	–	1.1	15	47[d]
XII	$(C_6H_5)_2AsSGM$	1.69							
	$C_{15}H_{15}AsO_2S$		15	14.3	1.0	–	1.2	32	82

[a] Relative retention time: RRT = retention time of analyte/retention time of pentadecane, retention time of pentadecane: GC–MS, 16.8 min; GC–AED, 11.2 min.

[b] The reference element carbon, is underlined; oxygen was not determined.

[c] Upon GC injection of 1 μl.

[d] Assuming the starting compound to be of 100% purity.

whereas under these conditions the halogenated compounds gave only poor yields, or none at all. Hence, the procedure described is the result of an optimization with regard to the slow-reacting compounds. By lowering the temperature, it may be possible to increase the yield of the most thermolabile derivatives, $As(SGM)_3$ and $ClC_2H_2As(SGM)_2$; however, the main losses, probably occur on the GC column [11]. Upon split–splitless injection into the hot injector (250°C), all TGM derivatives underwent thermal decomposition; hence, exclusively on-column injection was applied.

The reaction mixture should be acidic [12,13]; in fact, no chromatographable products could be extracted from slightly alkaline solutions. The content of dichloromethane, a common extracting solvent, in the reaction mixture should not exceed 10%; addition of 20% dichloromethane resulted in lower yields and several non-identified byproducts.

As mentioned above, the derivatives contain arsenic in the trivalent state; arsenic(V) compounds are reduced by the reagent, from which an equivalent amount of disulphide (RRT 0.94) is formed. This offers an opportunity for differentiating between arsenic(III) and arsenic(V) compounds.

From the test substances VI, IX and X, the same

product, $C_6H_5As(SGM)_2$, is formed, and VII, XI, XII all lead to $(C_6H_5)_2AsSGM$. In a water analysis, for example, a certain discrimination between the different starting compounds is still possible; upon extraction with dichloromethane, VI, VII and XII will be transferred into the organic phase, whereas the two acids IX and XI remain in the aqueous phase (the partitioning behaviour of phenylarsin oxide may be ambivalent). Direct GC of the organic phase will yield phenylarsin dichloride, VI (RRT 1.14, but not reliably chromatographable), diphenylarsinchloride, VII (RRT 1.37) and bis(diphenylarsin) oxide, XII (RRT 2.82); derivatization leads to $C_6H_5As(SGM)_2$ in an amount corresponding to VI and X, and to $(C_6H_5)_2AsSGM$ from VII and XII. Finally, derivatization in the (preconcentrated) aqueous phase yields the derivatives of IX + X and XI; the portion of IX in IX + X can be estimated from the amount of disulphide formed. In this context it should be noted, however, that repeated injections of arsenic tri- and dichlorides cause irreversible damage to the GC column.

ACKNOWLEDGEMENTS

We are indebted to the Niedersächsisches Umweltministerium, Hannover, Germany, for financial support, and to Dr. B. Appler, Munster, Germany, for helpful advice and discussions.

REFERENCES

1 K. E. Jackson, *Chem. Rev.*, 17 (1935) 251.
2 B. D. Quimby and J. J. Sullivan, *Anal. Chem.*, 62 (1990) 1027.
3 J. J. Sullivan and B. D. Quimby, *Anal. Chem.*, 62 (1990) 1034.
4 Z. Witkiewicz, M. Mazurek and J. Szulc, *J. Chromatogr.*, 503 (1990) 293.
5 C. J. Soderquist, D. G. Bowers and D. G. Crosby, *Anal. Chem.*, 46 (1974) 155.
6 F. T. Henry and T. M. Thorpe, *J. Chromatogr.*, 166 (1978) 577.
7 B. Beckermann, *Anal. Chim. Acta*, 135 (1982) 77.
8 Y. Taimi and D. T. Bostic, *Anal. Chem.*, 47 (1975) 2145.
9 H. Mukai and Y. Ambe, *Anal. Chim. Acta*, 193 (1987) 219.
10 S. Franke, *Militärchemie*, Vol. 2, Deutscher Militärverlag, Berlin, 2nd ed., 1976, p. 340.
11 U. Hannestad and B. Sörbo, *J. Chromatogr.*, 200 (1980) 171.
12 K. Dix, C. J. Cappon and T. Y. Torbara, *J. Chromatogr. Sci.*, 25 (1987) 235.
13 H. Haraguchi and A. Takatsu, *Spectrochim. Acta*, 42B (1987) 235.
14 J. K. Fowler, D. S. Stewart and D. S. Weinberg, *J. Chromatogr.*, 558 (1991) 235.

Journal of Chromatography, 605 (1992) 263–267
Elsevier Science Publishers B.V., Amsterdam

CHROM. 24 261

Separation of unsaturated fatty acid methyl esters by packed capillary supercritical fluid chromatography

Comparison of different column packings

Mustafa Demirbüker, Ingela Hägglund and Lars G. Blomberg

Department of Analytical Chemistry, Stockholm University, Arrhenius Laboratory, S-106 91 Stockholm (Sweden)

(First received December 30th, 1991; revised manuscript received April 13th, 1992)

ABSTRACT

Packed capillary supercritical fluid chromatography with ultraviolet detection was applied to the separation of methyl esters of unsaturated fatty acids obtained from a fish oil. Separation was attempted on three different types of column packing: cation exchanger impregnated with silver nitrate, silica and anion exchanger treated with potassium permanganate. Separation on the argentation column resulted in relatively good resolution of geometric isomers of dienes and trienes. Further, this column performed well in the separation of fatty acid methyl esters from a fish oil. Separatiaon of the same sample on a column packed with silica was somewhat less complete. Finally, a permanganate-treated anion exchanger separated the fatty acid methyl esters into groups according to the degree of unsaturation.

INTRODUCTION

Fatty acids are the distinctive structural components of lipids, and methods for their separation and analysis are of great significance. Gas chromatographic (GC) [1] as well as high-performance liquid chromatographic (HPLC) [2] methods have been successfully used. Silver ion or argentation chromatography has been of particular interest for the separation of complex mixtures of *cis/trans* isomers [3,4]. In this method, fatty acids are separated according to the number, position and geometrical configuration of their double bonds. Argentation columns for HPLC were orginally prepared by impregnation of silica with silver nitrate. The silver nitrate was, however, rapidly leached out from such columns, thus contaminating samples and reducing the working life of the column. It was demonstrated by Christie [5] that columns in which a silica-based cation exchanger has been impregnated with silver nitrate can be stable under HPLC conditions. Recently, it was shown that such columns also show excellent stability under supercritical fluid chromatographic (SFC) conditions [6,7].

Argentation columns of this stable type have been applied to the separation of derivatized fatty acids by HPLC using conventional column dimensions [1–4]. Two different approaches may be distinguished. First, the most complete separation may be sought, *e.g.* of *cis/trans* isomers [3]. Second, the conditions may be changed to give a separation into groups which subsequently will be further separated using a complementary chromatographic method, *e.g.* GC [1,4].

Oxides of transition metals, such as chromium [8], vanadium [9,10] and manganese [11], have been

Correspondence to: Dr. L. G. Blomberg, Department of Analytical Chemistry, Stockholm University, Arrhenius Laboratory, S-106 91 Stockholm, Sweden.

0021-9673/92/$05.00

chemically attached to silica in order to be used as catalysts. This type of modification often results in decreased silanol activity [12]. It was recently shown that silanol groups on silica and silica-based anion exchangers could be deactivated by treatment with potassium permanganate [13]. Under SFC conditions, manganese acts as a weak electron acceptor, and triacylglycerols could be separated into groups according to their degree of unsaturation.

Few separations of fatty acid derivatives using normal-phase HPLC have been reported, but it is considered that there is some potential for further development [2].

In this work, separation of fatty acid methyl esters (FAMEs) was attempted on packed capillary columns, using supercritical fluids as mobile phase. The performance of different types of column packing—silica, Ag^+/cation exchanger and potassium permanganate/anion exchanger—was evaluated.

EXPERIMENTAL

SFC was performed on a Lee Scientific 600 Series SFC system equipped with a Lee Scientific variable-wavelength absorbance detector. Detection was executed at 210 nm. Fused-silica capillary tubing (Polymicro Technologies, Phoenix, AZ, USA), 11 μm I.D., was used as restrictors in lengths of 20–25 cm.

Columns were prepared from fused-silica capillary tubing, 250 or 330 mm × 0.25 mm I.D. and 0.43 mm O.D. (Polymicro Technologies). Three types of packing were used: Nucleosil 4 SA and 5 SB (Macherey Nagel, Düren, Germany) and Superspher Si 60 4 μm (Merck, Darmstadt, Germany). Slurry packing and impregnation with silver nitrate were performed as described previously [6,7]. For the modification with permanganate, some columns were, after packing with Nucleosil 5 SB, washed successively with methanol, 400 μl of distilled water, 400 μl of 0.2 *M* potassium permanganate and 400 μl of distilled water. Finally, the columns were dried by flushing with carbon dioxide at 115°C and 275 atm [13].

The mobile phase consisted of carbon dioxide–acetonitrile–isopropanol. Different contents of modifier were used for the different column types. SFC-grade carbon dioxide (Scott Specialty Gases, Plumsteadville, PA, USA) was used. The content of isopropanol was *ca.* 10% of that of acetonitrile. The mobile phase mixture was prepared in the SFC pump as described previously [14]. Mobile phase velocity was 3.5 mm/s. Analytes were dissolved in HPLC-grade pentane at concentrations of 30 mg/ml. The injector was equipped with an internal loop, 200 nl, and injection was performed using a timed split of 0.2 s. In addition, a split ratio of 1:1 was applied. Using these conditions, *ca.* 60 nl were allowed to enter the column.

GC was performed on a Mega gas chromatograph (Carlo Erba). Open tubular columns coated with the stationary phase Sila C were prepared as described previously [15]. Hydrogen was used as mobile phase.

FAME standards and CPL fish oil 30 were obtained from Larodan Fine Chemicals (Malmö, Sweden). Saponification and methylation of triacylglycerols were performed according to Christie [16]. Mixtures of geometrical isomers were prepared from the parent compounds by nitric oxide-catalysed isomerzation [17].

RESULTS AND DISCUSSION

The separation of a mixture of geometrical isomers of dienes is shown in Fig. 1A. Isomers 9*t*,12*c*-18:2 and 9*c*,12*t*-18:2 could not be resolved, which was observed also for argentation HPLC [3]. Fig. 1B illustrates the separation of the geometrical isomers obtained from linolenic acid. This mixture should contain eight components. In argentation chromatography, *trans* isomers always migrate ahead of *cis* isomers [1], and the first peak in Fig. 1B thus ought to be the *t,t,t* isomer and the last peak the *c,c,c* isomer. Then there remain two groups of peaks; the first group ought to be the *t,t,c* isomers and the second group the *t,c,c* isomers. In the separation of the same type of sample with argentation HPLC, six peaks were obtained, and the analysis time was much longer, 40 min [3].

Separation of *t,t*-18:2 and *c,c*-18:2 was attempted on capillary columns packed with anion exchanger and modified *in situ* with potassium permanganate: an α-value of 1.02 was obtained.

Fish oil FAMEs

The SFC separation of the FAMEs from a fish oil on an argentation column is shown in Fig. 2, the

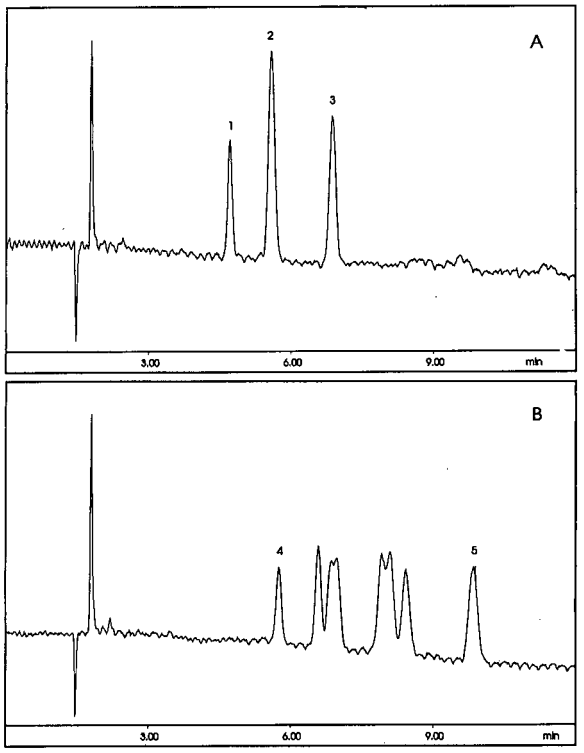

Fig. 1. Supercritical fluid chromatogram of methyl esters of geometrical isomers of (A) linoleic acid and (B) linolenic acid. Capillary column, 250 mm × 0.25 mm I.D., packed with 4-μm cation exchanger and impregnated *in situ* with silver nitrate. Injection at 115°C and 280 atm; after 2 min, programmed at −1°C/min and 2 atm/min to 75°C and 360 atm. Mobile phase: carbon dioxide–acetonitrile–isopropanol (97.1:2.6:0.3, mol%). UV detection at 210 nm. See the Experimental section for practical details. Peaks: 1 = 9*t*,12*t*-18:2; 2 = 9*c*,12*t*-18:2 + 9*t*,12*c*-18:2; 3 = 9*c*,12*c*-18:2; 4 = *t*,*t*,*t*-18:3; 5 = *c*,*c*,*c*-18:3.

content of acetonitrile in the mobile phase being 2.6 mol% in this case. A gas chromatogram of the same sample is shown in Fig. 3. Fractions were collected from the SFC eluate for further separation by open tubular GC, a relatively complete separation of the components thus being obtained. Further, the analysis of the fractions aided in the identification of the peaks in the SFC chromatogram.

The separation obtained on an anion exchanger treated *in situ* with potassium permanganate is shown in Fig. 4. Although the mobile phase contained only 0.6% acetonitrile in this case, the retention times were much shorter than for the Ag^+ column. Fig. 5 shows the separation obtained on a column packed with silica. The most complete separation was obtained with the argentation column, but the separation achieved with the column packed with pure silica was almost as good. Columns that had been treated with potassium permanganate gave inferior separations. Here, separation into groups according to the degree of unsaturation was achieved rather than separation of molecular species. The potential practical values of such a group

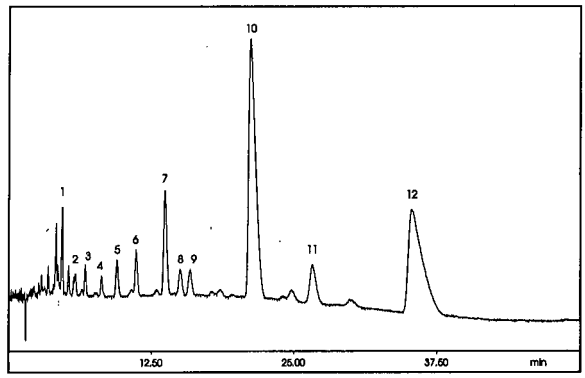

Fig. 2. Supercritical fluid chromatogram of FAMEs of CPL fish oil 30. Column, mobile phase and conditions as in Fig. 1. Peaks: 1 = 18:1; 2 = 20:1; 3 = 18:2; 4 = 22:1; 5 = 18:3; 6 = 16:4; 7 = 18:4; 8 = 20:4($n-6$); 9 = 20:4($n-3$); 10 = 20:5; 11 = 22:5; 12 = 22:6.

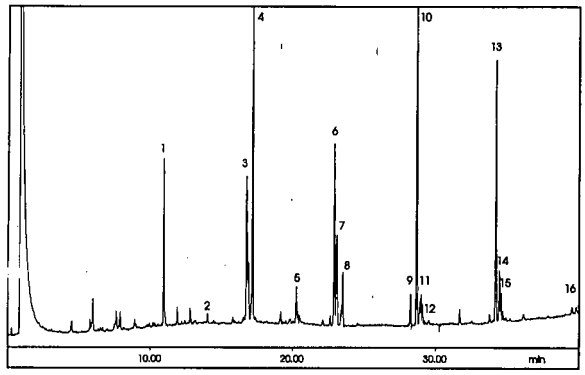

Fig. 3. Gas chromatogram (flame ionization detection) of FAMEs of CPL fish oil 30 on a 25 m × 0.25 mm I.D. fused-silica capillary column coated with Polymer S. Conditions: split injection at 130°C; after 2 min, programmed at 3°C/min to 250°C. Peaks: 1 = 14:0; 2 = 15:0; 3 = 16:1*c* + 16:4; 4 = 16:0 + 16:1*t* + 16:2; 5 = 17:1; 6 = 18:1*c* + 18:2*c*,*c* + 18:4 + 18:5; 7 = 18:1*t*; 8 = 18:0 + 18:2*t*,*t* + 18:3; 9 = 20:4($n-6$); 10 = 20:3 + 20:5; 11 = 20:1 + 20:2*c*,*c* + 20:4($n-3$); 12 = 20:0; 13 = 22:6; 14 = 22:5 + 22:1*c*; 15 = 22:1*t*; 16 = 24:1.

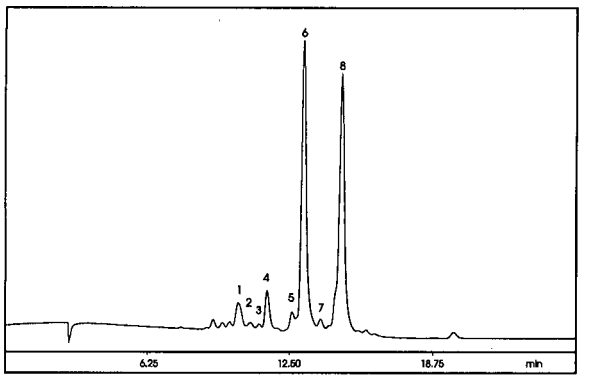

Fig. 4. Supercritical fluid chromatogram of FAMEs of CPL fish oil 30. Capillary column, 330 mm × 0.25 mm I.D., packed with 5-μm anion exchanger and modified *in situ* with potassium permanganate. Injection at 115°C and 220 atm; after 2 min, programmed at −2°C/min and 4 atm/min to 75°C and 300 atm. Mobile phase: carbon dioxide–acetonitrile–isopropanol (99.3:0.6:0.06, mol%). See Experimental section for practical details. Peaks: 1 = 18:1; 2 = 18:2; 3 = 18:3; 4 = 18:4; 5 = 20:4; 6 = 20:5; 7 = 22:5; 8 = 22:6.

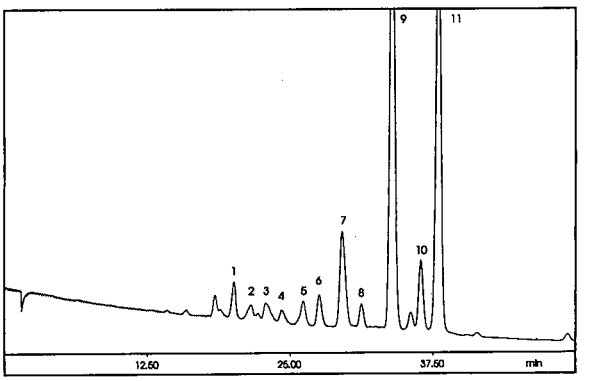

Fig. 5. Supercritical fluid chromatogram of FAMEs of CPL fish oil 30. Capillary column, 250 mm × 0.25 mm I.D., packed with 4-μm silica. Mobile phase and conditions as in Fig. 4. Peaks: 1 = 18:1; 2 = 20:1; 3 = 18:2; 4 = 22:1; 5 = 18:3; 6 = 16:4; 7 = 18:4 + 20:4($n-6$); 8 = 20:4($n-3$)?; 9 = 20:5; 10 = 22:5; 11 = 22:6.

separation may involve the use in hyphenated systems, where each group is being separated further in another dimension. Moreover, permanganate-treated columns could be of value in preparative work.

A relatively high content of acetonitrile in the mobile phase, 2.8%, is needed for the elution of FAMEs from Ag^+ columns. For elution on silica and permanganate-treated columns, 0.8% acetonitrile was sufficient. It seems that, for argentation columns, the main function of the acetonitrile is to partially deactivate the silver ions. Permanganate-treated columns were less retentive than silica columns, and it seems that such a treatment serves to deactivate residual silanol groups. However, silanol groups aid in the separation of molecular species of FAMEs. Triacylglycerols, on the other hand, are relatively poorly separated on columns packed with silica [13]. For the separation of such compounds, elimination of residual silanols on the column packing seems to be beneficial.

The column packing material became light brown on treatment with potassium permanganate. After rinsing with a solution of potassium persulphate, the packing was again white, and the colour of the eluate was purple. Further, the presence of managanese on the silica surface was detected by means of atomic absorption spectroscopy. Permanganate has an oxidizing effect on unsaturated lipids; such an effect would here lead to a consumption of permanganate ions and thus a reduction in retention times. However, the permanganate-treated columns showed excellent reproducibility of the retention under the conditions applied in this work. Further, the columns showed high stability at relatively high temperatures, the retention properties being unchanged after 12 h at 180°C. It is not known in what form the managanese occurs on the surface, but it seems unlikely that it is as permanganate.

ACKNOWLEDGEMENT

Financial support for M. D. from Karlshamns Research Council is gratefully acknowledged.

REFERENCES

1 W. W. Christie, *Gas Chromatography and Lipids*, The Oily Press, Ayr, 1989.
2 W. W. Christie, *HPLC and Lipids*, Pergamon Press, Oxford, 1987.
3 W. W. Christie and G. H. McG. Breckenridge, *J. Chromatogr.*, 469 (1989) 261.
4 W. W. Christie, E. Y. Brechany and K. Stefanov, *Chem. Phys. Lipids*, 46 (1988) 127.
5 W. W. Christie, *J. High Resolut. Chromatogr. Chromatogr. Commun.*, 10 (1987) 148.
6 M. Demirbüker and L. G. Blomberg, *J. Chromatogr. Sci.*, 28 (1990) 67.

7 M. Demirbüker and L. G. Blomberg, *J. Chromatogr.*, 550 (1991) 765.
8 G. Hierl and H. L. Krauss, *Z. Anorg. Allg. Chem.*, 415 (1975) 57.
9 B. Horvath, J. Geyer and H. L. Krauss, *Z. Anorg. Allg. Chem.*, 426 (1976) 141.
10 F. Roozeboom, T. Fransen, P. Mars and P. J. Gellings, *Z. Anorg. Allg. Chem.*, 449 (1979) 25.
11 B. Horvath, J. Strutz, R. Möseler and E. G. Horvath, *Z. Anorg. Allg. Chem.*, 449 (1979) 5.
12 H.-P. Boehm and H. Knözinger, in J. R. Anderson and M. Boudart (Editors), *Catalysis*, Vol. 4, Springer, Berlin, 1983, pp. 40–189.
13 M. Demirbüker and L. G. Blomberg, *J. Chromatogr.*, 600 (1992) 352.
14 S. Schmidt, L. G. Blomberg and E. R. Campbell, *Chromatographia*, 25 (1988) 775.
15 I. Hägglund, L. G. Blomberg, K. Janák, S. Claude and R. Tabacchi, *J. Microcol. Sep.*, 3 (1991) 459.
16 W. W. Christie, *J. Lipid Res.*, 23 (1982) 1072.
17 W. W. Christie, *J. Labelled Compd. Radiopharm.*, 16 (1979) 263.

Journal of Chromatography, 605 (1992) 269–275
Elsevier Science Publishers B.V., Amsterdam

CHROM. 24 228

Micellar electrokinetic capillary chromatography of the enantiomers of amphetamine, methamphetamine and their hydroxyphenethylamine precursors

Ira S. Lurie

Drug Enforcement Administration, Special Testing and Research Laboratory, 7704 Old Springhouse Road, McLean, VA 22102-3494 (USA)

(First received January 15th, 1992; revised manuscript received March 31st, 1992)

ABSTRACT

The separation of the enantiomers of amphetamine, methamphetamine, ephedrine, pseudoephedrine, norephedrine and norpseudoephedrine in a single run via micellar electrokinetic capillary chromatography (MECC) is described. The procedure, which involves preliminary derivatization with 2,3,4,6-tetra-O-acetyl-β-D-glucopyranosyl isothiocyanate (GITC) followed by MECC analysis, is far superior with respect to both resolution and speed of analysis versus similar efforts utilizing high-performance liquid chromatography. The MECC separation was obtained at 20 kV on a 48 cm × 50 μm I.D. (26 cm length to detector) capillary at 30°C using a run buffer consisting of 20% methanol and 80% sodium dodecyl sulfate (SDS) solution [100 m*M* SDS, 10 m*M* phosphate, 10 m*M* borate (pH 9.0)]. The effects of organic modifier type, organic modifier concentration, voltage, temperature and SDS concentration on the resolution of the GITC derivatives are described. The application of the above methodology to forensic samples is presented.

INTRODUCTION

The separation of optical isomers such as phenethylamines (amphetamine, methamphetamine, norephedrine, norpseudoephedrine, ephedrine and pseudoephedrine) is important for forensic analysis. Isomer determination can help identify synthetic methodolologies. For example, amphetamine or methamphetamine synthesized via the Leuckart reaction (*i.e.*, from phenylacetone) will exist as the racemate, whereas that synthesized via direct stereospecific reduction of one of the enantiomeric α-hydroxyphenethylamines (*i.e.*, from norephedrine, norpseudoephedrine, ephedrine or pseudoephedrine) will exist as an optically pure *d* or *l* isomer [1]. In addition, since these compounds are often encountered in combinations, the determination of their isomers could provide additional intelligence information other than synthetic route.

Gas chromatography (GC) and high-performance liquid chromatography (HPLC) have both been utilized previously for the separation of the enantiomers of phenethylamines [2–5]. Resolution of the optically active compounds was obtained either by derivatization with an optically active reagent with subsequent separation of the resulting diastereomers on a non-chiral stationary phase [2,4], or by direct analysis using a chiral stationary phase [3,5]. None of the reported procedures are capable of resolving the enantiomers of norephedrine, norpseudoephedrine, ephedrine, pseudoephedrine, amphetamine and methamphetamine (Fig. 1) in a single run.

One approach for the capillary electrophoretic (CE) separation of enantiomers involves the use of buffer additives such as cyclodextrin derivatives [6–8], chiral surfactants [9–12] or cyclodextrin plus

Correspondence to: I. S. Lurie, Drug Enforcement Administration, Special Testing and Research Laboratory, 7704 Old Springhouse Road, McLean, VA 22102-3494, USA.

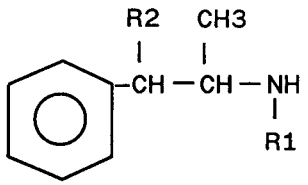

R1	R2	COMPOUND	ABSOLUTE CONFIGURATION
H	H	Amphetamine	2S - (+) 2R - (-)
CH_3	H	Methamphetamine	2S - (+) 2R - (-)
CH_3	OH	Ephedrine	1R, 2S - (-) 1S, 2R - (+)
CH_3	OH	Pseudoephedrine	1R, 2R - (-) 1S, 2S - (+)
H	OH	Norephedrine	1R, 2S - (-) 1S, 2R - (+)
H	OH	Norpseudoephedrine	1R, 2R - (-) 1S, 2S - (+)

Fig. 1. Structures, absolute configurations and optical rotations of phenethylamines examined.

chiral surfactant [13]. The use of cyclodextrin derivatives as mobile phase additives have been previously reported for the separation of the enantiomers of norephedrine, pseudoephedrine and ephedrine [6,7]. Another approach for the CE analysis of optical isomers involves the micellar electrokinetic capillary chromatographic (MECC) separation of diastereomers resulting from the reaction of enantiomers with chiral derivatizing reagents [14,15]. MECC, a form of CE developed by Terabe *et al.* [16], is capable of providing high resolution for both neutral and ionic compounds [15–18]. In this chromatographic technique, compounds may have different abilities to partition into a micelle which is retarded by electrophoretic migration. 2,3,4,6-Tetra-O-acetyl-β-D-glucopyranosyl isothiocyanate (GITC) has been previously shown to be an excellent chiral derivatization reagent for the analysis of primary and secondary amines (such as phenethylamines) via HPLC [4] and the analysis of amino acids via MECC [15]. Reactions proceed fairly quickly under mild conditions and give products with high UV extinction coefficients. This increased sensitivity is particularly advantageous for MECC in view of the small optical path lengths used for the on-column UV detection.

This paper describes the MECC separation of the enantiomers of amphetamine, methamphetamine, ephedrine, pseudoephedrine, norephedrine and norpseudoephedrine. In addition the effect of various chromatographic parameters on the separation is detailed.

EXPERIMENTAL

Equipment

A Model 270A-HT capillary electrophoresis unit (Applied Biosystems, San Jose, CA, USA) interfaced with a Turbochrom 3 chromatographic data handling system (PE Nelson, Cupertino, CA, USA) was used for all CE studies.

The fused-silica capillaries (Polymicro Technologies, Scottsdale, AZ, USA) used in this study were conditioned by successively aspirating with 1 *M* sodium hydroxide 10 min, water 10 min and the run buffer 10 min. For separations employing heptakis (di-O-methyl)-β-cyclodextrin, a 57 cm × 50 μm I.D. (35 cm length to detector) capillary was used. For separations using cyclodextrin plus sodium dodecyl sulfate (SDS) and for those runs using sodium taurocholate 72 cm × 50 mm I.D. (50 cm length to detector) capillaries were used. Finally, for separations using SDS, a 48 cm × 50 μm I.D. (26 cm length to detector) capillary was used. All separations were carried out with UV detection at 210 nm and with the autosampler cooled to 4°C.

For flow injection analysis a Series 4 liquid chromatograph (Perkin-Elmer, Norwalk, CT, USA) fitted with an ISS 100 autosampler (Perkin-Elmer) and a 1040 M diode array detection system (Hewlett Packard, Waldbronn, Germany) were used.

Materials

Heptakis(di-O-methyl)-β-cyclodextrin (Sigma, St. Louis, MO, USA), sodium taurocholate (Sigma) and SDS (Aldrich, Milwaukee, WI, USA) were used as received. Sodium borate, sodium phosphate (monobasic), tris(hydroxymethyl)aminomethane hydrochloride (trizma) buffer, phosphoric acid and sodium hydroxide were reagent grade. Deionized water from a Milli-Q system (Millipore, Bedford, MA, USA) was used to prepare all buffers. Methanol, acetonitrile and tetrahydrofuran were HPLC grade. GITC was obtained from Polysciences (Warrington, PA, USA). The drug standards used were

part of the reference collection of the Drug Enforcement Administration's Special Testing and Research Laboratory.

One run buffer consisted of a 0.01 *M* phosphate–borate buffer (pH 9.0) containing 0.015 *M* heptakis (di-O-methyl)-β-cyclodextrin and 100 m*M* SDS. Other run buffers consisted of a 0.01 *M* phosphate–borate buffer (pH 9.0) containing 0.05 *M* sodium taurocholate and this same solution adjusted to pH 11.7 with 1 *M* sodium hydroxide. For MECC analysis using GITC derivatives, a stock solution containing 10 m*M* borate and 10 m*M* phosphate (pH 9.0) was used for the preparation of all run buffers.

GITC derivatization procedure

A standard solution containing all six racemic phenethylamines was prepared by dissolving 4 mg of each substance in 1.0 ml of 50% (v/v) aqueous acetonitrile containing 0.2% triethylamine; complete solution was achieved by vortexing for 30 s. A 100-μl volume of the resulting solution was then reacted with 100 μl of (1.28%, w/v). GITC–acetonitrile solution; complete solution was achieved by vortexing for 60 s. After standing for 15 min (to complete the reaction), the solution was diluted to 1.0 ml with 0.01 *M* phosphate–borate buffer (pH 9.0) containing 100 m*M* SDS. After final vortexing for 20 s, the solution was filtered through a UniPrep filter (Whatman, Clifton, NJ, USA) and finally injected onto the capillary electrophoresis instrument using a vacuum-assisted injection of 0.5 s. This procedure is a modification of a previously described derivatization protocol [15]. The structure of GITC-derivatized amphetamine is shown in Fig. 2.

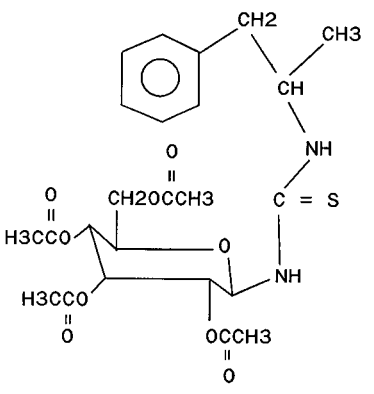

Fig. 2. Structure of GITC derivative of amphetamine.

RESULTS AND DISCUSSION

Use of chiral additives

The first approach investigated for the CE separation of the enantiomers of phenethylamines involved the use of a chiral cyclodextrin derivative as a additive. Using similar conditions as Swartz [7], attempts to separate the enantiomers of amphetamine and methamphetamine using cyclodextrins proved unsuccessful. It has been reported for HPLC that three points of interaction are required between the enantiomer and the β-cyclodextrin derivative for a separation to occur [19]. It appears that a benzylic hydroxyl can provide one of these points, since the enantiomers of ephedrine, pseudoephedrine, norephedrine and norpseudoephedrine all resolve using the above mobile phase conditions. In addition, use of the chiral surfactant taurocholate in buffers of pH values 9.0 and 11.7 failed to resolve the enantiomers of ephedrine or methamphetamine (separation of other phenethylamines were not attempted). At pH 9.0 the predominantly positively charged ephedrine and methamphetamine had little affinity for the micelle and eluted before t_0 (neutral marker; methanol peak), while at pH 11.7 these compounds existed predominantly as the free base and had affinity for the micelle and therefore eluted after t_0. Finally, the use of the non-chiral micelle dodecyl sulfate with cyclodextrin at pH 9.0 failed to resolve the enantiomers of ephedrine or methamphetamine.

MECC analysis of GITC derivatives

Effect of organic modifiers. Pre-column derivatization with optically pure GITC was investigated. As shown in Fig. 3, extensive overlap existed between the compounds of interest when MECC was employed with a run buffer containing SDS and no organic modifier. The addition of an organic modifier to the buffer (Fig. 4) greatly improved the separation by increasing the peak capacity and by decreasing the micelle–water partition coefficient. Organic modifiers have been previously shown to reduce electroosmotic flow in MECC systems, thus extending elution range, and also to reduce solute capacity factors [20]. Using the MECC conditions shown in Fig. 4 methanol appears to be the modifier of choice. Using 20% methanol in the run buffer results in at least partial resolution of all

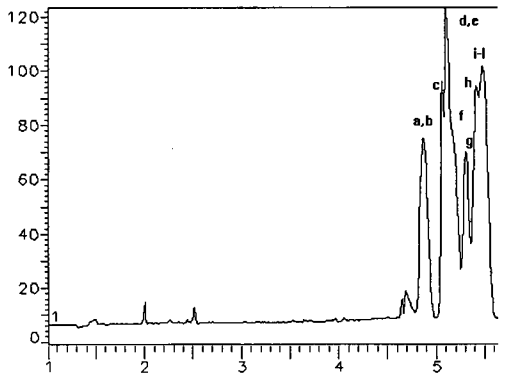

Fig. 3. MECC separation at 210 nm of phenethylamine-GITC derivatives with 100 m*M* SDS in 10 m*M* phosphate–10 m*M* borate buffer (pH 9.0) in a 48 cm (26 cm length to detector) × 50 μm capillary at 40°C with a voltage of 20 kV; current 86 μA. Peaks: a = 1*S*,2*S*-(+)-norpseudoephedrine; b = 1*R*,2*S*-(−)-ephedrine; c = 1*R*,2*S*-(−)-norephedrine; d = 1*R*,2*R*-(−)-norpseudoephedrine; e = 1*R*,2*R*-(+)-ephedrine; f = 1*S*,2*S*-(+)-pseudoephedrine; g = 1*S*,2*R*-(+)-norephedrine; h = 1*R*,2*R*-(−)-pseudoephedrine; i = 2R-(−)-methamphetamine; j = 2R-(−)-amphetamine; k = 2*S*-(+)-methamphetamine; l = 2*S*-(+)-amphetamine. Abscissa: time in min; ordinate: mAU.

enantiomers. In addition, for reasons that are presently unclear, amphetamine and methamphetamine exhibit reduced response in the presence of acetonitrile.

Since MECC is partially based on a liquid–liquid partition mechanism, it exhibits some similarity to reversed-phase HPLC. Therefore the percent organic modifier present for methanol, acetonitrile and tetrahydrofuran in the MECC separation were based on the relative percentages which gave equal solvent strength in a previously reported reversed-phase HPLC separation [21]. As shown in Fig. 4, this was a reasonable assumption for acetonitrile and tetrahydrofuran.

Effect of percent methanol

A study of the effect of % methanol indicates that when the run buffer contains 20% methanol, as shown in Fig. 5, all enantiomers are at least partially resolved. Amphetamine and methamphetamine again exhibit reduced response when 25% methanol is used. Changing the organic modifier concentration alters the partition coefficient as well as possibly changing the micellar size [22]. It is apparent from Figs. 4 and 5, and as was also observed by Gorse *et al.* [23], that both the type and amount of organic modifier used can alter selectivity. Interestingly, the elution order changes with different organic modifier types because partition coefficients are altered [20].

Effect of temperature

The effect of temperature on the separation is shown in Fig. 6. For these MECC conditions the best separation is obtained at 30°C where, except for 1*R*,2*S*-(−)-norephedrine and 1S,2*S*-(+)-pseudoephedrine, all compounds are well resolved. For reasons that are unclear it is apparent that lower

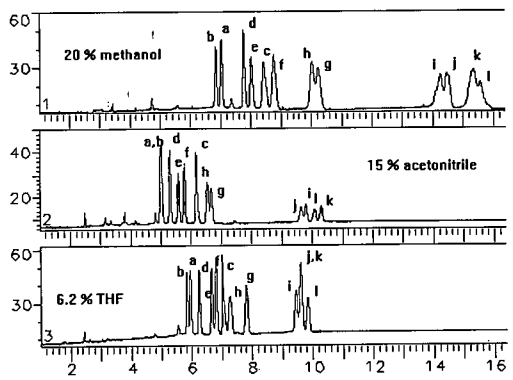

Fig. 4. Effect of organic modifier on MECC separation of phenethylamine-GITC derivatives. Conditions as in Fig. 3 except for organic modifier; methanol, current 54 μA; acetonitrile, current 88 μA; and tetrahydrofuran (THF), current 93 μA. Peaks and axes as in Fig. 3.

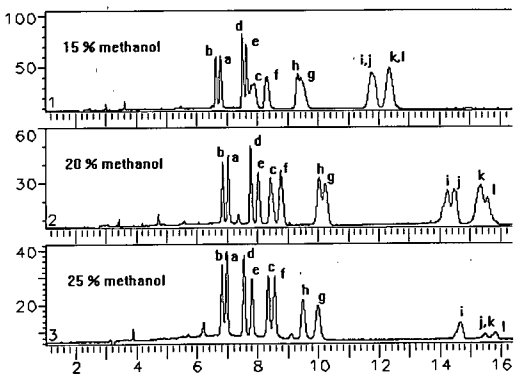

Fig. 5. Effect of methanol concentration on MECC separation of phenethylamine-GITC derivatives. Conditions as in Fig. 3 except for methanol concentration; 15% methanol, current 58 μA; 20% methanol, current 54 μA; and 25% methanol, current 45 μA. Peaks and axes as in Fig. 3.

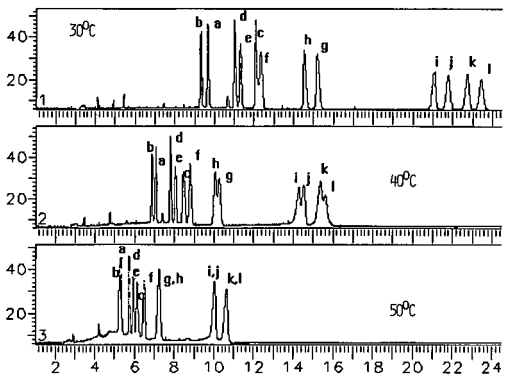

Fig. 6. Effect of temperature on MECC separation of phenethylamine-GITC derivatives. Conditions as in Fig. 3 except for temperature and the presence of 20% methanol in run buffer; 30°C, current 48 μA; 40°C, current 54 μA; and 50°C current 58 μA. Peaks and axes as in Fig. 3.

temperatures result in higher efficiencies. In fact, the efficiency (number of plates, N) for 2*R*-(−)-methamphetamine is 44 000, 27 000 and 22 000 at temperatures of 30, 40 and 50°C, respectively. In addition to its effect on column efficiency, temperature can also change selectivity in MECC by its effect on micelle partitioning [24]. A combination of these two factors could contribute to the overall increase in resolution at lower temperatures.

Effect of voltage

As shown in Fig. 7, lowering the voltage from 20 to 15 kV increases the overall resolution. Although the efficiency for 2*R*-(−)-methamphetamine decreases from 27 000 to 20 000, resolution increases for several pairs of compounds (including the late eluters) due to an apparent increase in selectivity. In describing column efficiency in MECC as related to voltage, Sepaniak and Cole [25] showed at low to moderate voltages the major contribution to plate height to be axial diffusion (which decreases with increasing voltage). The change in selectivity with voltage can be described in terms of joule heating effects inside the capillary which effect the solute distribution coefficient K [24]. At 25 kV, which represents a relatively high field strength of 521 V/cm, no peaks were detected presumably due to a degradation of separation due to joule heating effects.

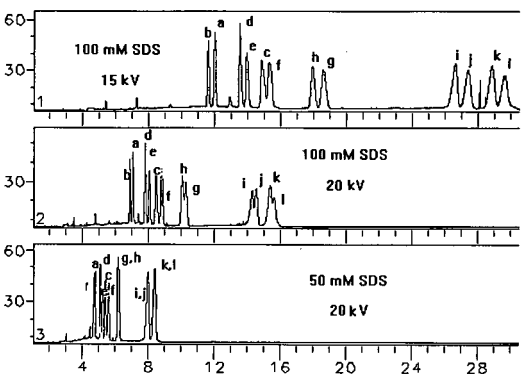

Fig. 7. Effect of voltage and SDS concentration on MECC separation of phenethylamine-GITC derivatives. Conditions as in Fig. 3 except for voltage, SDS concentration and the presence of 20% methanol in run buffer; 15 kV, 100 m*M* SDS, current 34 μA; 20 kV, 100 m*M* SDS, current 54 μA; and 20 kV, 50 m*M* SDS, current 34 μA. Peaks and axes as in Fig. 3.

Effect of SDS concentration

In addition, as shown in Fig. 7, lowering the SDS concentration results in decreased resolution. A similar result was obtained for diastereomers of GITC-derivatized amino acids due to changes in selectivity and migration times [15]. The efficiency (N) of 2R-(−)-methamphetamine decreased from 27 000 to 19 600 when the SDS concentration was lowered from 100 m*M* to 50 m*M*. Since resolution depends on the square root of N, it is apparent from Fig. 7 that a decrease in selectivity as well as migration times is playing a major role. The change in selectivity is due to differences in interactions of solutes with micelles, as detailed by Armstrong and Stine [26] in describing micellar pseudophase in HPLC. When an SDS concentration of 200 m*M* was used, no peaks were detected. This was presumably due to a degradation of separation as a result of joule heating effects caused by the increased current.

Resolution of twelve phenethylamine isomers

Using an organic modifier concentration of 20% methanol, a temperature of 30°C, a voltage of 20 kV and a 100 m*M* SDS concentration, all compounds are baseline resolved except for 1*R*,2*S*-(−)-norephedrine and 1*S*,2*S*-(+)-pseudoephedrine, which have a resolution of approximately 1 (see Fig. 6). This may not represent the best possible separation; however such determination is beyond the scope of this manuscript.

The use of a relatively short 48 cm capillary (26

cm length to detector) resulted in faster separations at the expense of plate number. A plate count of 44 000 for 2*R*-(−)-methamphetamine is significantly below what was reported for GITC derivatives of amino acids analyzed via MECC [15]. For these compounds, Nishi *et al.* [15] reported plate numbers in excess of 100 000 using capillary lengths of 65 cm (50 cm length to detector). Use of shorter columns resulted in a higher field strength where joule heating effects, *i.e.* temperature gradients within the column, might be expected to be responsible for the decreased plate count. However, several authors have shown the temperature gradient in the capillary to have a neglible effect on plate height [27–29].

MECC versus HPLC

In spite of the relatively low plate numbers obtained using the shorter capillaries, the MECC separations are still far superior to what is obtained via HPLC [4]. As shown in Fig. 8, the separation of GITC-derivatized amines via HPLC results in far less resolution and longer analysis time than obtained via MECC. For this same HPLC system, amphetamine–GITC derivatives failed to resolve in spite of a 60-min elution time. It is also of interest to compare the elution order of the individual optical isomers using HPLC *versus* MECC. For the optical isomers separated in Fig. 8, only ephedrine–GITC derivatives have the same elution order using both techniques. Since both separation techniques depend to a large extent on the hydrophobicity of the solutes, identical elution orders would not have been unexpected. Nishi *et al.* [15] reported identical elution orders via HPLC and MECC for the GITC derivatives of the optical isomers of five out of the six compounds. It would appear that mobile phase interactions such as hydrogen bonding and dipole interactions play a major role in both separation techniques. For the HPLC separation of GITC-derivatized phenethylamines, the mobile phase contains tetrahydrofuran for MECC, methanol is used as the organic modifier.

Application to forensic exhibit

The applicability of the MECC technique to a forensic sample is shown in Fig. 9. By comparison with the standard run shown in Fig. 6, the sample was found to contain 1*R*,2*S*-(−)-ephedrine and 2*S*-(+)-methamphetamine. This result was consistent

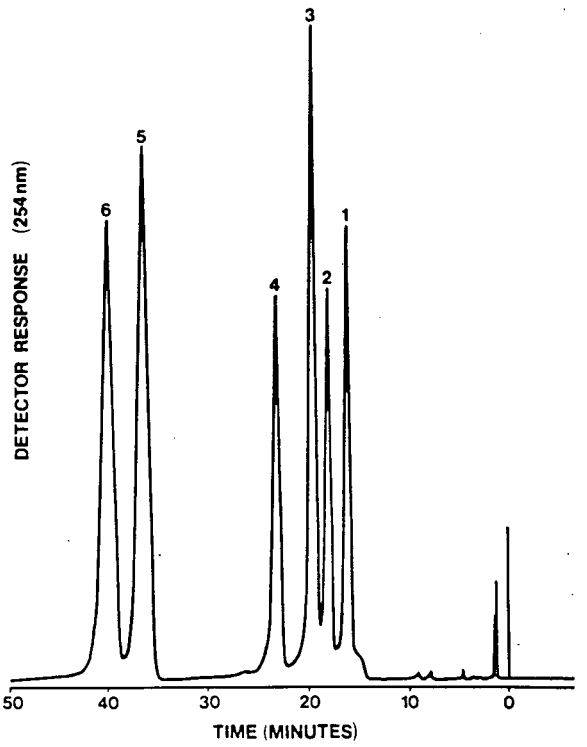

Fig. 8. HPLC separation of phenethylamine-GITC derivatized amines using tetrahydrofuran–water (3:7) mobile phase at a flow-rate of 1.5 ml/min. Peaks: 1 = 1*R*,2*R*-(−)-pseudoephedrine; 2 = 1*S*,2*S*-(+)-pseudoephedrine; 3 = 1*R*,2*S*-(−)-ephedrine; 4 = 1*S*,2*R*-(+)-ephedrine; 5 = 2*S*-(+)-methamphetamine; 6 = 2*R*-(−)-methamphetamine. From ref. 4.

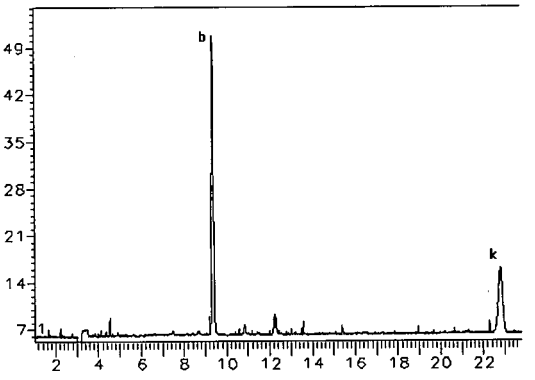

Fig. 9. MECC separation of GITC-derivatized exhibit. Conditions as in Fig. 3 except for a temperature of 30°C and the presence of 20% methanol in run buffer. Peaks and axes as in Fig. 3.

with what had been reported for this exhibit using a combination of GC-mass spectrometry and microscopic techniques.

Flow injection analysis using a diode array detector reveals that the extinction coefficient at 210 nm for the GITC derivative of methamphetamine is approximately twice that of both underivatized methamphetamine and that obtained at the UV maximum wavelength (254 nm) of the GITC derivative. For more selective detection the higher wavelength of 254 nm would be recommended since the extinction coefficient of GITC derivatized methamphetamine is approximately fifty times that of the underivatized methamphetamine. It has been previously shown that at 250 nm the molar extinction coefficient of GITC is 1000 whereas those of GITC-amino acids are approximately 12 000 [30]. Apparently the N,N′-disubstituted thiourea linkage where lone pair electrons on two amide groups can contribute to UV conjugation (see Fig. 2) is reponsible for the higher extinction coefficients of the GITC derivatives.

ACKNOWLEDGEMENTS

The author thanks Dr. Robert Weinberger (CE Technologies, Chappaqua, NY, USA) and Dr. Michael Albin (Applied Biosystems, Foster City, CA, USA) for helpful discussions. The author would also like to thank Charles Harper for the preparation of those figures containing chemical structures.

REFERENCES

1 H. F. Skinner, *Forensic Sci. Int.*, 48 (1990) 123.
2 A. H. Beckett and B. Testa, *J. Chromatogr.*, 69 (1972) 285.
3 H. Frank, G. J. Nicholson and E. Bayer, *J. Chromatogr.*, 146 (1978) 197.
4 F. T. Noggle and C. R. Clark, *J. Forensic Sci.*, 31 (1986) 732.
5 T. D. Doyle, W. M. Adams, F. S. Fry and I. W. Wainer, *J. Liq. Chromatogr.*, 9 (1986) 455.
6 S. Fanali, *J. Chromatogr.*, 474 (1989) 441.
7 M. E. Swartz, *J. Liq. Chromatogr.*, 14 (1991) 923.
8 J. Snopek, H. Soini, M. Novotny, E. Smolkova-Keulemansova and I. Jelinek, *J. Chromatogr.*, 559 (1991) 215.
9 S. Terabe, M. Shibata and Y. Miyashita, *J. Chromatogr.*, 480 (1989) 403.
10 K. Otsuka and S. Terabe, *J. Chromatogr.*, 515 (1990) 221.
11 H. Nishi, T. Fukuyama, M. Matsuo and S. Terabe, *J. Microcol. Sep.*, 1 (1989) 234.
12 K. Otsuka, J. Kawahara, K. Tatekawa and S. Terabe, *J. Chromatogr.*, 559 (1991) 209.
13 H. Nishi, T. Fukuyama and S. Terabe, *J. Chromatogr.*, 553 (1991) 503.
14 A. D. Tran, T. Blanc and E. J. Leopold. *J. Chromatogr.*, 516 (1990) 241.
15 H. Nishi, T. Fukuyama and M. Matsuo, *J. Microcol. Sep.*, 2 (1990) 234.
16 S. Terabe, K. Otsuka, K. Ichikawa, A. Tsuchiya and T. Ando, *Anal. Chem.*, 56 (1984) 113.
17 H. Nishi, N. Tsumagari, T. Kakimoto and S. Terabe, *J. Chromatogr.*, 465 (1989) 331.
18 R. Weinberger and I. S. Lurie, *Anal. Chem.*, 63 (1991) 63.
19 W. L. Hinze, T. E. Riehl, D. W. Armstrong, W. DeMond, A. Alak and T. Ward, *Anal. Chem.*, 57 (1985) 237.
20 A. T. Balchunas and M. J. Sepaniak, *Anal. Chem.*, 60 (1988) 617.
21 I. S. Lurie, A. C. Allen and H. J. Issaq, *J. Liq. Chromatogr.*, 7 (1984) 463.
22 A. Dobashi, T. Ono, S. Hara and J. Yamaguchi, *Anal. Chem.*, 61 (1989) 1986.
23 J. Gorse, A. T. Balchunas, D. F. Swaile and M. J. Sepaniak, *J. High Resolut. Chromatogr. Chromatogr. Commun.*, 11 (1988) 554.
24 A. S. Cohen, S. Terabe, J. A. Smith and B. L. Karger, *Anal. Chem.*, 59 (1987) 1021.
25 M. J. Sepaniak and R. O. Cole, *Anal. Chem.*, 59 (1987) 472.
26 D. W. Armstrong and G. Y. Stine, *Anal. Chem.*, 55 (1983) 2317.
27 J. H. Knox, *Chromatographia*, 26 (1988) 329.
28 E. Grushka, R. M. McCormick and J. J. Kirkland, *Anal. Chem.*, 61 (1989) 241.
29 S. Terabe, K. Otsuka and T. Ando, *Anal. Chem.*, 61 (1989) 251.
30 N. Nimura, H. Ogura and T. Kinoshita, *J. Chromatogr.*, 202 (1980) 375.

Journal of Chromatography, 605 (1992) 276–280
Elsevier Science Publishers B.V., Amsterdam

CHROM. 24 265

Short Communication

Assessment of the polarity of three liquid crystals used as gas chromatographic stationary phases

T. J. Betts

School of Pharmacy, Curtin University of Technology, GPO Box U1987, Perth, W. Australia (Australia)

(First received September 24th, 1991; revised manuscript received January 24th, 1992)

ABSTRACT

Attempts to evaluate the polarity of three liquid crystals used in packed gas chromatographic columns suggest that more than one method is required at different temperatures. At 120°C a triangular proportional plot of retention indices using three McReynolds' solute probes indicate azoxydiphenetole (ADP) and bis(methoxy-benzylidineanilchloroaniline) [$(MBCA)_2$] are reasonably strong in polarity. Bis(methoxybenzylidineanilbitoluidine) [$(MBT)_2$] is moderately polar, compared to normal-phase columns. At 160°C, however, using the sum of retention indices of three C_{10} volatile oil constituents, ADP and $(MBCA)_2$ rate as only moderately polar, with $(MBT)_2$ now exhibiting low polarity. The polarity sequence of the three liquid crystals (unmelted, melted and supercooled) is confirmed by the second method. Their polarity rating is method-sensitive, although they change in polarity more than normal chromatographic phases with temperature alterations. The selection of a liquid crystal for particular separations is discussed.

INTRODUCTION

This author has previously studied three liquid crystals as gas chromatographic stationary phases in packed columns [1,2] for volatile oil constituents. Following this work, the question of the polarity of these phases arose. Isenberg *et al.* [3] found that some diester aromatic liquid crystals "correspond to silicone phases of low polarity" using Rohrschneider solute probes at 100°C, and our observations on bis(methoxybenzylidineanilbitoluidine) [$(MBT)_2$] agreed with this [4] using a comparative retention index (I_R) method we devised in 1981 [5] with linalol, estragole and carvone as "LEC" solute probes at 160°C. Betts has also used three of McReynolds' [6] probes, *n*-butanol, pyridine and 2-octyne in connection with a triangular proportional I_R plot method of characterization [7] of a range of stationary phases. Butanol always eluted ahead of pyridine, but octyne appeared first for the group of "highly polar" phases, last from the "non-polar" phases, and between butanol and pyridine with the "intermediate polarity" phases at 120°C. This lower temperature, below all the liquid crystal melting points, allows them to be studied in the unmelted and the melted, supercooled condition. Having found that gas chromatography was readily possible with some of these supercooled liquid crystals, and having obtained interesting results with one of them at 120°C [2], it seemed appropriate to use the octyne procedure at this temperature to evaluate their polarity; supported by the higher temperature method [5] involving C_{10} volatile oil constituents of relevance to our studies rather than the smaller mol-

Correspondence to: Dr. T. J. Betts, Curtin University of Technology, GPO Box U1987, Perth, W. Australia, Australia.

0021-9673/92/$05.00

ecules (C_4–C_8) used at the lower temperature. However, only one of the liquid crystals can be evaluated at 160°C in the unmelted condition. Differing results prompted the selection of a modified set of three solute probes to allow evaluation of the polarity of these liquid crystal packed columns over a range of temperatures, with cineole instead of carvone in the LEC set.

EXPERIMENTAL

Instrumentation

A Pye-Unicam GCD gas chromatograph was used, fitted with a flame ionisation detector. This heated the columns rapidly, but on lowering the temperature setting, leaving the door closed, the oven cooled at about 4°C min^{-1} measured with a Technoterm probe. This allowed for slow supercooling of the melted column phases. Hewlett-Packard 3380A and 3390A recorder/integrators were used.

Columns

These were detailed in ref. 1 and contained about 3% (w/w) liquid crystal stationary phase. They were azoxy-phenetole (ADP), bis(methoxybenzylidineanilchloroaniline) [$(MBCA)_2$] and $(MBT)_2$. Normal-phase columns used are detailed in refs. 5 and 7.

Solutes

2-Octyne was obtained from T.C.I. (Tokyo). Some *n*-alkanes came from Sigma. (−)-Carvone was from Koch-Light, and sources of other solutes are as given previously [1,4] other than standard laboratory reagents.

Method

Injections were made from a microsyringe which

TABLE I

I_R, x AND McREYNOLDS VALUES FOR PACKED COLUMNS OF LIQUID CRYSTAL AND SOME CONVENTIONAL STATIONARY PHASES AT 120°C

x = (I_R of solute)/$\sum$(I_R three solutes). McR = I_R of solute on phase minus its I_R on squalane. Data in italics from ref. 7. Phases below the break show solute sequence of butanol–octyne–pyridine (last).

Stationary phase	Solute									$\sum(I_R)_3$	$\sum(McR)_3$
	2-Octyne			*n*-Butanol			Pyridine				
	I_R	*McR*	*x*	I_R	*McR*	*x*	I_R	*McR*	*x*		
PEG 20M polyglycol	*1041*	*200*		*1104*	*514*		*1180*	*481*		*3325*	*1195*
ADP UNmelted	854	13	0.281[a]	1090	500	0.358[b]	1098	399	0.361	3042	912
$(MBCA)_2$ new UNmelted	873	32	0.291	1010	420	0.337	1117	418	0.372	3000	870
SP-2330 PSX[c] CN-propyl			*0.292[d]*			*0.336*			*0.372[e]*		
ADP melted[f]	917	76	0.307	1009	419	0.338	1059	360	0.355	2985	855
PEG 1000 polyglycol			*0.306*			*0.337[e]*			*0.357*		
$(MBCA)_2$ old UN- or melt	909	68	0.309	922	332	0.314	1109	410	0.377[b]	2940	810
OV-225 PSX[c] CN-pr,Ph,Me	*980*	*139*	*0.330*	*939*	*349*	*0.317*	*1046*	*347*	*0.353*	*2965*	*835*
$(MBT)_2$ melted[f]	890	49	0.331	858	268	0.319	940	241	0.350	2688	558
OV-210 PSX[c] F_3-pr, Me	*891*	*50*	*0.332*	*815*	*225*	*0.304*	*977*	*278*	*0.364*	*2683*	*553*
$(MBT)_2$ UNmelted	892	51	0.340	813	223	0.309	922	223	0.351	2627	497

[a] Lower x value than observed previously [7]. See [d].
[b] Higher x value than observed previously. See [e].
[c] Polysiloxane (PSX). Side chains *Me*thyl, *Ph*enyl, F_3-*pr* = trifluoropropyl.
[d] Lowest x value observed previously.
[e] Highest x value observed previously.
[f] Slowly cooled from above liquid crystal melting point at about 4°C min^{-1}. [Above 138°C for ADP, above 154°C for $(MBCA)_2$, above 181°C for $(MBT)_2$].

TABLE II

I_R VALUES FOR PACKED COLUMNS OF LIQUID CRYSTAL AND SOME CONVENTIONAL STATIONARY PHASES

P rating = $\sum(I_R)_3$ for phase minus $\sum(I_R)_3$ for "base" SP-2250, all divided by three [5]. Data in italics from conventional phases.

160°C					Stationary phase			120°C			
Cineole	Linalol	Estragole	$\sum(I_R)_3$	*P* rating				Cineole	Linalol	Estragole	$\sum(I_R)_3$
1216	*1363*	*1531*	*4110*	*+137*	*OV-225 PSX CN-pr, Ph, Me*						
1125	1284	1453	3862	+ 55	← melted	ADP	melted[a] →	1082	1307	1407	3796
						ADP	UNmelted →	1076	1363	1243[b]	3682
1125	1321	1391	3837	+ 46	← melted	$(MBCA)_2$	melted[a] or UNmelted →	1106	1309	1326	3741
1139	*1198*[c]	*1361*[c]	*3698*	*0*	*SP-2250 PSX*[d] *Ph, Me (BASE)*						
[1054	1230	1423	3707		← melted	$(MBT)_2$	at 190°C]				
960	1183	1352	3495	− 68	← melted[a]	$(MBT)_2$	melted[a] →	1016	1208	1330	3554
1010	1177	1246	3433	− 88	← UNmelted	$(MBT)_2$	UNmelted →	1004	1191	1212	3407
1048	*1100*[c]	*1197*[c]	*3345*	*−118*	*SP-2100 PSX Me*						

[a] Slowly cooled from above liquid crystal melting point at about 4°C min^{-1}.

[b] Estragole precedes linalol (only case observed).

[c] Values a little different to those recorded over ten years ago [5] reflecting use of columns.

[d] PSX see Table I footnote *c*.

had been filled, then "emptied", apart from larger alkanes which required about 0.1 μl. Retention indices were obtained by a graphic method, plotting retention times of *n*-alkanes on a logarithmic scale against their carbon numbers, and then entering retention times of the probe solutes.

RESULTS AND DISCUSSION

Average results at 120°C for the octyne method are presented in Table I in sequence of decreasing sum of their I_R for the three solute probes. This indicates decreasing polarity, as it corresponds to increasing x values (proportion of I_R sum) for the lowest polarity probe octyne. $(MBCA)_2$ and ADP exhibit high polarity, shown by their elution sequence of solutes: octyne–butanol–pyridine (last). Their I_R sums are below that of polyethylene glycol 20M, however.

A new, never-melted column of $(MBCA)_2$ shows x values (not the actual I_R) very close to those of the highly polar cyanopropyl polysiloxane SP-2330 (see Table I and Fig. 1). After melting, a well-used mature column of $(MBCA)_2$ gives no change between melted and unmelted states (unlike the other two liquid crystals here) and has lower polarity than initially, particularly due to lower retention of butanol and stronger affinity for octyne. But it retains the same probe sequence indicating it is in the "highly polar" group of phases. It now exhibits a higher x value for pyridine than any seen previously [7], although this has increased only slightly (Table I, Fig. 1).

The other two mature liquid crystal columns always show different behaviour on changing from unmelted to melted (supercooled) condition. Previous study of volatile oil constituents with short retention times [2] also revealed this changing behaviour, again differing from $(MBCA)_2$. ADP decreases in polarity on melting, from having considerably the highest x value ever observed by this author for butanol (and the lowest for octyne) on any phase, to a set of x values very close to those of polyethylene glycol 1000. It retains the "highly polar" probe sequence.

$(MBT)_2$ in contrast increases in polarity on melting and exhibits the different probe sequence of butanol–octyne–pyridine, indicating only moderate polarity. Unmelted, it has I_R for octyne and butanol

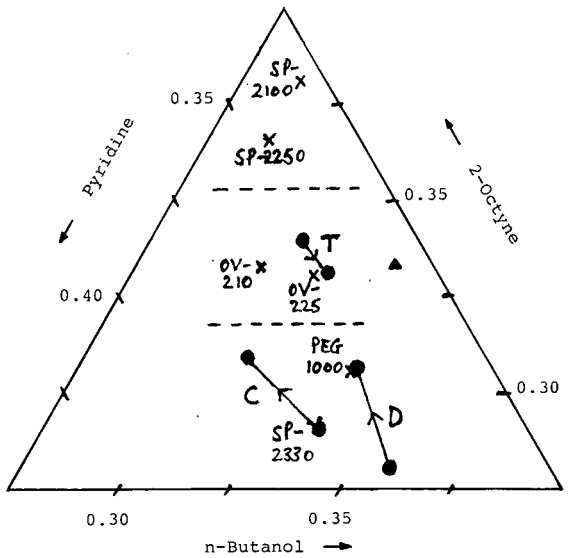

Fig. 1. Plot of relative I_R values of gas chromatographic stationary phases using solute probes of 2-octyne (right), pyridine (left) and *n*-butanol (base). ▲ = Centre of full triangular plot; ● = experimental values for liquid crystals $(MBCA)_2$ (C), ADP (D), and $(MBT)_2$ (T); × = values from ref. 7 for conventional phases explained in Tables I and II. Arrowed lines show changes from unmelted to melted liquid crystal condition. Dashed lines separate the strongly polar phases at the base of the triangle from the moderately polar phases across the middle and the low polarity phases at the top.

similar to the trifluoropropyl methyl polysiloxane OV-210 (see Table I). After melting, $(MBT)_2$ shows x values very close to the quarter-cyanopropyl polysiloxane OV-225 (Fig. 1), and slightly increased polarity, although x values for pyridine hardly alter. McReynolds' values are all low for octyne, but otherwise confirm the reasonably high polarities of the three liquid crystals (Table I).

As the study at 120°C indicated surprisingly high polarity, there was a need to assess this at another temperature. Davies [8] remarks that "temperature has ... quite marked effects on the (retention) indices on (polyethylene glycol) 20M" and records an increase of about 20 units over 20°C rise for caryophyllene on a methyl silicone. The probe solute carvone, previously used at 160°C [5] gave unsatisfactory broad peaks on two of these liquid crystal phases, as did some of the *n*-alcohols originally used as the basis for one set of I_R. Cineole, a low polarity terpenoid ether, replaced carvone and the three I_R were only determined against the traditional *n*-alkanes.

Table II gives the results for these revised LEC solute probes at 160°C in decreasing polarity, as indicated by their I_R sum; and at 120°C for comparison. They emerge in the sequence cineole-linalol-estragole apart from unmelted ADP, where linalol is last. From the sum of their three solute I_R $(MBCA)_2$ and ADP are distinctly more polar than $(MBT)_2$, confirming the sequence in Table I. They indicate an overall lower polarity than before, however, as the pair are only a little more polar than a low-polarity phenyl, methyl polysiloxane SP-2250 at 160°C, and $(MBT)_2$ a little more than a non-polar fully methyl polysiloxane SP-2100, which agrees with our earlier report [4]. At 160°C, melted ADP shows higher I_R for cineole and estragole than at 120°C in either its supercooled, or its unmelted condition: the latter is distinctively lower for estragole. Melted $(MBCA)_2$ at 160°C also shows the higher I_R compared to lower temperature values. There is thus no evidence that the polarity of these two phases is lower at 160°C than at 120°C. However, the LEC values at 160°C, and the derived P values in Table II, indicate considerably lower polarity than by the octyne method.

At 160°C, melted, supercooled $(MBT)_2$ has I_R lower than at 120°C for cineole and linalol and overall is slightly less polar. At both these temperatures, $(MBT)_2$ can be studied in the unmelted condition. It then has the lowest polarity observed here, especially at 120°C. Properly melted, at 190°C, it shows considerably higher polarity like the other two liquid crystals, with I_R close to a phenyl, methyl polysiloxane. Whilst there are some changes in I_R for LEC between 120° and 160°C for all three liquid crystals they do not account for the octyne procedure giving high polarity ratings at 120°C. Yet the results here are compared in each procedure with those of authentic normal phases of various polarities. The discrepancy can be illustrated in relation to the moderately polar cyanopropyl(25), phenyl (25), methyl(50)-polysiloxane OV-225. The octyne procedure sums (of I_R or McReynolds values) in Table I indicate the overall similar polarity of ADP and $(MBCA)_2$ to OV-225. With the LEC method at 160°C, the sums indicate these two liquid crystals to be considerably less polar than OV-225 (Table II). This is despite the three solute probes being, in both cases, an aromatic substance, an aliphatic alcohol, and a low polarity material. One method of polarity rating alone is apparently insufficient for liquid crystal phase assessment, probably because they change with alteration of temperature more than normal phases.

As it is the least polar liquid crystal here, $(MBT)_2$ should be the choice for studies of hydrocarbons, and it was previously found by Betts [2] to provide on melting a distinctive relative retention change for identifying terpinolene from other cyclic monoterpenes. However, it gave less resolution of a group of five such compounds when unmelted than the other two liquid crystals. None of these three liquid crystals gave the "non-polar" solute sequence butanol–pyridine–octyne, which would be optimum for such hydrocarbon studies.

From its results with estragole melted ADP should be the choice for studies of aromatics. However, previous studies made [1] show that relative to estragole the similarly linear aromatic safrole has a nearly constant retention time of about 1.6 on all three liquid crystals at various temperatures, with ADP showing the slightly highest value. $(MBCA)_2$ retains pyridine most strongly in the proportional plot (Fig. 1) and gives the best resolution of the "terpene-shaped" aromatic cuminal from safrole, but the worst separation of cuminal from the linear aromatic anethole. The "terpene-shaped" phenol thymol cannot be handled on ADP and is best resolved by $(MBT)_2$. Thus predictions of the appropriate phase for an analysis are not successful from I_R considerations.

ACKNOWLEDGEMENT

Thanks to Mr. B. MacKinnon for preparing the chromatographic columns and maintaining the rather old apparatus.

REFERENCES

1 T. J. Betts, *J. Chromatogr.*, 588 (1991) 231.
2 T. J. Betts, *J. Chromatogr.*, 587 (1991) 343.
3 A. Isenberg, G. Kraus and H. Zaschke, *J. Chromatogr.*, 292 (1984) 67.
4 T. J. Betts, C. M. Moir and A. I. Tassone, *J. Chromatogr.*, 547 (1991) 335.
5 T. J. Betts, G. J. Finucane and H. A. Tweedie, *J. Chromatogr.*, 213 (1981) 317.
6 W. O. McReynolds, *J. Chromatogr. Sci.*, 8 (1970) 685.
7 T. J. Betts, *J. Chromatogr.*, 354 (1986) 1.
8 N. W. Davies, *J. Chromatogr.*, 503 (1990) 1.

Journal of Chromatography, 605 (1992) 281–286
Elsevier Science Publishers B.V., Amsterdam

CHROM. 24 346

Short Communication

Simplified derivatization for determining sphingolipid fatty acyl composition by gas chromatography–mass spectrometry

Susan B. Johnson* and Rhoderick E. Brown

The Hormel Institute, University of Minnesota, 801 16th Avenue NE, Austin, MN 55912 (USA)

(First received February 3rd, 1992; revised manuscript received May 6th, 1992)

ABSTRACT

A simple procedure for simultaneously derivatizing non-hydroxy and hydroxy fatty acids prior to GC analysis [I. Ciucanu and F. Kerek, *J. Chromatogr.*, 284 (1984) 179] has been evaluated for its usefulness in determining sphingolipid acyl composition. The method uses methyl iodide in polar aprotic solvents to generate methyl esters of carboxyl groups and methyl ethers of hydroxyl groups. Methylation efficiency is examined as a function of hydroxyl group presence and location in free fatty acids as well as a function of 2-hydroxy fatty acid chain length. Conditions are also reported for efficient saponification and derivatization of sphingolipid fatty acyl chains as is illustrated using bovine brain galactosylceramide.

INTRODUCTION

Compared to glycerol-based lipids, sphingolipids require special conditions for accurate determination of their fatty acyl composition, in part because relatively large amounts of 2-hydroxy fatty acyl residues often are present [1–9]. Accordingly, derivatization prior to gas chromatographic analysis is typically accomplished by converting the carboxyl groups to methyl esters and the hydroxyl groups to trimethylsilyl (TMS) ether derivatives, which often are water-labile [10–13]. An alternative one-step procedure utilizing methyl iodide in polar aprotic organic solvents has been described by Ciucanu and Kerek [14] for simultaneously generating methyl esters of carboxyl groups and methyl ethers of hydroxyl groups in non-hydroxy and hydroxy fatty acids. Advantages of the methyl iodide method include simplicity and stability of the resulting methyl ether derivatives to water. However, the applicability to sphingolipids was not addressed in this initial report. For example, of the three hydroxy fatty acid standards studied, only one was a 2-hydroxy fatty acid and that was 2-hydroxypalmitic acid. Also, although the saponification rate of ester-linked fatty acyl chains in phosphoglycerides, glycerides, cholesteryl esters and methyl esters was reported, no information was provided for amide-linked fatty acyl chains typically found in sphingolipids. To assess the utility of the methyl iodide method for characterizing sphingolipid fatty acyl composition, we have examined methylation efficiency as a function

Correspondence to: Dr. Rhoderick E. Brown, The Hormel Institute, University of Minnesota, 801 16th Avenue NE, Austin, MN 55912, USA.

* Present address: Alfred Building, Lab 4-416, St. Mary's Hospital, Rochester, MN 55905, USA.

0021-9673/92/$05.00

of chain length in 2-hydroxy fatty acids and as a function of hydroxyl group presence and location. We have also defined conditions for application to sphingolipids as demonstrated using bovine brain galactosylceramide.

EXPERIMENTAL

Materials

Non-hydroxy fatty acid standards were obtained from NuChek Prep (Elysian, MN, USA) and 2-hydroxy fatty acid standards ($C_{18:0}$, $_{20:0}$, $_{22:0}$) were supplied by Analabs (South Norwalk, CT, USA). Bovine brain galactosylceramide (GalCer) was obtained from Avanti Polar Lipids (Birmingham, AL, USA). Bovine brain GalCer containing 99% 2-hydroxy fatty acids (Type I) or 99% non-hydroxy fatty acids (Type II) were supplied by Sigma (St. Louis, MO, USA). Dimethylacetamide and iodomethane were obtained from Sigma and Aldrich (Milwaukee, WI, USA), respectively. Other reagents were analytical grade.

Methods

Lipid purity was checked by thin-layer chromatography (TLC) using two solvent systems for GalCer [chloroform–methanol–water (85:15:1.5, v/v/v) or (50:21:3, v/v/v)] and one for free fatty acids [light petroleum (b.p. 00–00°C)–diethyl ether–acetic acid (80:20:1, v/v/v)]. Visualization of lipids was achieved by charring TLC plates after spraying with concentrated chromic–sulfuric acid (detection limit = 0.1 μg fatty acid), or by viewing under ultraviolet light after spraying with primulin (detection limit = 50 pmol diacyl lipid) or after spraying with orcinol (sugar specific; detection limit = 0.5 nmol). Scanning densitometry was performed with a Hoefer GS 300 instrument (San Francisco, CA, USA). All lipids were judged to be greater than 99% pure.

Free fatty acid derivatization. After dissolving free fatty acids in dimethylacetamide (1.0 ml), crushed NaOH (approx. 160 mg) was added and the sample was heated at 80°C for 1 h. Upon cooling, iodomethane (1.0 ml) was added and the sample was again heated for 1 hr at 80°C [14]. Fatty acid methy esters (FAMEs) were extracted using light petroleum (3 × 2 ml) after adding water (2 ml). The light petroleum phase was washed three times with water (2 ml) to remove residual NaOH. The resulting FAMEs are known to be stable for extended time periods in contrast to the limited stability of other derivatives (*e.g.*, TMS) [10–13]. As pointed out by Ciucanu and Kerek [14], the extremely low acidity of the hydroxyl group necessitates the use of a very strong base and the heating step was necessary for samples containing cholesteryl esters. While such conditions may induce isomerization of polyunsaturated fatty acyl residues, sphingolipids lack these acyl chains.

GalCer acyl chain derivatization. After drying aliquots (0.5 mg) of bovine brain GalCer in PTFE-lined screw-capped glass tubes under nitrogen, samples were hydrolyzed for 1 h at 100°C under nitrogen using 0.5 *M* HCl in acetonitrile–water [1 ml (9:1, v/v)] [15] and then were taken to dryness under nitrogen. Subsequent derivatization steps were performed as described above for free fatty acids.

Fatty acid analysis. After derivatization, FAMEs were quantitated using a Packard 427 gas chromatograph equipped with a 50 m × 0.25 mm free fatty acid phase (FFAP)–fused-silica capillary column (0.25 μm film thickness; Quadrex). The carrier gas was helium at a flow of 47.5 cm/s and the split ratio was set at 1:66. The column was programmed from 180–220°C at 2°C/min with an initial hold at 180°C for 13 min and a final hold at 220°C for 80 min. Peaks were integrated using a dedicated microprocessor.

In control experiments, the fatty acyl composition of bovine brain GalCer was determined either by simultaneously resolving non-hydroxy and 2-methoxy FAMEs by capillary gas chromatography (GC) or by separating non-hydroxy and 2-methoxy FAMEs by TLC prior to GC analysis. No significant differences were evident upon comparing results. In instances of partial peak overlap (*e.g.*, $C_{23:0(2\text{-OH})}$ and $C_{25:0}$; $C_{26:0}$ and $C_{24:0(2\text{-OH})}$; $C_{24:1(2\text{-OH})}$ and $C_{26:1}$), integration of deconvoluted peaks yielded results similar to those obtained when non-hydroxy and 2-methoxy FAMEs were separated by TLC and analyzed independently by GC. Other workers have reported complete resolution of non-hydroxy and 2-methoxy FAMEs using capillary GC [16].

A DuPont DP-102 mass spectrometer equipped with an all-glass jet separator and a SP-1000 fused capillary GC column (0.25 mm × 30 m; 0.25 μm film thickness; Supelco) was used for positive identi-

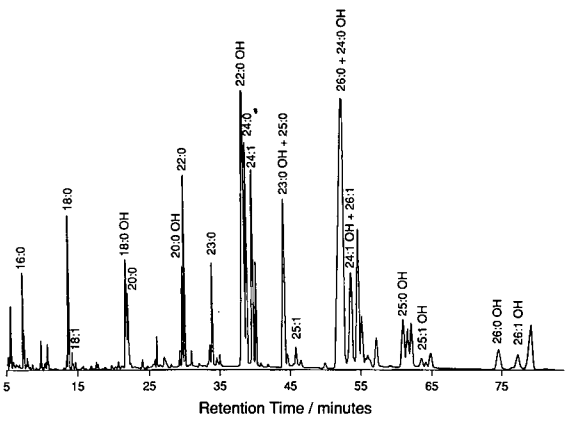

Fig. 1. Capillary GC profile of derivatized FAMEs from bovine brain GalCer. A FFAP-fused silica capillary column (Quadrex) was used as described in the *Methods* section.

fication of each FAME by electron impact mass spectrometric (MS) analysis. The column temperature was programmed from 120–220°C at 2°C/min with a final hold time of 120 min. Helium was used as the carrier gas (34 cm/s). Mass spectra were recorded at an ionization voltage of 70 eV. Ions from 43 to 500 were scanned at 300 amu/s.

Identification of derivatized fatty acids, when based solely on GC retention times, is not straightforward because certain 2-hydroxy fatty acid derivatives elute similarly to non-hydroxy fatty acid derivatives (Fig. 1). However, the electron impact mass spectral fragmentation patterns of non-hydroxy and 2-methoxy FAMEs are distinctly different (Fig. 2). The intense $m - 59$ peak and the lack of the base peak at m/z 74 are diagnostic for 2-methoxy FAMEs and clearly distinguishes them from non-hydroxy FAMEs [11]. This information, along with the mass of the molecular ion, allows definitive identification of each FAME.

RESULTS AND DISCUSSION

Free fatty acids studies

Initially, control experiments were performed to assess the feasibility of the methyl iodide method for determining sphingolipid fatty acyl composition. For example, because sphingolipids often contain long, saturated 2-hydroxyacyl chains, the effect of acyl chain length on derivatization efficiency was checked using representative 2-hydroxy fatty acids other than 2-hydroxypalmitic acid [14]. Following derivatization and TLC separation using light petroleum–diethyl ether–acetic acid (80:20:1, v/v/v), lipids were visualized by charring with concentrated chromic–sulfuric acid. Based on inspection and scanning densitometry, nearly quantitative methylation (>95%) was observed for 2-hydroxy fatty acids regardless of chain length ($C_{18:0}$, $C_{20:0}$, $C_{22:0}$).

To determine whether the presence and position of the hydroxyl group affects the extent of methylation, stearic acid, 2-hydroxybehenic acid, and 11-hydroxystearic acid derivatization (0.5 mg each) were compared by TLC analysis as described above. Both the stearic acid and 2-hydroxybehenic acids were methylated almost quantitatively (>95%), but methylation of 11-hydroxystearic acid was only about 50%. Increasing the reaction temperature to 100°C did not improve the extent of methylation.

Galactosylceramide studies

Based on the results obtained above with the free fatty acids, we anticipated that the methyl iodide method would work well if the amide-linked fatty acyl residues were released efficiently. Relatively harsh conditions are needed to release amide-linked acyl chains compared to those used with ester-linked fatty acids [1-6]. One method that reportedly releases sphingomyelin's acyl chains quantitatively involves heating in acidic aqueous acetonitrile [15]. To verify that this method is appropriate for galactosylceramides, experiments were run as described in the *Methods* section. Aliquots of the reaction mixture were analyzed by TLC using chloroform–methanol–water (85:15:1.5, v/v/v) to assess release of free fatty acid, and lipid products were visualized by charring with concentrated chromic–sulfuric acid. Based on inspection and scanning densitometry, over 90% release of fatty acids was achieved.

These findings were confirmed by including known amounts of N-palmitoyl galactosylsphingoid (GalSpd) and N-(2-hydroxy)-stearoyl GalSpd as internal standards in GalCer containing either 2-hydroxy or non-hydroxy fatty acyl chains, respectively. Following fatty acid release by heating with acidic aqueous acetonitrile and derivatization by the methyl iodide method, GC analysis revealed

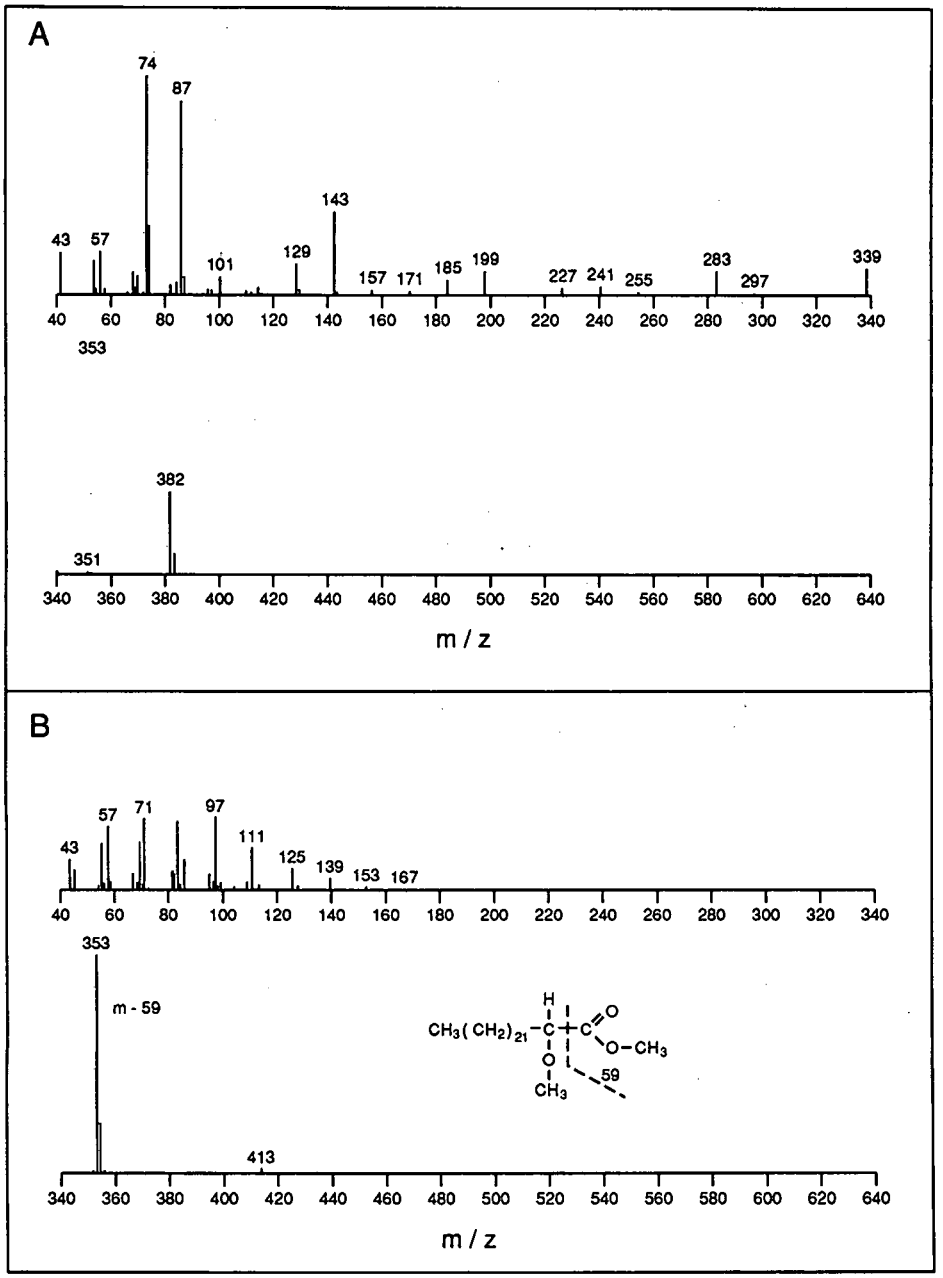

Fig. 2. Typical fragmentation patterns of non-hydroxy and 2-methoxy fatty acid methyl esters obtained by mass spectral analysis. (A) Tetracosanoic (24:0) methyl ester (mol.wt. 382); (B) 2-methoxy-tetracosanoic methyl ester (mol.wt. 412).

percentage recoveries of 96.2 ± 9.1% and 70.3 ± 6.2% for GalCer's non-hydroxy and 2-hydroxy fatty acyl residues, respectively. These recoveries appear to be adequate since the experimental conditions produce no bias amongst different 2-hydroxy fatty acids and agree well with determinations made by more complex procedures (see below).

Complete characterization of bovine brain Gal-

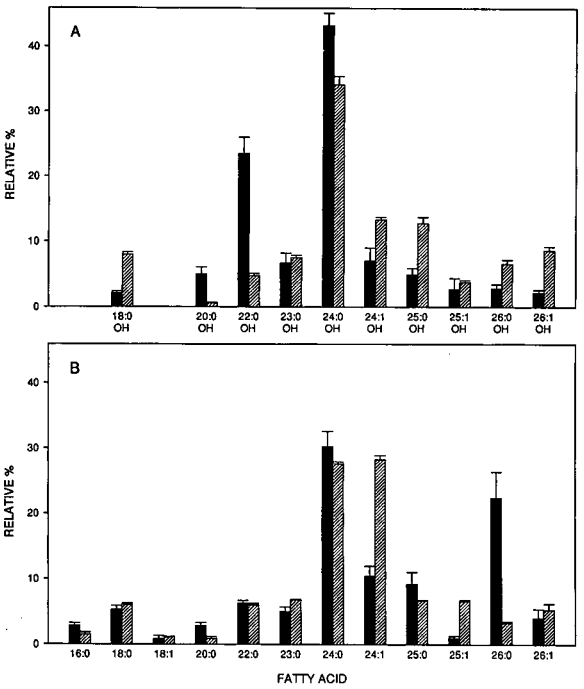

Fig. 3. Fatty acyl composition of bovine brain GalCer. Solid bars represent FAMEs derived from Avanti's bovine brain GalCer. Cross-hatched bars represent FAMEs derived from Sigma's Type I and Type II bovine brain GalCer (see *Methods*). Data are % (w/w). A FFAP–fused-silica capillary column was used as described in the *Methods* section.

Cer's fatty acyl composition is shown in Fig. 3 and reveals a preponderance of long, saturated or mono-unsaturated acyl chains with a large fraction being hydroxylated at the second carbon atom. In general, these findings agree well with earlier studies in which multi-step derivatization procedures were used and in which identifications were based solely on GC retention times [9, 17–21] rather than on GC–MS analysis. A survey of these earlier studies reveals that our results fall well within the expected range of variation. Most of this variation is probably due to differences in tissue developmental state and/or animal age [22–24] and as well as regional compositional differences within tissue [17].

One final experiment was performed to determine whether the methyl iodide method can be used directly on intact GalCer to saponify and derivatize the amide-linked fatty acyl chains as has been shown for ester-linked fatty acyl chains in phosphoglycerides, glycerides, cholesteryl esters [14]. After treatment of GalCer (0.5 mg) as described for the free fatty acids (see Methods section), the resulting lipids were analyzed by TLC using light petroleum–diethyl ether–acetic acid (80:20:1, v/v/v) to assess derivatization of released fatty acids. Inspection of TLC plates revealed that both release and derivatization of fatty acids were poor (< 50%) and many unidentified side-products were generated. Attempts to increase the yield by raising the incubation temperature (100°C) produced no net improvement. Although fatty acid release increased, the ensuing yield of derivatized hydroxy fatty acids decreased, apparently because of degeneration of the 2-hydroxy group. In contrast, if temperature was lowered, fatty acid release declined and the ensuing derivatization improved only slightly.

In summary, a simple and direct means of analyzing sphingolipids fatty acyl composition has been demonstrated. The method is particularly useful for sphingolipids containing mixtures of non-hydroxy and 2-hydroxy fatty acids since stable derivatives of both fatty acid types can be produced simultaneously and then positively identified by capillary GC–MS.

ACKNOWLEDGEMENTS

We would like to thank Dr. Shaukat Ali for synthesizing the sphingolipid internal standards, Drs. Hermann Schlenk and Herb Dutton for their helpful comments, Carmen Perleberg for secretarial services, and Core D of USPHS PPG HL08214 for the use of GC–MS equipment. This work was supported by USPHS Grant GM45928 and by the Hormel Foundation.

REFERENCES

1 Y. Kishimoto and N. S. Radin, *J. Lipid Res.*, 1 (1959) 72.
2 Y. Kishimoto and N. S. Radin, *J. Lipid Res.*, 4 (1963) 130.
3 N. S. Radin, *J. Am. Oil Chem. Soc.*, 42 (1965) 569.
4 H. E. Carter, J. A. Rothfus and R. Gigg, *J. Lipid Res.* 2 (1961) 228.
5 R. C. Gaver and C. C. Sweeley, *J. Am. Oil Chem. Soc.* 42 (1965) 294.
6 H. Kadowaki, E. G. Bremer, J. E. Evans, F. B. Jungalwala and R. H. McCluer, *J. Lipid Res.*, 24 (1983) 1389.
7 Y. Kishimoto and N. S. Radin, *J. Lipid Res.*, 4 (1963) 139.
8 K. K. Carroll, *J. Lipid Res.*, 3 (1962) 263.
9 J. S. O'Brien and G. Rouser, *J. Lipid Res.*, 5 (1964) 339.

10 M. Scheutwinkel-Reich, B. Reindl and H.-J. Stan, in A. Frigerio (Editor), *Recent Developments in Mass Spectrometry in Biochemistry, Medicine and Environmental Research, 8*, Elsevier, Amsterdam, 1983, p. 251.
11 R. A. Laine, N. D. Young, J. N. Gerber and C. C. Sweeley, *Biomed. Mass Spectrom.*, 1 (1974) 10.
12 C. F. Poole and A. Zlatkis, *J. Chromatogr. Sci.*, 17 (1979) 115.
13 J. Drozo, *J. Chromatogr.*, 113 (1975) 303.
14 I. Ciucanu and F. Kerek, *J. Chromatogr.*, 284 (1984) 179.
15 M. I. Aveldano and L. A. Horrocks, *J. Lipid Res.*, 24 (1983) 1101.
16 K. Abe and Y. Tamai, *J. Chromatogr.*, 232 (1982) 400.
17 G. H. DeVries and W. T. Norton, *J. Neurochem.*, 22 (1974) 251.
18 *Catalogue*, Avanti Polar Lipids Inc., Birmingham, AL, p. 4.
19 M. J. Ruocco and G. G. Shipley, *Biochim. Biophys. Acta*, 859 (1986) 246.
20 D. S. Johnston and D. Chapman, *Biochim. Biophys. Acta*, 937 (1988) 10.
21 J. D. Jones, P. F. Almeida and T. E. Thompson, *Biochemistry*, 29 (1990) 3892.
22 Y. Kishimoto and N. S. Radin, *J. Lipid Res.*, 1 (1959) 79.
23 L. F. Eng, B. Gerstl, R. B. Hayman, Y. L. Lee, R. W. Tietsort and J. K. Smith, *J. Lipid Res.*, 6 (1965) 135.
24 L. Svennerholm and S. Stallberg-Stenhagen, *J. Lipid Res.*, 9 (1968) 215.

Author Index

Errata

J. Chromatogr., 600 (1992) 133–137
Page 134, eqn. 11 should read:

$$c(x_1,z_1) = \sum_{n=0}^{n=\infty} B_n e^{-\lambda z_1 - E_0(x_1 - x_0)^2/2} u_n(x_1)$$

Page 134, eqn. 14 should read:

$$d^2u/dy^2 + \{[E_0 + Pe\lambda(E_0^2 f_0 + Pe\lambda)/(E_0^2 + + Pe\lambda)]/(E_0^2 + Pe\lambda)^{1/2} - y^2\}u = 0$$

J. Chromatogr., 600 (1992) 251–256
Page 253, 3rd line below eqn. 5, "C^{-1}" should read "C_G^{-1}".
Page 253, 1st line below eqn. 12, "MHE" should read "multistep CGE".
Page 255, 7th line below eqn. 18, "X = constant = 1" should read "X = constant $\neq$ 1".

Capillary Electrophoresis

Principles, Practice and Applications

by **S.F.Y. Li**, *National University of Singapore, Singapore*

Journal of Chromatography Library Volume 52

Capillary Electrophoresis (CE) has had a very significant impact on the field of analytical chemistry in recent years as the technique is capable of very high resolution separations, requiring only small amounts of samples and reagents. Furthermore, it can be readily adapted to automatic sample handling and real time data processing. Many new methodologies based on CE have been reported. Rapid, reproducible separations of extremely small amounts of chemicals and biochemicals, including peptides, proteins, nucleotides, DNA, enantiomers, carbohydrates, vitamins, inorganic ions, pharmaceuticals and environmental pollutants have been demonstrated. A wide range of applications have been developed in greatly diverse fields, such as chemical, biotechnological, environmental and pharmaceutical analysis.

This book covers all aspects of CE, from the principles and technical aspects to the most important applications. It is intended to meet the growing need for a thorough and balanced treatment of CE. The book will serve as a comprehensive reference work and can also be used as a textbook for advanced undergraduate and graduate courses. Both the experienced analyst and the newcomer will find the text useful.

Contents:

1992 xxvi + 586 pages
Price: US$ 225.50 / Dfl. 395.00
ISBN 0-444-89433-0

TO ORDER

Contact your regular supplier or:

ELSEVIER SCIENCE PUBLISHERS
P.O. Box 211
1000 AE Amsterdam
The Netherlands

Customers in the USA & Canada:
ELSEVIER SCIENCE PUBLISHERS
Attn. Judy Weislogel
P.O. Box 945
Madison Square Station
New York, NY 10160-0757, USA

No postage will be added to prepaid book orders. US $ book prices are valid only in the USA and Canada. In all other countries the Dutch guilder (Dfl.) price is definitive. Customers in The Netherlands please add 6% BTW. In New York State please add applicable sales tax. All prices are subject to change without prior notice.

ELSEVIER
SCIENCE PUBLISHERS

Announcement from the Publisher

ELSEVIER SCIENCE PUBLISHERS

prefers the submission of electronic manuscripts

Electronic manuscripts have the advantage that there is no need for the rekeying of text, thereby avoiding the possibility of introducing errors and resulting in reliable and fast delivery of proofs.

The preferred storage medium is a $5\frac{1}{4}$ or $3\frac{1}{2}$ inch disk in MS-DOS format, although other systems are welcome, e.g. Macintosh.

Your disk and (**exactly matching**) printed version (printout, hardcopy) should be submitted together to the accepting editor. In case of revision, the same procedure should be followed such that, on acceptance of the article, the file on disk and the printout are **identical**. Both will then be forwarded by the editor to Elsevier.

Please follow the general instructions on style/arrangement and, in particular, the reference style of this journal as given in 'Instructions to Authors'.

Please label the disk with your name, the software & hardware used and the name of the file to be processed.

Further information can be found under 'Instructions to Authors - Electronic manuscripts'.

Contact the Publisher for further information.

ELSEVIER SCIENCE PUBLISHERS B.V.
P.O. Box 330, 1000 AH Amsterdam
Netherlands
Fax: (+31-20) 5862-304

PUBLICATION SCHEDULE FOR 1992

Journal of Chromatography and *Journal of Chromatography, Biomedical Applications*

MONTH	O 1991–F 1992	M	A	M	J	J	
Journal of Chromatography	Vols. 585–593	594/1 + 2 595/1 + 2	596/1 596/2 597/1 + 2	598/1 598/2 599/1 + 2 600/1 600/2	602/1 + 2 603/1 + 2 604/1	604/2 605/1 605/2 606/1	The publication schedule for further issues will be published later.
Cumulative Indexes, Vols. 551–600							
Bibliography Section		610/1			610/2		
Biomedical Applications	Vols. 573 and 574	575/1 575/2	576/1	576/2 577/1	577/2	578/1 578/2	

[a] Cumulative Indexes will be Vol. 601, to appear early 1993.

INFORMATION FOR AUTHORS

(Detailed *Instructions to Authors* were published in Vol. 558, pp. 469–472. A free reprint can be obtained by application to the publisher, Elsevier Science Publishers B.V., P.O. Box 330, 1000 AH Amsterdam, The Netherlands.)

Types of Contributions. The following types of papers are published in the *Journal of Chromatography* and the section on *Biomedical Applications:* Regular research papers (Full-length papers), Review articles and Short Communications. Short Communications are usually descriptions of short investigations, or they can report minor technical improvements of previously published procedures; they reflect the same quality of research as Full-length papers, but should preferably not exceed five printed pages. For Review articles, see inside front cover under Submission of Papers.

Submission. Every paper must be accompanied by a letter from the senior author, stating that he/she is submitting the paper for publication in the *Journal of Chromatography*.

Manuscripts. Manuscripts should be typed in double spacing on consecutively numbered pages of uniform size. The manuscript should be preceded by a sheet of manuscript paper carrying the title of the paper and the name and full postal address of the person to whom the proofs are to be sent. As a rule, papers should be divided into sections, headed by a caption (*e.g.*, Abstract, Introduction, Experimental, Results, Discussion, etc.). All illustrations, photographs, tables, etc., should be on separate sheets.

Introduction. Every paper must have a concise introduction mentioning what has been done before on the topic described, and stating clearly what is new in the paper now submitted.

Abstract. All articles should have an abstract of 50–100 words which clearly and briefly indicates what is new, different and significant.

Illustrations. The figures should be submitted in a form suitable for reproduction, drawn in Indian ink on drawing or tracing paper. Each illustration should have a legend, all the *legends* being typed (with double spacing) together on a *separate sheet*. If structures are given in the text, the original drawings should be supplied. Coloured illustrations are reproduced at the author's expense, the cost being determined by the number of pages and by the number of colours needed. The written permission of the author and publisher must be obtained for the use of any figure already published. Its source must be indicated in the legend.

References. References should be numbered in the order in which they are cited in the text, and listed in numerical sequence on a separate sheet at the end of the article. Please check a recent issue for the layout of the reference list. Abbreviations for the titles of journals should follow the system used by *Chemical Abstracts*. Articles not yet published should be given as "in press" (journal should be specified), "submitted for publication" (journal should be specified), "in preparation" or "personal communication".

Dispatch. Before sending the manuscript to the Editor please check that the envelope contains four copies of the paper complete with references, legends and figures. One of the sets of figures must be the originals suitable for direct reproduction. Please also ensure that permission to publish has been obtained from your institute.

Proofs. One set of proofs will be sent to the author to be carefully checked for printer's errors. Corrections must be restricted to instances in which the proof is at variance with the manuscript. "Extra corrections" will be inserted at the author's expense.

Reprints. Fifty reprints of Full-length papers and Short Communications will be supplied free of charge. Additional reprints can be ordered by the authors. An order form containing price quotations will be sent to the authors together with the proofs of their article.

Advertisements. The Editors of the journal accept no responsibility for the contents of the advertisements. Advertisement rates are available on request. Advertising orders and enquiries can be sent to the Advertising Manager, Elsevier Science Publishers B.V., Advertising Department, P.O. Box 211, 1000 AE Amsterdam, Netherlands; courier shipments to: Van de Sande Bakhuyzenstraat 4, 1061 AG Amsterdam, Netherlands; Tel. (+31-20) 515 3220/515 3222, Telefax (+31-20) 6833 041, Telex 16479 els vi nl. *UK*: T. G. Scott & Son Ltd., Tim Blake, Portland House, 21 Narborough Road, Cosby, Leics. LE9 5TA, UK; Tel. (+44-533) 753 333, Telefax (+44-533) 750 522. *USA and Canada*: Weston Media Associates, Daniel S. Lipner, P.O. Box 1110, Greens Farms, CT 06436-1110, USA; Tel. (+1-203) 261 2500, Telefax (+1-203) 261 0101.

The most useful chiral separation column, ULTRON ES-OVM, for enantiomeric drugs.

Substance	Rs	Substance	Rs	Substance	Rs
Acetylpheneturide	2.74	Disopyramid	2.04	Nisoldipine	2.36
Alimemazine	6.06	Eperisone	1.15	Nitrendipine	1.80
Alprenolol	1.09[1)]	Ethiazide	1.42	Oxazepan	2.65[2)]
Arotinolol	1.95	Fenoprofen	0.80	Oxprenolol	1.38
Bay K 8644	5.92	Flurbiprofen	1.27	Pindolol	2.04
Benproperine	3.27	Glutethimide	1.36	2-Phenylpropionic acid	0.80
Benzoin	8.41	Glycopyrronium	1.73	Pranoprofen	0.63
Biperiden	3.17	Hexobarbital	1.70	Prenylamine	0.86
Bunitrolol	3.08	Homochlorcyclizine	3.04	Profenamine	3.31
Bupivacaine	1.26	Hydroxyzine	2.15	Promethazine	1.42
Chlormezanone	6.48	Ibuprofen	1.72	Propranolol	1.24
Chlorphenesin	2.23	Ketoprofen	1.37	Terfenadine	2.22
Chlorpheniramine	2.36	Lorazepam	2.55[2)]	Thioridazine	0.72
Chlorprenaline	2.34	Meclizine	3.71	Tolperisone	1.50
Cloperastin	2.85	Mepenzolate	1.40	Trihexyphenidyl	5.16
Dimethindene	4.33	Mephobarbital	1.70	Trimipramine	3.69
1,2-Diphenylethylamine	1.74	Methylphenidate	1.13[1)]	Verapamil	1.49

NOTE: 4.6×150mm column at room temp. except[1)] 6.0×150mm at room temp. and[2)] 6.0×150mm at 10°C

From trace analysis for metabolites

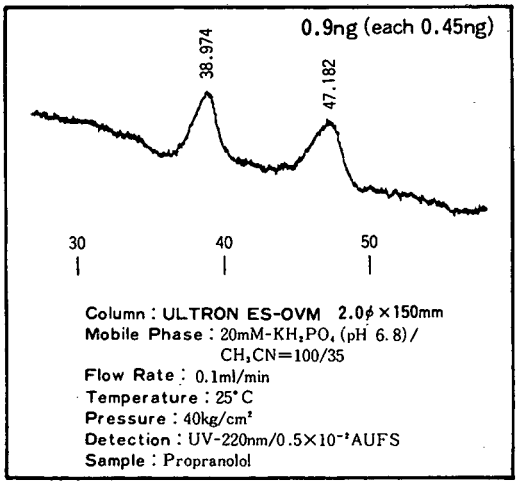

Column : ULTRON ES-OVM 2.0φ×150mm
Mobile Phase : 20mM-KH_2PO_4 (pH 6.8)/
CH_3CN=100/35
Flow Rate : 0.1ml/min
Temperature : 25°C
Pressure : 40kg/cm²
Detection : UV-220nm/0.5×10⁻²AUFS
Sample : Propranolol

to preparative scale

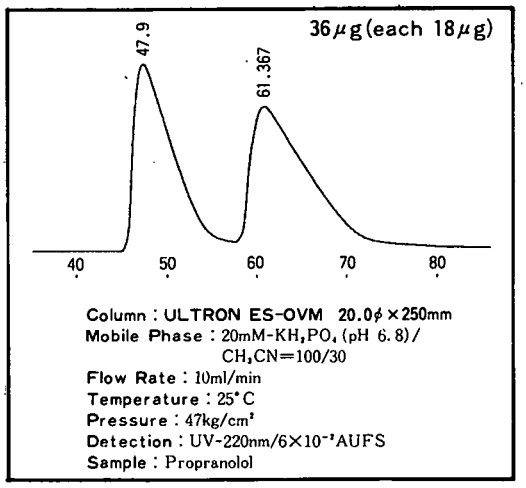

Column : ULTRON ES-OVM 20.0φ×250mm
Mobile Phase : 20mM-KH_2PO_4 (pH 6.8)/
CH_3CN=100/30
Flow Rate : 10ml/min
Temperature : 25°C
Pressure : 47kg/cm²
Detection : UV-220nm/6×10⁻²AUFS
Sample : Propranolol

SHINWA CHEMICAL INDUSTRIES, LTD

50 Kagekatsu-cho, Fushimi-ku, Kyoto 612, JAPAN

Phone: 80-75-621-2360 Fax : 80-75-602-2660

Please contact in United States of America and Europe to :

Rockland Technologies, Inc. 538 First State Boulevard, Newport, DE 19804, U.S.A.

Phone : 302-633-5880, Fax : 302-633-5893

This product is licenced by Eisai Co., Ltd.